




ADVERTIMENT. L'accés als continguts d'aquesta tesi queda condicionat a l'acceptació de les condicions d'ús establertes per la següent llicència Creative Commons:  <https://creativecommons.org/licenses/?lang=ca>

ADVERTENCIA. El acceso a los contenidos de esta tesis queda condicionado a la aceptación de las condiciones de uso establecidas por la siguiente licencia Creative Commons:  <https://creativecommons.org/licenses/?lang=es>

WARNING. The access to the contents of this doctoral thesis it is limited to the acceptance of the use conditions set by the following Creative Commons license:  <https://creativecommons.org/licenses/?lang=en>



UNIVERSITAT AUTÒNOMA DE BARCELONA

Facultat de Biociències

Dept. Biologia Animal, Biologia Vegetal i Ecologia

PhD thesis

Role and fine mapping of the minor QTLs *cmvqw3.1* and *cmvqw10.1* for resistance to *Cucumber mosaic virus* M6 in melon

PhD candidate

Lorena Beatriz Areco Ayala

Barcelona, Spain, July 2024

Universitat Autònoma de Barcelona
Facultat de Biociències
Dept. Biologia Animal, Biologia Vegetal i Ecologia
Estudis de Doctorat en Biologia i Biotecnologia Vegetal
PhD thesis

Role and fine mapping of the minor QTLs *cmvqw3.1* and *cmvqw10.1* for resistance to *Cucumber mosaic virus* M6 in melon

Dissertation presented by Lorena Beatriz Areco Ayala for the degree of Doctor of Biology and Plant Biotechnology by Universitat Autònoma de Barcelona (UAB) at the Centre de Recerca en Agrigenòmica (CRAG).

This work was performed in Centre de Recerca en Agrigenòmica (CRAG), Bellaterra and at the Institut de Recerca i Tecnologia Agroalimentaris (IRTA), Caldes de Montbui, Barcelona, Spain

Thesis director

Tutor

PhD candidate

Dra. Ana Montserrat
Martin Hernández

Dra. Ana Montserrat
Martin Hernández

Lorena Beatriz Areco
Ayala

Barcelona, Spain, July 2024

This thesis was carried out at the Plant Genetics Department of the Centre de Recerca en Agrigenòmica (CRAG) CSIC-IRTA- UAB-UB, Bellaterra, Barcelona. All the experimental fields were carried out at the Institut de Recerca i Tecnologia Agroalimentaris (IRTA), Caldes de Montbui, Barcelona. The research stay was carried out at the Leibniz Institute, German Collection of Microorganisms and Cell Cultures GmbH (DSMZ) and at the Julius Kühn Institute (JKI), located in Braunschweig, for three months in the group of Dr Björn Krenz from the Plant Viruses Department of the DSMZ.

Agradecimientos

Este periodo ha sido de gran importancia tanto a nivel personal como profesional y llega a su fin. A lo largo de estos cinco años, he vivido muchas experiencias, tanto buenas como malas, que me han dejado valiosas lecciones y aprendizajes. Estoy profundamente agradecida por haber compartido este tiempo con personas increíbles que me han acompañado en todos los momentos.

En primer lugar, quiero dedicar este logro a mi Papá, que en paz descanse, y a mi Mamá. Fueron los primeros en confiar en mí cuando tomé la decisión de dejar Paraguay para venir a realizar el máster y el doctorado. Su amor y apoyo han sido el cimiento de este logro.

Agradecimientos a “mi marido del alma querida santa maría y José Virgencita que bueno es” Kilian, que ha sido el pilar fundamental a lo largo de la tesis, desde el inicio hasta el final! Siempre ha estado a mi lado con su inquebrantable apoyo y sus palabras de aliento, recordándome constantemente que yo puedo. A mi gatito Oreo, mi protector espiritual, cuya presencia constante y afecto incondicional han sido un soporte emocional invaluable para mí. Aquellos que lo conocen saben cuán especial es y cuánto ha significado su compañía durante este viaje.

A mis hermanos Karina, Fernando y Romina, que me apoyaron desde la distancia cada uno con mis sobrinos loquitos Atenea, Santino y Allen y mis cuñis Tara (el más loco), Brenda (la más buena) y Marc (el chuchi). A mis suegros, quienes me acogieron en su casa durante la etapa más difícil de la tesis, la escritura. Siempre han respetado mi espacio y tiempo, tratándome como una hija. Agradezco profundamente tenerlos en mi vida.

A mis amigos del alma, Libni, Tina y Cristhian, quienes han estado conmigo desde que llegué aquí. Han sido un apoyo constante y cercano a lo largo de todo este proceso. Su amistad ha sido una luz en mi vida, el tipo de amistad que todos desean tener. Gracias por estar a mi lado cuando más lo necesitaba.

Mis agradecimientos a mi directora Montse Martin que me ha recibido con los brazos abiertos en su grupo. Gracias a ella pude aprender de cero todo lo relacionado a virus de plantas. Ella me ha enseñado a autogestionarme y ser autónoma. Su paciencia y orientación han sido incalculables y también su apoyo durante esos momentos difíciles de la vida, me han brindado mucho apoyo. Al igual que todo el periodo de la escritura de la tesis que ha sido duro, pero ¡lo hicimos Montse! Ahora es nuestro momento de festejar y disfrutar del resto.

I would like to thank Dr Bjorn Krenz, Dr Stephan Winter, Dra Samar Sheat and Dr Paolo Margaria for their warm welcome in Braunschweig, for their suggestions, constant support and invaluable guidance during my PhD stay at the Leibniz Institute DSMZ Julius-Kühn-Institut in Braunschweig, Germany. I would also like to thank Riny, Jessica and the greenhouse staff for their help during my stay. Además, a Kelly has sido una excelente amiga, espero que nos veamos pronto.

¡A los tres estudiantes que han llevado esta carga conmigo! Siempre llevar plantas a torre marimon, polinizar, cosechar, lavar semillas 😞, inocular plantas y extracciones con alta cantidad de muestras. Gracias Laia Pareras por preocuparse por

todo nuestro trabajo, una chica estupenda, muy trabajadora. El esmero que siempre tuviste te va a llevar lejos. A Emre (ya te escribo en castellano que sé que entiendes), el estudiante guapo por quien todos preguntaban, gracias por ayudarme con todo. Los trabajos de invernadero eran llevaderos gracias a las músicas turcas que siempre ponías y cantabas. Eres un chico muy genuino y simpático y eso te llevará lejos. Al final en mi defensa verás todos los avances que llegamos con la tesis. I would also like to thank Jochem for not letting me to forget about CRAG during the research stay jaja. Seriously, Jochem, I appreciate that you took care of everything when I was there! You have been a fundamental role in all the final experiments of this thesis. I would like to see you in my thesis presentation.

A mis compañeros del lab, Irene “La Ami”, una de las personas que más me ha apoyado y a la vez me ha regañado jejeje eres una mujer increíblemente fuerte con mucha determinación. Tendrás mucho éxito en tu vida y espero poder acompañarte en el proceso. Eres una amiga y una muy buena persona, y eso lo sabemos las personas que te conocemos sabemos que tienes un corazón enorme 😊. Ari, una de las chicas más encantadoras del lab, has sido importante en este periodo de mi vida y lo serás siendo. Espero que sigamos haciendo birras y nos descarguemos de las situaciones buenas y de la vida y luego salir de fiesta y disfrutar de la vida que a ti te falta poco también. Muchos ánimos con la tesis 😊. A Cris, otra de las mujeres más buenas y encantadoras que conocí en el CRAG, después de conllevar la maldición que nos cayó y queriendo apaciguar con la piedra que cargábamos con la luna llena, al final nos sirvió y terminamos juntas y exactamente el mismo día, hasta coincidimos en el día de la defensa de la tesis. Nuestra tesis en general del año cero del doctorado hasta el 23 de julio, serán solo 4 h de diferencia, el resto fue igual, Te deseo lo mejor en tu nuevo emprendimiento 😊

¡A grupo de CMV! Nuria, que también me ha enseñado desde los inicios, agradezco que hayas confiado en mí. Todo te irá genial. A Andrea, que siempre se ha preocupado de mis avances, te agradezco que siempre hayas sido muy buena conmigo. Thanks to Liu Bin, because he helped me to trust myself and my feelings, his support was significant during my first steps. Also, thanks to Weina, she was supporting me to be confident. I hope we will meet again.

¡Al grupo de melón! Miguel, ha sido un papel fundamental en mis inicios y durante el doctorado. Serás muy exitoso en todo lo que haces. Carlos, que ha estado conmigo también desde los inicios. Gracias por enseñarme cuando más lo necesitaba y llevarme en Torre Marimon cuando nadie iba, pero tú lo hacías. Éxitos en tu vida personal y profesional. A Laura, muchas gracias por darle buena onda siempre en los trabajos de invernaderos y me ayudabas con mis plantas hablándoles para que cuajen. ¡Eran complicadas ehh! Jeje ya lo sabes. Leandro el que está en todos los proyectos, más las 400 plantas de melón que tienes en torre maimón, espero que puedas con todo. Gracias por preocuparte siempre por mi tesis y como estaba. Satokoo, Satokitooo, thank you for your constant smile. The lab was always happy when you were there. I hope to travel to Japan with Irene as we always planned and meet there.

¡Al Grupo de Virus!, Juanjo por haber me apoyado desde el inicio de la tesis hasta ahora, muchas gracias. Tanto él como todo su grupo Ornela, Tarik y Clara, muy buena gente, me he pasado muy bien siempre.

A todo el personal de CRAG-IRTA. Fuensi, gracias por enseñarme de cero todo lo que se necesitó saber del Lab y ayúdame con mis experimentos. Enserio, muchas partes de la tesis no se hubieran llevado a cabo sin tu ayuda. Eres una persona muy buena en lo que hace y la más inteligente, “La Fuensi sabe todo”. Al Annnngeeel Que siempre ponía buenas músicas en el lab y en los invernaderos! gracias por la buena onda que siempre diste! Al final sos un brujo, porque muchas cosas que dijiste que me pasaría, le han pasado a la Luuurenaa. Elena, muchas gracias por tus enseñanzas y por haber estado ahí cuando necesitaba. Eres la mejor en lo que hace y todos sabemos. Noemí, gracias por la paciencia de siempre. Eres muy eficiente en lo que haces. Todavía no me olvido de las risas que nos tirábamos en el curso de inglés. Eran super divertidas gracias a ti. Kostas! Muchas gracias también a ti por la paciencia hasta en el último momento de mi tesis. Lo mejor para vos. A Joana, que me daba siempre buenas conversaciones diurnas. Se empezaba bien el día gracias a eso. Todo lo mejor para ti.

A todos los jefes del CRAG-IRTA, Marta, Jordi, Ibo, Amparo gracias por las sugerencias y orientaciones que me han dado durante el máster y la tesis. Gracias a ustedes también hoy estoy aquí.

A toda la unidad de Bioinformática del CRAG, Ignasi y Víctor sin ellos no hubiese llegado a nada de resultados. Gracias por guiarme y enseñarme en todo momento. Es especial a Ignasi, gracias por tu paciencia y tu predisposición, no hubiese hecho nada sin ti. Eres un chico muy inteligente que ayuda a los demás, ahora ya te liberaste oficialmente de mí.:)

Todo el personal de invernaderos del CRAG e IRTA Torre Marimón, gracias por la buena onda que siempre me han dado. Gloria, por aguantarme en todo momento cuando usaba “todos” los fitrotrones e invernaderos. Al igual que Alex y Albert, que estaba atrás mío siempre preguntando cuando los liberaba y siempre me ayudaban con mis plantas. Toñi gracias por preocuparse siempre que no me faltara insumos para mis plantas y por esas buenas conversaciones que siempre teníamos. Bernat, gracias por cuidar siempre de mis plantas incluso cuando estuve de estancia. Eres un chico muy trabajador. A Josep María, Manoli, Cristóbal, Teresita y Bernat, que siempre estuvieron conmigo durante toda la época del melón. Nos tirábamos unas risas e incluso bailábamos. Gracias a ustedes siempre los trabajos de invernadero eran llevaderos.

A todos mis compañeros de oficina, que han estado conmigo hasta el final en especial con los de animal Jesus, Yron, Magi que nos hemos reído un montón. Al igual que con Paloma y Montse, las nuevitas doctorandas, muchos éxitos en el doctorado. A todos los compañeros del departamento de Genética vegetal, Mariajo, Yanis, Nicole, Bea, Elisenda, Federico, Veredas, Ximo, Diana, Sergio y Dyllan gracias por la buena onda de siempre. Me ha encantado conocerlos, lo mejor para todos.

Dedicatoria

A mi papá que en paz descanse, a mi mamá, mi marido y mi gatito

“Déjalo ser al mundo”

-Cesar Domingo Areco Ferreira-

Indexes

Index of content

Abstract	I
Resumen	III
Resum	V
1. Introduction	1
1.1 Melon.....	2
1.1.1 Origin.....	2
1.1.2 Economic Importance of melon.....	4
1.1.3 Diseases in melon and yield losses.....	4
1.1.4 Genetics, genomics and breeding in melon	6
1.1.5 Collection of NILs in melon.....	7
1.2 Plant cell	10
1.2.1 Basic structure	10
1.2.2 Plant transport pathways.....	14
1.2.3 Veins anatomy	14
1.2.4 Bundle Sheath cells	15
1.2.5 Phloem.....	16
1.3 Plant viruses.....	17
1.3.1 Viral transport.....	18
.....	19
1.4 Resistance genes	20
1.4.1 Dominant resistance	20
1.4.2 Recessive resistance	21
1.5 Major and minor effects on the resistance.....	23
1.6. Cucumber mosaic virus	25
1.6.1 Host range and transmission.....	25
1.6.2 Genetic variability and evolution.....	26
1.6.3 Symptomatology.....	26

1.6.4 Genome organization.....	27
1.6.5 CMV cycle.....	28
1.7. Resistance to CMV in melon.....	31
1.7.1 Source of resistance to CMV in melon.....	31
1.7.2 Resistance to CMV in the accession Songwhan Charmi.....	32
1.8. Laser dissection microscopy.....	35
1.8.1 Fixation.....	36
1.8.2 Dehydration and cryoprotection.....	36
1.8.3 Embedding.....	37
1.8.4 Cell/Tissue isolation.....	38
2. Objectives	39
3. Materials and Methods	41
3.1 Plant material.....	42
3.1.1 Melon.....	42
3.1.2 Zucchini squash.....	43
3.2 In vitro plant culture.....	43
3.2.1 <i>In vitro</i> medium preparation.....	43
3.2.2 <i>In vitro</i> plant acclimatisation.....	44
3.3 Virus material.....	44
3.4 Visual phenotyping.....	45
3.5 DNA extraction.....	46
3.5.1 Quick DNA extraction.....	46
3.5.2 CTAB protocol, DNA extraction.....	46
3.6 RNA extraction.....	47
3.6.1 RNA extraction from melon tissue.....	47
3.6.2 RNA extraction from microdissected cells from fixed tissue sections after Laser dissection microscopy.....	47
3.7 Single Nucleotide Polymorphism Genotyping.....	49
3.8 Reverse transcription-polymerase chain reaction.....	49
3.8.1 RT-PCR using RNA extracted from melon tissue.....	49
3.8.2 The Polymerase chain reaction (PCR) in melon tissue.....	50
3.8.3 Real-time quantitative RT-PCR in melon tissue.....	51

3.8.4 RT-PCR using RNA extracted from microdissected cells.	52
3.8.5 The Polymerase chain reaction (PCR) for microdissected cells.....	52
3.9 Data Analysis.....	53
3.9.1 Infection scores.....	53
3.9.2 Quantification of virus (qRT-PCR) analysis	54
3.10 Laser dissection microscopy.....	54
3.10.1 Fixation.....	55
3.10.2 Cryoprotection.....	55
3.10.3 Embedding.....	55
3.10.4 Cryosectioning and OCT removal.....	56
3.10.5 Cell cut and sample isolation.....	56
4. Results.....	58
Chapter 1.....	59
Generation of melon pyramided lines with two QTLs containing minimal genetic contaminations.	60
1.1 Pyramiding and removal of undesirable regions	60
1.2 IL carrying <i>cmvqw3.1</i> and the <i>cmv1</i> gene.	61
1.2.1 Breeding strategy of IL 3-12 for <i>cmvqw3.1</i> and the <i>cmv1</i> gene selection.	63
1.2.2 Selected Pre-ILs 3-12	64
1.3 IL carrying <i>cmvqw10.1</i> and the <i>cmv1</i> gene.	66
1.3.1 Breeding scheme for selection of IL carrying <i>cmvqw10.1</i> and the <i>cmv1</i> gene...67	
1.3.2 Selected Pre ILs-10-12	69
1.4 IL 3-10-12. carrying <i>cmvqw3.1</i> , <i>cmvqw10.1</i> and <i>cmv1</i> gene.....	72
Chapter 2.....	74
Characterization of the resistance to CMV controlled by <i>cmvqw3.1</i> and <i>cmvqw10.1</i> QTLs in melon: Integration of laser dissection microscopy as a novel methodology in melon for determining the role of the minor QTLs in the Bundle Sheath cells.....	74

Section I: Characterization of the resistance to CMV controlled by <i>cmvqw3.1</i> and <i>cmvqw10.1</i> QTLs in melon.	75
2.1 Phenotyping of parent and melon pyramided lines.	75
2.1.1 Infection patterns of the melon pyramided lines	76
2.1.2 Minor QTLs <i>cmvqw3.1</i> and <i>cmvqw10.1</i> QTLs delay the virus phloem entry.	79
Section II: Integration of laser dissection microscopy as a novel methodology in melon for determining the role of the minor QTLs in the Bundle Sheath cells.	83
2.2 Exploring Bundle Sheath Cells in Melon.	83
2.3 Laser dissection microscopy.....	83
2.3.1 Influence of Vacuum on Tissue Fixation in Melon	84
2.3.2 Effects of levels of the cryoprotectant and its vacuum infiltration	84
2.3.3 Optimal freezing rate and their impact on tissue structure during embedding. ...	85
2.3.4 Thicker and transversal cryosections improve the cryosectioning process.	87
2.3.5 Microdissection of the Bundle Sheath cells.....	88
2.4 Identifying the BS cells in minor veins of the melon plant.	89
2.5 Detection of CMV in microdissected BS cells	89
Chapter 3	92
Construction of Fine Mapping Populations and Fine Mapping of the QTL <i>cmvqw3.1</i> and <i>cmvqw10.1</i>	92
Section I: Construction of Fine Mapping Populations	93
3.1 Recombinant plant selection in the F2 progeny.	94
Section II: Fine mapping of the QTL <i>cmvqw3.1</i>	97
3.2 Genotyping and phenotyping of R3 families.....	97
3.3 Genotyping and Phenotyping association of <i>cmvqw3.1</i> QTL	108
3.4 Candidate genes of <i>cmvqw3.1</i> QTL.	111
Section III: Fine mapping of the <i>cmvqw10.1</i> QTL	119
3.5 Genotyping and phenotyping of R10 families.....	119

3.6 Genotyping and Phenotyping Association of <i>cmvqw10.1</i> QTL	124
3.7 Candidate genes of <i>cmvqw10.1</i> QTL.....	126
5. General Discussion	127
5.1 Coordination of <i>cmvqw3.1</i> and <i>cmvqw10.1</i> QTLs with the <i>cmv1</i> gene in delaying infection from CMV subgroup I.....	128
5.2 The <i>cmvqw3.1</i> QTL appears to play a more significant role in resistance to CMV-M6 than the <i>cmvqw10.1</i> QTL.....	130
5.3 Laser dissection microscopy is a novel methodology in melon to isolate Bundle Sheath cells.....	132
5.4 Fine mapping of <i>cmvqw3.1</i> revealed two putative intervals.....	133
5.5 VPS33 a member of the HOPS and CORVET complex is a candidate gene for the <i>cmvqw3.1</i> QTL.....	135
6. Conclusions	140
7. Bibliography.....	143

Index of figures

Introduction

Figure I- 1. Geographical centre of origin of melon and the closer related species of <i>Cucumis melo</i> L. On the right side, drawing and picture of <i>Cucumis trigonus</i> (Adopted from Endl et al., 2018).	3
Figure I- 2. The collection of NILs in melon. The grey boxes in the specific Linkage group (LG) represent the SC introgression. The first number after “SC” indicates the chromosome, and the second number indicates the position of the introgression within the chromosome (Adopted from Eduardo et al., 2005).	9
Figure I- 3. Plant cell representation with the most important organelles. The picture was created with Biorender.....	10
Figure I- 4. Structure of melon veins. A) BS cells into the minor veins IV and V. B) BS cells surrounding the intermediary cells in a minor vein type V. C) Zoom of the minor vein type V of (B) where BS cells surrounding the sieve elements, intermediary cells and vascular parenchyma. chl: chloroplasts; T: tracheid, IC: intermediary cells, n: nucleus, VP: vascular parenchyma, SE: sieve elements (Adopted from Guiu-Aragonés et al., 2016).	16
Figure I- 5. General plant viruses transport either cell-to-cell or long-distance movement in plant tissues (Adopted from Hipper et al., 2013).....	19
Figure I- 6. Qualitative and quantitative resistance to disease in terms of mapping an interval in a reference genome (Adopted from Corwin and Kliebenstein 2017).	24
Figure I- 7. <i>Cucumovirus</i> non-enveloped, spherical virion about 29nm in diameter with T=3 icosahedral symmetry, composed of 180 coat proteins: 12 pentamers and 20 hexamers. Adopted from ExPASy https://viralzone.expasy.org/	27
Figure I-8. Current understanding of resistance to CMV in melon plants. A) Cellular localization of CMV by <i>in situ hybridization</i> in CMV-LS inoculated leaves of melon plants. The blue/dark colour indicates the presence of viral RNA. C-, samples from a non-inoculated plant; PS, susceptible cultivar; SC12-1-99, resistant accession	

carrying only *cmv1* gene. Ph, phloem; Xy, xylem (Adopted from Guiu-Aragonés et al., 2016). **B)** CMV movement in susceptible and resistant melon plants. The virus crosses the epidermis and moves from cell to cell to reach the VB, where the phloem is located. The CMV crosses the BS to reach the phloem and infect the whole plant in susceptible melon plants. In contrast, CMV stops in the BS cells in resistant melon plants. Red circle: CMV virions. Picture adapted from Real 2022 and was created with Biorender..... 34

Results

Chapter 1

Figure 1. 1. Breeding scheme for IL 3-12 to remove any undesired interval outside the QTLs of interest. F1, F2 and F3: represent the number of generations; BC: Backcross. 63

Figure1. 2. Breeding scheme for IL 10-12 for removing undesired SC contaminations outside the QTLs. F1, F2 and F3: represent the number of generations; BC: Backcross. 68

Chapter 2.

Figure 2. 1. A) PCA of the infection patterns of the melon pyramided lines including PS infections. PC1 showed 99.05% and PC2 0.92% of the variance. Cluster means the clustering of samples according to severity and the velocity of the infections. 77

Figure 2. 2. A) Plots of infection scores reached by individual plants of melon pyramided lines at each time point 7, 14, 21 and 28 dpi. **B)** Statistical significance (p-value <0.05) of all melon lines compared to each other using the mean score reached by the individual plants per group at each time point. In red highlight significantly different means of infection scores. The <0.0e+00 refers to p-values < 0.0e-293..... 78

Figure 2. 3. The plot of the Infection scores (scale from 0 to 5) of melon pyramided lines over time (7 to 28 dpi) of the melon pyramided lines. The number of replicates used in each melon pyramided line varies from 40 to 53 biological replicates. Each

dot represents the mean infection reached by the day. The bar corresponds to the standard deviation (SD). 79

Figure 2. 4. A) Relative virus accumulation within the petiole of the inoculated leaves in the melon pyramided lines and parent lines. **B)** Relative accumulation within the petiole of the inoculated leaves in the melon pyramided lines and SC excluding PS. The number of replicates used in each melon pyramided line for both varies between 3 to 7 biological replicates **C)** Statistical significance of all lines compared to each other. In red, statistically (p-value <0.05) different melon pyramided lines. 81

Figure 2. 5. Impact of sucrose concentration and vacuum infiltration time on sample sinking in melon leaves. 85

Figure 2. 6. A) Minor veins in melon leaves. **B)** positioning them into the mould to perform longitudinal cryosections. 86

Figure 2. 7. Velocity of the freezing of the minor veins. **A)** Morphology of the samples after quick freezing in liquid Nitrogen (N2 liquid), longitudinal cryosection. **B)** Morphology of the samples after slow freezing at -20 °C, longitudinal cryosection. 87

Figure 2. 8. Cryosection of minor veins Type IV and V, **A)** Longitudinal cryosection, **B)** Transversal cryosection of minor veins 88

Figure 2. 9. BS cell identification in longitudinal sections of the minor veins in PS melon. 89

Figure 2. 10. CMV detection by PCR of microdissected BS cells obtained by the LDM system. Each sample represents approximately >100 microdissected BS cells. For agarose gel amplification, the forward primer (F109-1600F/GGAGAGGAATGGGACGTG) and the reverse primer (F109-2000R/GGATCAACGGTAAAGTACG) correspond to the genomic RNA 1 sequence of CMV-SG I. The expected band size was 0.4 kb. The parent lines SC and, PS. Melon pyramided line: IL Q10-12-F50, ILQ3-12-H5 and IL3-10-12-18(64). Fast Ladder=Molecular weight marker, M=Mock-inoculated plant. 91

Chapter 3

Figure 3. 1. Construction of fine mapping populations for both QTLs *cmvqw3.1* and *cmvqw10.1* and consequently the recombinant plant selection..... 95

Figure 3. 2. A) Plant with typical viral symptoms characterized by a mosaic pattern on the leaves, which gradually develops into leaf curling. **B)** Plant with a combination of mosaic symptoms and necrosis in veins and petioles. These images represent individual plants of the R3-62 family at 28 dpi..... 98

Figure 3. 3. A) Genotyping results of informative R3 families of the first set of phenotyping. Chr: Chromosome, P: Physical position, O: Out of the QTL SNP: Single Nucleotide Polymorphism, FM: Flanking Markers, **B)** Scores and rate of mosaic and necrosis of R3 families phenotyped at 28 dpi. 99

Figure 3. 4. The first set of phenotyping results of each R3 family based on the scores of mosaics considering the time points 9, 13, 16, 20, 24, 28 dpi. The number of biological replicates was between 12 to 52 individuals per melon family. Each dot represents the replicate distributed along the graph using the `position_jitterdodge()` function of RStudio version 2024.04.2+764. The black diamond indicates the average infection reached by the family at each time point. The blue error indicates the standard deviation (SD) of each family and the black line represents the median of each R3 family. Each box corresponds to 25 to 75% of the data. Significant differences compared to IL 3-10-12-18(64) are marked with asterisks (p-values $* < 0.05$, $** < 0.005$, $*** < 0.0005$, $**** < 0.00005$). 101

Figure 3. 5. Preliminary mapping association of genotypes and phenotypes by visual paired comparisons of genotypes from eight R3 families..... 102

Figure 3. 6. A) Genotyping results of informative R3 families of the second set of phenotyping. Chr: Chromosome, P: Physical position, O Out of the QTL, SNP: Single Nucleotide Polymorphism, FM: Flanking Markers. **B)** Score of mosaics and necrosis of phenotyped R3 families at 28 dpi. 104

Figure 3. 7. The second set of phenotyping results of each R3 family based on the scores of mosaics considering the time points 9, 13, 16, 20, 24, and 28 dpi. The number of biological replicates was 12 to 52 individuals per melon family. Each dot

represents the replicate distributed along the graph using the `position_jitterdodge()` function of RStudio version 2024.04.2+764. The black diamond indicates the average infection reached by the family at each time point. The blue error indicates the standard deviation (SD) of each family and the black line represents the median of each R3 family. Each box corresponds to 25 to 75% of the data. Significant differences compared to IL 3-10-12-18(64) are marked with asterisks (p-values $* < 0.05$, $** < 0.005$, $*** < 0.0005$, $**** < 0.00005$). 105

Figure 3. 8. A) Phenotyping results for each R3 family, based on infection levels from 7 to 28 dpi. The dots represent the mean score of all individuals at each dpi and are distributed along the graph using the `position_jitterdodge()` function of RStudio version 2024.04.2+764. The red solid line indicates the average infection of the IL 3-10-12-18(64) line over time. The black diamond inside each box represents the average infection level, and the black line represents the median of each R3 family. Each box corresponds to 25 to 75% of the data. Significant differences from IL 3-10-12-18(64) indicating susceptibility are indicated by asterisks (p-values $* < 0.05$, $** < 0.005$, $*** < 0.0005$, $**** < 0.00005$). **B)** Genotyping results of R3 plants used for phenotyping assays with CMV-M6. Chr: Chromosome, P: Physical position, O: Out of the QTL SNP: Single Nucleotide Polymorphism, FM: Flanking Markers. 107

Figure 3. 9. A) Genotypes of 15 R3 families and the positive (IL Q10-12-F50) and the negative (IL 3-10-12-18(64)) controls. The molecular markers are distributed along the interval based on their physical position. The red markers indicate statistically significant SNPs and the black ones mean no association. The red dashed lines mean the fine mapping association. R: Resistant, S: Susceptible, Mb: Megabase **B)** Fine mapping association of the *cmvqw3.1* performed in different time points 9, 13, 16 and 20 dpi of infection scores. The X-axis shows the evenly distributed physical positions of SNPs within the *cmvqw3.1* interval, while the Y-axis shows $-\log_{10}(p\text{-value})$. The horizontal black line indicates a significance threshold of $p\text{-value} = 0.05$ 111

Figure 3. 10. The candidate gene CmVPS45 (Gene ID MELO3C008406.2.1) of QTL *cmvqw3.1*. The genome annotation is established in the SC genome with the

small variants in the PS genome. **A)** Representation of the gene structure with two SNPs in exons seven and eight. The numbers at the top indicate the physical position in the genome in kb: Kilobase. The numbers at the bottom indicate the position of the gene in bp: Base pairs. **B)** The coding sequence of the exon seven and eight in SC and PS. The red colour indicates the single mutation of SC, and the blue colour indicates the single mutation of PS. **C)** The protein sequence is translated from the original coding sequence, representing the protein translation of exons seven and eight in frame. 115

Figure 3. 11. The candidate gene CmVPS33 (Gene ID MELO3C029984.2.1) of QTL *cmvqw3.1*. The genome annotation is established in the SC genome with the variants in the PS genome. **A)** Representation of the gene structure with a SNP in exon four. The numbers at the top indicate the physical position in the genome in kb: Kilobase. The numbers at the bottom indicate the position of the gene in bp: Base pairs. **B)** The coding sequence of the gene in SC and PS. The red colour indicates the single mutation of SC, and the blue colour indicates the single mutation of PS. **C)** The protein sequence is translated from the original coding sequence..... 117

Figure 3. 12. A) Genotypes of the six R10 families inoculated with the CMV-M6. Chr: Chromosome, P: Physical position, SNP: Single Nucleotide Polymorphism, FM: Flanking Markers. B) Scores of mosaics and necrosis reached by phenotyped R10 families at 28 dpi. 120

Figure 3. 13. A) Phenotyping results of each R10 family based on the scores of mosaics considering time points 13, 16, 20, 24 and 28 dpi. Biological replicates ranged from 4 to 52 individuals per melon family. Each dot represents the replicate distributed along the graph using the `position_jitterdodge()` function of RStudio version 2024.04.2+764. The black diamond indicates the average infection reached by the family at each time point. The blue error indicates the SD of each family, and the black line represents the median of each R10 family. Each box corresponds to 25 to 75% of the data. Significant differences compared to IL 3-10-12-18(64) are marked with asterisks (p-values $* < 0.05$, $** < 0.005$, $*** < 0.0005$, $**** < 0.00005$). 122

Figure 3. 14. A) Genotypes of the six R10 families phenotyped with the CMV-M6. SNP: Molecular Markers, FM: Flanking Markers, P: Physical position, Chr: Chromosome. **C)** Boxplot of the phenotyping results for each R10 family, based on infection levels from 11 to 28 dpi. The dots represent the mean score of all individuals at each dpi and are distributed along the graph using the `position_jitterdodge()` function of RStudio version 2024.04.2+764. The red solid line indicates the average infection of the IL 3-10-12-18(64) line over time. The black diamond inside each box represents the average infection level, and the black line represents the median of each R10 family. Each box corresponds to 25 to 75% of the data. Significant differences from IL 3-10-12-18(64) indicating susceptibility are indicated by asterisks (p-values * <0.05 , ** <0.005 , *** <0.0005 , **** <0.00005).

..... 123

Figure 3. 15 A) Genotypes of six R10 families, the positive (IL Q3-12-H5) and the negative control (IL 3-10-12-18(64)). The molecular markers are distributed along the interval based on their physical position. The red markers indicate statistically significant SNPs and the black ones mean no association. The red dashed lines mean the fine mapping association. R: Resistant, S: Susceptible, Mb: Megabase. **B)** Fine mapping association of the *cmvqw10.1* in different time points 13, 16, 20, 24 and 28 dpi of infection scores. The physical positions of SNPs within the *cmvqw10.1* interval are distributed along the X-axis, while the Y-axis shows $-\log_{10}(\text{p-value})$. The horizontal line indicates a significance threshold of $\text{p-value}=0.05$ 125

General Discussion

Figure GD-1. Model of resistance conferred by QTL *cmvqw3.1* and *cmvqw10.1* in coordination with the *cmv1* gene. **A)** In susceptible PS plants, CMV SGI particles, once in the cytoplasm, move towards the late endosome, passing through the early endosome where the CORVET complex is located. Once in the late endosome, they interact with VPS41, VPS33 and unknown genes from the *cmvqw3.1* and *cmvqw10.1* QTL within the HOPS complex to hijack the melon cell machinery and move freely within the cell. They then cross the transvacuolar strands in the vacuole and reach

the tonoplast to finally enter the plasmodesmata. After that, the virus moves to the intermediate cells to reach the tonoplast of the vacuole and crosses the small transvacuolar strands in the various vacuoles present in ICs until it reaches the pore plasmodesmata unit. Then, the virus crosses the sieve element to establish a systemic infection. **B)** In resistant IL3-10-12-18(64) plants, the CMV SGI strain follows a similar pathway but interacts with mutant versions of VPS33, mutant VPS41 and unknown genes in the QTL *cmvqw3.1* and *cmvqw10.1* within the HOPS complex at the late endosome. The mutant VPS41, in the absence of the susceptible alleles of the other genes, can develop very few TVS and thus, cannot provide the way through the vacuole to the PDs to finally reach the ICs and SE. The very few viruses able to reach the phloem would, at a later time post-infection, have multiplied enough in some plants to produce a systemic infection. VPS41: Vacuolar protein sorting 41, VPS33: Vacuolar protein sorting 33, *cmvqw3.1* QTL: Quantitative trait locus on chromosome III of SC melon, *cmvqw10.1* QTL: Quantitative trait locus on chromosome X of SC melon, CORVET: Class C core vacuole/endosome tethering.

Index of Tables

Materials and Methods

Table M&M- 1. Original melon ILs used to segregate out genetic contaminations (Yan, 2018).	42
Table M&M- 2. Component of the <i>in vitro</i> culture medium	43
Table M&M- 3. The scale of the mosaic symptoms in melon.	45
Table M&M- 4. The scale of the necrotic observations in melon to characterize the HR.	46
Table M&M-5. Reverse primers to synthesize the first strand cDNA specific for the viral RNA (RNA1, RNA2 or RNA3).....	50
Table M&M- 6. PCR conditions to detect CMV infection in melon tissues. Primers for CMV detection are specified in Supplementary Table 1.S1 Excel sheet Primers.	51
Table M&M- 7. Real-time quantitative qPCR conditions to quantify the CMV. .	52
Table M&M- 8. PCR conditions to detect CMV infection in microdissected cells.	53

Results

Chapter 1

Table 1. 1. Genotype of the original ILs that have been used to segregate out genetic contaminations.	60
Table 1. 2. Physical and genetic distance of the resistance QTLs in the melon genome.	61
Table 1. 3. Genetic contaminations contained in the IL 3-12.	62
Table 1. 4. The genotype of the selected Pre-IL H5 and Pre-IL H218.	64
Table 1. 5. Final genotypes of ILs Q3-12 H5 and IL Q3-12 H218 that were chosen for further experiments.....	65
Table 1. 6. Genetic contaminations contained in the parent lines SC 10.2 and SC 12.1.99.....	67
Table 1. 7. The genotype of the selected Pre-IL F50 and Pre-IL F193.....	70

Table 1. 8. Final lines IL Q10-12 F50 and F193 after segregating out the genetic contaminations. 71

Table 1. 9. The genotype of the IL 3-10-12. 73

Chapter 2

Table 2. 1. Melon pyramided lines that were used in this study. 75

Chapter 3

Table 3. 1. Genotypes of the F1: ILQ3-12-H218 x ILQ10-12-F193 plants and segregating out the genetic contaminations. 94

Table 3. 2. Genotypes of the four groups from the progeny of F2: ILQ3-12-H218 x ILQ10-12-F193 population to select recombinant plants. These groups are R3, R10, R3-HH, and R10-HH. 96

Table 3. 3. List of candidate genes of the first interval of *cmvqw3.1* between 5,307,083 and 5,703,825 bp in the melon genome annotation and structural variations in PS. The genes are annotated in the melon genome assembly version V4.0 and V3.6.1 In blue are the two candidate genes for the QTL *cmvqw3.1*. 112

Index of the digital supplementary material

Materials and Methods

Table 1.2 S1, Excel sheets:

SNPs: The physical position of the SNPs in v3.61 genome assembly.

Primers: Primers used to detect CMV and the reverse primers

qPCR: the sequence of the primers to quantify the CMV and the housekeeping

Chapter 1

Table 1.1 S2, Excel sheets: genotyping of melon pyramided lines carrying *cmvqw3.1* and the *cmv1* gene.

IL Q3-12 (H5)

Table 1.2 S2, Excel sheets: genotyping of melon pyramided lines carrying *cmvqw10.1* and the *cmv1* gene.

IL Q10-12 (F50)

IL Q10-12 (F193)

Chapter 3

Table 1.1 S3, Excel sheets:

cmvqw3.1 Recombinant plant generation

Association Time points, Statistical analyses performed per time point in the fine mapping of *cmvqw3.1* QTL.

Candidate genes, List of candidate genes of *cmvqw3.1* in v4.0 genome assembly

CmVPS4, coding sequence and protein sequence

CmVPS3, coding sequence and protein sequence

R3 families, Pictures of recombinant plants for the QTL *cmvqw3.1*

Table 1.2 S3, Excel sheets:

cmvqw10.1 Recombinant plant generation

Association Time points, Statistical analyses performed per time point in the fine mapping of *cmvqw10.1* QTL.

Candidate genes, List of candidate genes of *cmvqw10.1* in v4.0 genome assembly

R10 families, Pictures of recombinant plants for the QTL *cmvqw10.1*

Abstracts

Abstract

Cucumber mosaic virus (CMV) affects over 1,300 plant species, including important agricultural species, including the *Cucurbitaceae* family. CMV strains are divided into Subgroup I (SGI) and II (SGII). The Korean accession “Songwan Charmi” (SC) carries an oligogenic, recessive and quantitative resistance to CMV. SC was crossed with the Spanish cultivar “Piel de Sapo” (PS), which is susceptible to CMV, to further investigate the resistance trait. The *cmv1* gene, encoding a Vacuolar Protein Sorting 41 (VPS41), acts as a gatekeeper for viral phloem entry in melon and has a major effect on resistance to CMV-LS, from SGII strain. *cmv1* restricts CMV-LS in the bundle sheath cells (BS), preventing systemic infection, but is ineffective against CMV-SGI strains (CMV-M6). In addition, two Quantitative Trait Loci (QTLs) with minor effects on resistance were identified: *cmvqw3.1* (chromosome III) and *cmvqw10.1* (chromosome X). Full resistance to SGI requires the presence of *cmv1* and these minor QTLs. This thesis, divided into three chapters, investigates the role of the minor QTLs *cmvqw3.1* and *cmvqw10.1* together with the *cmv1* gene and addresses their fine mapping.

In the **First Chapter**, melon pyramided lines carrying one or the two QTLs and the *cmv1* gene were developed carrying minimal genetic contaminations from SC.

In the **Second Chapter**, the melon pyramided lines were used to characterise the resistance conferred by these genes. The minor QTLs, cooperating with the *cmv1* gene, delayed CMV-M6 infection. The QTL *cmvqw3.1* plays a more relevant role in resistance than *cmvqw10.1*. A methodology for laser dissection microscopy in melon for cell-specific studies was also developed.

In the **Third Chapter**, two fine mapping populations for the minor QTLs were generated. Mapping of *cmvqw3.1* suggested two intervals, narrowing them to 0.39 Mb, with 25 genes, and 15.28 Mb and identifying a Vacuolar Protein Sorting Associated Protein 33-Like Protein (VPS33) as a strong candidate because of its role in protein trafficking and relationship with the VPS41. In contrast, the mapping of

cmvqw10.1 narrowed the interval from 3.62 Mb to 1.76 Mb, implicating 294 genes in CMV M6 resistance.

Resumen

El *Virus del mosaico del pepino* (CMV) afecta a más de 1.300 especies de plantas, incluidas importantes especies agrícolas como las *Cucurbitáceas*. Las cepas de CMV se dividen en Subgrupo I (SGI) y II (SGII). La accesión coreana “Songwan Charmi” (SC) tiene una resistencia oligogénica, recesiva y cuantitativa ante el CMV. SC se cruzó con el cultivar español “Piel de Sapo” (PS), el cual es susceptible al CMV para investigar más a fondo el rasgo de resistencia. El gen *cmv1* codifica la proteína Vacuolar Protein Sorting 41 (VPS41) que actúa como guardián de la entrada del virus al floema del melón. Este gen tiene un efecto importante sobre la resistencia al CMV-LS, de la cepa SGII. *cmv1* restringe CMV-LS en las células de la vaina del haz (BS), previniendo la infección sistémica, pero es ineficaz contra las cepas de CMV-SGI (CMV-M6). Para ello se identificaron otros dos Quantitative Trait Loci (QTL) con efectos menores en la resistencia: *cmvqw3.1* (cromosoma III) y *cmvqw10.1* (cromosoma X). La resistencia total a SGI requiere la presencia de *cmv1* y estos QTL. Esta tesis, dividida en tres capítulos, investiga el papel de los QTL menores *cmvqw3.1* y *cmvqw10.1* junto con al gen *cmv1* y aborda su mapeo fino.

En el **Primer Capítulo**, se desarrollaron líneas piramidadas de melón que portaban uno o dos QTL y el gen *cmv1* con mínimas contaminaciones genéticas de SC.

En el **Segundo Capítulo** se utilizaron las líneas piramidadas de melón para caracterizar la resistencia conferida por estos QTLs. Los QTL que cooperan con el gen *cmv1*, retrasaron la infección por CMV-M6. El *cmvqw3.1* tiene un papel más relevante en la resistencia que *cmvqw10.1*. Además, se desarrolló una metodología de microscopía de disección láser en melón para estudios de células específicas.

En el **Tercer Capítulo**, se generaron dos poblaciones de mapeo fino para los QTL. El mapeo de *cmvqw3.1* sugirió dos intervalos, reduciéndolos a 0,39 Mb con 25 genes y 15,28 Mb. La proteína Vacuolar Protein Sorting Associated Protein 33-Like Protein (VPS33) se identificó como un fuerte candidato debido al role en el tráfico de proteínas y su relación con la VPS41. Por el contrario, el mapeo de *cmvqw10.1* se

redujo el intervalo de 3,62 Mb a 1,76 Mb, lo cual involucra unos 294 genes en la resistencia al CMV M6.

Resum

El *Virus del mosaic del cogombre* (CMV) afecta més de 1.300 espècies vegetals, incloses espècies agrícoles importants, com ara la família *Cucurbitaceae*. Les soques de CMV es divideixen en el subgrup I (SGI) i II (SGII). L'accessió coreana "Songwan Charmi" (SC) té una resistència oligogènica, recessiva i quantitativa al CMV. SC es va creuar amb el cultivar espanyol "Piel de Sapo" (PS), que és susceptible al CMV, per investigar més la seva resistència. El gen *cmv1*, que codifica un Vacuolar Protein Sorting 41 (VPS41), actua com a guardià de l'entrada del virus al floema del meló i té un efecte important sobre la resistència a CMV-LS, de la soca SGII. *cmv1* restringeix CMV-LS a les cèl·lules de la beina (BS), evitant la infecció sistèmica, però és ineficaç contra les soques de CMV-SGI (CMV-M6). A més, es van identificar dos Quantitative Trait Loci (QTL) amb efectes menors sobre la resistència: *cmvqw3.1* (cromosoma III) i *cmvqw10.1* (cromosoma X). La resistència total a SGI requereix la presència de *cmv1* i aquests QTL menors. Aquesta tesi, dividida en tres capítols, investiga el paper dels QTL menors *cmvqw3.1* i *cmvqw10.1* vinculats al gen *cmv1* i aborda el seu mapeig fi.

Al **Primer Capítol**, es van desenvolupar línies piramitades de meló que portaven un o dos QTL i el gen *cmv1* amb contaminacions genètiques mínimes de SC.

En el **Segon Capítol**, es van utilitzar les línies piramitades del meló per caracteritzar la resistència que confereixen aquests QTLs. Els QTL, que van cooperar amb el gen *cmv1*, van retardar la infecció per CMV-M6. El QTL *cmvqw3.1* té una funció més rellevant en la resistència que el *cmvqw10.1*. També es va desenvolupar una metodologia per a la microscòpia de dissecció làser en meló per a estudis específics de cèl·lules.

Al **Tercer Capítol**, es van generar dues poblacions de mapeig fi per als QTL. El mapeig de *cmvqw3.1* va suggerir dos intervals, reduint-los a 0,39 Mb amb 25 gens i 15,28 Mb. La proteïna Vacuolar Protein Sorting Associated Protein 33-Like Protein (VPS33) es va identificar com a un fort candidat. En canvi, el mapeig de *cmvqw10.1*

el va reduir de 3,62 Mb a 1,76 Mb, implicant 294 gens per a la resistència del meló al CMV-M6.

1. Introduction

1. Introduction

1.1 Melon

1.1.1 Origin

Melon (*Cucumis melo*) is a diploid species ($2x=2n=24$ chromosomes) belonging to the botanical family *Cucurbitaceae* (Schaefer and Renner, 2011; Renner and Shaefer, 2017; Chomicki et al. 2020). Members of the *Cucurbitaceae* family include other important crops such as cucumber (*Cucumis sativus*), watermelon (*Citrullus lanatus*), pumpkin (*Cucurbita spp*), squash and zucchini (*Cucurbita pepo*), bitter gourd (*Momordica charantia*), Sandia (*Citrullus amarus*) and bottle gourd (*Lagenaria siceraria*) (Schaefer and Renner, 2011; Renner and Shaefer, 2017). *Cucurbitaceae* is divided into two subfamilies, *Cucurbitoidae* and *Zanonioidae*, while *Cucumis melo* is divided into three subspecies. *Cucumis melo subsp. melo*, *Cucumis melo subsp. agrestis* and *Cucumis melo subsp. meloides* (Schaefer and Renner, 2011; Renner and Shaefer, 2017; Chomicki et al. 2020).

Recent studies have shown that the melon originated in Asia millions of years ago during the Late Cretaceous (Schaefer and Renner, 2011). Since then, transoceanic long-distance dispersal has spread the lineages repeatedly to the African, American and Australian continents (Schaefer et al. 2009). However, the exact centre of origin remains controversial (Renner et al. 2007, Sebastian et al. 2010). The latest research has identified three possible geographic centres of origin: The first clade includes African accessions called “African Agrestis”. The second clade included an accession from Australia and New Guinea called “Australian Agrestis”. Finally, the largest clade, the third one includes accessions from Asia and also accessions from Madagascar and islands in the Indian Ocean, described as a new geographical centre of origin called “Asian Agrestis”. *Cucumis melo* is more closely related to the wild Australian and Indian accessions such as *Cucumis pirocarpus* and *Cucumis trigonous* respectively, as shown in Figure I-1 (Renner et al. 2007, Sebastian et al. 2010; Endl et al. 2018).

1. Introduction

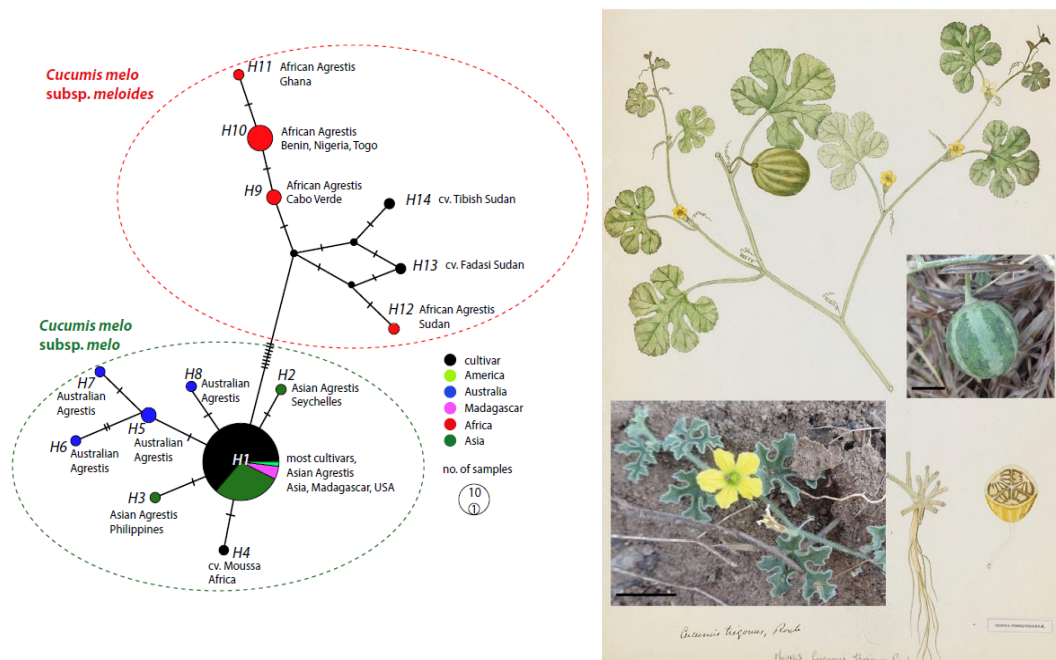


Figure I- 1. Geographical centre of origin of melon and the closer related species of *Cucumis melo* L. On the right side, drawing and picture of *Cucumis trigonus* (Adopted from Endl et al., 2018).

The first domesticated melon was described in Asia and Africa 5,000 and 6,000 years ago. The wild melons of India (*Cucumis melo subsp. melo*) and Africa (*Cucumis melo subsp. agrestis*) are the ancestors of the commercial melons cultivated in agriculture today. Although the *Cucumis melo subsp. melo* group is less important in terms of quality, it provides a rich source of genetic variability for new potential cultivars. Some modern melon cultivars such as “Galia”, “Cantaloupe” and “Yellow Honeydew” are derived from Asian accessions. Domestication of the most common melon cultivars, such as *Inodorus*, *Cantaloupensis*, *Reticulatus*, *Adzhur*, *Chinensis*, *Conomon* and *Makuwa*, occurred mainly in India. Asian accessions include Southeast, Central and Far East Asia. Australian/New Guinean accessions were apparently never domesticated, whereas African accessions include “Tibish” and “Fadasi” melons. (Endl et al., 2018).

1.1.2 Economic Importance of melon

Melons are consumed for their culinary, nutritional and health benefits. Domestication has been based on the protein and lipid-rich seeds and subsequently on the flesh (Saltveit, 2011; Manchali et al. 2021). Melon fruits are used worldwide in various types of desserts, salads, snacks and pickles for culinary preparation, and the seeds are used for cooking oil (Manchali et al., 2021). Meanwhile, the unripe fruit is used for salad or pickling (Pitrat 2008). Additionally, the fruit contains proteins and important antioxidants such as carotenes, folic and ascorbic acids, potassium, bioactive compounds and phenolic compounds (Lester and Hodges 2008; Menon and Rao 2012; Manchali et al., 2021). They are also an important source of vitamins A, C, B6, niacin and folate (Saltveit, 2011).

World melon production has increased by 7.5 million tonnes (Mt), reaching 28.55 Mt of world production between 2002 and 2022, according to FAOSTAT 2022 (accessed January 2024). In the last 20 years, Spain has become one of the main producers of melons in the world, after China, Turkey, India, Kazakhstan, Afghanistan, Guatemala, Iran, Brazil, Bangladesh, Italy, Mexico, and the United States (USA). Spain is currently the second producer in Europe and the 13th in the world, with a production of 652,600 tonnes (t) (FAOSTAT 2022, Ministerio de Agricultura, Ganadería y Pesca 2022, accessed January 2024). Recent data on melon exports from Spain show that the volume of exports has remained stable in recent years, ranging from 406,017 to 451,471 t of fruit, generating around €312.8 million per year (Ministerio de Agricultura, Ganadería y Pesca, 2021, from 2002 to 2022, FAOSTAT 2022, accessed January 2024).

1.1.3 Diseases in melon and yield losses.

Melon plants are susceptible to various diseases, including bacterial, fungal, and viral infections. One such bacterial disease is Bacterial leaf blight, which is caused by

1. Introduction

Pseudomonas syringae (Song et al., 2024). Common fungal diseases are Powdery mildew, which is caused by *Podosphaera xanthii-21* races or *Golovinomyces orontii* and Downy mildew, caused by *Pseudoperonospora cubensis* (Cui et al., 2022), Alternaria leaf spot, caused by *Alternaria alternata* (Yu et al., 2022, Ahmed et al., 2021) or Fusarium wilt, caused by *Fusarium oxysporum* (Joobeur et al., 2004, Wechter et al., 1995).

Viruses affecting melon include *Watermelon Mosaic Virus* (WMV), *Zucchini Yellow Mosaic Virus* (ZYMV), *Cucumber Mosaic Virus* (CMV) and *Cucurbit Aphid-Borne Yellows Virus* (CABYV) (Lecoq and Desbiez 2012; Martín-Hernández and Pico 2021), *Papaya Ringspot Virus* (PRSV), *Tomato Leaf Curl New Delhi Virus* (ToLCNDV) (Martín- Hernández and Pico 2021), *Cucurbit Yellow Stunting Disorder Virus* (CYSDV) or *Cucumber Green Mottle Mosaic* (CGMV) (Cui et al., 2022). WMV, PRSV, ZYMV, and CMV are the melon viruses that cause the most economic losses. Recently, ToLCNDV has also emerged as a significant problem in certain regions, affecting many countries (Martín- Hernández and Pico 2021).

CMV affects 26-66% of plants grown in conventional agriculture in Spain and is considered the third most important virus in this sector, after WMV and CABYV. Between 2019 and 2020, mixed infections were identified of CMV and CABYV, *Moroccan Watermelon Mosaic Virus* (MWMV) and with ToLCNDV but at lower rates, and most frequently in mixed infections with WMV and triple infection of WMV, CABYV and CMV. Most of the infections were widespread in many regions of Spain, where they were detected more frequently by growers in Valencia, Andalusia, Murcia, Castilla- la Mancha and Extremadura. Also, (López-Martín et al., 2024).

1.1.4 Genetics, genomics and breeding in melon

The melon genome sequence was published in 2012, with an approximate size of 450 Mbp (Garcia-Mas et al, 2012). Recent advances in the refinement of the melon reference, as reported by Argyris et al. (2015) Sanseverino et al. (2015) and Ruggieri et al. (2018), have led to the assembly of the complete melon genome assembly (version v3.61) and genome version (version v4.0), which measures 375.3 Mbp. Castanera et al (2019) improved the genome assembly to 357.64 Mbp in version v4.0 through error correction of the v3.61 genome assembly. This improvement made significant contributions to minimise unclassified sequences and identify novel genes and transposon variants associated with important phenotypes reaching.

Several genetic and molecular tools have been developed for melon over the years, including genetic maps (Périn et al., 2002; Díaz et al., 2011), ESTs and RNAseq databases (Clepet et al., 2011), and reverse genetics tools such as TILLING platforms (Dahmani-Mardas et al., 2010) and CRISPR-Cas (Liu et al. (2022); Giordano et al. (2022)). Next-generation sequencing (NGS) has enabled the construction of high-resolution genetic maps using Single Nucleotide Polymorphisms (SNPs) (Argyris et al., 2015) derived from Genotyping-by-sequencing (GBS) (Xu et al., 2022). Genetic maps have been generated to support Marker-assisted breeding and Map-based cloning using Amplified Fragment Length Polymorphism (AFLP), microsatellites, Random Amplified Polymorphic DNA (RAPD) (Wang et al., 1997; Xu et al., 2022), Simple Sequence Repeats (SSRs) (Gonzalo et al., 2005) and SNPs (Argyris et al., 2015). Several population resources such as collections of Near Isogenic Lines (NILs) (Eduardo et al., 2005; Perpiñá et al., 2016; Pereira et al., 2021; Campos et al., 2023), Double Haploid Lines (DHLs) (Gonzalo et al., 2011) and Recombinant Inbred Lines (RILs) (Pereira et al., 2017) have been generated in melon to study the desired traits.

1. Introduction

The expansion of genetic tools provides the resources to study different traits, mainly disease resistance and fruit quality, in melons. Genetic mapping has allowed the identification of Quantitative Trait Loci (QTL) for CMV resistance (Guiu-Aragonés et al., 2014; Giner et al., 2017). The mechanisms of resistance to CMV have been investigated, providing valuable insights into the complex resistance and the host factors that interact with CMV (Guiu-Aragonés et al., 2016; Pascual et al., 2019; Real et al., 2023). In addition, have investigated fruit quality, including ripening, and aroma production (Vegas et al. 2013; Pereira et al. 2020; Santo Domingo et al. 2022b and 2022b; Mayobre et al., 2024). Functional validation of genes in melon through stable transformation was documented (Giner et al. 2017; Ma et al., 2022). Using the CRISPR-Cas9 gene editing technique, Liu et al. (2022) and Giordano et al. (2022) successfully investigated genes associated with fruit ripening in melon. The melon gene *prv* for resistance to *Papaya ringspot virus* (PRSV) was validated also via CRISPR/Cas9 (Nizan et al., 2023).

1.1.5 Collection of NILs in melon

NILs are plant populations characterised by homozygous introgression from a donor parent into the genome of a recipient or recurrent parent, typically an elite cultivar (Kaepler et al., 1993; Eshed and Zamir 1995). This method is a key tool for the mapping of QTLs associated with complex desirable traits such as melon resistance and fruit quality (Eduardo et al., 2005; Eduardo et al., 2007; Obando-Ulloa et al, 2010; Perpiñá et al., 2016; Argyris et al., 2017; Pereira et al., 2021; Santo Domingo et al., 2022b; Campos et al., 2023), tomato (José et al., 2005), watermelon (Dou et al., 2022, Lee et al., 2022), strawberries (Urrutia et al., 2015) and peach (Kalluri et al., 2022). In addition, NILs play a key role in introducing genetic diversity into commercial cultivars derived from exotic germplasm sources (Tanksley and McCouch 1997, Eduardo 2005). A NIL collection was developed by crossing the Korean accession "Songwhan Charmin PI 161375" (SC), which represents an exotic donor parent, with the Spanish parent "Piel de Sapo" (PS) (Eduardo et al. 2005) as

1. Introduction

shown in Figure I-2. SC has resistance to CMV (Essafi et al., 2009; Guiu Aragonés et al., 2014; Giner et al., 2017; Pascual et al., 2019) and increased ethylene production during melon ripening (Dos-Santos et al., 2023; Santo Domingo et al., 2022b), making it a suitable parent for future breeding programmes to study these agronomic traits.

Besides trait identification, NILs are essential for assessing the influence of QTLs under different environmental conditions and for exploring interactions between QTLs and genotypes (Alpert and Tanksley 1996; José et al. 2005; Vegas et al. 2013; Guiu Aragonés et al. 2014; Santo Domingo et al. 2022a; Dos Santos et al. 2023). NILs are also a valuable resource for detecting the linkage between QTLs and molecular markers (Kaeppeler et al., 1993). They are ideal materials for fine mapping, gene function research and breeding by molecular Marker Assisted Selection (MAS) (Dou et al., 2022).

1. Introduction

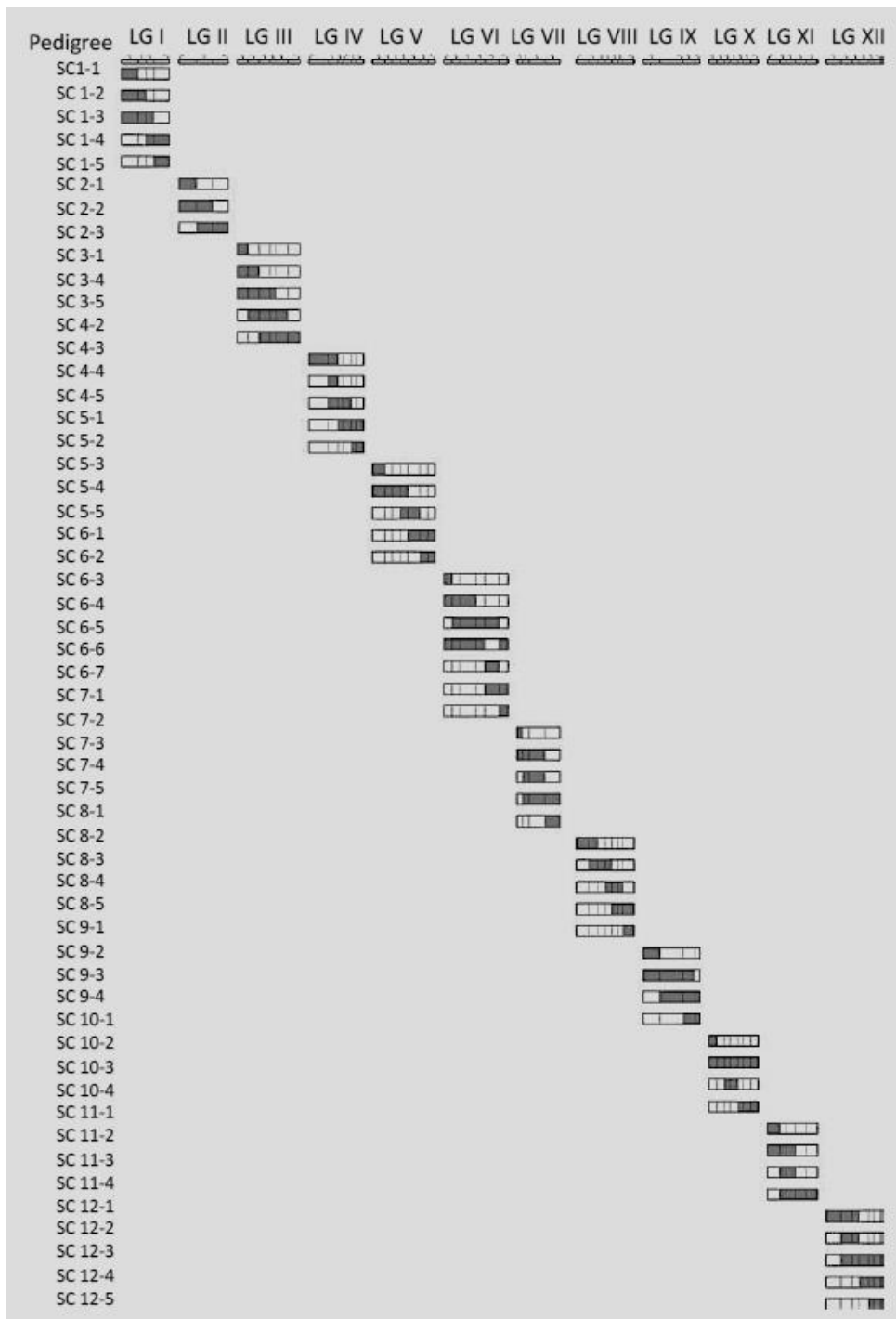


Figure I- 2. The collection of NILs in melon. The grey boxes in the specific Linkage group (LG) represent the SC introgression. The first number after “SC” indicates the chromosome, and the second number indicates the position of the introgression within the chromosome (Adopted from Eduardo et al., 2005).

1.2 Plant cell

1.2.1 Basic structure

The plant cell has the characteristic properties of eukaryotic cells, including a plasma membrane, ribosomes, a nucleus, various cytoplasmic organelles, and a cytoskeleton (Figure I-3). The nucleus contains chromosomes which serve as the repository of genetic information, controlling DNA replication and RNA synthesis. The translation of RNA into proteins takes place in ribosomes in the cytoplasm. The cytoplasm of the cell is surrounded by membrane-bound organelles that define specialised compartments for different metabolic activities. Two critical organelles are mitochondria and chloroplasts, which are central to energy metabolism.

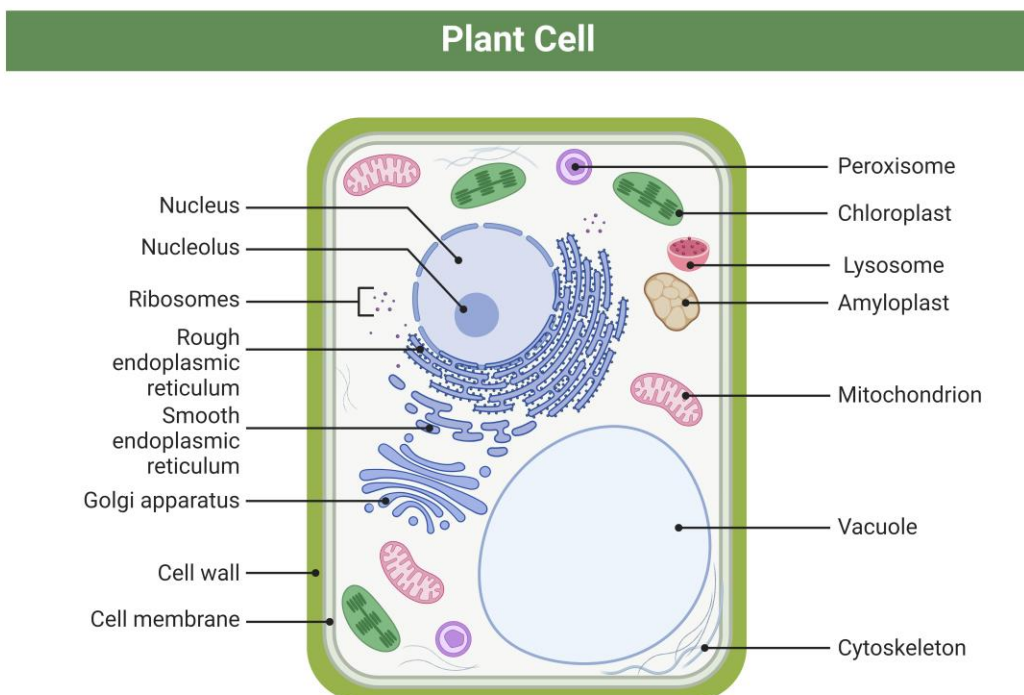


Figure I- 3. Plant cell representation with the most important organelles. The picture was created with Biorender.

1. Introduction

Photosynthesis takes place in chloroplasts. Lysosomes and peroxisomes are specialised metabolic compartments that facilitate the digestion of macromolecules and various oxidative reactions. Most plant cells contain large vacuoles that perform multiple functions, including the digestion of macromolecules and the storage of waste and nutrients (Gunning and Steer 1996; Cooper 2000). This compartment also stores proteins, carbohydrates, secondary cell metabolites, ions and pigments, keeps homeostasis and water balance, and carries out detoxification and lysis of unwanted compounds. (Crang et al., 2019; Kang et al., 2021).

Within the cytoplasm, the endoplasmic reticulum (ER) forms an extensive network of membranes extending from the nuclear membrane throughout the cell. It plays a wide variety of roles, including protein processing and transport, and lipid synthesis. The Golgi apparatus has a role in protein transport, serves as a site for lipid synthesis and, in plant cells, for synthesizing certain cell wall polysaccharides. Proteins are transported from the ER to the Golgi apparatus in membrane vesicles, where they are further processed and sorted for transport to their destination (Gunning and Steer 1996; Cooper 2000). The plant secretory pathway connects several organelles: the ER, Golgi apparatus, trans-Golgi network, endosomes, pre-vacuoles, vacuoles, and plasma membrane. This pathway is essential for the biosynthesis of proteins, lipids, and cell wall polysaccharides. The process begins in the rough ER, where proteins are synthesized, while lipids are produced in the smooth ER. Polysaccharides are also assembled here. These molecules are then transported to the Golgi apparatus. Cisternae are stacked membrane compartments in the Golgi apparatus that collect membranes and ER contents. They process and sort these materials to the trans-Golgi network, vacuole, and plasma membrane (Kim and Brandizzi 2014; Kim and Brandizzi 2016; van de Meene et al., 2017). Mature proteins enter the trans-Golgi network, where they are classified and secreted to either the plasma membrane, vacuole, or endosomal system. Proteins destined for the vacuole interact with

1. Introduction

Vacuolar sorting receptors (VSR) to be trafficked to pre-vacuolar compartments (Gu and Thomas 2001; Kim and Brandizzi 2016).

The plant cell wall is a unique component of plant cells. It is an extracellular matrix that surrounds every cell in a plant (Alberts et al., 2002). The cell wall provides structural integrity to maintain internal hydrostatic pressure, flexibility to support cell division, and a pathological and environmental barrier to protect against stress. (Hamann et al., 2012; Houston et al., 2016; Anderson and Kieber 2020; Hoffmann et al., 2021).

Plasmodesmata (PD) mediate intercellular communication between the plasma membranes (PM) of two neighbouring cells through the cell wall and a constricted form of the ER, the desmotubule, which spans the pore at its centre. The size of these intercellular channels is typically 30-60 nm. (Bhatla 2018; Crang et al., 2019; Faulkner and Bayer 2017). They also provide pathways for short and long-distance communication (Kang et al., 2021). PDs are key to the movement of water, small molecules (Sevilem et al. 2015), plant hormones involved in development such as auxin (Mellor et al. 2020), and control the loading, transport, and release of substances from the phloem (Ross-Elliott et al. 2017). Overall, PDs are involved in facilitating cell-to-cell and vascular loading and unloading of metabolites, proteins, and other signalling molecules (Benitez-Alfonso 2014). The permeability of plasmodesmata is not only regulated by physiological and developmental signals but is also increased by some of the proteins that are trafficked across them (Wayne 2010). Plant viruses manipulate PD pathways to deliver their proteins and nucleic acids (Reagan et al., 2020, Bui et al., 2014; Peña et al., 2012). During movement, transcription factors, mRNAs and even whole viral genomes have been tracked (Bui et al., 2014; Daum et al., 2014; Crang et al., 2019).

1. Introduction

The Size Exclusion Limit (SEL) is a critical parameter that determines molecular flux through the PD. This parameter indicates the maximum size of a molecule that can pass through the PD pores without causing dilation. The physical size of a molecule's mass, charge and hydrophobicity are critical in determining whether a particular molecule can pass through PD (Bui et al., 2014; Bhatla 2018). Pore plasmodesmal units (PPUs) are specialised PDs that have multiple channels on the companion cell's side and a single channel towards the Sieve element's side. These structures exhibit higher SEL than PDs between other cells, indicating increased permeability. Macromolecules such as proteins or RNAs can diffuse into the sieve element without strict regulatory control (Oparka and Turgeon, 1999; Hipper et al., 2013).

Transport phenomena across the PD can be classified as either passive or active processes. In passive diffusion, molecules, water and solutes move between cells without the intervention of any external force (Bui et al., 2014; Di Donato and Amari 2015). Such diffusion is important as intercellular signalling during plant development, such as embryogenesis (Xu et al., 2012), and pathogen defence (Heinlein and Epel, 2004; Maule et al., 2011). In contrast, active transport allows the trafficking of molecules that exceed the SEL of PDs. This process involves the interaction of cargo with transport proteins, contributing to various functions such as docking cargo to PDs, gating PD pores or delivering cargo to the neighbouring cell. The first cases of active transport have been observed in viral movement, with an increase in the SEL of PDs to pass the movement protein (MP) of the *Tobacco Mosaic Virus* (TMV) (Peña and Heinlein 2012). Also, it was demonstrated that the MP of TMV targets mRNA to PD (Luo et al., 2018). and The MP of CMV disrupts actin filaments to increase the SEL of PD in tobacco (Su et al., 2010).

1.2.2 Plant transport pathways

The plant moves water and solutes through the xylem and phloem as long-distance transport. The xylem moves water from the soil to the leaves (“up-flow” transport), while the phloem moves photoassimilates (products of photosynthesis) from the leaves to the whole plant organs (“up-flow” and “down-flow” transport) (Crang et al., 2019). There are two types of short-distance molecular transport, apoplastic and symplastic, which transport solutes, water, ions, and organic molecules. They are critical for plant growth, cell signalling, nutrition, and cellular homeostasis (Bhatla 2018). The apoplast is the outer plasma membrane space that includes the cell walls and xylem channels. The symplast is the inner cell space surrounded by plasma membranes that connect cells through plasmodesmata (PD) (Lambers et al., 2008).

1.2.3 Veins anatomy

Veins are vascular structures in plant leaves that transport photosynthate and water. They are formed by xylem, phloem and sclerenchyma cells surrounded by Bundle Sheath (BS) cells. Based on their class, function and structure, veins can be divided into two groups: Major and Minor veins. Major veins are the midribs (Class I, II and III) (Lambers et al., 2008; Crang et al., 2019), which are the central veins of the leaf. Its main function is to transport water and photosynthate and provide mechanical support to the mesophyll. The cells included in the major veins are xylem, phloem, BS, undifferentiated parenchyma, sclerenchyma and collenchyma cells (Crang et al., 2019). They play a critical role in the distribution of transpiration and photosynthates across the mesophyll, BS cells, and companion cells towards the loading into sieve elements (Lambers et al., 2008; Crang et al., 2019). The mesophyll encloses the minor veins, which contain a small number of phloem cells, SEs and xylem tracheary elements. These are enclosed by the BS cells (Crang et al., 2019). BS cells are a tightly packed layer of mesophyll cells that surrounds the veins and are located

1. Introduction

between the vascular bundle (VB) and mesophyll cells (Gao et al., 2014). Due to their importance in this research, we will focus on them in the next section.

1.2.4 Bundle Sheath cells

BS cells provide mechanical support, water and assimilates transport, storage of ions and carbohydrates, starch and sulphur assimilation and jasmonic acid synthesis. They are involved in carbon assimilation and have a photosynthetic capacity (Popovic et al., 1987; Tsutsumi et al., 2007; Leegood 2008; Hua et al., 2021). Transport through the BS cells occurs throughout the cycle, but the load changes depending on the stage of the plant. For instance, the loading of photosynthates into sieve elements occurs during leaf development and the unloading of photosynthates into sieve elements occurs during senescence (Leegood 2008; Bezruczyk et al., 2021). Moreover, in C4 plants, high concentrations of carbon in the bundle sheath (BS) cells enhance photosynthetic capacity. This leads to significantly higher photosynthetic efficiency than C3 plants (Griffiths et al. 2013; Liu and Cheng 2024). In melon, BS cells contain large vacuoles and chloroplasts, mostly filled with starch, as well as a large nucleus as shown in Figure I-4 (Guiu-Aragonés et al. 2016).

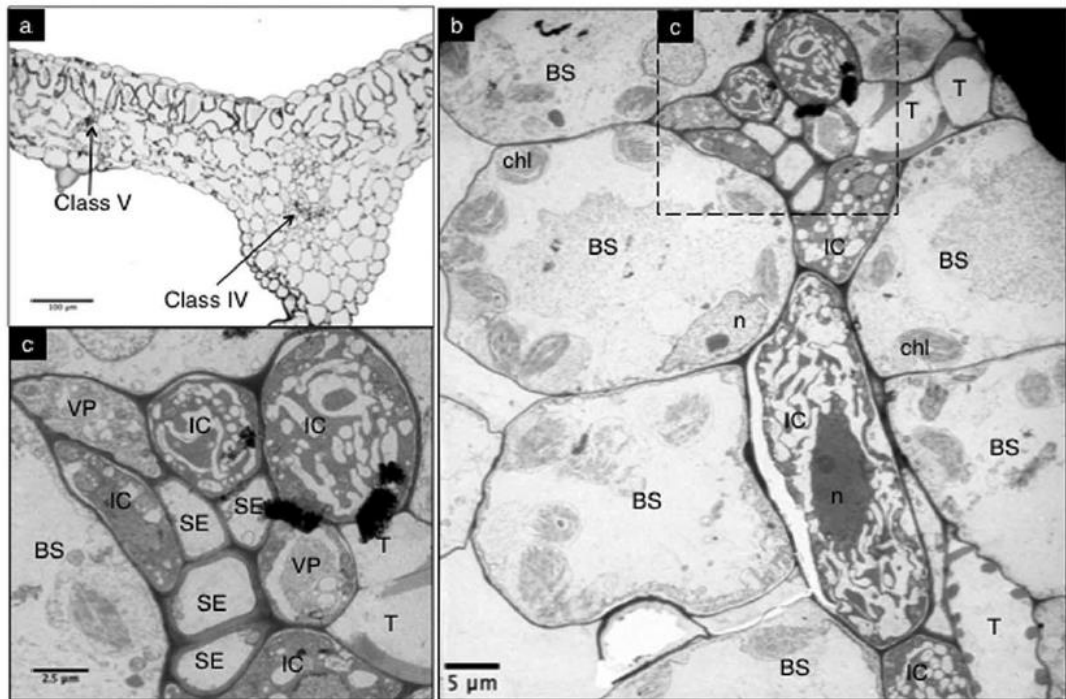


Figure I- 4. Structure of melon veins. **A)** BS cells into the minor veins IV and V. **B)** BS cells surrounding the intermediary cells in a minor vein type V. **C)** Zoom of the minor vein type V of (B) where BS cells surrounding the sieve elements, intermediary cells and vascular parenchyma. chl: chloroplasts; T: tracheid, IC: intermediary cells, n: nucleus, VP: vascular parenchyma, SE: sieve elements (Adopted from Guiu-Aragonés et al., 2016).

1.2.5 Phloem

Phloem is the plant vascular system responsible for the long-distance transport of photosynthates produced in mature leaves or reserves such as cotyledons (source) to flowers, roots, developing structures, fruits, and seeds (sink). Mediated transport moves photosynthetically derived sugars, amino acids, plant growth regulators, essential nutrients, and other compounds. The vascular system consists of sieve tube elements (STEs), companion cells (CC), phloem parenchyma (PP) and fibres. Together, they load, unload and transport elements while protecting the STES from external damage (Zhang and Turgeon 2018; Lambers et al., 2008; Crang et al., 2019). The phloem interface depends on the frequency, morphology, and connections of

1. Introduction

PDs, which enable the translocation of photosynthates from source to sink (Lee and Frank, 2018; Navarro et al., 2019).

1.3 Plant viruses

Plant viruses are obligate parasites consisting of one or more nucleic acid molecules as a genome enclosed in a coat protein. Despite their ability to replicate and adapt, viruses are not considered living organisms. They have a very small genome with minimal coding capacity (Wang 2015) and rely on the host cell machinery for replication, which involves the synthesis of viral proteins and nucleic acids using host cell resources. Viruses display genetic diversity, with variations in nucleic acid type and sense, and can undergo genetic changes through mechanisms such as mutation, recombination, and acquisition of sequences from unrelated viruses or the host genome. Plant viruses manipulate intracellular communication systems to facilitate infection within the host plant. They vary in size from 16 to 2000 nm and structure, with shapes ranging from isometric to rod-shaped capsids. (Hull, 2009; Sastry et al., 2019; Reagan et al., 2020; Navas-Castillo and Fiallo-Olivé 2021).

The first classification of viruses was published by the International Committee on Taxonomy of Viruses (ICTV) (Wildy 1971). However, virus classification is challenging due to the important factors that drive virus evolution, such as mutation, recombination and reassortment. The 30th ICTV report published the classification of plant viruses into 122 families, 735 genera and 4404 species (Lefkowitz et al., 2018). Virus classification was based on particle morphology, physicochemical properties, the gene expression program used to produce the virus proteins, serological relationships, mode of transmission, nucleic acid type, symptoms, and host range. The viral genome is organised based on its nucleic acid, which can be either RNA or DNA and can be single-stranded (ss) or double-stranded (ds). The genome can be positive (+) or negative (-), referring to whether the viral RNA sequence can be translated directly (+) or needs to copy first a + strand, which is then

translated (-) (Hull 2014). The type of viral genome, such as dsDNA, ssDNA, dsRNA, ssRNA(+) and ssRNA(-), is included in the annotation for each species (King et al., 2012). Common symptoms include effects on plant size, mosaic patterns, leaf yellowing, necrotic tissue, chlorotic leaves, leaf curling, ring spots, wilting of aerial parts and growth abnormalities (Hull, 2009).

1.3.1 Viral transport

Plant virus infection involves several key stages, including virus entrance, genome replication, translation, encapsulation, short- and long-distance movement, and inter-plant transmission. When an infection begins in an epidermal cell, the virus must replicate and translate viral proteins, and move sequentially from cell to cell in the mesophyll until it reaches host vascular cells (Carrington et al., 1999; Hipper et al., 2013; Kumar and Dasgupta 2021). PDs are critical for short-distance virus movement (Reagan et al., 2020; Kappagantu et al., 2020) and are dependent on SEL for virus passage. While closed PDs inhibit all traffic, open PDs allow traffic of molecules below 1 kDa, and dilated PDs are permeable to larger molecules such as proteins and mRNAs. (Navarro et al., 2019). During viral infection, the SEL of the PD is modified to allow systemic movement of viral complexes (Kumar and Dasgupta 2021). The MP encoded by the viral genome is responsible for movement by increasing the SEL for its translocation, thereby increasing the pore of the PD. This is achieved through the interaction of MP with host proteins able to modify the SEL for viral entry (Rojas et al., 2016; Bhatla 2018). MPs have been reported to interact with various host factors to ensure successful viral movement across cells (Boevink and Oparka 2005; Kumar and Dasgupta 2021).

The virus translocates several cells including M, BS, VP, CC, and SE cells of the vasculature. Once the virus reaches the host vasculature, it causes a systemic infection. In contrast, long-distance movement is rapid, and the virus moves with the

1. Introduction

photosynthates through the vasculature. Systemic virus movement involves six major sequential steps: Virus translocation from MS to BS cells, entry into VP through BS, entry into the phloem CC/SE complex (or, for some viruses, from VP into xylem-associated cells), rapid transport to systemic uninfected plant organs through the SE (or xylem in some cases), unloading from the CC/SE complex into uninfected VP, exit from VP through BS cells and into the MS cells of systemic plant organs (Figure I-5) (Ueki and Citovsky 2007).

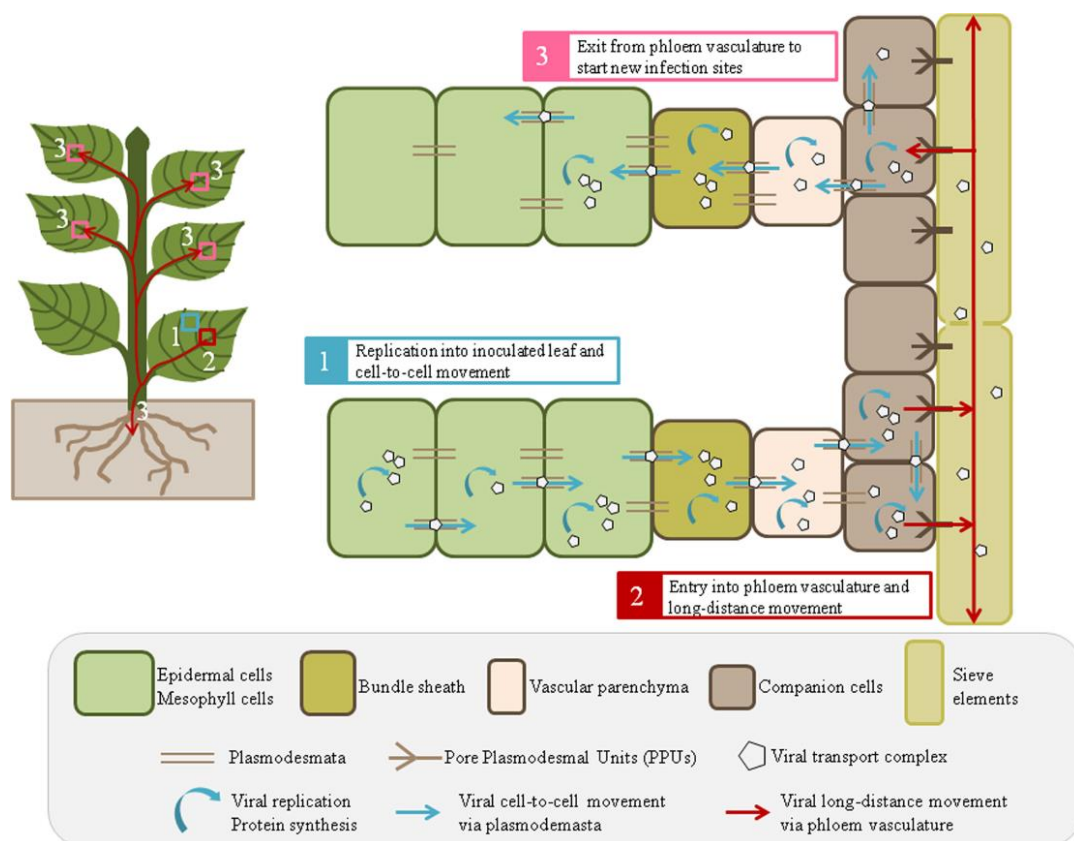


Figure I- 5. General plant viruses transport either cell-to-cell or long-distance movement in plant tissues (Adopted from Hipper et al., 2013)

Studies reported that the BS cell interface was found to play a critical role in viral trafficking by regulating viral load in the VB through successful virus-host interactions. Several studies have reported that the BS is a barrier to viral infection. For instance, research has shown that CMV is restricted in the BS cells in resistant

19

1. Introduction

melon plants (Guiu-Aragonés et al., 2016). Similarly, Thompson and García-Arenal (1998) reported that the BS interface prevents systemic infection by CMV and *Tomato Aspermy Virus* (TAV) in *Cucumis sativus*. Transgenic tobacco plants also restrict CMV and TAV at the BS interface (Wintermantel et al., 1997). Additional studies show that CMV is restricted in the BS cells of *Cucumis figarei* (Kobori et al., 2000) and *Grapevine Pinot Gris Virus* (GPGV) is inhibited in the BS cells of grapevine leaves (Tarquini et al., 2018). These findings highlight the important role of BS cells in restricting viral infection and protecting plants.

Similarly, the phloem is considered a critical physical and physiological collection point for plant viruses to establish infection in the plant (Kappagantu et al., 2020). The movement of the virus is dependent on defence molecules present at the PD interface before long-distance transport (Reagan et al., 2020). In a study of the CMV-infected melon phloem sap's proteome, several proteins were identified to be involved in defence responses and protection against oxidative stress in sieve tube elements (Malter and Wolf, 2011).

1.4 Resistance genes

A plant susceptible to viruses provides a favourable environment for replication, movement, and subsequent infection of the entire plant (Truniger and Aranda, 2009; Kobayashi et al., 2014). Plant hosts include two types of resistance: Dominant and Recessive.

1.4.1 Dominant resistance

The first is dominant resistance, in which resistance proteins intercept pathogen effector molecules or avirulence (Avr) factors and activate signalling mechanisms to initiate defence against the specific pathogen (Bishnoi et al., 2023). Such activation triggers programmed cell death, which is manifested in the plant as the

1. Introduction

hypersensitive response (HR). The dominant genes, known as R-genes, encode Nucleotide Binding Site and Leucine-Rich Repeat (NB-LRR) proteins that, together with other proteins within the same family, confer resistance to bacterial, viral and fungal pathogens (Moffett, 2009; Kobayashi et al., 2014; Hashimoto et al., 2016).

1.4.2 Recessive resistance

About half of the resistances already being used in virus resistance breeding programmes are recessive (Kang et al., 2005; Truniger and Aranda, 2009; Hashimoto et al., 2016). This type of resistance is primarily controlled by S-genes, which are host factors that facilitate pathogen entry and proliferation through compatible plant-pathogen interactions, leading to disease development. Recessive resistance is achieved by mutations that inactivate those S-genes. This leads to inhibition of replication or movement, possibly due to the inability of viral RNAs to be translated or properly transported within the cell (Rojas et al., 2016). S-genes provide a more durable and broader spectrum resistance than R-genes.

Several recessive genes reported by Garcia-Ruiz (2018) are involved in viral RNA translation, replication, movement, accumulation, RNA silencing suppression, and virion assembly. The S genes responsible for this type of resistance can act in different stages of infection. The best-known type of recessive resistance involves variants of the Elongation Initiation Factor (eIF) proteins, namely eIF4E, and eIF4G, which are used by viruses for their initial translation. Mutations in those genes impair the translation of viral proteins (Pestova et al., 2001; Nicaise 2014; Sanfaçon 2015). However, more recently, S-genes involved in other steps of the viral cycle have been reported (Agaoua et al., 2021). The gene “*cmvI*” was the first natural recessive resistance gene whose function is to prevent CMV trafficking in a specific cell type (Essaffi et al., 2009). A recessive gene, *zym*, has been identified in *Cucumis sativus* as providing resistance to ZYMV. This gene encodes a protein called Vacuolar Protein Sorting 4 (VPS4), which is part of the Endosomal Sorting Complex (ESCRT)

1. Introduction

required for virus replication (Amano et al., 2013). VPS4 interferes not only with ZYMV replication but also with *Tomato bushy stunt virus* (TBSV) replication (Barajas et al., 2009; Barajas et al., 2014). In addition, another recessive gene, *rwm1*, was found to confer resistance to WMV (Ouibrahim et al., 2014). Indeed, the S-genes play their roles in both physiological processes (such as plant growth and development) and susceptibility (by facilitating pathogen growth and infection) leading to resistance with pleiotropic effects (van Schie and Takken, 2014, Bishnoi et al. 2023). For example, CRISPR-Cas9-mediated mutation in the natural resistance gene eIF4E in *Arabidopsis thaliana* led to the loss of susceptibility to *Clover Yellow Vein Virus* (CIYVV), but an increased susceptibility to *Turnip Mosaic Virus* (TuMV). In addition, the mutant plants exhibited significant developmental defects such as early senescence and disruption of primordia development (Zafirov et al., 2021). These mutations also confer resistance to some pathogens on the host, while favouring infection by others (Gallois et al., 2018). For instance, the knockout of the Glyceraldehyde-3-phosphate dehydrogenase (GAPDH) disrupts the replication of TBSV tested in yeast. However, this knockout did not affect susceptibility in *Nicotiana benthamiana* to TMV (Wang and Nagy, 2008). Interestingly, in *Nicotiana benthamiana* the knockout of GAPDH enhances the susceptibility to the *Bamboo Mosaic Virus* (BaMV) (Prasanth et al., 2011).

Also, resistance can be classified as qualitative or quantitative based on phenotypic symptoms and mode of inheritance. Qualitative resistance is primarily controlled by a single gene with a significant effect and typically results in complete resistance (Pilet-Nayel et al., 2017; Gou et al., 2023). In contrast, quantitative resistance is typically controlled by multiple QTLs with small to moderate effects on each one and, depending on the number of genes carried, can manifest as incomplete or reduced resistance (Gou et al., 2023). Rather than completely blocking pathogen reproduction, it attenuates pathogen multiplication, plant colonisation and/or symptom severity (Pilet-Nayel et al., 2017). The environment strongly influences

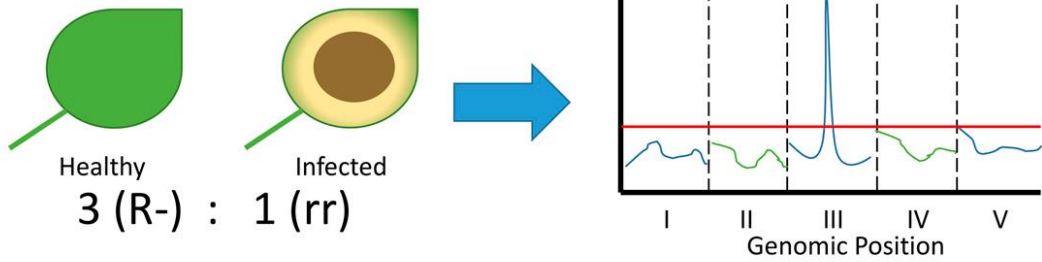
1. Introduction

quantitative resistance, which poses greater challenges than qualitative resistance. Quantitative resistance genes include those involved in immune signal perception, metabolite transport and biosynthesis, vesicle transport, and other functions (Gou et al., 2023). Broad-spectrum resistance, either to multiple races of the same pathogen or to different pathogens, can be conferred by QTLs or minor effect genes (Corwin and Kliebenstein, 2017).

1.5 Major and minor effects on the resistance

Plants respond differently to different pathogen strains, resulting in conflicting selective pressures on pathogen evolution. This diversity in plant responses can also influence various pathogen life history traits, including latency, infection efficiency, plant colonisation and pathogen multiplication. To increase resistance levels in crops, several QTLs and genes with major and minor effects on resistance have been used. The complex biological and technical characteristics of quantitative resistance have made it challenging to identify the causal genes and perform subsequent molecular analyses. The use of minor effect QTLs is challenging and requires better methods for phenotyping in plants (Figure I-6). This is particularly important for evaluating resistance components that can accurately predict resistance in the field. Breeding strategies for quantitative resistance require a better understanding of the genetic, ecological and agronomic factors that influence how pathogens adapt and cause loss of QTL function. In addition, we need more insight into the evolutionary capacity of pathogens, which depends on factors such as mutation rate, reproduction, dispersal ability, and population size (McDonald and Linde, 2002; Pilet-Nayel et al., 2017). Breeding programs have been developed to combine these resistance QTLs and key genes to combine different resistance mechanisms to restrict pathogen infection (Baumgartner et al., 2015).

Qualitative Resistance



Quantitative Resistance

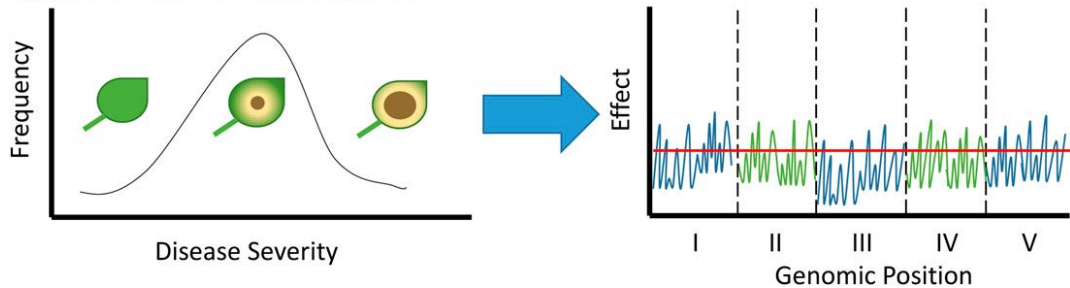


Figure I- 6. Qualitative and quantitative resistance to disease in terms of mapping an interval in a reference genome (Adopted from Corwin and Kliebenstein 2017).

Several pyramiding QTLs plus a major gene were reported to increase the resistance to viruses, such as: in barley with two recessive genes plus a QTL conferring tolerance to *Barley Yellow Dwarf* (BYD) (Riedel et al., 2011); and in soybean with multiple resistance genes against seven strains of *Soybean Mosaic Virus* (SMV) (Shi et al., 2009); in *Capsicum annum*, two consistent QTLs and one major gene were mapped by Genome-wide association studies (GWAS) and biparental mapping which led to increasing the resistance to *Potato Virus Y* (PVY) (Tamisier et al., 2020). In breeding programs of tomatoes, four important genes from different donor parents in the background cultivar line provided resistance to the devastating *Tomato leaf curl virus* (ToLCV) (Prabhandakavi et al., 2021). In melon, two resistance QTLs against CMV were identified that, in cooperation with the gene *cmvI*, encoding a VPS41, have a minor effect on resistance to the CMV subgroup I strain (see section 6.2) (Guiu-Aragonés et al., 2014). Seven QTLs with phenotypic variation between 3.57 and 17.10% were found in sugarcane to provide resistance to *Sugarcane Mosaic*

1. Introduction

Virus (SCMV) and *Sorghum Mosaic Virus* (SrMV) (Lu et al., 2023). Similarly, six QTLs were consistently identified as giving resistance to the Begomovirus *Pepper leaf curl virus* (PepLCV) in *Capsicum annum* (Dwivedi et al., 2024).

1.6. Cucumber mosaic virus

1.6.1 Host range and transmission

CMV, a member of the genus *Cucumovirus*, of the family *Bromoviridae*, is one of the most destructive viruses in temperate regions. CMV is known to cause significant agronomic and economic losses in several crops worldwide and has one of the broadest host ranges of any plant virus, infecting more than 1,300 plant species in over 500 genera in more than 100 families including cultivated, ornamental, and wild species (García-Arenal and Palukaitis 2008; Joshi et al., 2023). Some of these species have high agricultural relevance, such as *Cucurbitaceae*, *Solanaceae*, *Leguminosae*, *Brassicaceae*, *Gramineae* and many other plant species. CMV is used as a research model to study plant-virus interactions due to features such as mechanical transmission, robust accumulation in infected hosts allowing for easy purification, and the availability of infectious cDNAs for multiple strains (Palukaitis et al., 1992; Palukaitis and García-Arenal 2003; García-Arenal and Palukaitis 2008; Jacquemond 2012; Joshi et al., 2023). The weed species not only serve as potential reservoirs for the virus but also provide refuge for insect vectors (Joshi et al., 2023).

CMV is primarily transmitted by aphids in a non-persistent manner, with at least 86 aphid species identified as vectors for CMV. Seeds can also transmit CMV, with reports of transmission in the embryo, endosperm and tegument. Pollen has also been implicated as a CMV vector via bumblebee-mediated cross-pollination (Murphy et al., 2023). The coat protein of CMV plays a crucial role in its transmissibility by aphids. *Aphis gossypii* and *Myzus persicae* are among the most common vectors of

CMV in field environments (Palukaitis and García-Arenal 2003, Moury and Verdin, 2012, Joshi et al., 2023).

1.6.2 Genetic variability and evolution

CMV is one of the most successful RNA viruses for host adaptation and dispersion. CMV exhibits extensive genetic variability, resulting in many strains. These strains are divided into two subgroups, I (SGI) and II (SGII), based on their biological, serological and molecular properties. SGI is further subdivided into two subgroups, IA and IB. Nucleotide sequence comparisons show an overall similarity of 92% to 94% (IA/IB), 74% to 78% (IA/II) and 73% to 78% (IB/II) between the different subgroups. This genetic diversity provides valuable insights into the role of viral genes in CMV virulence (Roossinck, 2001; Mochizuki and Ohki, 2012). Under field conditions, SGI predominates due to the higher prevalence of isolates favoured by warmer climates. In contrast, SGII strains are more common in cooler regions, favoured by the lower temperatures. SGIB has been reported from East Asia, but Apalowo et al, (2022) have identified SGIB strains in various locations in West Africa as they provide a comprehensive description of recombinant CMVs. SGI strains have also been reported in the Mediterranean region, Brazil, Australia (Joshi et al, 2023) and California and Florida (Babu et al, 2014). In addition, Anwer et al. (2019) documented natural isolates of CMV-SGIB and SGII affecting tomatoes in Pakistan and Mrkvová et al. (2022) reported Slovakian CMV-SGIA and SGII isolates. The rapid mutation rate of CMV has led to the emergence of newly described strains that may lose their ability to infect traditional hosts while gaining the ability to infect new hosts.

1.6.3 Symptomatology

CMV causes a wide range of symptoms in plants, including mosaic patterns, leaf distortion, spotting, vein chlorosis, dwarfing, stunting and deformed fruits with

1. Introduction

pinpoint depressions (Lecoq and Desbiez, 2012; Mochizuki and Ohki, 2012). Together, these symptoms result in a significant reduction in plant vigour and yield. The manifestation of symptoms is influenced by factors such as cultivar, age at infection, ambient temperature, and the specific virus strain (Palukaitis et al., 1992; Joshi et al., 2023). Typically, SGI strains are more virulent than SGII strains. SGI strains usually cause severe symptoms, including mosaic patterns and stunted growth, whereas most SGII strains cause only mild symptoms or may even be asymptomatic. In addition, even within SGI strains, there can be considerable variation in the severity of disease symptoms (Roossinck, 2001; Mochizuki and Ohki, 2012). These symptom patterns are not observed in melon lines, where both SGs show similar phenotypes (M. Martín-Hernández, personal communication).

1.6.4 Genome organization

CMV virions are encapsulated in 29 nm icosahedral particles (T = 3 icosahedral symmetry) and consist of 180 capsid subunits with 18% RNA (Figure I-7) (Roossinck 2001, Lecoq and Desbiez 2012, Jacquemond 2012).

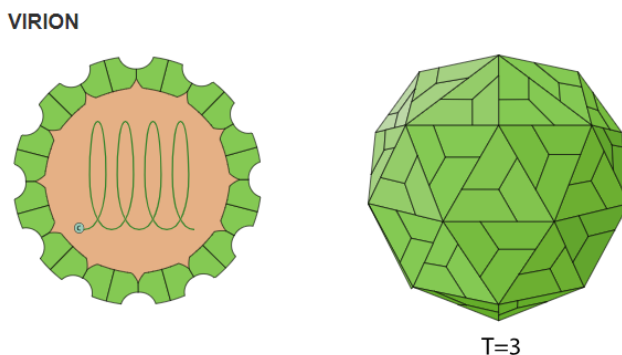


Figure I- 7. *Cucumovirus* non-enveloped, spherical virion about 29nm in diameter with T=3 icosahedral symmetry, composed of 180 coat proteins: 12 pentamers and 20 hexamers. Adopted from ExPASy <https://viralzone.expasy.org/>

CMV, a multicomponent single-stranded virus (+) ssRNA, has three Capped positive-sense RNAs: RNA1, RNA2 and RNA3, and two subgenomic RNAs: RNA4A and RNA 4. Small RNAs are also encapsidated in CMV particles, two of

1. Introduction

which, RNA5 and satellite RNA (satRNA), are well characterised (Jacquemond 2012). The 1a protein contains a methyltransferase and a helicase domain. The 2a protein is an RNA-dependent RNA polymerase (RdRp). Together they are involved in viral replication. In addition, RNA2 also encodes the multifunctional protein 2b, a determinant of symptoms and viral suppressor of RNA silencing (VSR), which is involved in long-range movement but not in viral replication (Ding et al., 1996). RNA3 is bicistronic and encodes two proteins: the 3a or movement protein (MP), involved in the cell-to-cell movement of the virus, and the coat protein (CP), involved in long-distance movement and encapsidation of the viral RNAs (Palukaitis et al., 1992, Palukaitis and García-Arenal 2003, Moury and Verdin 2012, Joshi et al., 2023). Guiu-Aragonés et al. (2015) identified the MP as the virulence factor of CMV involved in phloem entry and thus, in systemic infection in melon. They found that four mutation sites in the MP of CMV-FNY are responsible for conferring virulence in the melon accession SC, resistant to the strain CMV-LS, which lacks those same residues in the MP. The two subgenomic RNAs (RNA 4A and RNA4) code for 2b and CP respectively (Jacquemond 2012). Contrary to the genomic and subgenomic RNAs, RNA5 is not capped and no polypeptides associated with it have been observed. The function of RNA5 is unknown and is only present in the CMV-SGII (García-Arenal and Palukaitis 2008). Finally, CMV carries satellite RNAs, which are small 5'-capped non-coding RNAs that depend completely on the viral genome as a helper virus for their replication, encapsidation and dissemination (Jacquemond 2012; Palukaitis 2016) that attenuate the symptoms or produce necrosis (Roossinck 2001; Xu et al., 2003; Hou et al., 2011).

1.6.5 CMV cycle

1.6.5.1 CMV replication

Once inside the cell, the virus particles shed their coats, releasing their genomic RNAs for translation of the (+) ssRNAs into viral proteins. The replication process

1. Introduction

of CMV involves complex interactions between viral proteins and host cell components primarily with those involved in viral replication. Replication occurs primarily in the cytoplasm where proteins 1a and 2a, derived from RNA 1 and RNA 2 respectively, interact with host factors at the tonoplast, to initiate viral genome replication (Cillo et al., 2002; Jacquemond 2012). The protein 1a plays also a critical role in viral translation (Seo et al., 2009).

In *Arabidopsis thaliana*, two Tonoplast Intrinsic Proteins (TIPs), TIP1 and TIP2 were found to interact with the protein 1a in the tonoplast, the vacuole membrane. Also, these interactions permitted the production of a CMV replication complex anchoring to the tonoplast (Kim et al., 2006). Then, the plus-stranded RNA, which is in the cytoplasm, is the template for replicating a minus-stranded RNA, translation, and encapsidation whereas the minus-stranded genomic RNA, which is in the tonoplast, synthesizes new plus-stranded genomic RNA and starts again the process (Cillo et al., 2002; García-Arenal and Palukaitis 2008; Jacquemond 2012). The protein 1a carried the methyltransferase domain, which is critical for RNA capping and the helicase domain which harboured the replicase useful for the initial virus-host interactions (Cillo et al., 2002; Kim et al., 2006; Joshi et al., 2023) whereas the protein 2a carries the RNA-dependent RNA polymerase domain and is used for synthesizing positive-strand RNAs (Cillo et al., 2002; Mochizuki and Ohki 2012) whereas both proteins 1a and 2a are necessary for the minus-strand RNAs (Seo et al., 2009).

1.6.5.2 CMV movement

Once the virus infects a host cell, it moves from cell to cell through PD to reach the sieve element as a ribonucleoprotein complex containing viral RNA, coat protein, and protein 3a MP derived from RNA3. (Blackman et al., 1998). The CMV-MP is a member of the 30K superfamily (Palukaitis and Garcia-Arenal, 2003) and is known to increase the SEL in Tobacco to pass through the cell wall by severing actin

1. Introduction

filaments of PD (Su et al, 2010). Certain amino acids of CMV-MP can be phosphorylated, altering symptom formation and affecting PD localisation (Sáray et al, 2021). Some amino acids of CMV-MP modify the subcellular localization and the efficient trafficking cell-to-cell into and/or out of the cell suggesting that factors other than zinc-binding activity are required. Also, these amino acids are involved in the enhancement of pathogenesis (Sasaki et al., 2006; Jacquemond 2012). Through chimeric CMV viruses, four sequence positions of CMV-MP have been reported to determine virulence against *cmv1*-mediated resistance in melon (Guiu-Aragónés et al., 2015). *In vitro* and *in vivo* validation showed that CMV-MP interacts with an enzyme from the cell wall, an Apoplastic Ascorbate Oxidase (CsAO4) in *Cucumis sativus* for early CMV movement (Kumari et al., 2016).

Long-distance movement requires three distinct steps: loading into sieve elements, movement within them, and then unloading from these elements, all of which may constitute many barriers to invading the whole plant (Jacquemond 2012). This process involves passage through cellular boundaries and access to the phloem for systemic transport (Palukaitis and García-Arenal 2003). However, this requires compatible interactions between viral hosts to promote systemic movement. Less information is available on the long-distance movement of viruses. CMV, like other viruses, uses the phloem route of photosynthate movement for invasion (Moreno et al., 2004). Three viral proteins MP, CP and 2b of CMV appear to be viral determinants of long-distance movement (Jacquemond 2012; Khaing et al., 2020). Mutations in the MP showed that it was involved in the long-range movement (Li et al., 2001). In the case of CP, some sequences of its genome affect interactions involved in long-distance movement through the phloem (Taliensky and García-Arenal, 1995). In addition, basic amino acids of the CP influence the stability of the virus and can form a nucleoprotein complex with the viral RNA to provide some protection for the viral RNA and promote systemic infection (Kaplan et al, 1998). Three amino acids of CP situated in a loop are implicated in the long-distance

1. Introduction

movement in Cucumber (Salánki et al., 2011). The 2b protein mediates long-distance migration in a host-specific manner (Lewsey et al., 2009). Specific sites of RNA1 have been shown to influence systemic infection kinetics in squash (Yamaguchi et al., 2005). In addition, the interaction of 1a protein with Tcoi1 promotes systemic infection and symptom development in tobacco plants (Kim et al., 2008). Recently, the N-terminal region of the 2a protein was identified as a mediator of systemic CMV infection in *Brassica juncea* (Park et al., 2024). Concerning the host proteins which interact with the abovementioned viral proteins, AtBiP1/2, a protein from *Arabidopsis thaliana*, located in the ER lumen forms a complex with CMV-MP in the plasmodesmal ER-mediated by AtERdj2A, located in ER integral membrane, to establish cell connections (Ham et al., 2023). At the phloem level, three cucumber proteins (p69, p48 and p44) of phloem exudates, which are a part of the stream composition, were reported to interact with CMV-CP as part of the translocating virions. Among them, the interaction of the CMV-CP with proteins p48 and p44 appeared to strengthen the CMV encapsidation for the transport to long distances by inhibiting the RNase A activity. The results indicate that the p48 (cucumber homologue of PP1) interaction with the CMV CP modifies the structure of the CMV particle during translocation in the sieve tubes. (Requena et al., 2006).

1.7. Resistance to CMV in melon

1.7.1 Source of resistance to CMV in melon

The resistance in melon is normally oligogenic, recessive (Pitrat and Lecoq 1980), quantitative and frequently, strain specificity (Dogimont et al., 2000; Díaz et al., 2003). Natural resistance to CMV is very limited and geographically dispersed. Melon accessions from Asia, the Japanese "Freeman's Cucumber" melon (Karchi et al., 1975) and the Korean accession PI 161375 cultivar "Songwhan Charmi" (SC) have been the most widely used in breeding programmes (Risser et al., 1977). Pitrat and Lecoq (1980) identified several resistant melon accessions from the Makuwa

1. Introduction

group, such as *Ginsen* and *Kanro makuwa*. The Japanese accession (C-189) showed strain specificity, was resistant to M6, and showed heterogeneous responses to the CMV strain B20.2 (Díaz et al., 2003). In addition, Indian accessions IC 274014 (Dhillon et al., 2007), AM 25 and AM 82 (Fergany et al., 2011), three *Momordica* accessions (MM 3974, MM 3982 and MM 3994) and one *Cantalupensis* accession (MM 4067) were highly resistant to CMV-SGIB (Malik et al., 2014). In recent years, more natural resistance to CMV has been identified in melon accessions belonging to the *Conomon*, *Makuwa* and *Dudaim* melon groups (Giner et al., 2017; Pascual et al., 2019).

1.7.2 Resistance to CMV in the accession Songwhan Charmi

1.7.2.1 QTL and genes for resistance to CMV in melon.

The Korean melon accession SC is one of the few CMV-resistant accessions identified to date, carrying oligogenic, recessive and quantitative resistance (Karchi et al., 1975; Risser et al., 1977; Dogimont et al., 2000). Several QTLs controlling resistance to CMV have been identified using Recombinant Inbred Lines (RILs) from a cross of SC and PS. The major one, the *cmvqw12.1* QTL, with a large effect, is located on chromosome XII (Dogimont et al., 2000, Essafi et al., 2009) and confers complete resistance to CMV-SGII (P9 and P104.82), but it was not sufficient to restrict CMV-SGI strains (M6 and TL) (Essafi et al., 2009). Later, by fine mapping, the *cmv1* gene was mapped within *cmvqw12.1* and found to encode a Vacuolar Protein Sorting 41 (VPS41) (Giner et al., 2017), which is a general gatekeeper for virus phloem entry in melon (Pascual et al., 2019). Two-point mutations in CmVPS41, the changes L348R and G85E, are responsible for the resistance in several accessions (Giner et al., 2017; Pascual et al., 2019) belonging to the *Conomon*, *Makuwa* and *Dudaim* melon groups. The VPS41 has been identified as forming transvacuolar strands (TVS) in the susceptible plant, whereas mutations L348 and G85E impede the formation of TVS. TVS are, thus, strictly associated with

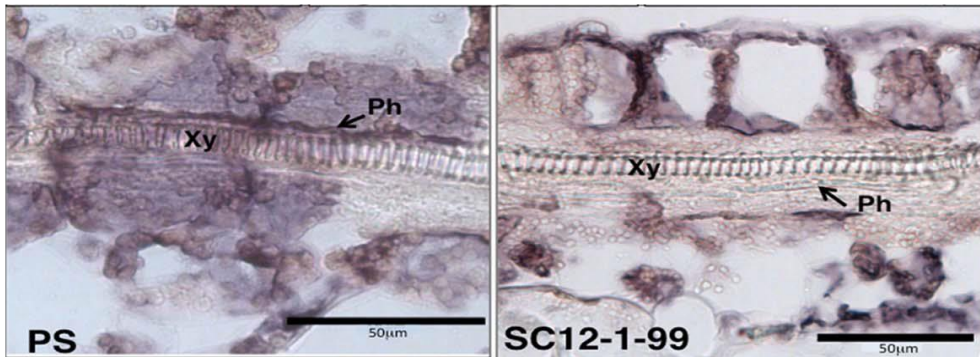
1. Introduction

susceptibility to CMV and could be necessary for the virus to reach some specific PDs (Real et al, 2023). Since the *cmv1* gene is not sufficient to restrict the infection by CMV-SGI strains, two additional QTLs were identified on chromosomes III and X, named *cmvqw3.1* and *cmvqw10.1*, respectively. The *cmv1* gene is necessary and explains most of the phenotypic variance but is not sufficient and requires cooperation with the identified minor QTLs *cmvqw3.1* and *cmvqw10.1*. Indeed, a fourth QTL may be required in cooperation to stop CMV-FNY infection from the CMV-SGI strains (Guiu-Aragonés et al., 2014).

1.7.2.2 Resistance at cell-specific level

In the resistant accession SC, CMV-LS can replicate and move from cell to cell but cannot enter the phloem and cause systemic infection, The resistance mechanism consists of limiting CMV-LS in the BS cells (Guiu-Aragonés et al., 2016) (Figure I-8). Immunogold labelling and electron microscopy revealed that resistant melon restricts viral particles in the BS cells and the virus is no longer able to move to the VP or IC, thereby preventing systemic infection. In contrast, the susceptible accession PS shows significantly more gold particles in the VP and IC. However, *cmv1* alone cannot prevent CMV-FNY from being transported through the BS cells to the phloem and can cause a systemic infection. The resistant gene *cmv1* acts as a gatekeeper for systemic infection depending on the MP of the infecting strain, so that chimeric LS viruses carrying the MP from FNY can overcome the resistance posed by *cmv1*, whereas chimeric FNY carrying the MP from LS are unable to overcome this resistance (Guiu-Aragonés et al., 2016). Upon entry into the phloem, the virus is free to move throughout the phloem. Therefore, the combination of minor QTLs and the *cmv1* gene plays a role in restricting virus entry into the phloem for the CMV-FNY strain, from SGI (Yan, 2018), similar to how *cmv1* restricts phloem entry for the CMV-SGII strains (Guiu-Aragonés et al., 2016). In addition, melon ILs harbouring *cmv1* and at least one minor QTL, either *cmvqw3.1* or *cmvqw10.1*, or the two minor QTLs, delayed systemic infection of CMV FNY (Yan, 2018).

A



B

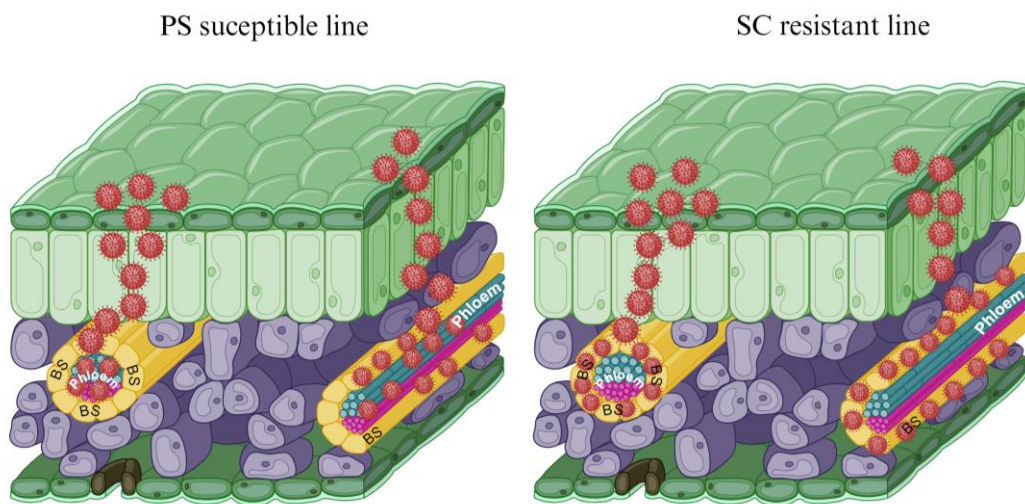


Figure I-8. Current understanding of resistance to CMV in melon plants. **A)** Cellular localization of CMV by *in situ hybridization* in CMV-LS inoculated leaves of melon plants. The blue/dark colour indicates the presence of viral RNA. C-, samples from a non-inoculated plant; PS, susceptible cultivar; SC12-1-99, resistant accession carrying only *cmv1* gene. Ph, phloem; Xy, xylem (Adopted from Guiu-Aragonés et al., 2016). **B)** CMV movement in susceptible and resistant melon plants. The virus crosses the epidermis and moves from cell to cell to reach the VB, where the phloem is located. The CMV crosses the BS to reach the phloem and infect the whole plant in susceptible melon plants. In contrast, CMV stops in the BS cells in resistant melon plants. Red circle: CMV virions. Picture adapted from Real 2022 and was created with Biorender.

1. Introduction

1.8. Laser dissection microscopy

Laser dissection microscopy (LDM) is a technique whereby specific groups or individual cells can be isolated under a microscope by picking up the collected cells with a specialized Eppendorf tube cap. The harvested cells can be used for molecular and cell biology studies. DNA, RNA and proteins from individual cells would be analyzed for genomics studies and relationships between gene expression and cell-specific functions. (Zhu et al., 2016; Kerk et al., 2003). The small number of cells can be used to isolate RNA, DNA and protein and the samples are suitable for real-time PCR, ELISA, Western blotting and protein microarray analysis (Mustafa et al., 2012). In addition, specific markers can help to identify the cells of interest before or after isolation but are not a prerequisite for LDM. The goal of LDM is to preserve enough visual detail to identify specific cells for harvest while allowing maximum subsequent recovery of RNA, DNA or protein from the harvested cells (Kerk et al., 2003).

The LDM technique has been used to isolate RNA for gene expression profiling in vascular systems to study phytoplasmas in *Arabidopsis thaliana* (Rossi et al., 2018), xylem tissue in woody plants (Blokhina et al., 2017) and epidermal cells of *Arabidopsis embryos* (Sakai et al., 2018). Berkowitz et al. (2021) conducted RNA-seq analyses on *Arabidopsis* cells. They studied the epidermis, mesophyll, and vasculature tissues. These tissues were isolated using laser microdissection to examine expression profiles at the cellular level under abiotic stresses. Furthermore, for biological cell studies, Shunmugam et al. (2018) proposed an efficient method to study the staging and isolation of meiocytes in the prophase I sub-stages of meiosis in wheat. In addition, rolling circle amplification of begomoviral DNA from infected *Nicotiana benthamiana* epidermal cells and nuclei was performed for plant health studies (Sicking and Krenz 2022). The complete laser microdissection process requires the following steps: sample preparation, fixation, cryoprotection,

embedding, cryosectioning and sample isolation under microscope visualisation, RNA, DNA or protein extraction and analysis (Teixeira and Pereira, 2010).

1.8.1 Fixation

Fixation is required to maintain histological integrity and secure cell contents during tissue sectioning and cell harvesting (Kerk et al, 2003; Bussolati, 2022). Tissue fixation can be either physical or chemical. Physical methods include heating, microwaving and freeze-drying. On the other hand, various combinations of chemicals are used as fixative reagents. The most common fixatives are aldehydes, which cause cross-linking between adjacent proteins, and alcohols, which fix tissues by dehydration (Molin et al, 1978; Matsuno et al, 2000; Kiernan., 2000; Eltoun et al, 2001; Teixeira and Pereira, 2010; Kim, 2020). Formalin 10% does not cause excessive tissue shrinkage or distortion of cell structure (Thavarajah et al, 2012) and provides excellent morphological quality (Rodriguez-Canales et al, 2013).

1.8.2 Dehydration and cryoprotection

A dehydration step is used to remove water from the tissue to make it compatible with subsequent cryoprotection steps. Alcohol is most used in histology. Dehydration should be gradual, especially for vacuolated plant cells. Rapid dehydration can cause rapid diffusion, leading to plasmolysis and the collapse of the cells. The duration of each dehydration step ranges from 30 min to overnight, depending on the size of the fixed tissue (Stasolla and Yeung 2015).

Cryoprotection aims to preserve tissues, cells and other biological materials at ultra-low using liquid nitrogen temperatures (-80°C or -196°C) (Nagashima et al., 1995; Chang and Zhao, 2021). A major challenge in cryopreservation is the formation of ice crystals during the freeze-thaw process, which is particularly detrimental to tissue viability. When cooling is slow, ice crystals form on the outside of the cells, causing

1. Introduction

damage. Meanwhile, water inside the cells is displaced, leading to increased solute concentration and osmotic injury. Rapid cooling leads to intracellular ice dominance, causing mechanical damage to cell structures. During rewarming, recrystallisation produces large ice crystals that cause severe cell damage (Chang and Zhao, 2021; Chen et al, 2023). For that reason, several cryoprotectants are used in laboratories to preserve the samples. For instance, Zamecnik et al., (2021) reported three types of cryoprotectants based on the way of penetrate the cells (I) Substances that can penetrate through the cell wall and plasma membrane such as glycerol, dimethyl sulfoxide, ethylene glycol and others, (II) Substances that can penetrate through the cell wall such as glucose, sorbitol, sucrose and others and (III) Substances that do not penetrate the cell walls and the plasma membrane such as soluble proteins, polyethylene glycol, polysaccharides and others. Sucrose is a cryoprotectant that helps with dehydration before or during cryoprotection (Zamecnik et al, 2021). The concentration of sucrose varies in different methods, ranging from 5% to 50%, with 40% sucrose commonly used in many studies either for cryopreservation or general studies (Sakai et al, 1990; Nishizawa et al., 1993; Suzuki et al., 2008; Sopalun et al, 2010)

1.8.3 Embedding

Embedding medium in tissue provides adequate support for cells and tissue stability over time and does not require immediate processing (Kerk et al., 2003) for subsequent sectioning procedures (Stasolla and Yeung 2015). This technique facilitates the identification of individual cells in complex biological samples (Kulak et al., 2023). There are several types of embedding, including cryosectioning (Abbott et al., 2010), paraffin embedding (Gomez et al., 2009, Chavan et al., 2023, Thomas et al., 2023), Steedman's wax embedding (Shiono et al., 2014, Hoge Kamp et al., 2011), polyethylene glycol embedding (Romanov and Kirchoff 2021), and resin embedding (Thomas et al., 2023), among others.

1. Introduction

Optimal Cutting Temperature Compound (OCT) medium is the superior embedding medium because it is the best in preserving the quality and yield of biomolecules. It can be used in a variety of molecular assays, including high-throughput platforms for large-scale molecular profiling (Liu et al., 2014). It was also useful for transcriptome analysis of plant reproductive tissues in phylogenetically distant angiosperms (Kivivirta et al., 2019). Cryosectioning was also suitable for providing discrete plant tissues for indole-3-acetic acid (IAA) quantification, while preserving plant tissues in the best possible condition to avoid auxin degradation (Muñoz-Sanhueza et al., 2018). In addition, cryosectioning reduced sample preparation time and allowed the processing of tissue sections for high-resolution imaging of targeted fluorescent proteins in all plant tissues (Knapp et al., 2012). Cryosectioning generally results in higher-quality RNA (Kulak et al., 2023).

1.8.4 Cell/Tissue isolation

LDM requires a specialised microscope with specifications that are easy to use (Kalof et al., 2015). Several microdissection microscopes use lasers to perform single-cell/tissue sectioning. Microscopes include the Arcturus system (Life Technologies), the Leica system (Leica Microsystems), the PALM Zeiss system (Zeiss) and the MMI CellCut laser microdissection system (Molecular Machines & Industries). The LDM process involves several steps: first, the cells of interest are visualised under a microscope. The selected area is then marked, and the cells and tissue are cut using a laser. Next, laser pulses directed at the underneath of the tissue are used to propel the excised tissue into a collection cap positioned upside down above the sample. The collected samples are then transferred to a collection tube for further analysis (Edgley et al, 2010).

2. Objectives

2. Objectives

2. Objectives

The main objective of this thesis was to investigate the resistance to CMV-M6 conferred by the QTLs *cmvqw3.1* and *cmvqw10.1* in coordination with the *cmv1* gene and to fine-map the genes associated with these QTLs.

The specific objectives to address the main objective were:

- ✓ The generation of new introgression lines (ILs) containing minimal contaminations and different degrees of resistance to the SGI strain CMV-M6.
- ✓ Characterization of the resistance given by either two or three QTLs against CMV M6.
- ✓ The generation of mapping populations for the QTLs *qwcmv3.1* and *qwcmv10.1*.
- ✓ The fine mapping of the QTLs *qwcmv3.1* and *qwcmv10.1*.

3. Materials and Methods

3. Materials and Methods

3.1 Plant material

3.1.1 Melon

For our experiments, Piel de Sapo (PS) and Songwhan Charmi (SC) genotypes were used as controls and four different initial Introgression lines (ILs) of melon were used to segregate genetic contaminations outside the QTL regions (Table M&M-1)

Table M&M- 1. Original melon ILs used to segregate out genetic contaminations (Yan, 2018).

Previous name	Carrying	From now on
12.1.99	<i>cmv1</i> gene	IL 12
2013 III-XII_2_2014(9)	<i>cmvqw3.1</i> and <i>cmv1</i> gene,	IL 3-12
H III-20-28(59)_9	<i>cmvqw10</i> and <i>cmv1</i> gene	IL 10-12
2013_III-X-XII 18(64)	<i>cmvqw3.1</i> , <i>cmvqw10</i> and <i>cmv1</i> gene	IL 3-10-12

Melon seeds were treated with either Captan (2.5 g/l) or Thiamethoxam 80% (2.5 g/l) to avoid microbial contamination. Seeds were placed in petri dishes and germinated under the following conditions: 28/26°C, 12/12 hours (h) light/dark for 4-5 days. Seedlings were then transplanted into fertile pots with Substrate N° 2 (Mixture of sphagnum peat with wood fibre, calcium carbonate 9g/l and N-P-K fertilizer 2.0g/l and microelements) and grown under different conditions depending on the experiments. For plant selection, seedlings were grown for three weeks under the following conditions: 16/8 h at 24/22 °C/ 1600 lux. Then, the plants with the desired genotype were selected and transferred for complete growth until fruit production to the greenhouses of the IRTA experimental fields, located in Caldes de Montbui, Barcelona. For infection experiments, melon lines were grown in fitotrons ARALAB 1200 maintained with a long day (LD) photoperiod of 16 hours of light at 22°C and 5000 lux, followed by 8 hours of darkness at 18°C.

3. Materials and Methods

3.1.2 Zucchini squash

Zucchini squash (*Cucurbita pepo* L.) Chapin F1 (Semillas Fitó SA, Barcelona, Spain) was used to reproduce CMV. Plants were grown in SANYO MLR 350H growth chambers (16/8, 24/22 °C/ 1600 lux).

3.2 In vitro plant culture

3.2.1 In vitro medium preparation

The culture medium prepared is a maintenance medium without hormones. Table M&M-2 shows components and amounts for 1 litre (L) of media. All components were weighed with an electronic balance and DUCHEFA, CuSO₄, was diluted in an Erlenmeyer flask containing 0.5 L of distilled water. 5H₂O, Murashige and Skoog (MS) and sucrose in the same order and placed on a magnetic agitator to mix the components. The mixture was diluted to a final volume of 1 L using a 1000 mL graduated cylinder and the pH was adjusted to 5.8 with a calibrated pH meter. Finally, agar was added to the medium and placed on a hot plate to dilute. Once dissolved, it was dispensed into test tubes at a 14 mL/tube dose using an automatic dispenser. Finally, the filled tubes were autoclaved at 120 °C under 1.2 atmosphere (atm) and allowed to cool to RT for two days without any abrupt movements. They were then stored at 4°C until they were used.

Table M&M- 2. Component of the *in vitro* culture medium

Medium MS	
Reagents	Amount/L
DUCHEFA M 0231 MS	4.4141
CuSO ₄ . 5H ₂ O (1mg/ml)	1
MES (Medio básico)	0.6
Sacarosa	30
Agar	8
pH	5.8

3.2.2 *In vitro* plant acclimatisation

Plants with enough roots and a favourable stem length (between two and four nodes and approximately three or four leaves) were selected for acclimatisation. For that, *in vitro*, selected plants were planted in Fitotron conditions adapted to melon (LD photoperiod of 16 hours of light at 26°C and 5000 lux, followed by 8 hours of darkness at 22°C). *In vitro* selected plants were extracted from the tube, the roots of which were carefully washed to remove the culture medium to avoid a medium favourable to the growth of microorganisms. The plants were then transplanted into pre-prepared fertilizer pots containing Substrate N°2. The pots were covered with a plastic lid to facilitate gradual opening until they were completely open. This procedure allowed the plants to harden through changes in temperature and humidity, thus ensuring their survival. After a week, the door was opened completely, and the plants were transplanted to the Torre Marimon greenhouses.

3.3 Virus material

In this study, CMV strain M6 was used (CMV-M6), which belongs to the SGI strains (Diaz et al., 2003). For viral inoculation, CMV-M6 was extracted from dry infected leaves adding 0.2% diethyl dithiocarbamate of sodium (DIECA) and activated carbon. The cotyledons of the zucchini squash were covered with carborundum to induce micro-injuries and facilitate the infection. Once the plant and the inoculum were prepared, mechanical rub inoculation was performed to introduce the virus into the zucchini squash cotyledons. Symptoms became apparent in zucchini squash leaves within 5-10 days post-inoculation (dpi). To inoculate melon plants, fresh virus inoculum was prepared as indicated previously by using the youngest and infected zucchini squash leaves 5 to 10 days after symptoms appeared. Then, the virus sap was gently rubbed onto the cotyledons of the melon plants. Symptoms indicative of virus infection were observed in PS melon at 7-10 dpi. For virus monitoring,

3. Materials and Methods

symptoms were recorded by visual observation at intervals of 2-5 days up to 28-30 dpi.

3.4 Visual phenotyping

Visual phenotyping involved systematically assessing CMV-M6 infection within 30 days by visual observation. Symptoms were defined by the presence or absence of viral mosaic patterns, while hypersensitive responses were defined by the presence or absence of necrotic tissue on leaves, veins, stems, or petioles. Mosaic symptoms were scored from 0 to 5, as detailed in Table M&M-3 (Guiu-Aragonés et al., 2014). A score of 0 indicated no symptoms, while a score from 1 to 5 indicated a scale of severity of symptoms.

Table M&M- 3. The scale of the mosaic symptoms in melon.

Score	Mosaic Symptoms
0	no symptoms
1	very mild mosaic only in the first or two leaves
2	mild mosaic in all leaves
3	stronger mosaic in all leaves without curly leaves
4	very strong mosaic with some curly leaves
5	very strong mosaic with very small, curled leaves and small plants.

In addition, necrotic tissue was recorded on a scale of 0 to 4 (in Table M&M-4). Score 0 indicated the absence of necrosis observations, while 1 to 4 represented the severity of necrotic tissue to plant death.

Table M&M- 4. The scale of the necrotic observations in melon to characterize the HR.

Score	Necrosis
0	no symptoms
1	Necrosis on one petiole
2	Necrosis on one leaf and petiole
3	Necrosis on more petioles and leaves
4	Plant dying from necrosis

3.5 DNA extraction

3.5.1 Quick DNA extraction

For short-term DNA preparations (lasting up to one week) and swift genotyping analysis of selected populations, a high-throughput Quick genomic DNA Extraction (Lu et al., 2020) protocol was used with some modifications. Approximately 100 mg of young leaves were collected and placed in individual wells with 57 μ L of 0.3M NaOH. After that, a rapid mechanical homogenization using tungsten balls was performed in a TissueLyser (30 sec at 30 Hz) and then incubated at 96°C for 1 min. Subsequently, 200 μ L of 0.75M Tris-HCl (pH= 7.5-7.8) were added to the samples and centrifuged at 3000 rpm for 1 min. The supernatant was transferred to a fresh plate and stored at -20°C for short-term use to ensure efficient DNA preservation.

3.5.2 CTAB protocol, DNA extraction

For long-term DNA preparations, the CTAB genomic DNA extraction protocol (Doyle, 1992) was used with some modifications. Young leaves were harvested and placed in 96-well plates or 1.5 ml or 1.9 ml Eppendorf tubes in individual wells. 340 μ L of CTAB was added to each tube at room temperature (up to 500 μ l for Eppendorf tubes) and the plant material was ground using a TissueLyser (1 min at 30 Hz). After 30 to 45 min incubation at 65°C, 340 μ L of chloroform: isoamlic acid 24:1 was added to precipitate the DNA, mixed by inversion, and centrifuged at 3000 rpm for 10 min. The supernatant was collected and 200 μ L of isopropanol was added to wash

3. Materials and Methods

the DNA and mixed by inversion. After centrifugation at 3000 rpm for 30 min (or 10000 for 5 min for Eppendorf tube extraction). The supernatant was removed, 200 μ L of 70% ethanol (stored at -20°C) was added and centrifuged at 3000 rpm for 10 min (up to 10000 rpm for 3 min for Eppendorf tube extraction). Finally, the supernatant was removed, and the samples were dried. For long-term use, 50 μ L of ultrapure water was added and stored at -20°C .

3.6 RNA extraction

3.6.1 RNA extraction from melon tissue

100 mg melon tissue was collected in a 1.5 ml Eppendorf tube and immediately immersed in N_2 liquid. Frozen tissue was homogenized using the TissueLyser with tungsten balls. All steps were performed on ice and under RNase-free conditions. 1 ml TRI-REAGENT® (Isolation Reagent, Sigma) and 0.2 ml chloroform were added to each sample and vortexed for 15 sec followed by incubation at room temperature (RT) for 10 min. Individual samples were centrifuged under the following conditions 4°C , 12.000 g for 15 min. All centrifugations were performed consistently at 4°C and 12000 g. The supernatant was collected and transferred to a new RNase-free Eppendorf tube for RNA purification. Thus, 0.5 ml of isopropanol (stored at 4°C) was added to each sample, followed by incubation at RT for 7 min and centrifugation for 10 min. Then, 0.5 ml of 70% ethanol (stored at 4°C) was added and centrifuged for 5 min. RNA pellet was dried at RT for a maximum of 1 h. After that, 20-50 μ L RNase-free H_2O was added to resuspend the pellet and stored at -80°C for long-term storage.

3.6.2 RNA extraction from microdissected cells from fixed tissue sections after Laser dissection microscopy

Total RNA was extracted from microdissected cells of melon plants through the application of the RNeasy® FFPE Kit (Isolation, Qiagen, RNeasy® FFPE

3. Materials and Methods

Handbook, 2021) according to the manufacturer's instructions. This RNA extraction protocol is appropriate for a cell quantity greater than 150 cells. Briefly, melting was chosen as the deparaffinization method for the fixed tissues. The protocol involved the addition of 150 μ L of Buffer PKD followed by mixing through vortexing. Following this, the samples were heated to 55°C for 3 min, vortexed vigorously for 10 sec and then centrifuged at full speed for 2 min. To digest the tissue, 10 μ l of Proteinase K was added and gently mixed. The solidified layer was pierced to add the Proteinase K into the MMI IsolationCap® RNase-free Eppendorf tube (Molecular Machines & Industries MMI®, Germany). The samples were incubated at 56°C for 15 min, followed by a second incubation at 80°C for 15 min. The second incubation was essential for ensuring maximum RNA yield. This means that the heater must reach 80°C before starting the incubation step. Subsequently, the samples were incubated on ice for 3 min and centrifuged at 20,000 gravities (g) for 15 min. The supernatant was transferred to a new Eppendorf tube, taking care not to disturb the pellet. To treat the supernatant, DNase Booster Buffer was added to approximately 16 μ l (one-tenth of the total sample volume), and 10 μ l of DNase I stock solution (lyophilised DNase I 1500 Kunitz units in 550 μ l RNase-free water). Samples were mixed by inversion and centrifuged briefly to collect residual liquid, then incubated at RT for 15 min. To adjust the binding conditions, 320 μ l of RBC buffer was gently mixed with the lysate. For RNA purifications, 720 μ l of 100% ethanol was added and mixed thoroughly by pipetting. Immediately, 700 μ l of the sample was transferred into a RNeasy MinElute spin column (stored at 4°C) and placed in a 2 ml collection tube. Centrifugation was performed according to the following conditions: 15 sec \geq 8000 g. Afterwards, the flow-through was eliminated and the collection tube was re-used to repeat the same step. To wash the spin column membrane, 500 μ L buffer RPE was added and centrifuged for 15 sec \geq 8000 g. This step was repeated twice. The flow-through and the collection tube were discarded. RNeasy MinElute spin columns were placed in a new 2 ml collection tube, centrifuged at full speed for 5 min and the collection tube discarded. Finally, 15 μ L

3. Materials and Methods

of RNase-free water was added directly to the spin column membrane, placed in a new 1.5 ml collection tube and centrifuged twice for 1 min (reusing the flow-through). To ensure long-term storage, the RNA samples were stored at a temperature of -80°C.

3.7 Single Nucleotide Polymorphism Genotyping

Single nucleotide polymorphisms (SNPs) were used as molecular markers. SNPs were identified and designed based on comprehensive resequencing data from both parental lines PS and SC (Sanseverino et al. 2015) and IL resequencing, including IL 3-12, IL 10-12, and IL 3-10-12 (Yan, 2018). All SNP positions were confirmed in the reference genome version V3.6.1 (<http://www.melonomics.net>). Flanking markers (FM) for specific QTLs were sourced from Illumina Assay Design Tool (ADT) validation (Argyris et al., 2015) as described in Supplementary Table 1.S1 Excel sheet SNPs. Primers were designed in the PrimerPicker software (KBioscience, 2009), resulting in the generation of two Forward primers (A1, A2) and one Reverse common primer (C1). Subsequently, genotyping was performed using two different Master Mix methods: the KASPar SNP Genotyping System (KBiosciences, Herts, United Kingdom) and the PACE™ 2.0 Genotyping Master Mix chemistry provided by 3CR Bioscience (United Kingdom). The Polymerase chain reaction (PCR) amplification was conducted on the LightCycler® 480 Real-time PCR instrument according to the technical instructions (Roche Diagnostics, Germany).

3.8 Reverse transcription-polymerase chain reaction

3.8.1 RT-PCR using RNA extracted from melon tissue.

First-strand cDNA synthesis was carried out using the PrimeScript RT Reagent Kit™ (Takara, Japan) with specific modifications. The RT reaction involved mixing 300 to 500 ng of RNA with 1.54 µM of reverse primer (10 µM), followed by the

3. Materials and Methods

addition of 10 μ L of sterile water to reach a final volume of 13 μ L. Depending on the experiment, different types of reverse primers were used. For virus cDNA synthesis, gene-specific primers were employed (F109-3'R for RNA 1, F209-3'R for RNA 2, and F309 3'R for RNA 3, as outlined in Table M&M-5). On the other hand, in preparations where both melon and viral cDNA were synthesized, Random Primers (Applied BiosystemsTM) were used.

Table M&M-5. Reverse primers to synthesize the first strand cDNA specific for the viral RNA (RNA1, RNA2 or RNA3).

Primer name	Sequence 5'-3'	nt
F109-3'R	TGGTCTCCTTTTAGAGACCC	20
F209-3'R	TGGTCTCCTTTTGGAGGC	18
F309-3'R	TGGTCTCCTTTTGGAGGCC	19

nt: Nucleotide

The mixture was incubated at 70°C for 10 min. Then, a reaction mixture containing RT-PrimeScript (200 U/ μ L), RNase OUTTM recombinant ribonuclease inhibitor (11.1 mM, Invitrogen, United Kingdom), 1x PrimeScript buffer and RNase-free dNTPs (1.1 mM) was added to the sample to reach a final volume of 22 μ L. The reaction mixture was gently vortexed and incubated at 50°C for 1 h. The RT polymerase was deactivated by heating the reaction at 70°C for 15 min. The resulting cDNA was kept at -20°C for long-term storage.

3.8.2 The Polymerase chain reaction (PCR) in melon tissue

To detect CMV in the tissue, PCR was performed using, 1x buffer A (FastGene® DNA Polymerase, Nippon Genetics Europe GmbH, Germany), 0.2 mM dNTP, 0.5 μ M forward primer, 0.5 μ M reverse primer and 0.2 μ l volume of 500 U/ μ l FastGene® Taq with 2 μ l cDNA in 20 μ l final volume. The PCR was conducted in a SimpliAmpTM Thermal Cycler by Applied BiosystemsTM, USA following specific conditions (see Table M&M-6 below).

3. Materials and Methods

Table M&M- 6. PCR conditions to detect CMV infection in melon tissues. Primers for CMV detection are specified in Supplementary Table 1.S1 Excel sheet Primers.

Step	Temperature	Duration	Cycles
Initial denaturation	94°C	1 min	1X
Denaturation	94°C	30 sec	
Annealing	55°C	30 sec	35X
Extention	72°C	1 min/kb	
Final Extention	72°C	5 min	1X

3.8.3 Real-time quantitative RT-PCR in melon tissue

The qRT-PCR procedure followed technical guidelines provided by Roche Diagnostics, Germany and was performed on the LightCycler® 480 Real-time PCR system. qRT-PCR reaction contained 1x SYBR® Green Master Mix (Roche Diagnostics, Germany), 0.3 µl of forward primer (10 µM), 0.3 µl of reverse primer (10 µM) and 2 µl of cDNA in a final volume of 10 µl. For viral quantification, specific CMV primers were used as shown in Table 1.S1 (Kong et al., 2016). In addition, two housekeeping genes were used: *Cyclophilin ROC7 (CmCYP7)* and *Ribosomal Protein L (CmRPL)*. The qPCR conditions are described below (Table M&M-7 below).

Table M&M- 7. Real-time quantitative qPCR conditions to quantify the CMV.

Step	Temperature	Duration	Cycles
Initial denaturation	95°C	5 min	1X
Denaturation	95°C	10 sec	
Annealing	60°C	10 sec	45X
Extention	72°C	10 sec	
	95°C	5 sec	
	65°C	1 min	
Melting curve		Continuously with a ramp rate of 0.11 °C/sec	1X
Cooling	40°C	30 sec	1X

3.8.4 RT-PCR using RNA extracted from microdissected cells.

The initial complementary cDNA strand was produced from micro-dissected cells, using Moloney Murine Leukemia Virus-Reverse Transcriptase (M-MLV-RT, Invitrogen™, United Kingdom) and random primer according to the manufacturer's instructions with minor modifications. Briefly, total RNA between 1 and 5 µg was combined with 0.83 mM RNAase-free dNTP and 0.83 µM reverse primer in a final volume of 12 µl in an RNAase-free Eppendorf tube. The mixture was incubated at 65°C for 5 min followed by rapid cooling on ice. In the meantime, 1 x first strand buffer, 9.52 nM DTT and 1 µl of RT enzyme M-MLV RT (200 U/ µl) were prepared. This was combined with the RT reaction and incubated at 37°C for 50 min with gentle shaking at 150 rpm. The polymerase was then deactivated by heating the reaction to 70°C for 15 min and stored at -20°C for long-term storage.

3.8.5 The Polymerase chain reaction (PCR) for microdissected cells

To detect CMV infection at the single cell level, a PCR reaction was conducted on the cDNA based on established protocols. The PCR was prepared by mixing 1x Q5®

3. Materials and Methods

High-Fidelity 2X Master Mix (Q5® High-Fidelity DNA Polymerase, New England Biolabsinc (USA), 0.5 µM forward primer and 0.5 µM reverse primer) with 2 µl of cDNA to a final volume of 20 µl. To detect CMV at the single-cell level, the PCR reaction was performed with some modifications (Table M&M-8).

Table M&M- 8. PCR conditions to detect CMV infection in microdissected cells.

Step	Temperature	Duration	Cycles
Initial denaturation	94°C	1 min	1X
Denaturation	94°C	30 sec	
Annealing	55°C	30 sec	60X
Extention	72°C	1 min/kb	
Final extention	72°C	5 min	1X

kb: Kilobase

3.9 Data Analysis

All the statistical analyses and the plotting were performed in the software R version 4.2.2 (R Core Team 2022) and RStudio version 2024.04.2+764. The results were imputed in the RStudio for all statistical analysis and plotting without any missing data to be analysed for time points or overtime infections and virus quantification per time point.

3.9.1 Infection scores

For the mosaic score, the Principal Component Analysis (PCA) was constructed using the R package “stats”. The distribution of all mosaic score data followed a non-parametric distribution, allowing for non-parametric statistical analysis. This analysis included the Kruskal-Wallis test, followed by post-hoc analysis using the Dunn test to determine which groups were significantly different. Multiple statistical analyses were corrected using the Holm correction method, resulting in p-adjusted results. The R packages used for statistical analyses were “stats” for the Kruskal-Wallis test and “FSA” for the Dunn test and Holm p-adjusted correction. All graphs

3. Materials and Methods

were carefully plotted using the “ggplot2” package. Key steps included adjusting aesthetic parameters such as colours, shapes and sizes, adjusting scales for clear axis labels and boundaries, and applying positional adjustments such as dodging and stacking to manage overlapping data points. Additional layers for titles, labels and themes were added to enhance the representation and effectively communicate the statistical findings.

3.9.2 Quantification of virus (qRT-PCR) analysis

In all experiments, qRT-PCR data were normalized using two reference genes: *CmCYP7* and *CmRPL*. The stability of the reference genes was assessed for each treatment across all samples. The quantification cycle (C_t) values of the genes were converted into relative quantities (RQs), which were then normalised to the geometric mean of the RQs of the two reference genes (NRQs) following the method described by Hellemans et al. (2007). The NRQs were log-transformed ($\log_2\text{NRQ}$) to correct for variance heterogeneity (Rieu and Powers, 2009) and were used for statistical analysis using the pairwise t-tests with the Holm method correction per time point (7, 14, 21 dpi). The R package used for this analysis was the “stats”. The plot of the qPCR data was generated using NRQ values per time point. All generated plot was performed using the R package “ggplot2” as in the infection scores plots.

3.10 Laser dissection microscopy

The Laser dissection microscopy (LDM) technique was employed to isolate individual Bundle sheath (BS) cells from minor veins melon pyramid lines. Note that all procedures were performed at 4 °C, and harvested cells were prepared in a cold, RNase-free environment to maintain RNA stability. Melon plants were grown in pots under greenhouse conditions at 26/24 °C with a 16/8-hour light/dark cycle in the greenhouse at the department of the German Collection of Microorganisms and Cell Cultures GmbH (DSMZ) located at the Julius Kühn Institute (JKI), Braunschweig,

3. Materials and Methods

Germany. Once the melons produced their first true leaves, they were inoculated with CMV-M6, as described in section 3.3.

3.10.1 Fixation

To maintain the integrity of cells and tissue in the melon pyramided line, formalin 10% fixation was employed as follows. First, the trichomes were removed to allow the fixative to penetrate the leaf. Subsequently, minor veins (type IV and V) were dissected carefully from the whole leaf. The following steps (fixation and cryoprotection) were carried out at 4°C. Each set of minor veins was individually placed in vials and subjected to fixation with 10% formalin under vacuum conditions for 30 min. The formalin solution was then refreshed and vacuum-treated overnight (o/n).

3.10.2 Cryoprotection

To remove residual formalin, the fixed sample was washed twice with 1X Phosphate-buffered saline (PBS) with pH= 8. The next step was dehydration using a series of ethanol gradients of 30-50-70%. The process was followed by rehydration, which was repeated in reverse for at least 30 min each time. To protect the cells from freezing, the samples were cryoprotected by successive immersion in 10%, 20% and 30% sucrose solutions (prepared in 1X PBS). A minimum incubation period of 2 hours was necessary for every cryoprotection step to guarantee successful penetration of the sucrose solution. Specifically, the 30% sucrose solution was incubated overnight to ensure complete infiltration and cellular cryoprotection.

3.10.3 Embedding

Following cryoprotection of the minor veins, any residual sucrose was eliminated by desiccation through a membrane and immersion in Neg-50™ Frozen Section Medium (OCT medium, Enhancing precision for cancer diagnostics, EpreDia™,

3. Materials and Methods

United States) for at least 2 min. To protect the tissues during the freezing process, they were fully embedded in Neg-50™ Frozen Section Medium in a square or triangular plastic mould. Afterwards, the mould containing the protected tissue was immediately cooled in liquid nitrogen for around 20 sec. Subsequently, these samples were stored at either -20°C for rapid usage or -80°C for long-term preservation.

3.10.4 Cryosectioning and OCT removal

Embedded samples were cryosectioned into separate 25 µm thick pieces of tissue, which is optimal for future LDM with the MMI Microscope® (Molecular Machines & Industries MMI®, Germany). Cryosectioning was performed at -20°C using a cryostat (Leica Biosystems, USA). The longitudinal sections produced were placed on MMI MembraneSlide® RNase-free slides (Molecular Machines & Industries MMI®, Germany) pretreated with Poly L-Lysine® solution 0.1% (w/v) in H₂O (Sigma-Aldrich®, United States). To prevent any undesired rolling of the sections, the samples were placed immediately at RT. To completely remove and hydrate the cryosections, the slides were incubated twice in ultrapure water for 30 sec each time. For dehydration, the samples were immersed sequentially in increasing ethanol concentrations of 70%, 90%, and ultimately 100%, with each step lasting for 30 sec. Finally, the samples were left to dry at RT for at least 5 min.

3.10.5 Cell cut and sample isolation.

The cryosectioned samples were positioned on MMI MembraneSlide® RNase free slides (Molecular Machines & Industries MMI®, Germany) following the instructions given in the preceding section. The MMI Cell Cut tool was employed to perform precise calibrations and tool settings for the laser microdissection following the technical guidelines provided for the MMI Microscope® by Molecular Machines & Industries LLC (MMI®, Germany). The BS cells, located adjacent to the Vascular

3. Materials and Methods

Bundle (VB), were delineated using the MMI Cell Cut tool. The cells were isolated and collected in MMI IsolationCap® RNase-free Eppendorf tubes. Samples were stored at -80°C for subsequent RNA extraction and quality analysis assurance.

4. Results

4. Results

Chapter 1

**Generation of melon pyramided lines with two
QTLs containing minimal genetic
contaminations**

Chapter 1: Melon Pyramided Lines Development

Generation of melon pyramided lines with two QTLs containing minimal genetic contaminations.

1.1 Pyramiding and removal of undesirable regions

Introgression Lines (ILs) carrying resistant QTLs to CMV in melon (shown in Table 1.1) were developed using flanking markers (FM) (listed in Table 1.2). However, these ILs carried genetic contamination beyond the QTL of interest. Genetic contamination in this context refers to alleles originating from the SC parent or hybrid alleles (SC/PS=H) outside the designated QTL regions. Genetic contamination could complicate the clear association between phenotyping and genotyping. Resistance or susceptibility of plants may therefore be difficult to determine as the phenotyping results may be inconclusive. To improve result accuracy, we aimed to minimize genetic contamination in the ILs that would be used to develop the mapping populations in Chapter 3.

Table 1. 1. Genotype of the original ILs that have been used to segregate out genetic contaminations.

Previous name	Reference	From now on	<i>cmvqw3.1</i>	<i>cmvqw10.1</i>	<i>cmv1 gene</i>
SC 12.1.99	Essafi et al. 2009	IL 12	PS	PS	SC
SC 10.2	Eduardo et al., 2005	IL 10	PS	SC	PS
2013 III-XII_2_2014(9)	Resequencing unpublished	IL 3-12	SC	PS	SC
2013_III-X-XII 18(64)	Resequencing unpublished	IL 3-10-12	SC	SC	SC

■ PS: Piel de Sapo

■ SC: Songwhan Charmi PI 161375

Chapter 1: Melon Pyramided Lines Development

Table 1. 2. Physical and genetic distance of the resistance QTLs in the melon genome.

QTLs	Chr	FM	P of FM (bp)	P of the QTL (Mb)	G (cM)	References	
<i>cmvqw3.1</i>	III	AI_14-B01	2,804,514	20.81	1.6	Guiu Aragonés et al., 2014	
		AI_33_H11	23,616,908		8		
<i>cmvqw10.1</i>	X	CMPSNP1117	1,122,396	3.62	1.6		
		CMPSNP671	4,747,687		28.8		
<i>cmv1 gene</i>	XII	cmv1 marker	9,320,908		2.2		Dogimont et al., 2000, Essafi et al., 2009, Giner et al. 2017

P: Physical position, G: Genetic position, FM: Flanking marker, Mb: Megabase, cM: Centimorgan.

1.2 IL carrying *cmvqw3.1* and the *cmv1* gene.

IL 3-12 harboured the *cmvqw3.1* QTL and the *cmv1* gene. However, these ILs carried genetic contaminations in external regions of the *cmvqw3.1* QTL which expands around 20.81 Mb due to the SC allele between physical positions 24,802,439 and 24,421,885 base pairs (bp). Moreover, the SC allele was also detected in two regions, before and after the *cmv1* locus: 2,391,541 to 6,122,217 bp and 9,344,699 to 11,095,411 bp, respectively. In addition, the H allele was also present on chromosome (Chr) VIII detected by the marker CMPSNP510, at position 6,823,101 bp in the indicated region (see Table 1.3).

Chapter 1: Melon Pyramided Lines Development

Table 1. 3. Genetic contaminations contained in the IL 3-12.

Chr	III					VIII	XII											
QTL and gene	<i>cmvqw3.1</i>		O			G	O				<i>cmv1 gene</i>		O					
SNP	FM: AI_14-B01	FM: AI_33_H11	CMPSNP64	Chr3_25764960	CMPSNP979	CMPSNP510	Chr12_251545	Chr12_2391541	Chr12_4268062	Chr12_6122217	Chr12_9319960	SNP: <i>cmv1</i>	Chr12_9330070	Chr12_9344699	Chr12_11095411	Chr12_13397309	Chr12_16256846	Chr12_24021497
P	2,804,514	23,616,908	24,802,439	25,764,960	26,421,885	6,823,101	251,545	2,391,541	4,268,062	6,122,217	9,319,960	9,320,908	9,330,070	9,344,699	11,095,411	13,397,309	16,256,846	24,021,497
IL 3-12	SC	SC	SC	SC	SC	H	PS	SC	SC	SC	SC	SC	SC	SC	SC	PS	PS	PS

Chr: Chromosome, O: Out the QTL and the gene, G: Genome, SNP: Single Nucleotide Polimorfism, FM: Flanking Markers, P: Physical position.

- PS: Piel de Sapo
- H: Heterozygosity
- SC: Songwhan Charmi PI 161375,
- QTL and *cmv1* gene.

1.2.1 Breeding strategy of IL 3-12 for *cmvqw3.1* and the *cmv1* gene selection.

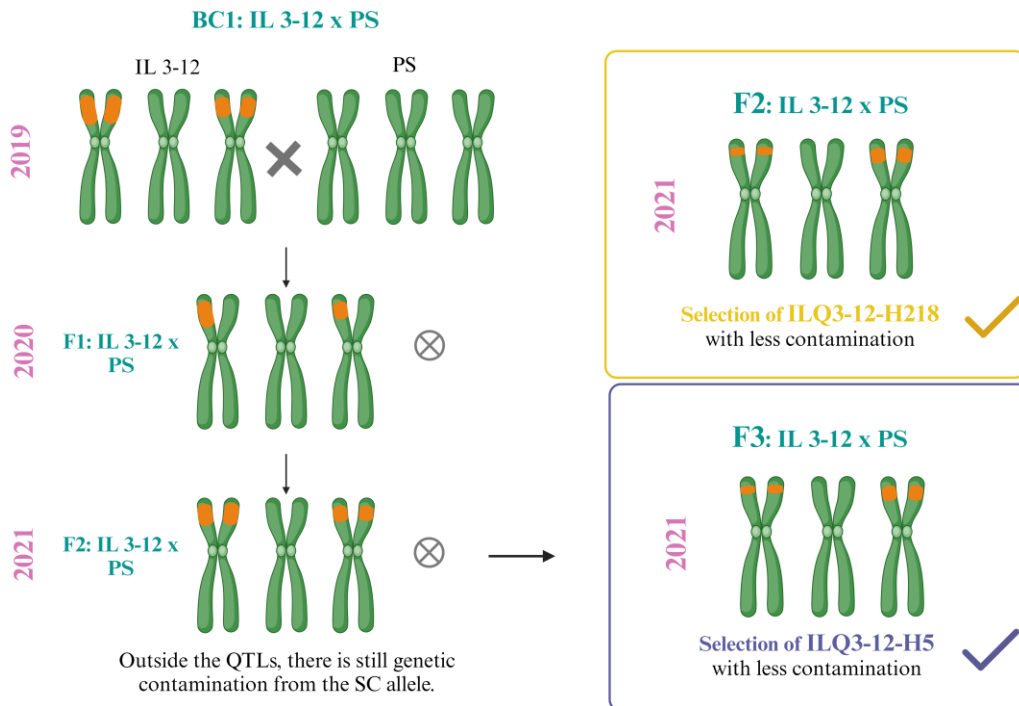


Figure 1. 1. Breeding scheme for IL 3-12 to remove any undesired interval outside the QTLs of interest. F1, F2 and F3: represent the number of generations; BC: Backcross.

- PS: Piel de Sapo
- SC: Songwhan Charmi PI 161375

As shown in Figure 1.1 above, a backcross (BC) between IL 3-12 and PS (BC1: IL 3-12 x PS) was performed in 2019 to remove genetic contamination in regions beyond the QTLs (details in Table 1.3). In 2020, 20 F1 plants were genotyped to confirm heterozygosity within the two QTLs using the *cmv1* marker (sitting in the *cmv1* gene locus). For the *cmvqw3.1* QTL, we used the FM: AI_14-B01 (P=2,804,514 bp) and AI_33_H11 (P=23,616,908 bp). In addition, the SNP CMPSNP550 (P=6,823,101 bp), mapping on Chr VIII, was used to select the PS allele.

Chapter 1: Melon Pyramided Lines Development

The F1: IL 3-12 x PS plants were self-pollinated to produce the F2 generation. Next year, 2116 F2:IL 3-12 x PS plants were genotyped. First, they were selected for the *cmv1* gene and then for the *cmvqw3.1* QTL in homozygosity for the SC allele. Finally, 34 F2 individuals with these characteristics were chosen. To assess the length of SC introgression of the *cmvqw3.1* QTL, the F2 individuals were genotyped beyond the QTL. We focus on selecting the PS and H alleles within the intervals 24,802,439 and 26,421,885 of Chr III. Nevertheless, the segregation showed SC, PS and H alleles (Table 1.1 S2). Only 24 melon fruits were obtained from the 34 F2 individuals in the field.

1.2.2 Selected Pre-ILs 3-12

Based on the 24 genotypes, we selected two Pre-ILs, H218 and H5 (hereafter referred to as Pre-IL H218 or Pre-IL H5), listed in Table 1.4.

Table 1. 4. The genotype of the selected Pre-IL H5 and Pre-IL H218.

Chr	III					VIII	XII											
	<i>cmvqw3.1</i>		O			G	O				<i>cmv1</i> gene		O					
QTL and gene	FM: AL_14-B01	FM: AL_33_H11	CMPSNP64	Chr3_25764960	CMPSNP979	CMPSNP510	Chr12_251545	Chr12_2391541	Chr12_4268062	Chr12_6122217	Chr12_9319960	SNP: <i>cmv1</i>	Chr12_9330070	Chr12_9344699	Chr12_11095411	Chr12_13397309	Chr12_16256846	Chr12_24021497
P	2,804,514	23,616,908	24,802,439	25,764,960	26,421,885	6,823,101	251,545	2,391,541	4,268,062	6,122,217	9,319,960	9,320,908	9,330,070	9,344,699	11,095,411	13,397,309	16,256,846	24,021,497
Pre-IL-H5	SC	SC	H	H	H	PS	PS	SC	SC	SC	SC	SC	SC	SC	SC	PS	PS	PS
Pre-IL-H218	SC	SC	SC	H	H	PS	PS	SC	SC	SC	SC	SC	SC	SC	SC	PS	PS	PS

Chr: Chromosome, O: Out the QTL and the gene, G: Genome, SNP: Single Nucleotide Polimorfism, FM: Flanking Markers, P: Physical position.

- PS: Piel de Sapo
- H: Heterozygosity
- SC: Songwhan Charmi PI 161375,
- QTL and *cmv1* gene.

Chapter 1: Melon Pyramided Lines Development

Both Pre-IL (H218 and H5) shared the SC introgression of the *cmvqw3.1* QTL (between 2,804,514 and 23,616,908 bp). The Pre-IL H5 had genetic contamination with the H allele outside the QTL (between 24,802,439 and 26,421,885 bp), but no further contamination in the contiguous regions of Chr III. The Pre-IL H218 carried both the SC allele (24,802,439 bp) and the H allele (between 25,764,960 and 26,421,885 bp) on Chr III, with no further contamination in contiguous regions, as did the Pre-IL H5. The two Pre-ILs carried the SC introgression on Chr XII between positions 2,391,541 and 6,122,217bp and 9,344,699 and 11,095,411 bp with no further contamination between 13,397,309 and 24,021,497 bp. Only the Pre-IL-H5 was further self-pollinated to remove the H allele by selection for PS, as shown in Table 1.5 and Figure 1.1.

Table 1. 5. Final genotypes of ILs Q3-12 H5 and IL Q3-12 H218 that were chosen for further experiments.

Chr	III					VIII	XII											
QTL and gene	<i>cmvqw3.1</i>		O			G	O				<i>cmv1 gene</i>		O					
SNP	FM: AL_14-B01	FM: AL_33_H11	CMPSNP64	Chr3_25764960	CMPSNP979	CMPSNP510	Chr12_251545	Chr12_2391541	Chr12_4268062	Chr12_6122217	Chr12_9319960	SNP: cmv1	Chr12_9330070	Chr12_9344699	Chr12_11095411	Chr12_13397309	Chr12_16256846	Chr12_24021497
P	2,804,514	23,616,908	24,802,439	25,764,960	26,421,885	6,823,101	251,545	2,391,541	4,268,062	6,122,217	9,319,960	9,320,908	9,330,070	9,344,699	11,095,411	13,397,309	16,256,846	24,021,497
IL Q3-12-IL-H5	SC	SC	PS	PS	PS	PS	PS	SC	SC	SC	SC	SC	SC	SC	SC	PS	PS	PS
IL Q3-12-H218	SC	SC	SC	H	H	PS	PS	SC	SC	SC	SC	SC	SC	SC	SC	PS	PS	PS

Chr: Chromosome, O: Out the QTL and the gene, G: Genome, SNP: Single Nucleotide Polimorfism, FM: Flanking Markers, P: Physical position.

■ PS: Piel de Sapo

■ H: Heterozygosity

■ SC: Songwhan Charmi PI 161375,

■ QTL and *cmv1* gene.

Chapter 1: Melon Pyramided Lines Development

Therefore, both Pre-IL H218 (F2 generation) and Pre-IL H5 (F3 generation) were selected as final lines and used for different further purposes (hereafter referred to as IL Q3-12-H5 and IL Q3-12-H218) (see Table 1.5): IL Q3-12 H5 was used for experiments to characterise the resistance conferred by two QTLs (Chapter 2), and IL Q3-12 H218 was used for crosses to create the mapping population of QTL3 (Chapter 3) since line IL Q3-12-H5 was not ready at the time to start developing the mapping populations.

1.3 IL carrying *cmvqw10.1* and the *cmv1* gene.

We started IL development with an F2 from the crossing of lines SC 10.2 with SC 12.1.99 to produce an IL10-12 carrying the *cmvqw10.1* QTL and the *cmv1* locus. However, both parent lines carried genetic contaminations. Specifically, the SC 10.2 contaminations were observed in the external regions of the *cmvqw10.1*, spanning 3.62 Mb, carrying the SC allele on Chr X between 11,280,612 and 22,048,252 bp. In the parent line SC 12.1.99, SC introgressions were observed between 251,545 and 6,122,217 bp before the *cmv1* locus and between 9,344,699 and 13,397,309 bp after it. Also, an SC introgression was observed at position 28,908,331 bp on Chr VII as shown in Table 1.6 below.

Chapter 1: Melon Pyramided Lines Development

Table 1. 6. Genetic contaminations contained in the parent lines SC 10.2 and SC 12.1.99.

Chr	VII	X								XII											
QTL and gene	G	<i>cmvqw10.1</i>		O						O		<i>cmv1 gene</i>		O							
SNP	Chr7_28908331	FM: CMPSNP1117	FM: CMPSNP671	CMPSNP113	CMPSNP530	CMPSNP2035	CMPSNP666	AI_38_B09B	CMPSNP550	Chr12_251545	Chr12_2391541	Chr_12_4268062	Chr12_6122217	Chr12_9319960	SNP: <i>cmv1</i>	Chr12_9330070	Chr12_9344699	Chr12_11095411	Chr12_13397309	Chr12_16256846	Chr12_24021497
P	28,908,331	1,122,396	4,747,687	11,280,612	14,320,096	17,528,871	20,319,699	21,800,391	22,048,252	251,545	2,391,541	4,268,062	6,122,217	9,319,960	9,320,908	9,330,070	9,344,699	11,095,411	13,397,309	16,256,846	24,021,497
SC 10.2	PS	SC	SC	SC	SC	SC	SC	SC	SC	PS	PS	PS	PS	PS	PS	PS	PS	PS	PS	PS	PS
SC 12.1.99	SC	PS	PS	PS	PS	PS	PS	PS	PS	SC	SC	SC	SC	SC	SC	SC	SC	SC	SC	PS	PS

Chr: Chromosome, O: Out the QTL and the gene, G: Genome, SNP: Single Nucleotide Polimorfism, FM: Flanking Markers, P: Physical position.

■ PS: Piel de Sapo

■ SC: Songwhan Charmi PI 161375,

■ H: Heterozygosity

■ QTL and *cmv1* gene.

1.3.1 Breeding scheme for selection of IL carrying *cmvqw10.1* and the *cmv1* gene.

In 2020 we screened 2,300 plants from the F2 generation (F2: SC 10.2 x SC 12.1.99) of this cross to fix the *cmvqw10.1* QTL and the *cmv1* locus in homozygosity for the SC allele and to fix the PS allele outside the QTL region (Figure 2.2). First, we selected the *cmv1* gene (*cmv1* marker) from the progeny. Then, we chose plants with homozygous SC introgression of *cmvqw10.1* among those containing the *cmv1* locus. We used the FMs CMPSNP1117 (P=1,122,396 bp) and CMPSNP671 (P=4,747,687 bp) to make the selection. As a result of the selection, 17 F2 individuals were obtained to self-pollinate and grow melon for fruit production in the greenhouse (F2 plants in Table 1.2. S2).

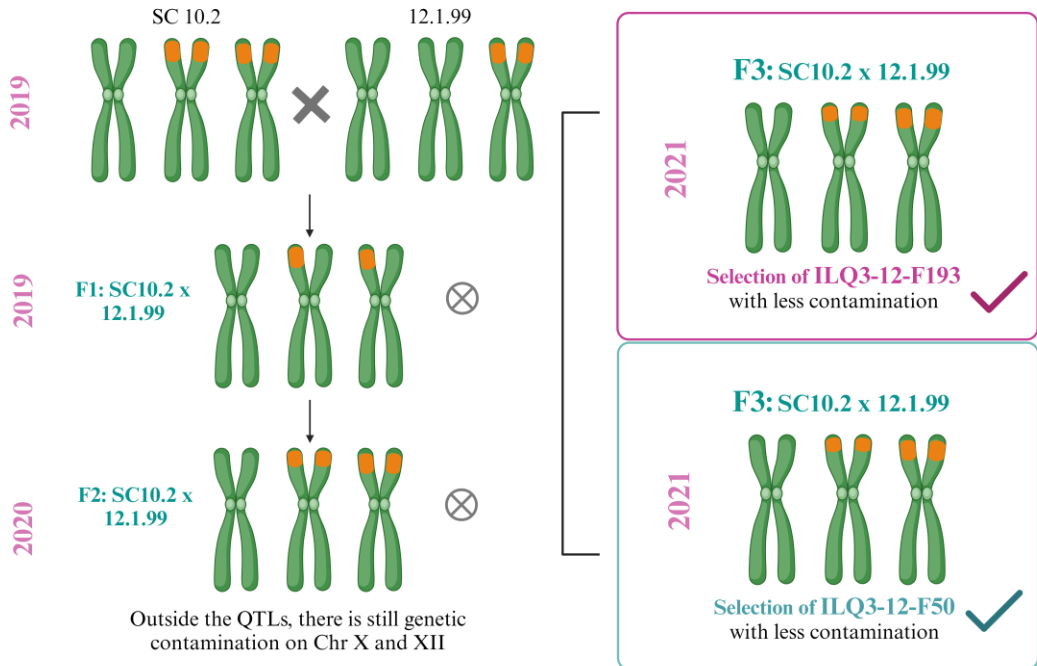


Figure1. 2. Breeding scheme for IL 10-12 for removing undesired SC contaminations outside the QTLs. F1, F2 and F3: represent the number of generations; BC: Backcross.

- PS: Piel de Sapo
- SC: Songwhan Charmi PI 161375

The 17 F2 individuals were genotyped to determine the length of introgression outside the *cmvqw10.1* QTL in Chr X (from 11,280,612 to 22,048,252 bp) to preferably select the PS allele. Nevertheless, the progeny displayed SC, PS and H alleles in this interval. The same selection was applied in Chr XII before and after the *cmv1* gene. However, the SC alleles could not be removed in the interval between 9,344,699 and 13,397,309 bp. Within the interval between 251,545 and 6,122,217 bp before the *cmv1* locus and at position 28,908,331 bp on Chr VII SC alleles were segregating. Only five of the 17 selected plants produced melons in the field by self-pollination at that moment. Therefore, the remaining 12 individuals were maintained under *in vitro* conditions for more than six months to avoid their loss (for more details, check Table 1.2 S2).

Chapter 1: Melon Pyramided Lines Development

1.3.2 Selected Pre ILs-10-12

Two genotypes were selected as more desirable to remove the remaining genetic contamination in the external regions of the *cmvqw10.1* QTL and the *cmv1* gene. Pre-IL F50 (from in vitro and acclimation conditions) and Pre-IL F193 (which produced fruit in the F2 screening selection), hereafter referred to as Pre-IL F193 and Pre-IL F50. Both Pre-ILs shared the same SC introgression within the *cmvqw10.1* QTL (between 1,122,396 and 4,747,687 bp). However, they have different genotypes outside of the QTL *cmvqw10.1* and the *cmv1* locus (Table 1.7). The Pre-IL F193 carried the H allele within the interval of 11,280,612 and 21,800,391 bp beyond the *cmvqw10.1* QTL. In contrast, the Pre-IL F50 did not have any contamination in that interval. On Chr XII, the Pre-IL F193 contained the SC alleles before the *cmv1* locus (between 2,391,541 and 6,122,217 bp) and after it (between 9,344,699 and 13,397,309 bp). On the other hand, Pre-IL F50 carried the H allele between 2,391,541 and 6,122,217 bp before the *cmv1* locus and between 9,344,699 and 13,397,309 bp after it, as did Pre-IL F193. Additionally, the H allele was present at position 28,908,331 bp of Chr VII.

Chapter 1: Melon Pyramided Lines Development

Table 1. 7. The genotype of the selected Pre-IL F50 and Pre-IL F193.

Chr	VII	X								XII											
QTL and gene	G	<i>cmvqw10.1</i>		O						O		<i>cmv1 gene</i>		O							
SNP	Chr7_28908331	FM: CMPSNP1117	FM: CMPSNP671	CMPSNP113	CMPSNP530	CMPSNP2035	CMPSNP666	AL_38_B09B	CMPSNP550	Chr12_251545	Chr12_2391541	Chr12_4268062	Chr12_6122217	Chr12_9319960	SNP: <i>cmv1</i>	Chr12_9330070	Chr12_9344699	Chr12_11095411	Chr12_13397309	Chr12_16256846	Chr12_24021497
P	28,908,331	1,122,396	4,747,687	11,280,612	14,320,096	17,528,871	20,319,699	21,800,391	22,048,252	251,545	2,391,541	4,268,062	6,122,217	9,319,960	9,320,908	9,330,070	9,344,699	11,095,411	13,397,309	16,256,846	24,021,497
Pre-IL-F193	PS	SC	SC	H	H	H	H	H	PS	PS	SC	SC	SC	SC	SC	SC	SC	SC	SC	PS	PS
Pre-IL-F50	H	SC	SC	PS	PS	PS	PS	PS	PS	PS	H	H	H	SC	SC	SC	SC	SC	SC	PS	PS

Chr: Chromosome, O: Out the QTL and G: Genome the gene, SNP: Single Nucleotide Polimorfism, FM: Flanking Markers, P: Physical position.

- PS: Piel de Sapo
- SC: Songwhan Charmi PI 161375,
- H: Heterozygosity
- QTL and *cmv1* gene.

To segregate the contaminations from Pre-IL F193, we genotyped 92 F3 plants to fix the PS allele within the interval outside the *cmvqw10.1* QTL (11,280,612 to 21,800,391 bp). The introgression of SC has not been removed in the interval before and after the *cmv1* locus at 2,391,541 and 9,204,842 bp and 9,344,699 and 13,397,309 bp. Finally, 22 out of 92 plants were identified as final lines (hereafter referred to as IL Q10-12 F193) with no genetic contamination beyond the *cmvqw10.1* QTL. (See Table 1.8 and for further details refer to Table 1.2. S2).

Chapter 1: Melon Pyramided Lines Development

Table 1. 8. Final lines IL Q10-12 F50 and F193 after segregating out the genetic contaminations.

Chr	VII	X							XII													
QTL and gene	G	<i>cmvqw10.1</i>		O					O			<i>cmv1 gene</i>		O								
SNP	Chr7_28908331	FM: CMPSNP117	FM: CMPSNP671	CMPSNP113	CMPSNP530	CMPSNP2035	CMPSNP666	AL_38_B09B	CMPSNP550	Chr12_251545	Chr12_2391541	Chr12_4268062	Chr12_6122217	Chr12_9319960	SNP: <i>cmv1</i>	Chr12_9330070	Chr12_9344699	Chr12_11095411	Chr12_13397309	Chr12_16256846	Chr12_24021497	
P	28,908,331	1,122,396	4,747,687	11,280,612	14,320,096	17,528,871	20,319,699	21,800,391	22,048,252	251,545	2,391,541	4,268,062	6,122,217	9,319,960	9,320,908	9,330,070	9,344,699	11,095,411	13,397,309	16,256,846	24,021,497	
Pre-IL-F193	PS	SC	SC	PS	PS	PS	PS	PS	PS	PS	SC	SC	SC	SC	SC	SC	SC	SC	SC	PS	PS	
Pre-IL-F50	H*	SC	SC	PS	PS	PS	PS	PS	PS	PS	PS	PS	PS	SC	SC	SC	SC	SC	SC	SC	PS	PS

Chr: Chromosome, O: Out the QTL and the gene, G: Genome, SNP: Single Nucleotide Polimorfism, FM: Flanking Markers, P: Physical position. *The progeny is segregating into the H and PS alleles

- PS: Piel de Sapo
- H: Heterozygosity
- SC: Songwhan Charmi PI 161375,
- QTL and *cmv1* gene.

On the other hand, after maintenance *in vitro*, the Pre-IL F50 (introduced *in vitro* at the time of F2 sampling) was acclimatised under controlled conditions for two weeks before being planted in a greenhouse. At least 10 F2 *in vitro* replicates of Pre-IL F50 were then planted in the field to self-pollinate and produce melons. The F3 individuals of the Pre-IL F50 were genotyped to segregate genetic contaminations as much as possible. From the 169 individuals obtained, 19 plants were selected as the final line (hereafter referred to as IL Q10-12-F50) with no genetic contamination between 2,391,541 and 6,122,217 bp on Chr XII. However, genetic contamination with the SC allele persisted between 9,344,699 and 13,397,309 bp. A few years later, we discovered that the Pre-IL F50 carried the H allele at position 28,908,331 bp of Chr VII, thus the progeny of IL Q10-12-F50 segregate at this position, as shown in Table 1.8 (for further details see Table 1.2. S2). IL Q10-12 (F50) was used to characterise resistance to CMV (Chapter 2), while IL Q10-12 (F193) was used to

Chapter 1: Melon Pyramided Lines Development

construct the fine-mapping populations (Chapters 3), as IL Q10-12-F50 was not available at the time of their development.

1.4 IL 3-10-12. carrying *cmvqw3.1*, *cmvqw10.1* and *cmv1* gene.

IL 3-10-12 contained the QTL *cmvqw3.1*, *cmvqw10.1* and the *cmv1* locus in homozygosity for the SC introgressions. However, resequencing of this line (unpublished) revealed genetic contamination beyond the *cmvqw10.1* region by the H allele (11,280,612 and 22,048,252 bp). In addition, SC introgressions were found on Chr XII before and after the *cmv1* locus, between 2,391,541 and 6,122,217 bp and 9,344,699 and 13,199,889 bp, respectively. Table 1.9 shows that Chr VII was contaminated by the SC allele at position 28,908,331 bp. However, no contaminations were found in the external region of the *cmvqw3.1* QTL (refer to Table 1.9). The sequenced IL 3-10-12 was used for all infection experiments, with further crosses to remove the SC alleles from the QTL intervals. However, we were unable to produce an IL 3-10-12 without any external contamination due to time limitations.

Chapter 1: Melon Pyramided Lines Development

Table 1. 9. The genotype of the IL 3-10-12.

QTL and gene	<i>cmvqw3.1</i>			O	G	<i>cmvqw10.1</i>			O			O			<i>cmv1</i> gene			O								
SNP	FM: AL_14_B01	FM: AL_33_H11	CMPSNP64	Chr3_25764960	CMPSNP979	Chr7_28908331	FM: CMPSNP1117	FM: CMPSNP671	CMPSNP113	CMPSNP530	CMPSNP2035	CMPSNP666	AL_38_B09B	CMPSNP550	Chr12_251545	Chr12_2391541	Chr12_4268062	Chr12_6122217	Chr12_9319960	SNP: cmv1	Chr12_9330070	Chr12_9344699	Chr12_11095411	Chr12_13397309	Chr12_16256846	Chr12_24021497
P	2,804,514	23,616,908	24,802,439	25,764,960	26,421,885	28,908,331	1,122,396	4,747,687	11,280,612	14,320,096	17,528,871	20,319,699	21,800,391	22,048,252	251,545	2,391,541	4,268,062	6,122,217	9,319,960	9,320,908	9,330,070	9,344,699	11,095,411	13,397,309	16,256,846	24,021,497
IL 3-10-12	SC	SC	PS	PS	PS	SC	SC	SC	SC	SC	SC	SC	SC	SC	PS	SC	SC	SC	SC	SC	SC	SC	SC	SC	PS	SC

Chr: Chromosome, O: Out the QTL and the gene, G: Genome, SNP: Single Nucleotide Polimorfism, FM: Flanking Markers, P: Physical position.

- PS: Piel de Sapo
- H: Heterozygosity
- SC: Songwhan Charmi PI 161375,
- QTL and *cmv1* gene.

Chapter 2

Characterization of the resistance to CMV controlled by *cmvqw3.1* and *cmvqw10.1* QTLs in melon: Integration of laser dissection microscopy as a novel methodology in melon for determining the role of the minor QTLs in the Bundle Sheath cells

Chapter 2

Section I: Characterization of the resistance to CMV controlled by *cmvqw3.1* and *cmvqw10.1* QTLs in melon.

2.1 Phenotyping of parent and melon pyramided lines.

The melon pyramided lines used in this study were IL Q3-12-H5, which carries *cmvqw3.1* QTL and the *cmv1* gene, IL Q10-12-F50, which carries *cmvqw10.1* and the *cmv1* gene, and IL 3-10-12, which carries *cmvqw3.1*, *cmvqw10.1* QTL and the *cmv1* gene. The control lines were Songwhan Charmi (SC), the resistant accession, and Piel de Sapo (PS), the cultivar susceptible to CMV (see Table 2.1). The melon pyramided lines were constructed to obtain lines with as few genetic contaminations as possible (Chapter 1).

Table 2. 1. Melon pyramided lines that were used in this study.

Melon pyramided lines	<i>cmvqw3.1</i>	<i>cmvqw10.1</i>	<i>cmv1 gene</i>
PS	PS	PS	PS
SC	SC	SC	SC
IL Q3-12-H5	SC	PS	SC
IL Q10-12-F50	PS	SC	SC
IL 3-10-12-18(64)	SC	SC	SC

■ PS: Piel de Sapo

■ SC: Songwhan Charmi PI 161375

The lines were phenotyped by inoculation with CMV-M6 form SGI to assess the contribution of the individual and collective role of the minor QTLs in cooperation with the *cmv1* gene in resistance to CMV. To this end, two types of phenotyping were performed. First, the severity and speed of infection were phenotyped visually using infection scores based on a scale from 0 to 5 between 7 and 28 days post-inoculation (dpi) (see Materials and Methods section 3.4 for more details). Secondly,

Chapter 2-I: Characterization of the resistance

to assess the movement of CMV at a local level, we quantified its viral RNA within the petiole of the inoculated leaf at three time points (7, 14 and 21 dpi). The pattern of virus accumulation within the petiole tells us whether the virus has reached the phloem and whether these QTLs restrict or delay phloem entry to produce a systemic infection.

2.1.1 Infection patterns of the melon pyramided lines

Principal component analyses (PCA) were performed to obtain a general overview of the infection patterns of the melon lines with the infection levels achieved by each melon line. The analyses were performed with and without infection scores of PS. The data set included the average severity (infection scores) and the velocity of infection over time. The PCAs were able to cluster into different groups according to the infection patterns and we noticed an interesting infection trend (Figure 2.1). The PCA with PS showed an isolated cluster where the PS cultivar (in pink) represented the most significant variance in PC1 (explaining 99.05% of the variance) compared to the others (Figure 2.1). When focusing only on the melon pyramided lines, IL Q10-12-F50 seems to be the most susceptible melon pyramided line (cluster in green). This line is located at the average of the infection data set. In contrast, SC and IL 3-10-12-18(64) (in red) are clustered together and close to the cluster of IL Q3-12-H5 (in blue).

At the experimental level, PS showed 100% infection with severe/fast-progressing symptoms over time. IL Q10-12-F50 showed higher infection and in a shorter time than the other melon pyramided lines. The IL Q3-12-H5 showed similar symptoms, but less aggressive and later than the IL Q10-12-F50 plants. The IL 3-10-12-18(64) plants were occasionally infected with late symptoms and were less aggressive than F50. However, the SC accession did not show any symptoms over time. Regarding PC2, only explains a 0.92% variance of the mean of the infections.

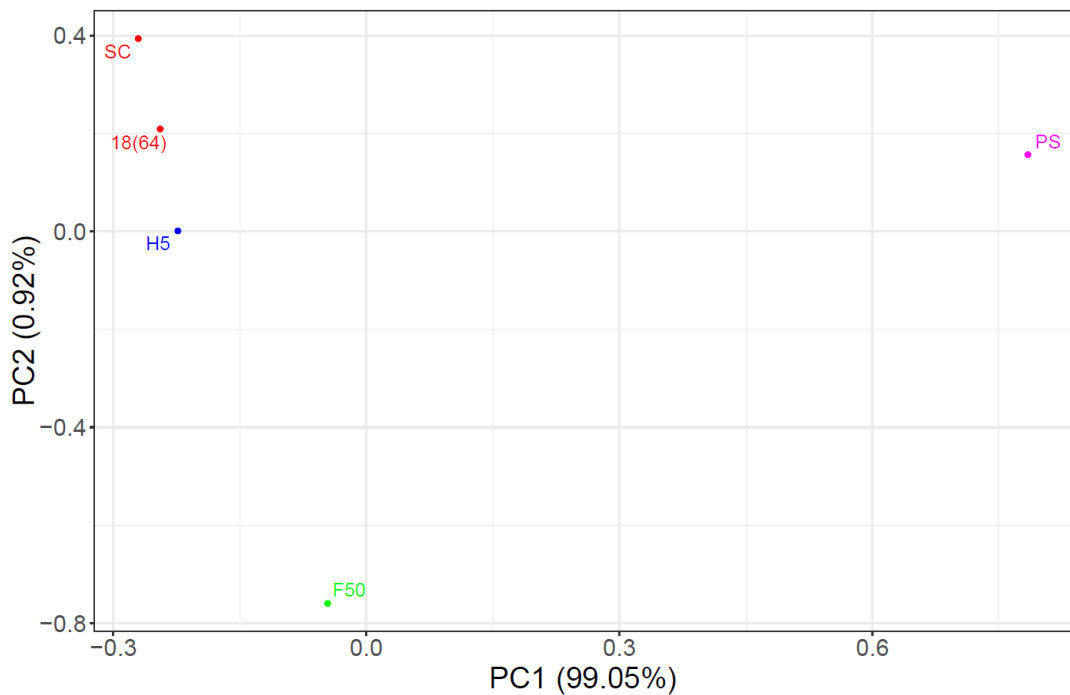


Figure 2. 1. A) PCA of the infection patterns of the melon pyramided lines including PS infections. PC1 showed 99.05% and PC2 0.92% of the variance. Cluster means the clustering of samples according to severity and the velocity of the infections.

We analysed the visual phenotype to determine the level of infection (infection scores achieved by individual plants). This phenotyping indicates the severity and speed of infection. The Kruskal-Wallis test was used to analyse the infection of the melon pyramided lines, as the distribution of the data set was not parametric. The post-hoc Dunn's test was used to determine which groups differed significantly from the resistant control IL 3-10-12-18(64). Multiple testing was corrected (p-adjusted) using the Holm method (Figure 2.2B). Figure 2.2A, below shows the infection scores achieved at different time points 7, 14, 21 and 28 dpi in each melon pyramided line and the controls.

Chapter 2-I: Characterization of the resistance

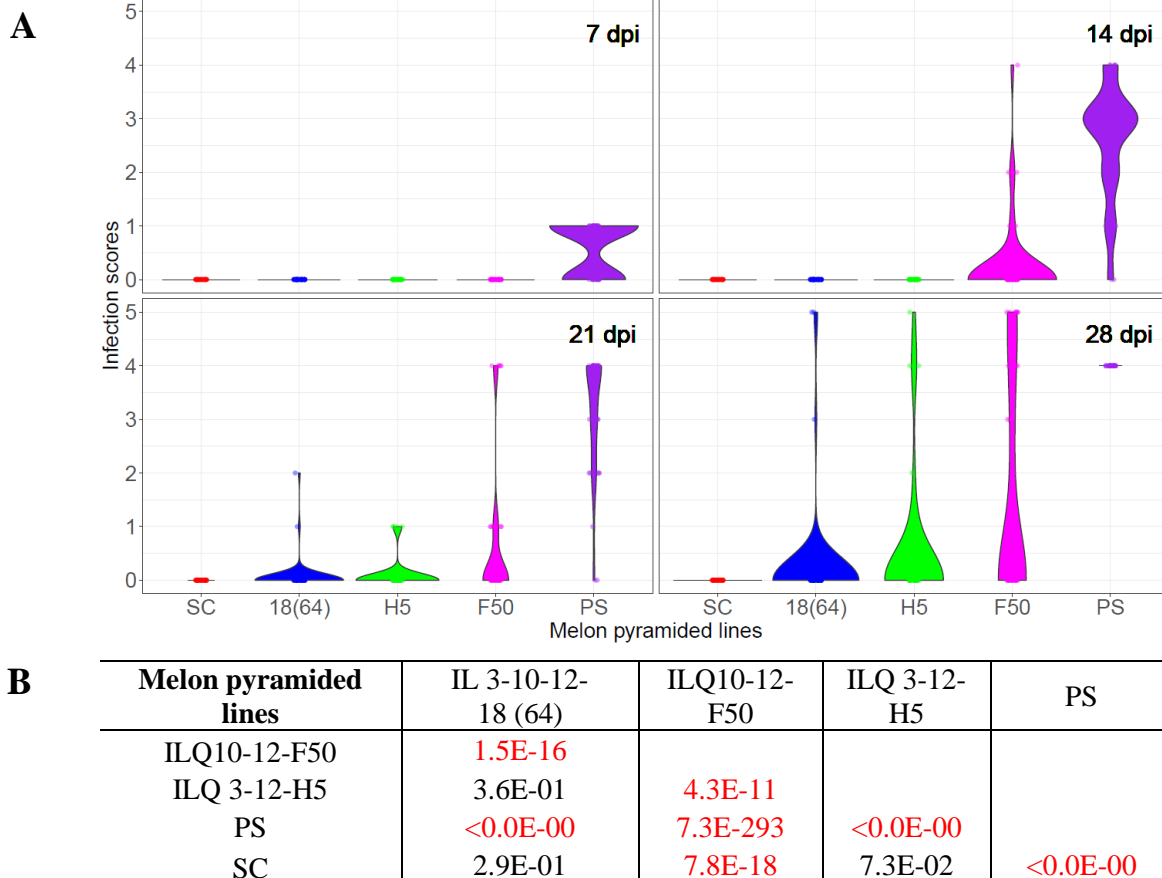


Figure 2. 2. A) Plots of infection scores reached by individual plants of melon pyramided lines at each time point 7, 14, 21 and 28 dpi. **B)** Statistical significance (p -value <0.05) of all melon lines compared to each other using the mean score reached by the individual plants per group at each time point. In red highlight significantly different means of infection scores. The $<0.0e+00$ refers to p -values $< 0.0e-293$.

The PS infection scores were significantly different (p -value <0.05) compared to the SC accession and all melon pyramid lines, as mentioned above. In contrast, SC showed no symptoms over time (infection score 0). Similarly, IL3-10-12-18(64) and IL Q3-12-H5 showed resistance compared to the susceptible lines PS and IL Q10-12-F50 (p -value <0.05) and were not statistically different from each other. The two melon lines behaved similarly in terms of infection levels. However, IL Q10-12-F50 behaved as a mildly resistant line and showed significance (p -value <0.05) compared to PS and SC.

Regarding the time of infection appearance, melon pyramided lines carrying at least one minor QTL in coordination with the *cmv1* gene showed delayed infection compared to PS, which became infected around day 7. IL Q10-12-F50 was delayed until around 13 dpi, IL Q3-12-H5 until 17 dpi, and IL 3-10-12-18(64) until about 17 to 23 dpi, when occasionally showed infection. IL Q3-12-H5 had lower infection scores at later infection times than IL Q10-12-F50, as shown in Figure 2.3. Therefore, the gene behind the *cmvqw3.1* QTL would have a major role in CMV-M6 viral infection than the gene residing in the *cmvqw10.1* QTL.

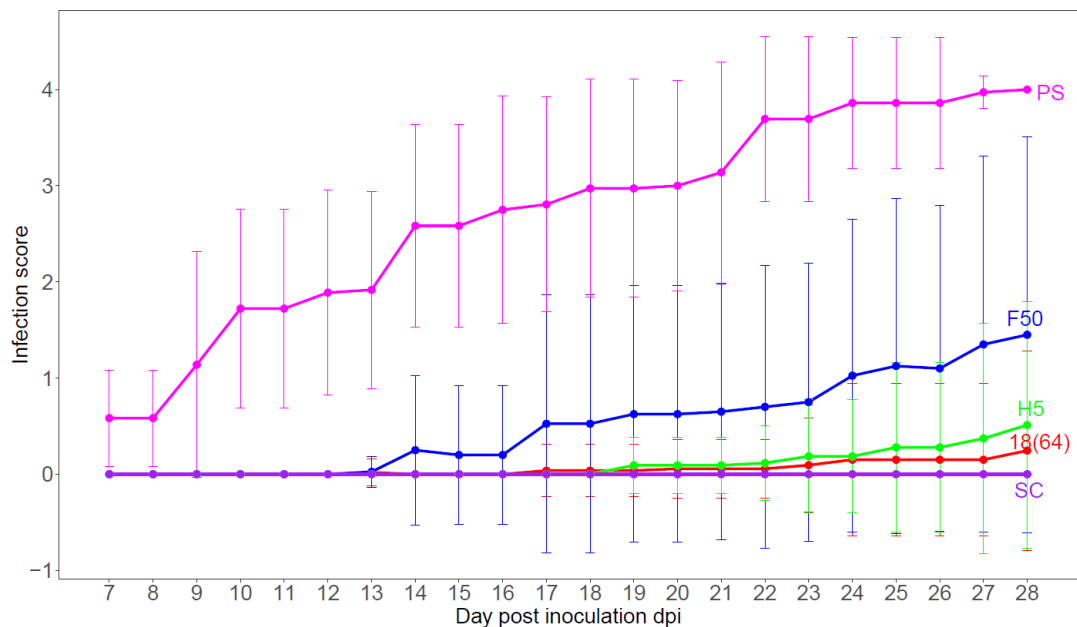


Figure 2. 3. The plot of the Infection scores (scale from 0 to 5) of melon pyramided lines over time (7 to 28 dpi) of the melon pyramided lines. The number of replicates used in each melon pyramided line varies from 40 to 53 biological replicates. Each dot represents the mean infection reached by the day. The bar corresponds to the standard deviation (SD).

2.1.2 Minor QTLs *cmvqw3.1* and *cmvqw10.1* QTLs delay the virus phloem entry.

To investigate whether the delay in infection observed in certain melon lines was due to a delay in virus entry into the phloem, we analysed the initial time of CMV

Chapter 2-I: Characterization of the resistance

inoculation in these lines. We determined the virus load within the petiole of the inoculated leaf at three different time points (7, 14 and 21 dpi) to assess the contribution of each minor QTL in delaying virus infection. The amount of virus within the petiole in all melon lines was analysed by multiple T-tests with a corrector of the analyses using the Holm method. As expected, the PS had a significantly higher viral load than the other melon lines at all time points (p-value <0.05) (Figure 2.4A and 2.4B). Although non-significant, IL Q3-12-F50 showed a trend towards being more permissive to CMV phloem entry than ILQ3-12-H5 at 21 dpi (Figure 2.4A). Both IL 3-10-12-18 (64) and IL Q3-12-H5 tended to be always more restrictive.

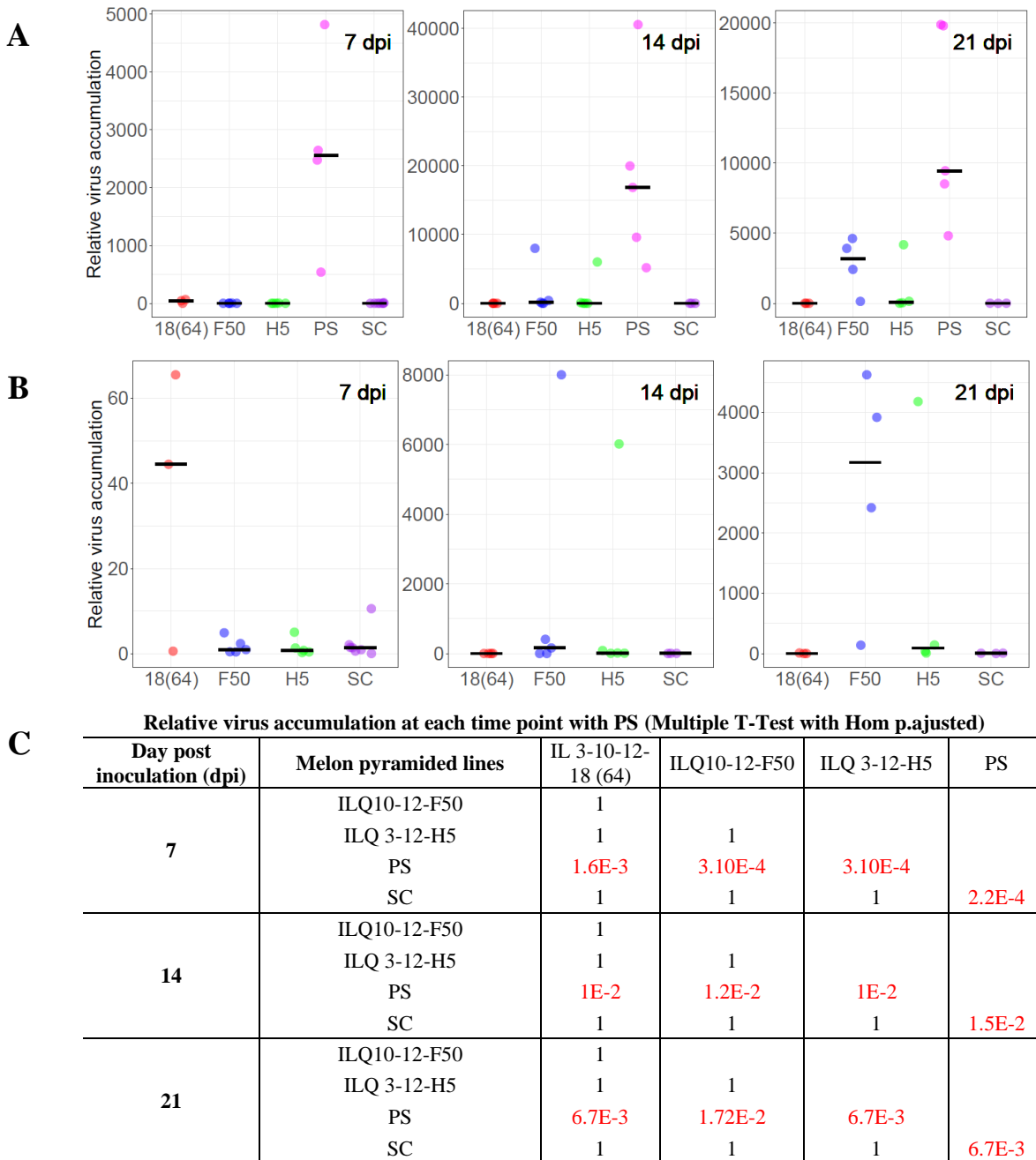


Figure 2. 4. A) Relative virus accumulation within the petiole of the inoculated leaves in the melon pyramided lines and parent lines. **B)** Relative accumulation within the petiole of the inoculated leaves in the melon pyramided lines and SC excluding PS. The number of replicates used in each melon pyramided line for both varies between 3 to 7 biological replicates **C)** Statistical significance of all lines compared to each other. In red, statistically (p-value <0.05) different melon pyramided lines.

Chapter 2-I: Characterization of the resistance

Interestingly, we observed inconsistencies between results in the two QTL lines Q3-12-H5 and Q10-12-F50 from visual phenotyping, at late times post-infection, and viral load quantification, which is analysed at early steps of the infection. This is, there are inconsistencies between two different moments of the infection. At the visual level, IL-Q3-12-H5 appeared to be more resistant than IL-Q10-12-F50, developing fewer and later symptoms. However, at the phloem entry-level, these melon pyramided lines carrying two QTLs did not show statistically significant differences between them, despite the IL Q10-12-F50 line appearing to be more susceptible to virus infection than the IL Q3-12-H5 line. This suggested that the gene(s) residing in IL Q10-12-F50 may facilitate more efficient viral invasion and replication throughout the phloem of the plant compared to the gene/genes residing in IL Q3-12-H5. In contrast, IL-3-10-12-18(64) and IL-3-12-H5 had revealed a higher resistance at the systemic level compared to PS, developing fewer symptoms and at much later stages.

Therefore, since CMV-M6 phloem entry is delayed in melon pyramided lines compared to the susceptible control PS, the minor QTLs, in cooperation with the *cmv1* gene, play a role in phloem entry of CMV-M6 as *cmv1* does for CMV-LS (Guiu-Aragonés et al, 2016). Moreover, the *qwcmv3.1* QTL seems to play a more important role in phloem entry than the *qwcmv10.1* QTL.

Section II: Integration of laser dissection microscopy as a novel methodology in melon for determining the role of the minor QTLs in the Bundle Sheath cells.

2.2 Exploring Bundle Sheath Cells in Melon.

As CMV-LS is blocked in the Bundle Sheath (BS) cells of melon lines that contain only the *cmv1* gene (Guiu-Aragónés et al., 2016), we focused on the BS cells and investigated their role in conferring resistance to CMV infection. Furthermore, we examined their effect on resistance through the contribution of the minor QTLs *cmvqw3.1* and *cmvqw10.1*. This required the development of a system to isolate BS cells from the leaves. Since there was no established method for cell isolation in melon plants, we chose to investigate and establish a method using Laser Dissection Microscopy (LDM) for specific cell studies in melon. Here we report a methodology of LDM adapted to melon plants for specific cell studies.

2.3 Laser dissection microscopy

The LDM methodology described here involves fixing, cryoprotecting, embedding, cryosectioning, and cell isolating. CMV can be detected in BS cells and the phloem of susceptible PS lines at 5 dpi, as previously reported in our laboratory (Guiu-Aragónés et al., 2016). Therefore, we chose to investigate the role of BS cells in phloem entry at this time point. At 5 dpi, inoculated leaves were harvested from both inoculated and mock-inoculated plants. To facilitate fixation, the thick trichomes on the melon leaves were removed. Then, minor veins were collected and prepared for tissue preparation using the LDM technique.

2.3.1 Influence of Vacuum on Tissue Fixation in Melon

Fixation is crucial for maintaining histological integrity and protecting cell contents during tissue cryosectioning and cell isolating. It is the most critical factor in preserving the structural and molecular components of cells and tissues under normal conditions (Kerk et al, 2003; Bussolati, 2022). A commercial fixative was employed: Formalin 10% (a 1:10 solution of commercial formaldehyde in water) to provide high morphological quality without causing excessive distortion of cell structure (Rodriguez-Canales et al, 2013; Thavarajah et al, 2012).

Tissue fixation is necessary to ensure rapid and effective penetration of fixative into the inner cell layer. To ensure successful fixation and subsequent processing, fixation should be combined with two vacuum infiltration steps, an initial vacuum and a final vacuum, most typically performed overnight (o/n) (Pasternak et al., 2015). Minor veins of melons were placed in separate vials with 10% formalin at 4°C, followed by two vacuum infiltration steps. To compare the effect of proper fixation, two initial vacuum infiltration periods were used: 15 and 30 min. The longest infiltration time (30 min) preserved the morphological quality of the cells under the microscope. After the first vacuum, the formalin solution was refreshed before applying the second vacuum, treated (o/v).

2.3.2 Effects of levels of the cryoprotectant and its vacuum infiltration

After fixation, cryoprotection was required to protect tissues, cells and other biological materials from very low temperatures (-80°C or -195.8°C), minimise damage from ice crystals and preserve cell morphology (Chen et al, 2023; Chang and Zhao, 2021; Nagashima et al, 1995). To remove the formalin, the fixed minor veins were first washed twice with 1X PBS for 15 min without shaking. Then, they were dehydrated through a series of ethanol gradients (30%, 50%, and 70% in 1X

Chapter 2-II: Laser dissection microscopy methodology

PBS), repeated in reverse for at least 30 min each time. Sucrose has been used as a cryoprotectant for melon tissue to facilitate dehydration before or during cryopreservation. The concentration of sucrose in cryopreservation methods varies from 5% to 50% (Zamecnik et al, 2021; Sopalun et al, 2010; Suzuki et al, 2008; Nishizawa et al, 1993; Sakai et al, 1990). We tested the effect of different concentrations of sucrose (10%, 20%, and 30%) and different vacuum infiltration periods of sucrose on melon tissue. The sucrose was infiltrated on the tissue samples by vacuum for 15 min, 1 h and 2 h. The sinking of the tissue samples into the sucrose solution indicates complete sucrose integrity within the cells (see Figure 1 below). The cryoprotection procedure for melon tissue was established using 10%, 20%, and 30% sucrose with a 2 h vacuum infiltration period. These steps guarantee complete tissue sinking and a suitable tissue morphology with no cell disruption.



Figure 2. 5. Impact of sucrose concentration and vacuum infiltration time on sample sinking in melon leaves.

2.3.3 Optimal freezing rate and their impact on tissue structure during embedding.

Following cryoprotection, any residual sucrose was removed by brief desiccation through a thin tissue. To protect the tissues during freezing, they were fully embedded in Neg-50™ Frozen Section Medium (OCT Medium, enhancing precision for cancer diagnostics, EpreDia™, United States) in a triangular plastic mould. The minor veins were embedded horizontally to facilitate cryosectioning (Figure 2.6).

Chapter 2-II: Laser dissection microscopy methodology

Embedding provides long-term tissue stability and does not require immediate processing (Kerk et al., 2003).

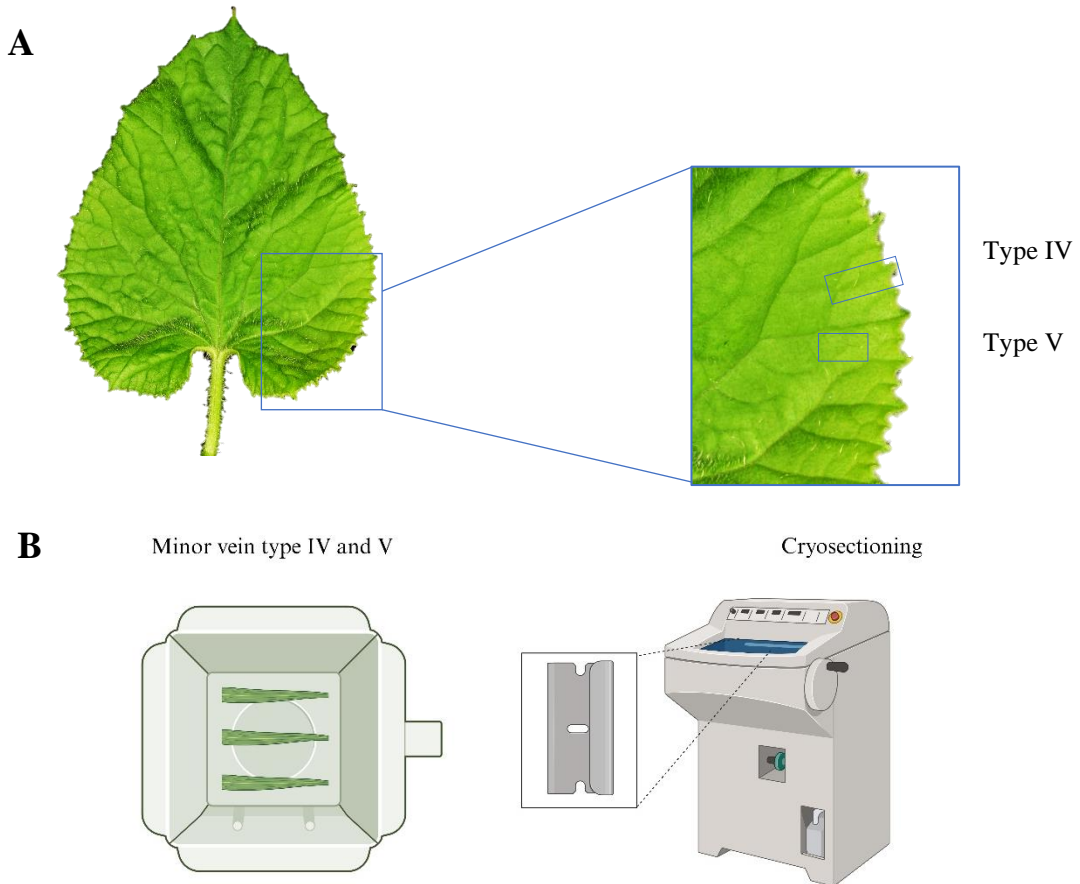


Figure 2. 6. A) Minor veins in melon leaves. **B)** positioning them into the mould to perform longitudinal cryosections.

To compare the effects of tissue freezing speed, two different speeds were used: slow freezing at $-20\text{ }^{\circ}\text{C}$ for at least 1 h or immediate freezing in N_2 liquid (liquid nitrogen) at $-195.8\text{ }^{\circ}\text{C}$ for approximately 20 sec (fast freezing). Tissue integrity was assessed using microscopy (refer to Figure 2.7). Fast freezing produced high-quality tissue morphology (Figure 2.7A), while slow freezing damaged cell structure and nearly destroyed the tissue (Figure 2.7B). Therefore, fast freezing was the preferred method

Chapter 2-II: Laser dissection microscopy methodology

for melon tissue. Once immersed in liquid nitrogen, samples were stored at either -20°C for rapid use or -80°C for long-term storage.

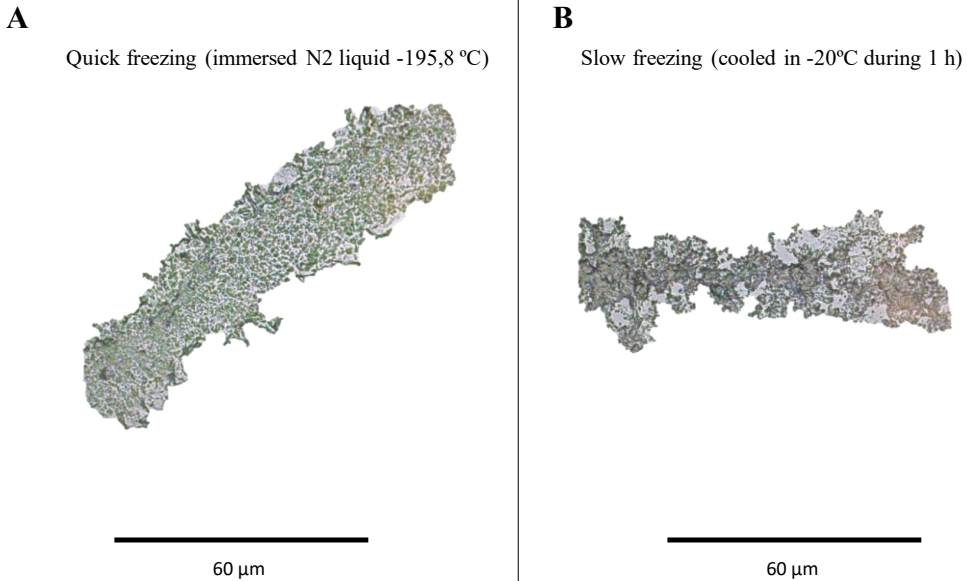


Figure 2. 7. Velocity of the freezing of the minor veins. **A)** Morphology of the samples after quick freezing in liquid Nitrogen (N₂ liquid), longitudinal cryosection. **B)** Morphology of the samples after slow freezing at -20°C , longitudinal cryosection.

2.3.4 Thicker and transversal cryosections improve the cryosectioning process.

Two types of cryosections were performed: longitudinal and transversal. In the longitudinal cryosections, the BS cells were easily identified using the vascular bundle (VB) and mesophyll (M) cells as references. However, identifying BS cells in the transversal cryosections (Figure 2.8) was rather difficult. Cryosections at 14, 20 and 25 μm (the upper limit of the laser settings) were also compared in terms of thickness. As would be expected, the samples in the thicker cryosections remained of better histological quality (20 and 25 μm). In contrast, the thinner samples (14 μm) resulted in cell disruption. Therefore, thicker samples are more suitable for cryosectioning and subsequent cell dissection.

Chapter 2-II: Laser dissection microscopy methodology

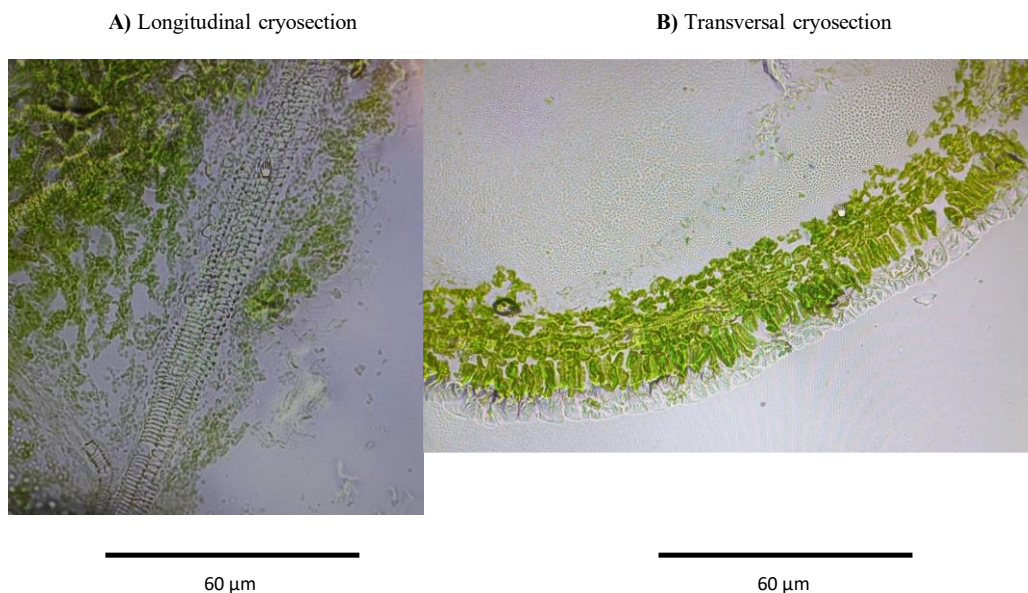


Figure 2. 8. Cryosection of minor veins Type IV and V, **A)** Longitudinal cryosection, **B)** Transversal cryosection of minor veins

The embedded minor veins were cryosectioned into separate 25 µm thick slices at -20°C using a cryostat (Leica Biosystems, USA). The longitudinal sections were placed on MMI MembraneSlide® RNase-free slides (Molecular Machines & Industries MMI®, Germany) pretreated with Poly L-Lysine® solution 0.1% (w/v) in H₂O (Sigma-Aldrich®, United States). To avoid any rolling of the sections, the MMI MembraneSlide® RNase-free slides (MMI®, Germany) were immediately brought to RT. For complete rinsing and hydration, the cryosections were incubated twice in ultrapure water for 30 sec each time. For dehydration, the samples were immersed sequentially in increasing ethanol concentrations of 70%, 90% and 100% for 30 s in each step. Finally, the samples were dried at RT for at least 5 min.

2.3.5 Microdissection of the Bundle Sheath cells

The LDM microscope was calibrated and set up using the MMI Cell Cut tool according to the technical guidelines for the MMI Microscope®. The BS cells

adjacent to the VB were collected using MMI IsolationCap® RNase-free Eppendorf tubes (MMI®, Germany). Afterwards, the samples were stored at -80°C for subsequent RNA and protein extraction.

2.4 Identifying the BS cells in minor veins of the melon plant.

Following all the suitable procedures for melon tissues (fixing, cryoprotecting, embedding, cryosectioning), we identified the BS cells in the intercellular space between VB and M which were the main references for the identification (Figure 2.9).

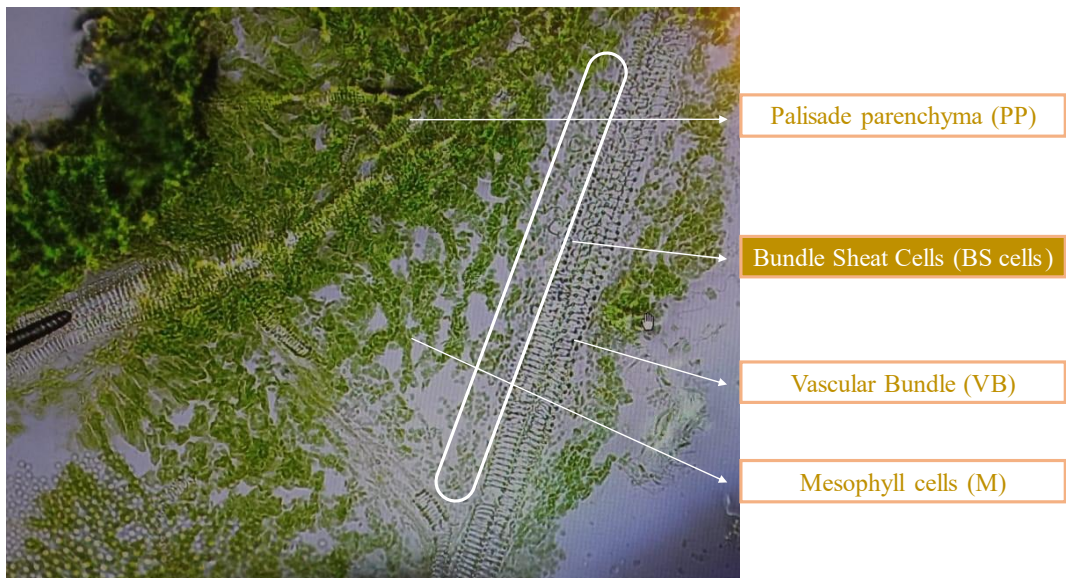


Figure 2. 9. BS cell identification in longitudinal sections of the minor veins in PS melon.

2.5 Detection of CMV in microdissected BS cells

After BS identification, we focused on assessing the influence of the minor QTLs *cmvqw3.1* and *cmvqw10.1* in cooperation with the *cmv1* gene in the expression of other genes. For this purpose, total RNA was purified from BS cells collected from minor veins. The samples were first deparaffinised by melting. RNA from

Chapter 2-II: Laser dissection microscopy methodology

microdissected BS cells was then purified using the RNeasy® FFPE Kit following the supplier's protocol (Isolation, Qiagen, RNeasy® FFPE Handbook, 2021). This kit is designed to extract total RNA from microdissected, formalin-fixed, paraffin-embedded (FFPE) tissue sections containing very low amounts of RNA. The RNA extraction for RT-PCR application requires the collection of more than 150 microdissected cells.

RNA was extracted from microdissected cells, and first-strand complementary DNA (cDNA) was prepared using Monoley Murine Leukaemia Virus reverse transcriptase (M-MLV-RT, Invitrogen™, United Kingdom) and random primers. PCR reactions were performed as normal virus detection PCR (for more details see Materials and Methods, section 3.8.5) with minor modifications for PCR of microdissected BS cells. For this purpose, the denaturation, annealing and extension cycles were increased up to 60.

The collected BS cells of parental lines (SC and PS) and the melon pyramided lines (see Figure 2.10) showed amplification of CMV, as expected. However, it should be noted that the mock-inoculated (M) plants also showed an amplified band, indicating CMV virus infection. This suggests technical difficulties in preventing contamination during the procedure before isolating the LDM-MMI cell sections. At the end of this work, there was no time to perform further extractions to ensure the absence of cross-contaminated RNA for the RNA-seq experiment.

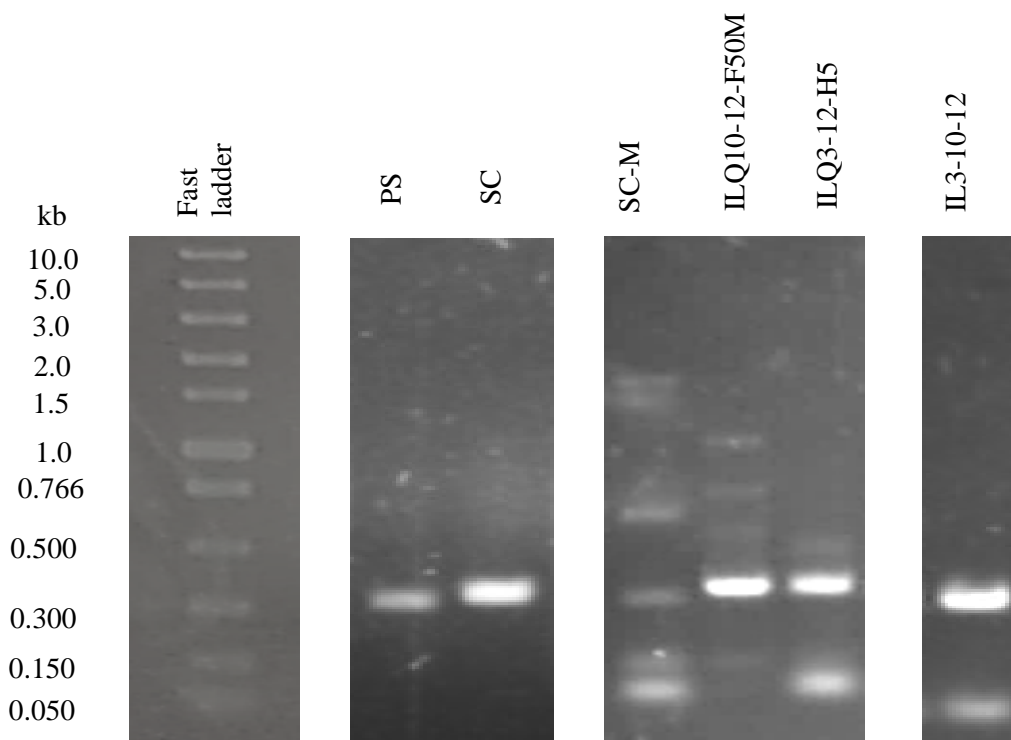


Figure 2. 10. CMV detection by PCR of microdissected BS cells obtained by the LDM system. Each sample represents approximately >100 microdissected BS cells. For agarose gel amplification, the forward primer (F109-1600F/GGAGAGGAATGGGACGTG) and the reverse primer (F109-2000R/GGATCAACGGTAAAGTACG) correspond to the genomic RNA 1 sequence of CMV-SG I. The expected band size was 0.4 kb. The parent lines SC and, PS. Melon pyramided line: IL Q10-12-F50, ILQ3-12-H5 and IL3-10-12-18(64). Fast Ladder=Molecular weight marker, M=Mock-inoculated plant.

Chapter 3

**Construction of Fine Mapping Populations and
Fine Mapping of the QTL *cmvqw3.1* and
*cmvqw10.1***

Chapter 3

Section I: Construction of Fine Mapping Populations

To develop the fine-mapping populations for the two minor QTLs, *cmvqw3.1* and *cmvqw10.1*, we crossed two ILs, on one side, ILQ3-12-H218, carrying the *cmvqw3.1* QTL and the *cmv1* gene, and on the other side, ILQ10-12-F193, carrying the *cmvqw10.1* QTL and *cmv1* gene. This cross was the starting point for selecting recombinant plants carrying at least one minor QTL and the *cmv1* gene, while the other QTL segregates in the F2 generation (Table 3.1. For more details, see Table 1.1.S3, Excel sheet *cmvqw3.1* QTL, and Table 1.2.S3, Excel sheet *cmvqw10.1*).

The heterozygosity of the F1: ILQ3-12-H218 x ILQ10-12-F193 individuals was checked within the two QTLs; for the *cmvqw3.1* QTL we used the flanking markers AI_14-B01 (P=2,804,514 bp) and AI_33_H11 (P=23,616,908 bp) and for the *cmvqw10.1* QTL we used CMPSNP1117 (P=1,122,396 bp) and CMPSNP671 (P=4,747,687) (Table 3.1). In this same F1 plants, the region outside the QTL *cmvqw3.1* around position 24,802,439 bp was heterozygous, while the PS allele was selected in the regions between 25,764,960 and 26,421,885 bp. No genetic contamination was observed in regions outside the *cmvqw10.1* QTL (Table 1.1.S3, sheet *cmvqw3.1* QTL). For the *cmv1* locus on Chr XII, the H allele was present between positions 13,397,309 and 16,256,846 bp and the PS allele was fixed at 24,021,497 bp on Chr XII. In the field, plants were self-pollinated to produce the F2 generation for recombinant selection of the *cmvqw3.1* and *cmvqw10.1* QTLs. For more details see the F1 generation F1: F193 x H218 in the Excel sheet *cmvqw3.1* QTL in Table 1.1.S3 and *cmvqw10.1* in Table 1.2.S3.

Chapter 3-I: Fine mapping populations

Table 3. 1. Genotypes of the F1: ILQ3-12-H218 x ILQ10-12-F193 plants and segregating out the genetic contaminations.

Chr	III					X		XII											
QTL and gene	<i>cmvqw3.1</i>		O			<i>cmvqw10.1</i>		O				<i>cmv1 gene</i>			O				
SNP	FM: AL_14-B01	FM: AL_33_H11	CMPSNP64	Chr3_25764960	CMPSNP979	FM: CMPSNP1117	FM: CMPSNP671	Chr12_251545	Chr12_2391541	Chr12_4268062	Chr12_6122217	Chr12_9319960	SNP: Cmv1	Chr12_9330070	Chr12_9344699	Chr12_11095411	Chr12_13397309	Chr12_16256846	Chr12_24021497
P	2,804,514	23,616,908	24,802,439	25,764,960	26,421,885	1,122,396	4,747,687	251,545	2,391,541	4,268,062	6,122,217	9,319,960	9,320,908	9,330,070	9,344,699	11,095,411	13,397,309	16,256,846	24,021,497
F1-9	H	H	H	PS	PS	H	H	PS	SC	SC	SC	SC	SC	SC	SC	SC	H	H	PS
F1-10	H	H	H	PS	PS	H	H	PS	SC	SC	SC	SC	SC	SC	SC	SC	H	H	PS
F1-11	H	H	H	PS	PS	H	H	PS	SC	SC	SC	SC	SC	SC	SC	SC	H	H	PS
F1-12	H	H	H	PS	PS	H	H	PS	SC	SC	SC	SC	SC	SC	SC	SC	H	H	PS
F1-13	H	H	H	PS	PS	H	H	PS	SC	SC	SC	SC	SC	SC	SC	SC	H	H	PS
F1-14	H	H	H	PS	PS	H	H	PS	SC	SC	SC	SC	SC	SC	SC	SC	H	H	PS
F1-15	H	H	H	PS	PS	H	H	PS	SC	SC	SC	SC	SC	SC	SC	SC	H	H	PS
F1-16	H	H	H	PS	PS	H	H	PS	SC	SC	SC	SC	SC	SC	SC	SC	H	H	PS
F1-17	H	H	H	PS	PS	H	H	PS	SC	SC	SC	SC	SC	SC	SC	SC	H	H	PS
F1-18	H	H	H	PS	PS	H	H	PS	SC	SC	SC	SC	SC	SC	SC	SC	H	H	PS
F1-19	H	H	H	PS	PS	H	H	PS	SC	SC	SC	SC	SC	SC	SC	SC	H	H	PS
F1-20	H	H	H	PS	PS	H	H	PS	SC	SC	SC	SC	SC	SC	SC	SC	H	H	PS
F1-21	H	H	H	PS	PS	H	H	PS	SC	SC	SC	SC	SC	SC	SC	SC	H	H	PS

Chr: Chromosome, O: Out the QTL and the gene, SNP: Single Nucleotide Polymorphism, P: Physical position, FM: Flanking Markers, F1: different plants from the cross ILQ3-12-H218 x ILQ10-12-F193.

- PS: Piel de Sapo
- SC: Songwhan Charmi PI 161375
- H: Heterozygosity
- QTL and *cmv1 gene*
- F1 individuals used for the screen in the F2 generation.

3.1 Recombinant plant selection in the F2 progeny.

2,000 plants from F2: ILQ3-12-H218 x ILQ10-12-F193 were genotyped to develop the two mapping populations for each of the two QTLs. The process followed is depicted in Figure 3.1. For the mapping population of the *cmvqw3.1* QTL, we selected plants with the SC allele in all markers of the *cmvqw10.1* QTL. Conversely, for the mapping population of the *cmvqw10.1* QTL, we selected plants with the SC allele in all markers of the *cmvqw3.1* QTL. Many of these plants were already

Chapter 3-I: Fine mapping populations

recombinant between the flanking markers of the second minor QTL. The combinations chosen were SC-PS, SC-H and vice versa. The combinations of H-PS or PS-H alleles were discarded, as these would only result in susceptible plants since resistance is recessive. Therefore, they would not provide useful information for mapping.

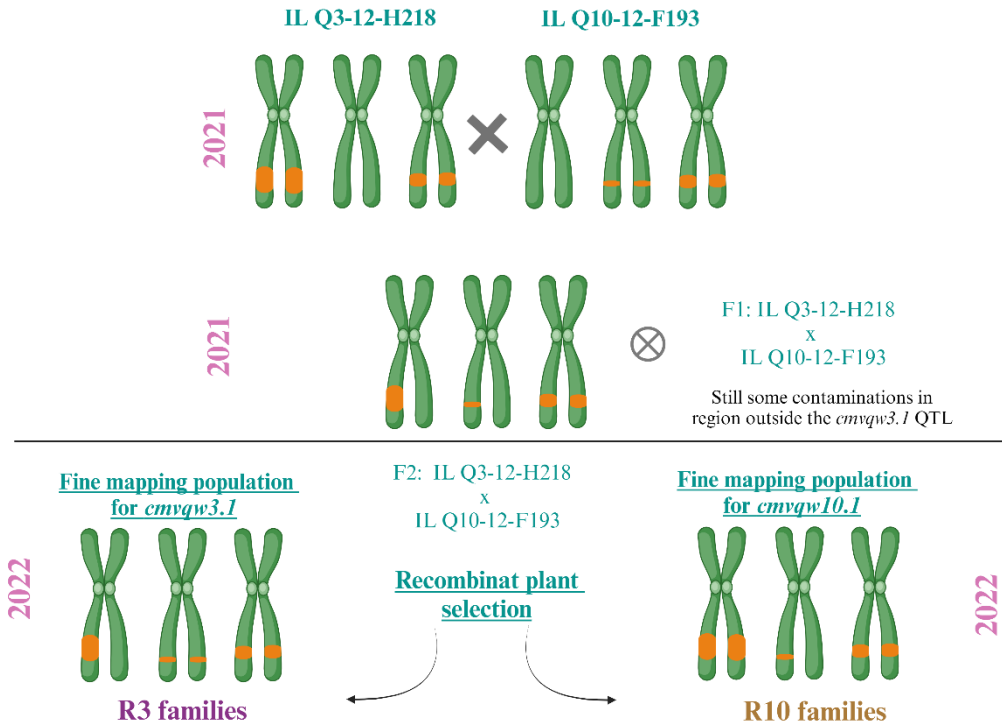


Figure 3. 1. Construction of fine mapping populations for both QTLs *cmvqw3.1* and *cmvqw10.1* and consequently the recombinant plant selection.

To map the *cmvqw3.1* QTL, 20 F2 plants were already recombinants and were selected from this population, called R3 lines. Among these, 15 produced fruits and seeds. To map the *cmvqw10.1* QTL, 52 plants were identified as recombinant from this population and were called R10 families (Table 3.2). From these R10 lines, 45 fruits were produced for the phenotyping assays in the next generation. For both populations, plants with H alleles in the whole segregating QTL were selected as the starting point for generating more recombinants in the next generation and were

Chapter 3-I: Fine mapping populations

named R3-HH and R10-HH, respectively. From the R3-HH progeny, we obtained a further 36 R3 lines with different allele combinations, which were self-pollinated in the field to produce seeds. In the end, we produced seeds of 72 R3 lines from the F2, R3-HH (Table 3.2 and Table 1.1 S3, Excel sheet named *cmvqw3.1* QTL). For the R10 lines, we produced 57 fruits with seeds. Both R3 and R10 lines were ready to perform the phenotyping assays for each fine mapping. (Table 3.2 and Table 1.2 S3, Excel sheet named *cmvqw10.1* QTL).

Table 3. 2. Genotypes of the four groups from the progeny of F2: ILQ3-12-H218 x ILQ10-12-F193 population to select recombinant plants. These groups are R3, R10, R3-HH, and R10-HH.

Chr		III	X	XII				
P (Mb)		20.8	3.62	<i>cmv1 gene</i>				
G (cM)		17.6	27.2	2.2				
QTL and gene		<i>cmvqw3.1</i>	<i>cmvqw10.1</i>	<i>cmv1 gene</i>				
Selected lines	SNP	FM: AI_14- 201	FM: AI_33_H11	FM: CMPSNP1117	FM: CMPSNP671	Chr12_931996 0	SNP: <i>cmv1</i>	Chr12_933007 0
	P	2,804,514	23,616,908	1,122,396	4,747,687	9,319,960	9,320,908	9,330,070
R3	R3-1	SC	PS	SC	SC	SC	SC	SC
	R3-2	SC	H	SC	SC	SC	SC	SC
	R3-3	PS	SC	SC	SC	SC	SC	SC
	R3-4	H	SC	SC	SC	SC	SC	SC
R10	R10-1	SC	SC	SC	PS	SC	SC	SC
	R10-2	SC	SC	SC	H	SC	SC	SC
	R10-3	SC	SC	PS	SC	SC	SC	SC
	R10-4	SC	SC	H	SC	SC	SC	SC
Plants with the H allele in the <i>cmvqw3.1</i> QTL interval		R3-HH	H	H	SC	SC	SC	SC
Plants with the H allele in the <i>cmvqw10.1</i> QTL interval		R10-HH	SC	SC	H	H	SC	SC

Chr: Chromosome, P: Physical position, Mb: Megabase, G: Genetic position, cM: Centimorgan, SNP: Single Nucleotide Polymorphism, FM: Flanking Markers.

■ PS: Piel de Sapo

■ SC: Songwhan Charmi PI 161375,

■ H: Heterozygosity

■ QTL and *cmv1* gene.

Section II: Fine mapping of the QTL *cmvqw3.1*

3.2 Genotyping and phenotyping of R3 families

The length of SC introgression in each R3 family was assessed by genotyping to identify putative recombination points (as described in the current Chapter Section I). The interval is physically large (20.81 Mb) and contains up to 1040 genes. Due to the large size of the interval, we genotyped with internal markers to cover the entire region. The R3 lines were then divided into groups containing recombination points at markers AI_14-B01 (P = 2,804,514 bp) and AI_33_H11 (P = 23,616,908 bp) (Figure 3.3A). Hence, we made those groups to discard one-half of the introgression and focus on the informative R3 families recombinant in the informative interval.

Two sets of phenotyping assays were performed, both based on visual symptoms taken from 7 to 28 dpi and scored on a scale of infection severity from 0 and 5, as in Chapter 2. Phenotyping refers to the severity and velocity of infection observed in individual plants from the progeny of R3 families (we can also refer to this as infection levels). Due to the slow appearance of symptoms on the leaves, we scored them approximately every 3 to 5 dpi. Infected plants showed two types of symptoms: mosaic and necrosis. Mosaic symptoms included mild and severe mosaics, curled leaves, and, sometimes, dwarf plants, which are typical symptoms of melon plants susceptible to CMV (as shown in Figure 3.2A). In addition, we observed necrosis on the leaf, vein (all vein types), petiole, and stem. Necrosis symptoms almost always followed mosaic symptoms (see Figure 3.2B), but occasionally some individual plants showed necrotic tissue in most organs with almost no mosaic symptoms. Necrosis occasionally caused some plants to die around 26-28 dpi.



Figure 3. 2. **A)** Plant with typical viral symptoms characterized by a mosaic pattern on the leaves, which gradually develops into leaf curling. **B)** Plant with a combination of mosaic symptoms and necrosis in veins and petioles. These images represent individual plants of the R3-62 family at 28 dpi.

The resistant IL 3-10-12-18(64) and the susceptible (IL Q10-12-F50) controls were phenotyped in all experimental assays. The first R3 families genotyped and phenotyped were R3-108, R3-115, R3-78, R3-62, R3-61, R3-113, R3-134, and R3-143 (see Figure 3.3A and for more details, the Excel file sheet *cmvqw3.1* QTL in Table 1.1 S3).

A

Chr	III									X		XII			Mosaic (%)	Necrosis (%)	
	<i>cmvqw3.1</i>									O	<i>cmvqw10.1</i>		<i>cmv1 gene</i>				
P											FM: CMPSNP1117	FM: CMPSNP671	Chr12_9319960	SNP: <i>cmv1</i>	Chr12_9330070		
SNP	AL_14_B01	CMPSNP307	CMPSNP9	CMPSNP260	CMPSNP316	CMPSNP556	CMPSNP543	AL_33_H11	CMPSNP64								
Melon lines	2,804,514	3,386,271	8,331,515	9,859,048	15,166,216	21,840,665	23,170,306	23,616,908	24,802,439	1,122,396	4,747,687	9,319,960	9,320,908	9,330,070			
18(64)	SC	SC	SC	SC	SC	SC	SC	SC	SC	SC	SC	SC	SC	SC	9,9	9,9	
F50	PS	PS	PS	PS	PS	PS	PS	PS	PS	SC	SC	SC	SC	SC	30,0	26,7	
R3-108	PS	H	H	H	H	H	H	H	H	SC	SC	SC	SC	SC	87,5	75,0	
R3-115	H	H	H	H	H	SC	SC	SC	SC	SC	SC	SC	SC	SC	21,4	21,4	
R3-78	H	H	H	H	SC	SC	SC	SC	PS	SC	SC	SC	SC	SC	71,4	64,3	
R3-62	PS	H	SC	SC	SC	SC	SC	SC	SC	SC	SC	SC	SC	SC	81,8	81,8	
R3-61	H	H	SC	SC	SC	SC	SC	SC	SC	SC	SC	SC	SC	SC	21,4	7,1	
R3-113	SC	SC	H	H	H	H	H	H	H	SC	SC	SC	SC	SC	41,7	58,3	
R3-134	SC	SC	PS	PS	PS	PS	PS	PS	PS	SC	SC	SC	SC	SC	30,8	34,6	
R3-143	H	SC	SC	SC	SC	SC	SC	SC	SC	SC	SC	SC	SC	SC	29,2	12,5	

B

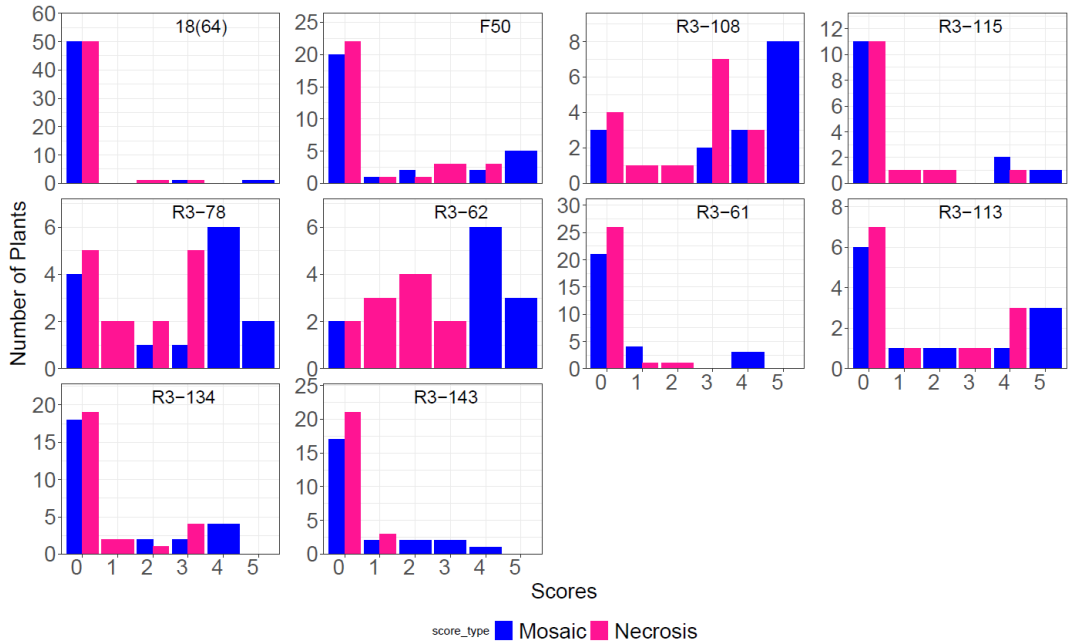


Figure 3.3. A) Genotyping results of informative R3 families of the first set of phenotyping. Chr: Chromosome, P: Physical position, O: Out of the QTL SNP: Single Nucleotide Polymorphism, FM: Flanking Markers, B) Scores and rate of mosaic and necrosis of R3 families phenotyped at 28 dpi.

- PS: Piel de Sapo
- H: Heterozygosity
- SC: Songwhan Charmi PI 161375,
- QTL and *cmv1* gene.

Chapter 3: Fine mapping of QTL *cmvqw3.1*

The controls and the R3 families showed mosaic and necrosis symptoms as shown in Figure 3.3B. The scale of mosaic was from 0 to 5 and necrosis from 0 to 4 as described in Materials and Methods, Section 3.4. The IL Q10-12-F50 showed all infection scores with only 30% of plants infected and the higher scores reached were 4 and 5, achieved at 28 dpi. When present, necrotic tissue was also found in all organs, scoring from 1 to 4 and some individual IL Q10-12-F50 plants were almost dead (score 3) or dead (score 4). Only a few plants of IL 3-10-12-18(64) showed a low percentage of mosaic and necrosis (9.9%). Regarding the results of the infections shown by the R3 families, we observed different infections reached at 28 dpi. The families R3-108, R3-78 and R3-62 behaved similarly in terms of mosaic and necrosis, with high scores. The R3-113 showed a lower percentage of mosaic compared to them. R3-115 and R3-61 behaved similarly in terms of mosaic but the R3-115 presented three times more necrosis than R3-61. In addition, R3-134 showed similar percentages of mosaic and necrosis, reaching high scores in both whereas R3-143 reached medium to low scores in both mosaic and necrosis (Figure 3.3).

Additionally, we plotted the mosaic score results achieved by individual plants of the R3 families at different time points to see the infection trend of each family (Figure 3.4). The time points to record the infections had been selected every 3-4 days because the symptoms of infection develop slowly and do not appear until at least 9 dpi. The selected time points were 9, 13, 16, 20, 24 and 28 dpi. The R3 families were statistically analysed using the mosaic scores achieved by individual plants per family at each time point to see the trend of mosaic infections achieved by family. The statistical analysis was the same as we applied in Chapter 2 because all mosaic scores followed non-parametric data. The statistical analyses showed at 24 dpi that the family R3-108 was significantly different (p -value <0.05) from the resistant line IL 3-10-12-18(64). Nevertheless, the families R3-78 and R3-62 together with the R3-108 were significantly different at 28 dpi. There were no

significant differences (p-value >0.05) between the R3 families and the resistant IL 3-10-12-18(64) before the 24 dpi.

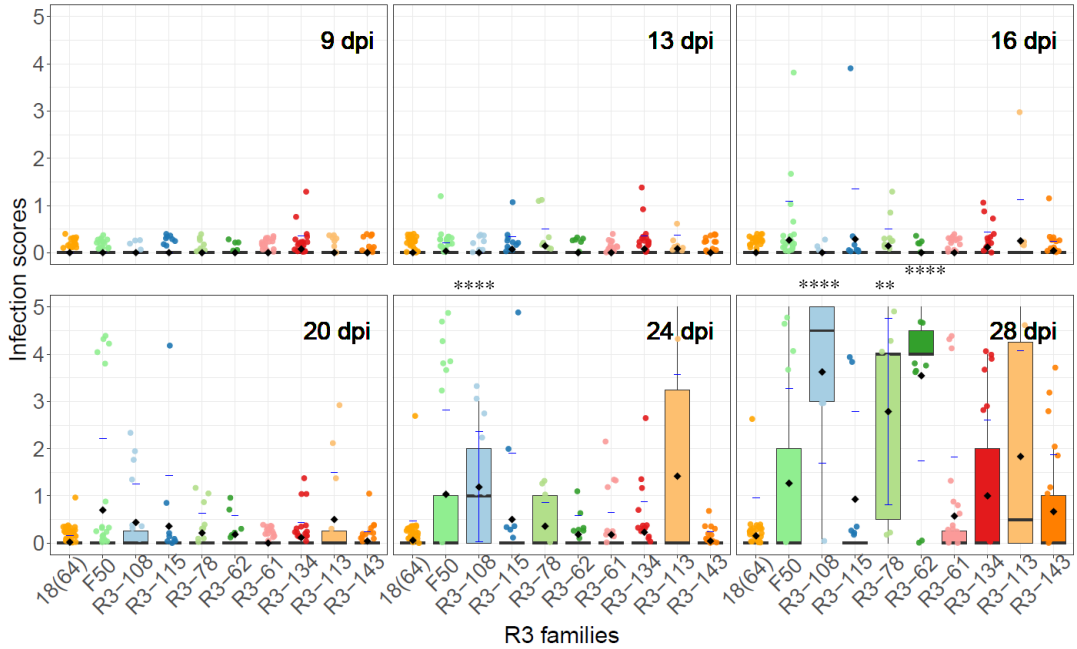


Figure 3. 4. The first set of phenotyping results of each R3 family based on the scores of mosaics considering the time points 9, 13, 16, 20, 24, 28 dpi. The number of biological replicates was between 12 to 52 individuals per melon family. Each dot represents the replicate distributed along the graph using the `position_jitterdodge()` function of RStudio version 2024.04.2+764. The black diamond indicates the average infection reached by the family at each time point. The blue error indicates the standard deviation (SD) of each family and the black line represents the median of each R3 family. Each box corresponds to 25 to 75% of the data. Significant differences compared to IL 3-10-12-18(64) are marked with asterisks (p-values *<0.05, **<0.005, ***<0.0005, ****<0.00005).

The preliminary phenotyping results allowed the first association of genotyping and phenotyping through visual pair comparisons. For the association, we only considered the mosaic symptoms, not the necrosis symptoms. We decided to follow the pattern of PS infection with mosaics, as PS does not follow the pattern of necrosis. According to the first set of phenotypes, strong mosaic infections are present when the PS allele is present on the left side of the interval, between the markers AI_14-B01 and CMPSNP9. Hence, the data appeared to discard the right

Chapter 3: Fine mapping of QTL *cmvqw3.1*

side of the interval, between markers CMPSNP9 and the flanking marker AI_33_H11. Therefore, the gene behind the QTL should map to the left of the marker CMPSNP9, between 2,804,514 and 8,331,515 bp as shown in Figure 3.5. Thus, we focused on developing more markers and phenotyping more R3 lines only on the left side of the QTL interval, where the putative gene (s) can be located.

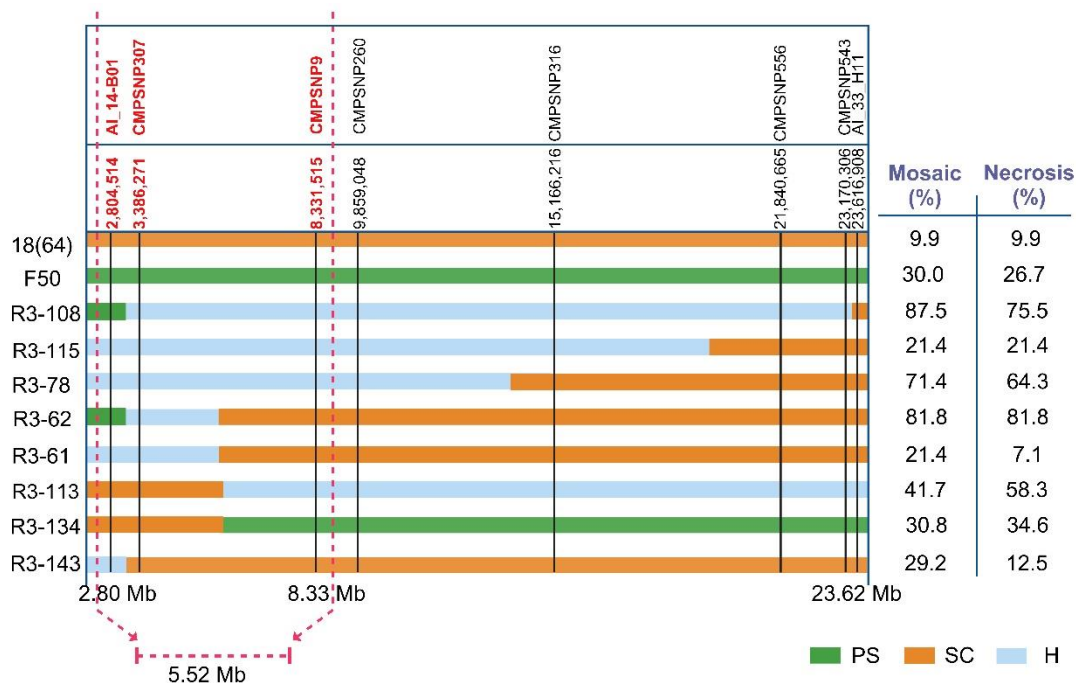


Figure 3. 5. Preliminary mapping association of genotypes and phenotypes by visual paired comparisons of genotypes from eight R3 families.

Thus, we selected for the second set of phenotyping new R3 families: R3-57, R3-53, R3-48, R3-69, R3-56, R3-214, and R3-121 carrying different recombination points in the region between 2,804,514 and 8,331,515 bp (Figure 3.6A). These new R3 lines were genotyped with new SNPs to increase the resolution of the introgression in the relevant interval. For more details on the new R3 lines, see the Excel sheet named *cmvqw3.1* QTL in Table 1.1 S3. The infection results in this second set of phenotypes generally showed infections with lower scores than in the first set of phenotyping

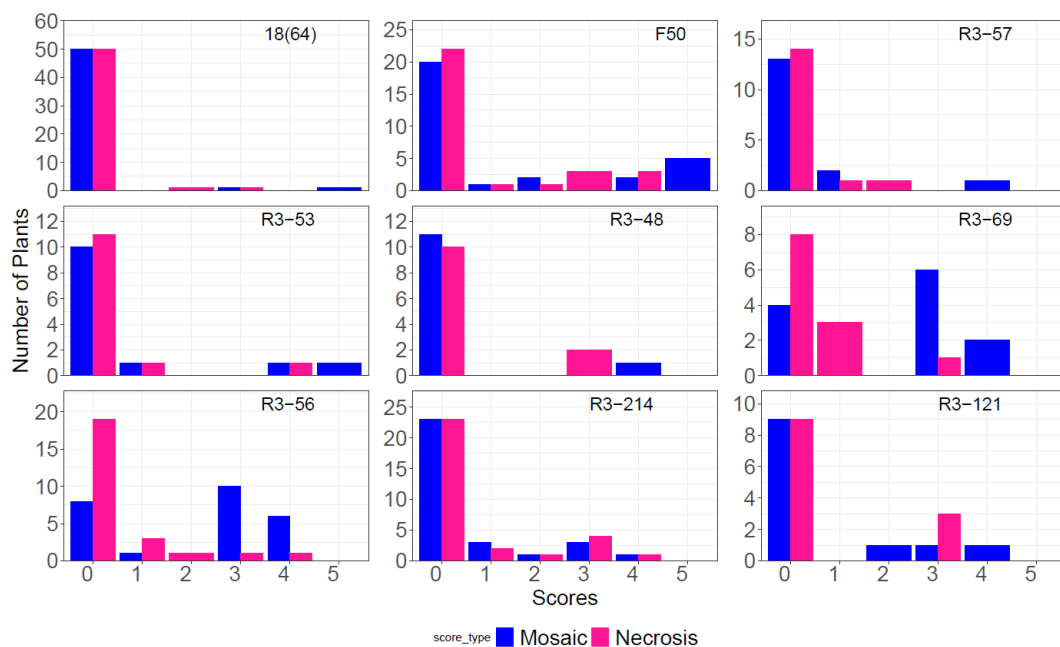
Chapter 3: Fine mapping of QTL *cmvqw3.1*

(Figure 3.6B). R3-56 and R3-69 showed similar mosaics with high scores and necrosis with low and high scores. R3-53, R3-214 and R3-121 showed similar numbers of plants affected by mosaics and necrosis. R3-57 and R3-48 showed low levels of mosaic and necrosis (<20%) with high scores only in a few plants

A





Chr P	III													X		XII		Mosaic (%)	Necrosis (%)	
	<i>cmvqw3.1</i>													O	<i>cmvqw10.1</i>	<i>cmv1 gene</i>				
SNP	AL_14-B01	CMPSNP307	PS_09-H05	CMPSNP31	Chr03_5417850	chr03_5703825	chr03_6087025	CMPSNP918	Chr03_6308614	Chr03_6390744	chr03_6898329	CMPSNP9	CMPSNP64	FM: CMPSNP1117	FM: CMPSNP671	Chr12_9319960	SNP: cmv1	Chr12_9330070		
Melon lines	2,804,514	3,386,271	4,756,219	5,307,083	5,417,850	5,703,825	6,087,025	6,150,771	6,308,614	6,390,744	6,898,329	8,331,515	24,802,439	1,122,396	4,747,687	9,319,960	9,320,908	9,330,070		
18(64)	SC	SC	SC	SC	SC	SC	SC	SC	SC	SC	SC	SC	SC	SC	SC	SC	SC	SC	11,3	9,9
F50	PS	PS	PS	PS	PS	PS	PS	PS	PS	PS	PS	PS	PS	SC	SC	SC	SC	SC	30,0	26,7
R3-57	PS	PS	PS	PS	PS	PS	PS	PS	PS	PS	PS	PS	SC	SC	SC	SC	SC	SC	18,8	12,5
R3-53	H	H	-	PS	PS	PS	PS	PS	PS	PS	PS	SC	SC	SC	SC	SC	SC	SC	23,1	15,4
R3-48	PS	PS	PS	PS	PS	PS	PS	PS	PS	PS	PS	SC	SC	SC	SC	SC	SC	SC	16,7	16,7
R3-69	PS	PS	PS	PS	PS	PS	PS	PS	PS	PS	SC	SC	SC	SC	SC	SC	SC	SC	66,7	33,3
R3-56	PS	PS	H	H	H	H	H	H	H	H	SC	SC	SC	SC	SC	SC	SC	SC	68,0	28,0
R3-214	PS	PS	PS	PS	PS	PS	SC	SC	SC	SC	SC	SC	SC	SC	SC	SC	SC	SC	29,0	25,8
R3-121	SC	SC	SC	SC	SC	H	H	H	H	H	H	H	H	SC	SC	SC	SC	SC	25,0	25,0

B



Chapter 3: Fine mapping of QTL *cmvqw3.1*

Figure 3. 6. A) Genotyping results of informative R3 families of the second set of phenotyping. Chr: Chromosome, P: Physical position, O Out of the QTL, SNP: Single Nucleotide Polymorphism, FM: Flanking Markers. **B)** Score of mosaics and necrosis of phenotyped R3 families at 28 dpi.

- | | |
|--|---|
|  PS: Piel de Sapo |  H: Heterozygosity |
|  SC: Songwhan Charmi PI 161375, |  QTL and <i>cmv1</i> gene. |

Also, we analysed statistically the mosaic score achieved at each time point. This analysis showed that at 16 dpi R3-56 was significantly different compared to IL 3-10-12-18(64) (p-value <0.05). However, at 20 dpi and 24 dpi, most families, including some individual plants of IL 3-10-12-18(64), displayed mosaic symptoms. Consequently, R3-56 did not show a significant difference (p-value > 0.05) at these time points. Significance was not observed again until 28 dpi, at which time R3-56, together with R3-69, became significant (Figure 3.7).

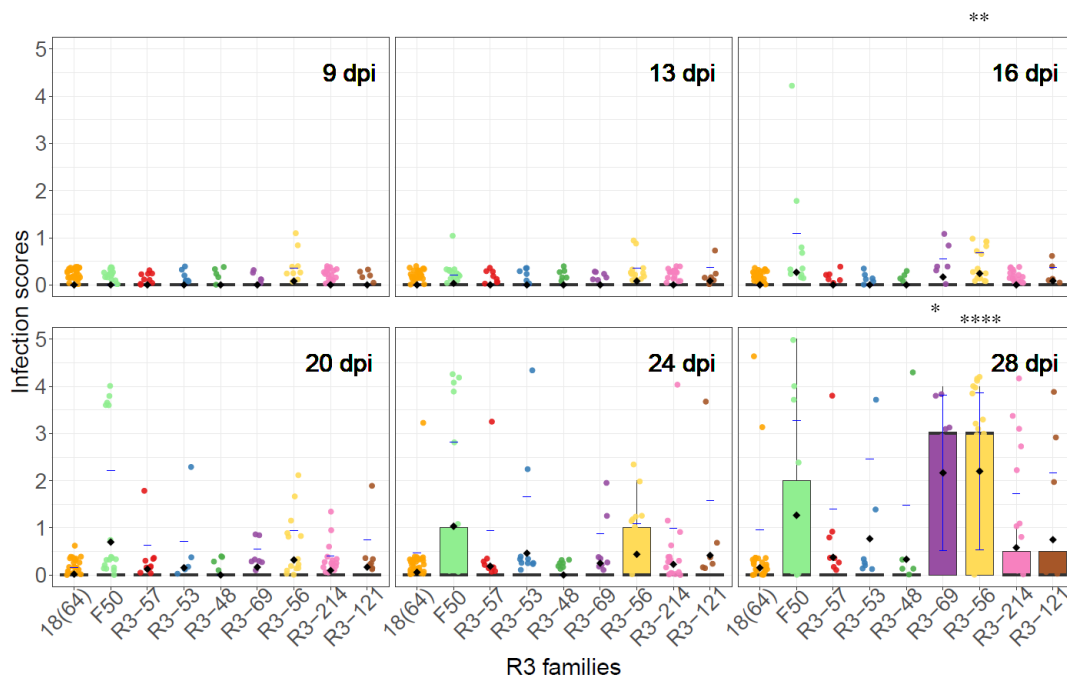


Figure 3. 7. The second set of phenotyping results of each R3 family based on the scores of mosaics considering the time points 9, 13, 16, 20, 24, and 28 dpi. The number of biological replicates was 12 to 52 individuals per melon family. Each dot represents the replicate distributed along the graph using the position_jitterdodge() function of RStudio version 2024.04.2+764. The black diamond indicates the average infection reached by the family at each time point. The blue error indicates the standard deviation (SD) of each family and the black line represents the median of each R3 family. Each box corresponds to 25 to 75% of the data. Significant differences compared to IL 3-10-12-18(64) are marked with asterisks (p-values * <0.05 , ** <0.005 , *** <0.0005 , **** <0.00005).

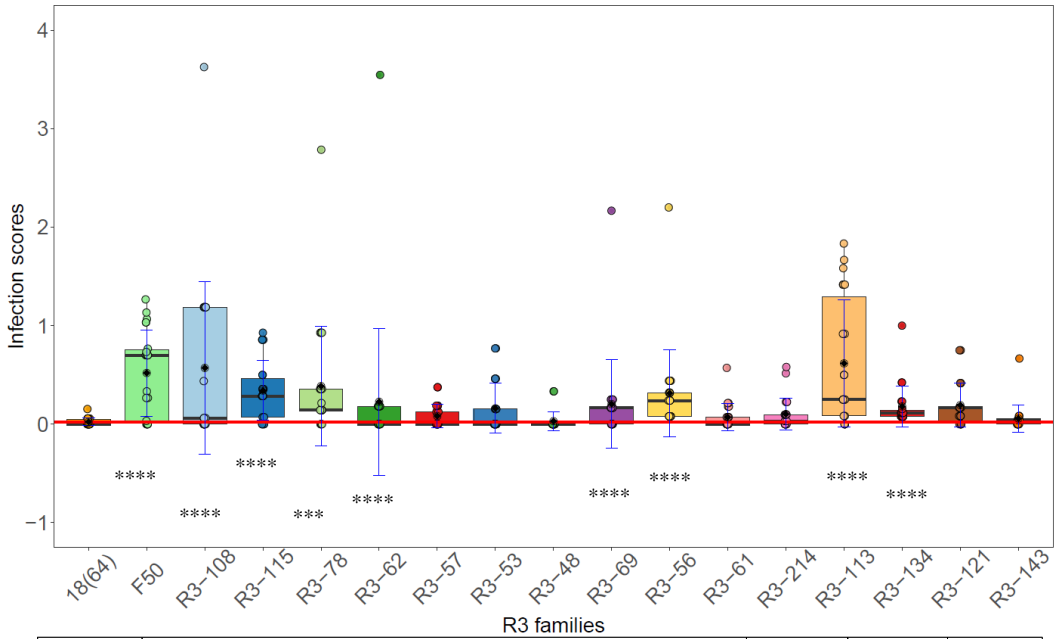
To assess the resistance and susceptibility of the R3 families, we analysed the mosaic scores using statistical analyses over time. However, we cannot consider only the analysis of the 28 dpi time point, as we had done previously to analyse the phenotyping results. In addition, as we have seen in the results per time point, we actually do not see a statistically significant difference between the resistant IL 3-10-12-18(64) and IL Q10-12-F50 at any fixed time point. This is because the infections in the R3 families and the controls were very complex during the time.

For that reason, we analysed the 15 phenotyped R3 families to determine whether they are resistant and susceptible considering the mosaic score over time.

Chapter 3: Fine mapping of QTL *cmvqw3.1*

Specifically, the statistical analyses used the mean of the score at each dpi per family group. Significant differences (p-value <0.05) compared to the resistant line IL 3-10-12-18(64) were considered susceptible. The results showed that the positive control IL Q10-12-F50 was significantly different in comparison with the resistant line (p-value<0.05). In addition, the R3 families R3-108, R3-78, R3-62, R3-69, R3-56, R3-113 and R3-134 and R3-115 (p-value<0.05) were considered susceptible compared to IL 3-10-12-18(64). The R3 families R3-121, R3-143, R3-214, R3-48, R3-53, R3-57, and R3-61, were considered resistant since they showed no significant differences (p-value>0.05) with IL 3-10-12-18(64) (see Figure 3.8A). The final genotype of all lines is shown in Figure 3.8B.

A



B

Chr	III																X		XII		Phenotype			
	<i>cmvqw3.1</i>																O	<i>cmvqw10.1</i>	<i>cmv1 gene</i>					
P																								
SNP	AL_14-B01	CMPSNP307	PS_09-H05	CMPSNP31	Chr03_5417850	chr03_5703825	chr03_6087025	CMPSNP918	Chr03_6308614	Chr03_6390744	chr03_6898329	CMPSNP9	CMPSNP260	CMPSNP316	CMPSNP556	CMPSNP543	AL_33_H11	CMPSNP64	FM: CMPSNP111	FM: CMPSNP671	Chr12_9319960	SNP: cmv1	Chr12_9330070	
Melon lines	2,804,514	3,386,271	4,756,219	5,307,083	5,417,850	5,703,825	6,087,025	6,150,771	6,308,614	6,390,744	6,898,329	8,331,515	9,859,048	15,166,216	21,840,665	23,170,306	23,616,908	24,802,439	1,122,396	4,747,687	9,319,960	9,320,908	9,330,070	
18(64)	SC	SC	SC	SC	SC	SC	SC	SC	SC	SC	SC	SC	SC	SC	SC	SC	SC	SC	SC	SC	SC	SC	SC	R
F50	PS	PS	PS	PS	PS	PS	PS	PS	PS	PS	PS	PS	PS	PS	PS	PS	PS	PS	SC	SC	SC	SC	SC	S
R3-108	PS	H	H	H	H	H	H	H	H	H	H	H	H	H	H	H	H	SC	SC	SC	SC	SC	SC	S
R3-115	H	H	H	H	H	H	H	H	H	H	H	H	H	H	SC	SC	SC	SC	SC	SC	SC	SC	SC	S
R3-78	H	H	H	H	H	H	H	H	H	H	H	H	H	SC	SC	SC	SC	SC	SC	SC	SC	SC	SC	S
R3-62	PS	H	H	H	H	H	H	H	H	H	H	SC	SC	SC	SC	SC	SC	SC	SC	SC	SC	SC	SC	S
R3-57	PS	PS	PS	PS	PS	PS	PS	PS	PS	PS	PS	SC	SC	SC	SC	SC	SC	SC	SC	SC	SC	SC	SC	R
R3-53	H	H	-	PS	PS	PS	PS	PS	PS	PS	PS	SC	SC	SC	SC	SC	SC	SC	SC	SC	SC	SC	SC	R
R3-48	PS	PS	PS	PS	PS	PS	PS	PS	PS	PS	PS	SC	SC	SC	SC	SC	SC	SC	SC	SC	SC	SC	SC	R
R3-69	PS	PS	PS	PS	PS	PS	PS	PS	PS	PS	SC	SC	SC	SC	SC	SC	SC	SC	SC	SC	SC	SC	SC	S
R3-56	PS	PS	H	H	H	H	H	H	SC	SC	SC	SC	SC	SC	SC	SC	SC	SC	SC	SC	SC	SC	SC	S
R3-61	H	H	H	H	H	H	H	H	SC	SC	SC	SC	SC	SC	SC	SC	SC	SC	SC	SC	SC	SC	SC	R
R3-214	PS	PS	PS	PS	PS	PS	SC	SC	SC	SC	SC	SC	SC	SC	SC	SC	SC	SC	SC	SC	SC	SC	SC	R
R3-113	SC	SC	H	H	H	H	H	H	H	H	H	H	H	H	H	H	H	SC	SC	SC	SC	SC	SC	S
R3-134	SC	SC	SC	SC	H	H	H	H	PS	PS	PS	PS	PS	PS	PS	PS	PS	SC	SC	SC	SC	SC	SC	S
R3-121	SC	SC	SC	SC	SC	H	H	H	H	H	H	H	H	H	H	H	H	SC	SC	SC	SC	SC	SC	R
R3-143	H	SC	SC	SC	SC	SC	SC	SC	SC	SC	SC	SC	SC	SC	SC	SC	SC	SC	SC	SC	SC	SC	SC	R

Figure 3. 8. A) Phenotyping results for each R3 family, based on infection levels from 7 to 28 dpi. The dots represent the mean score of all individuals at each dpi and are distributed along the graph using the position_jitterdodge() function of RStudio version 2024.04.2+764. The red solid line indicates the average infection of the IL 3-10-12-18(64) line over time.

Chapter 3: Fine mapping of QTL *cmvqw3.1*

The black diamond inside each box represents the average infection level, and the black line represents the median of each R3 family. Each box corresponds to 25 to 75% of the data. Significant differences from IL 3-10-12-18(64) indicating susceptibility are indicated by asterisks (p-values $* < 0.05$, $** < 0.005$, $*** < 0.0005$, $**** < 0.00005$). **B)** Genotyping results of R3 plants used for phenotyping assays with CMV-M6. Chr: Chromosome, P: Physical position, O: Out of the QTL SNP: Single Nucleotide Polymorphism, FM: Flanking Markers.

- | | |
|---------------------------------|----------------------------|
| ■ PS: Piel de Sapo | ■ R: Resistant line |
| ■ SC: Songwhan Charmi PI 161375 | ■ S: Susceptible line |
| ■ H: Heterozygosity | ■ QTL and <i>cmv1</i> gene |

3.3 Genotyping and Phenotyping association of *cmvqw3.1*

QTL

Overall, 15 R3 families were phenotyped and used to perform the fine-mapping association analysis to identify the target interval (Figure 3.9A). Hence, the susceptible R3 families were the most useful for understanding the fine-mapping association. The *cmvqw3.1* QTL spans a 17.6 cM interval in genetic distance and 20.81 Mb physical distance, with 1,040 genes within the interval. Fine mapping association with the target interval was performed by associating the genotype vs phenotype results from all experiments (Figure 3.9). Then, to provide a comprehensive association analysis, we selected six different time points to assess the association and to detect SNPs significantly associated with the phenotype. As we explained above in the first set of phenotyping, the time points chosen were: 9, 13, 16, 20, 24, and 28 dpi. Due to the complexity of the infection outcomes, we performed several analyses to narrow down the target interval considering the time points. First, two contingency tables (2x2) were constructed, with the phenotypes distributed in two columns (resistance and susceptibility) and the genotypes in two rows (SC allele and PS+H). The plant with a score of 0 was considered resistant (R) whereas plants with a score of 1-2-3-4-5 were considered susceptible. The contingency table provides the frequency distribution of resistant and susceptible genotypes at each physical location of the SNPs when it has the susceptible allele (PS+H alleles) compared to the resistant allele (SC allele) at all time points. Thus,

Chapter 3: Fine mapping of QTL *cmvqw3.1*

the SNP was significant if the distribution was significantly different. In the beginning, PS was considered the susceptible control of all infections coming from CMV-M6. For precision, we performed all analyses using infection results with and without PS to check if the strong and early PS infections were masking any association. We consistently used Fisher tests for two types of analysis: 1) Fisher with PS infections, and 2) Fisher without PS infections. Association analysis including results of PS infections was inconclusive as all SNPs were significant at all time points. Thus, the general significance complicated the identification of specific QTL intervals associated with resistance. As shown in Chapter 2, PS is significantly different (p-value <0.05) from the lines harbouring one QTL and the *cmv1* gene, providing a much higher susceptibility that masked the results of the real significant SNP. Therefore, we focused on performing the Fisher test analyses without including PS infection results and using IL Q10-12-F50 as a susceptible control for this fine mapping, which showed the closest susceptibility to the recombinant lines since both carry the QTL *cmvqw10.1* and *cmv1* gene, but not QTL *cmvqw3.1*.

The fine mapping association is shown in Figure 3.9B, where the significant SNPs (p-value<0.05) at each time point 9, 13, 16 and 20 dpi indicate the putative intervals. The data from 24 and 28 dpi were not informative as the majority of R3 plants were already infected at these times and almost all SNPs were significant (p-values <0.05). Thus, we excluded 24 and 28 dpi in these analyses. Since in this fine mapping, we are working with a gene that delays virus transport, resistance may be lost at late time points due to sufficient virus accumulation to produce a phenotype. Finally, the statistical results of the association showed two possible target intervals based on the significant SNPs of 16 and 20 dpi: one interval between positions 5,307,083 and 5,703,825 bp and the other between 8,331,515 and 23,616,908 bp. No associations (p-value>0.05) were found between intervals 2,804,514 and 4,756,219 and intervals

Figure 3. 9. A) Genotypes of 15 R3 families and the positive (IL Q10-12-F50) and the negative (IL 3-10-12-18(64) controls. The molecular markers are distributed along the interval based on their physical position. The red markers indicate statistically significant SNPs and the black ones mean no association. The red dashed lines mean the fine mapping association. R: Resistant, S: Susceptible, Mb: Megabase **B)** Fine mapping association of the *cmvqw3.1* performed in different time points 9, 13, 16 and 20 dpi of infection scores. The X-axis shows the evenly distributed physical positions of SNPs within the *cmvqw3.1* interval, while the Y-axis shows $-\log_{10}(\text{p-value})$. The horizontal black line indicates a significance threshold of $\text{p-value}=0.05$.

Further narrowing down the intervals could not be carried out because we did not have time to phenotype enough R3 families carrying different recombination points in the regions 5,307,083 to 5,703,825 bp and 8,331,515 to 23,616,908 bp. Further phenotyping assays with R3 families carrying recombination points within the first or second intervals are required. So far, we have narrowed down the interval from 20.81 Mb to 0.39 Mb for the first interval. For the second interval, we have narrowed the interval down to 15.28 Mb. In our fine mapping, we initially focused on the left interval (AI-14-B01 and CMPSNP9 molecular markers) because the first association data suggested that this was the primary region of interest. This interval appeared to be more clearly defined, so we developed markers and selected R3 families with recombination in that interval. However, the association analysis later revealed the presence of the second putative interval. Unfortunately, we did not have enough time to investigate the second putative interval in detail. Therefore, there might be two or more genes in the QTL *cmvqw3.1* that play a minor role with the *cmv1* gene in the resistance to CMV-M6.

1.7 3.4 Candidate genes of *cmvqw3.1* QTL.

The first interval, between positions 5,307,083 and 5,703,825 bp contains 25 annotated genes (see Table 3.3). To get an overview of the potential candidate genes, we compared structural variations in the coding sequences between the SC (reference genome) and PS genome annotations.

Chapter 3: Fine mapping of QTL *cmvqw3.1*

Table 3. 3. List of candidate genes of the first interval of *cmvqw3.1* between 5,307,083 and 5,703,825 bp in the melon genome annotation and structural variations in PS. The genes are annotated in the melon genome assembly version V4.0 and V3.6.1 In blue are the two candidate genes for the QTL *cmvqw3.1*.

Gene ID	Description in Songwham Charmi accession	Small variants SC/PS	Marker SNP	Physical position V3.6.1	Physical position V4.0
MELO3C008392.2.1	Mitochondrial_carrier_protein,_putative	SNP	CMPSNP31	5,307,083	5,313,909
MELO3C029848.2.1	Unknown_protein	SNP			
MELO3C008394.2.1	L-type_lectin-domain_containing_receptor_kinase_S.6	SNP			
MELO3C008396.2.1	Unknown_protein	SNP			
MELO3C029975.2.1	NBS-LRR_type_resistance_protein	-			
MELO3C008397.2.1		-			
MELO3C008398.2.1	protein_MKS1-like	-			
MELO3C016646.2.1	maker-chr03-exonerate_est2genome-gene-54.2-mRNA-1	-	Chr03_5417850	5,417,850	5,423,140
MELO3C008400.2.1	Dof_zinc_finger_protein	SNP			
MELO3C008403.2.1	glycolipid_transfer_protein_3-like	-			
MELO3C008404.2.1	Pathogen-related_protein	SNP			
MELO3C008405.2.1	Protein_LAZ1_homolog_1	SNP			
MELO3C008406.2.1	Vacuolar_protein_sorting_45	SNP			
MELO3C008407.2.1	Hexosyltransferase	SNP			
MELO3C008408.2.1	Ribosome_maturation_factor_RimP	SNP			
MELO3C008410.2.1	Carboxypeptidase	-			
MELO3C000105.2.1	maker-chr03-exonerate_est2genome-gene-55.3-mRNA-1	-			
MELO3C027328.2.1	maker-chr03-exonerate_est2genome-gene-55.4-mRNA-1	SNP			
MELO3C035478.2.1	maker-chr03-exonerate_est2genome-gene-56.48-mRNA-1	SNP			
MELO3C029854.2.1	maker-chr03-exonerate_est2genome-gene-56.51-mRNA-1	SNP			
MELO3C008413.2.1	Acyl-[acyl-carrier-protein]_desaturase	SNP			
MELO3C008414.2.1	Transcription_elongation_factor_SPT5	SNP			
MELO3C029984.2.1	Vacuolar_protein_sorting-associated_protein_33-like_protein	SNP			
MELO3C032494.2.1	maker-chr03-exonerate_est2genome-gene-56.71-mRNA-1	-			
MELO3C008415.2.1	Exostosin_family_protein	SNP			
MELO3C008416.2.1	Unknown_protein	SNP	Chr03_5703825	5,703,825	5,705,564

Chapter 3: Fine mapping of QTL *cmvqw3.1*

We found that 18 out of 25 annotated genes have SNPs in their coding sequences. All SNPs used for the mappings were present in the genome version v3.6.1. However, some genes in this list have some INDELs in v3.6.1 that we did not find in the genome version v4.0. Hence, we decided to use v4.0 the latest melon genome assembly and annotation version to analyse the candidate genes. Among 18 annotated genes, there are two candidate genes whose function is related to intracellular movement, and therefore, could be related to VPS41, a Vacuolar Protein Sorting 45 (VPS45) (Gene ID MELO3C008406.2.1) and a Vacuolar Protein Sorting Associated Protein 33 Like Protein (VPS33) (Gene ID MELO3C029984.2.1).

VPS45 is involved in protein trafficking to the vacuole, probably at the level of vesicle fusion at the trans-Golgi network (TGN), and not in trafficking from the TGN to the pre-vacuolar compartment. In mammals, VPS45 also plays a critical role in regulating trafficking through the endosomal system (Frey et al., 2021). In contrast, VPS33 is a subunit of the Class C Core Endosomal Vacuole Tethering (CORVET) and of the Homotypic Fusion and Vacuole Protein Sorting (HOPS) complex, which interact with soluble N-ethylmaleimide-sensitive Factor Attachment Protein Receptors (SNARE) proteins, which facilitate all fusion events essential for vesicle maturation and endosomal trafficking (Sato et al., 2000; Zhang and Hughson, 2021). The VPS33, as part of the Vacuolar Protein Sorting (VPS) core (VPS-C) of the CORVET complex, affects the endosomal biogenesis and vacuole morphology (Balderhaar and Christian Ungermann 2013). VPS41 is in the HOPS complex, but not in CORVET and helps endosomal/lysosomal membranes fusion for transport of cargo proteins (Wang et al., 2011). VPS33 and VPS41 accumulate in late endosomes and together they mediate protein trafficking. The lack of any of them could affect the vacuole morphology and function and compromise plant viability. VPS41 is also located in the tonoplast (Brillada et al., 2018; Real et al., 2023).

Chapter 3: Fine mapping of QTL *cmvqw3.1*

We analysed the SNPs located in the exons between SC (genome reference) and PS (genome alternative) using the JBrowse (v4.0) for both candidates. The CmVPS45 gene expands by 5,927 bp with 13 exons and 12 introns and the coding sequence expands by 1,707 bp. There are SNPs in the coding sequence of VPS45 at positions of 921 bp (T/C) and 1,059 bp (A/G) in exons seven and eight respectively. The protein CmVPS45 has a length of 568 amino acids (64,8 kDa). The two SNPs in its coding sequence were synonymous. Hence, there was no change of amino acid between PS and SC proteins that could explain the resistance given by the QTL *cmvqw3.1* (Figure 3.10A). For further sequence information, check Table 1.1.S3 Excel sheet VPS45.

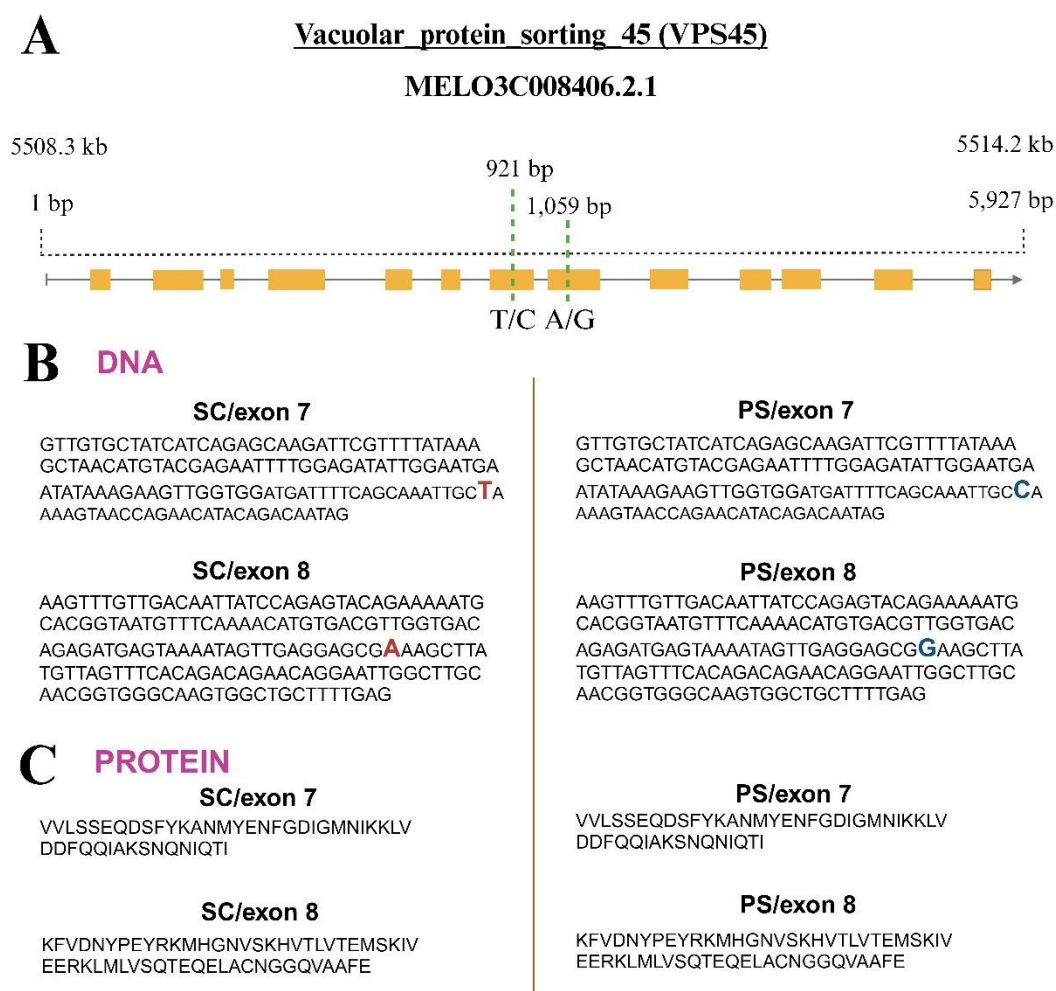


Figure 3. 10. The candidate gene CmVPS45 (Gene ID MELO3C008406.2.1) of QTL *cmvqw3.1*. The genome annotation is established in the SC genome with the small variants in the PS genome. **A)** Representation of the gene structure with two SNPs in exons seven and eight. The numbers at the top indicate the physical position in the genome in kb: Kilobase. The numbers at the bottom indicate the position of the gene in bp: Base pairs. **B)** The coding sequence of the exon seven and eight in SC and PS. The red colour indicates the single mutation of SC, and the blue colour indicates the single mutation of PS. **C)** The protein sequence is translated from the original coding sequence, representing the protein translation of exons seven and eight in frame.

In contrast, CmVPS33 expands by 4,406 bp with nine exons and eight introns and the coding sequence expands by 726 bp. In the coding sequence, there is a SNP (G/A)

Chapter 3: Fine mapping of QTL *cmvqw3.1*

at 308 bp exon four (Figure 3.11A) which results in an amino acid change from Gly (PS) to Glu (SC) at position 103 (G103E) of the protein sequence as CmVPS41 from some CMV-LS resistant melon accessions carried in its coding sequence (Pascual et al., 2019) (Figure 3.11C). Therefore, the amino acid change carried in the protein structure of CmVPS33 would not help CmVPS41 to support the trafficking of CMV-SGI (M6 and FNY) to the phloem. For further sequence information, check Table 1.1.S3 Excel sheet VPS33.

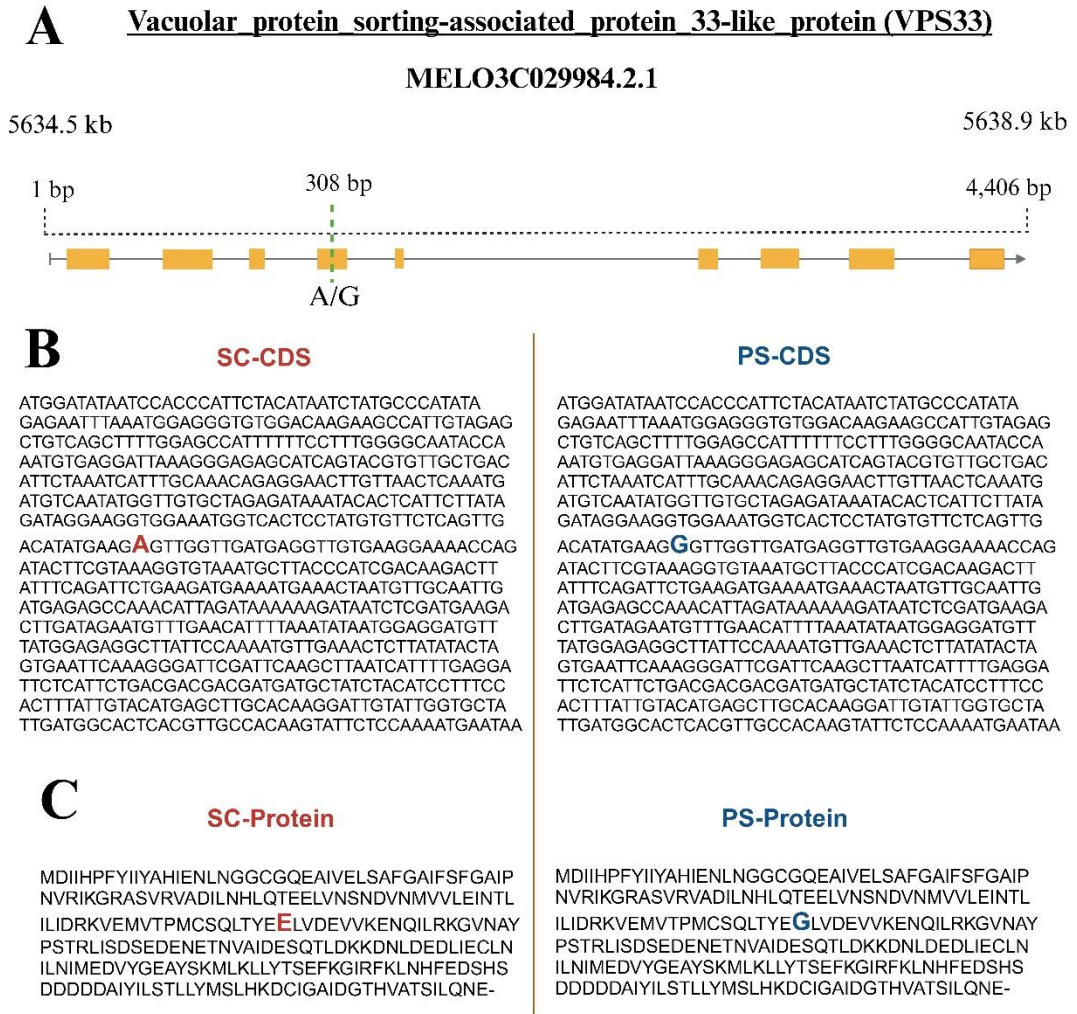


Figure 3. 11. The candidate gene CmVPS33 (Gene ID MELO3C029984.2.1) of QTL *cmvqw3.1*. The genome annotation is established in the SC genome with the variants in the PS genome. **A)** Representation of the gene structure with a SNP in exon four. The numbers at the top indicate the physical position in the genome in kb: Kilobase. The numbers at the bottom indicate the position of the gene in bp: Base pairs. **B)** The coding sequence of the gene in SC and PS. The red colour indicates the single mutation of SC, and the blue colour indicates the single mutation of PS. **C)** The protein sequence is translated from the original coding sequence.

Chapter 3: Fine mapping of QTL *cmvqw3.1*

Regarding the second interval between 8,331,515 and 23,616,908 bp, we still have 740 genes (see supplementary Table 1.1.S3, Candidate genes) and would be necessary to narrow down the relevant region using new recombinants before looking at the possible candidate genes.

Section III: Fine mapping of the *cmvqw10.1*

QTL

3.5 Genotyping and phenotyping of R10 families

In the first section of Chapter 3 (Section I), we identified many families carrying different combinations of the SC, PS or H allele at the flanking markers CMPSNP1117 and CMPSNP671 of the QTL *cmvqw10.1*. Compared to the QTL *cmvqw3.1* (20.81 Mb), this QTL is physically much smaller, spanning 3.62 Mb, but it has a higher genetic recombination rate. It was therefore easier to obtain recombinants from the QTL *cmvqw10.1* (R10 families) than from the *cmvqw3.1* QTL (for more details see the Excel sheet *cmvqw10.1* QTL in Table 1.2 S3).

Once we had many R10 families with different recombination points in the interval (Figure 3.12A), we proceeded with the phenotyping assays (Figure 3.12B). However, since the role of the resistance given by the QTL *cmvqw10.1* is very low as shown in Chapter 2, the phenotyping assays were more complex than during the mapping of QTL *cmvqw3.1*. The phenotyping system was the same as that used for the characterisation of the resistance of melon pyramided lines (Chapter 2) and the fine mapping of the *cmvqw3.1* QTL (previous section of this Chapter). Phenotyping assays were performed using IL Q3-12-H5 as positive control, IL 3-10-12-18(64) as negative control, and informative R10 families. The symptoms of the R10 lines took longer to appear than in the R3 families as happened in the IL Q3-12-H5 line (see Chapter 2 for more details). We phenotyped six R10 families (Figure 3.12A and 3.12B and Figure 3.14A). In this series of experiments IL Q3-12-H5 resulted in infection in some plants with 18% mosaic symptoms and 7% necrotic tissue

Chapter 3-III: Fine mapping of QTL *cmvqw10.1*

A

Chr	III		X																XII			Mosaic (%)	Necrosis (%)		
	P	<i>cmvqw3.1</i>	<i>cmvqw10.1</i>																<i>cmv1 gene</i>						
SNP	FM: AI_14-B01	FM: AI_33_H11	CMPSNP1117	CMPSNP528	CMPSNP1053	PS_15-H02	Chr10_2425868	chr10_2711871	chr10_2886704	chr10_2953598	chr10_3211060	CMPSNP183	Chr10_3457312	Chr10_3563772	Chr10_3665757	Chr10_3711131	Chr10_3823449	Chr10_3884492	CMPSNP762	CMPSNP671	Chr12_9319960	SNP: cmv1	Chr12_9330070		
Melon lines	2,804,514	23,616,908	1,122,396	1,722,779	1,786,379	2,295,138	2,425,868	2,711,871	2,886,704	2,953,598	3,211,060	3,390,408	3,457,312	3,563,772	3,665,757	3,711,131	3,823,449	3,884,492	3,983,992	4,747,687	9,319,960	9,320,908	9,330,070		
18(64)	SC	SC	SC	SC	SC	SC	SC	SC	SC	SC	SC	SC	SC	SC	SC	SC	SC	SC	SC	SC	SC	SC	SC	11,3	9,9
H5-1	SC	SC	PS	PS	PS	PS	PS	PS	PS	PS	PS	PS	PS	PS	PS	PS	PS	PS	PS	PS	SC	SC	SC	18,6	7,0
R10-16	SC	SC	H	H	H	H	H	H	-	SC	SC	SC	SC	SC	SC	SC	SC	SC	SC	SC	SC	SC	SC	20,6	17,6
R10-72	SC	SC	H	H	H	H	H	H	H	-	SC	SC	SC	SC	SC	SC	SC	SC	SC	SC	SC	SC	SC	75,0	25,0
R10-60	SC	SC	H	H	H	H	H	H	H	-	SC	SC	SC	SC	SC	SC	SC	SC	SC	SC	SC	SC	SC	17,5	12,5
R10-75	SC	SC	H	H	H	H	H	H	H	H	H	H	-	-	-	-	-	-	SC	SC	SC	SC	SC	9,1	9,1
R10-21	SC	SC	SC	H	H	H	H	H	H	H	H	H	-	-	-	-	-	-	-	-	SC	SC	SC	16,7	8,3
R10-32	SC	SC	SC	SC	SC	H	H	H	H	H	H	H	-	-	-	-	-	-	-	-	SC	SC	SC	12,5	12,5

B

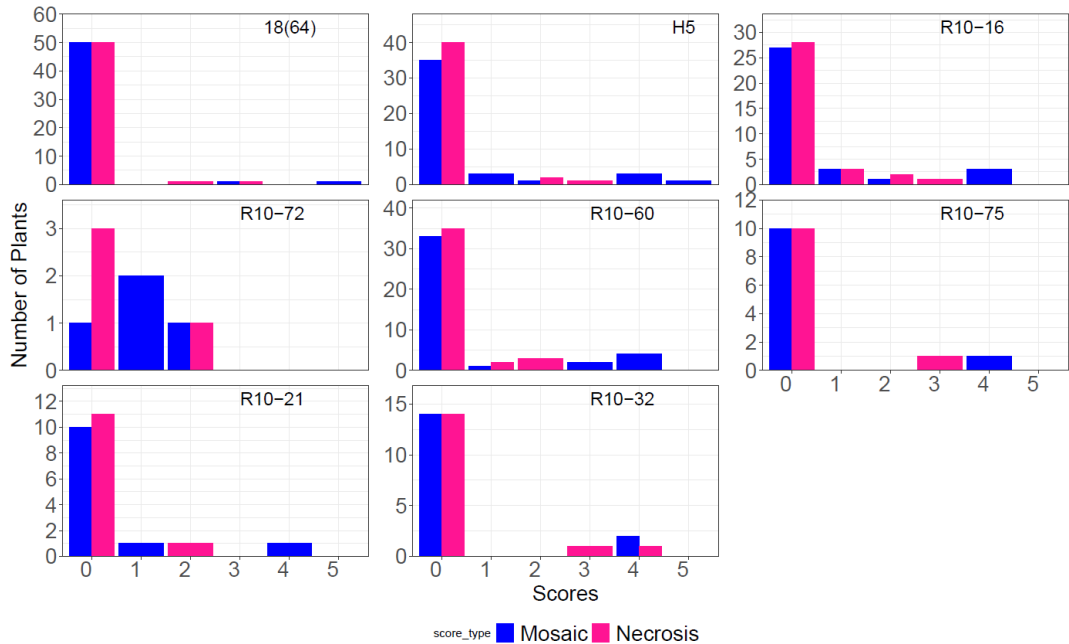


Figure 3. 12. A) Genotypes of the six R10 families inoculated with the CMV-M6. Chr: Chromosome, P: Physical position, SNP: Single Nucleotide Polymorphism, FM: Flanking Markers. B) Scores of mosaics and necrosis reached by phenotyped R10 families at 28 dpi.

- PS: Piel de Sapo
- SC: Songwhan Charmi PI 161375,
- H: Heterozygosity
- QTL and *cmv1* gene.

Most of the R10 families had less than 20% plants with mosaic symptoms and less than 17% necrotic tissue, as shown in Figure 1A. R10-72 was an exception among

Chapter 3-III: Fine mapping of QTL *cmvqw10.1*

the R10 families, producing more plants with mosaic (75%) and more necrotic tissue (25%) than the others and with low scores, although only a few R10-72 plants were tested. Both R10-16 and R10-60 behaved similarly in terms of infected plants. The R10-16 plants showed almost all mosaic scores and the R10-60 presented slightly higher mosaic scores but at a later time post infections as shown in Figure 3.12. Necrotic tissue presented low scores in both of them. R10-75 had very few infected plants but at early time post infections (Figure 3.13). R10-21 showed a similar infected rate of plants and necrosis symptoms than IL Q3-12-H5. Finally, R10-32 had the same percentage of infected plants and necrosis symptoms and was similar to IL 3-10-12-18(64) as shown in Figure 3.11B. The statistical analyses showed that the R10-75 differed statistically from the IL 3-10-12-18(64) at 13 dpi. Nevertheless, as the infections of the R10 families and even single plants of IL 3-10-12-18(64) started around 16 to 24 dpi, the R10-75 was not significant anymore. At 28 dpi, the R10-72 was significantly different compared to IL 3-10-12-18(64). There were no significant differences (p -value >0.05) between the R10 families and the resistant IL 3-10-12-18(64) at 16, 20 and 24 dpi.

Chapter 3-III: Fine mapping of QTL *cmvqw10.1*

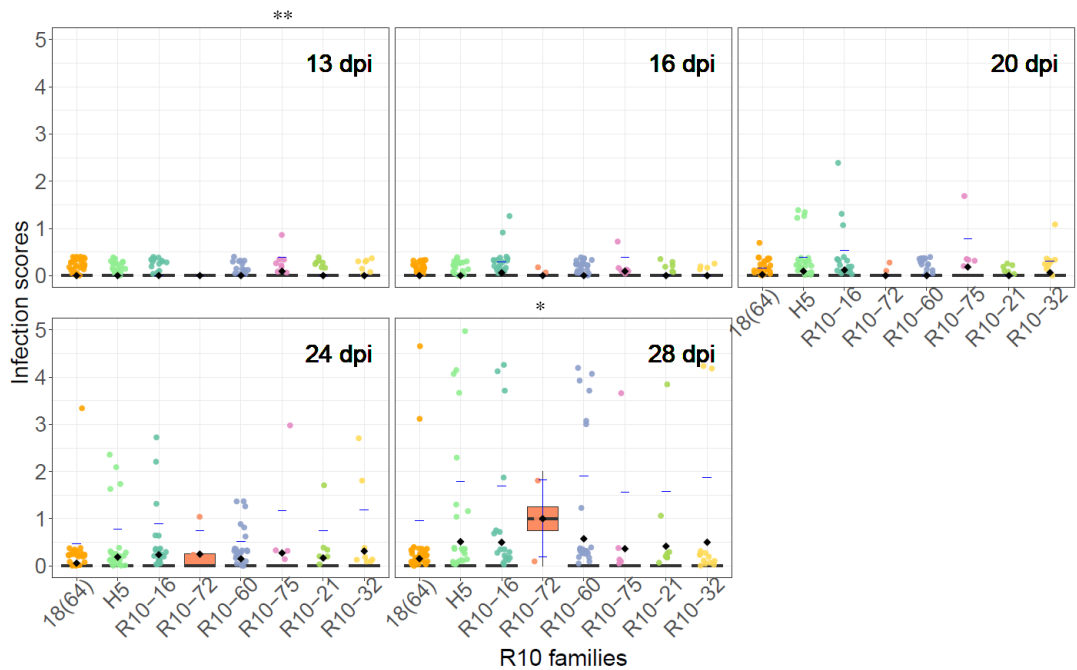


Figure 3. 13. A) Phenotyping results of each R10 family based on the scores of mosaics considering time points 13, 16, 20, 24 and 28 dpi. Biological replicates ranged from 4 to 52 individuals per melon family. Each dot represents the replicate distributed along the graph using the `position_jitterdodge()` function of RStudio version 2024.04.2+764. The black diamond indicates the average infection reached by the family at each time point. The blue error indicates the SD of each family, and the black line represents the median of each R10 family. Each box corresponds to 25 to 75% of the data. Significant differences compared to IL 3-10-12-18(64) are marked with asterisks (p-values $* < 0.05$, $** < 0.005$, $*** < 0.0005$, $**** < 0.00005$).

To assess infection levels and determine whether each R10 family is resistant or susceptible, we analysed the average infection achieved by individual plants over time from 11 to 28 dpi as shown in Figure 3.13A (Genotypes) and Figure 1.13B (Phenotypes). We selected these time points because we did not observe any symptoms before 11 dpi and the symptoms' appearance was at very late stages. The R10 families considered susceptible (p-value < 0.05) were R10-72, R10-75 and R10-16 with significantly different infection levels from the resistant control IL3-10-12-18(64) as shown in Figure 3.13B. In the R10-75 family, only one plant was infected over time, but early post-infection. Since the statistical analysis considered all dpi

and all mosaic scores of the individuals per family group, R10-75 was considered a susceptible plant. By contrast, because individuals of R10-60 were infected at a late time post-infection, the statistical analysis considered this family as resistant (Figure 3.14B).

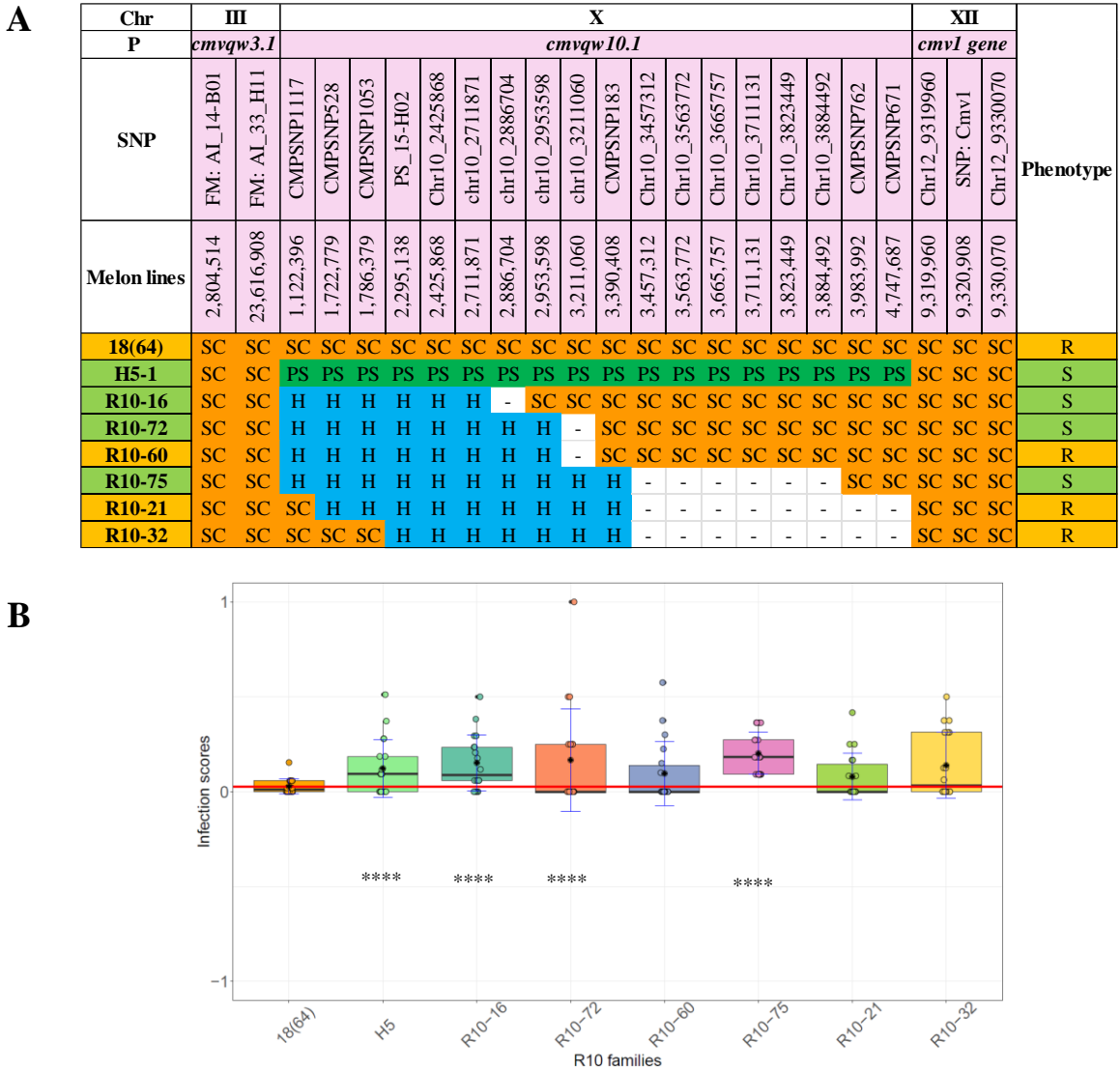


Figure 3. 14. A) Genotypes of the six R10 families phenotyped with the CMV-M6. SNP: Molecular Markers, FM: Flanking Markers, P: Physical position, Chr: Chromosome. **C)** Boxplot of the phenotyping results for each R10 family, based on infection levels from 11 to 28 dpi. The dots represent the mean score of all individuals at each dpi and are distributed

Chapter 3-III: Fine mapping of QTL *cmvqw10.1*

along the graph using the `position_jitterdodge()` function of RStudio version 2024.04.2+764. The red solid line indicates the average infection of the IL 3-10-12-18(64) line over time. The black diamond inside each box represents the average infection level, and the black line represents the median of each R10 family. Each box corresponds to 25 to 75% of the data. Significant differences from IL 3-10-12-18(64) indicating susceptibility are indicated by asterisks (p-values $* < 0.05$, $** < 0.005$, $*** < 0.0005$, $**** < 0.00005$).

- | | |
|---------------------------------|----------------------------|
| ■ PS: Piel de Sapo | ■ QTL and <i>cmv1</i> gene |
| ■ SC: Songwhan Charmi PI 161375 | ■ R: Resistant line |
| ■ H: Heterozygosity | ■ S: Susceptible line |

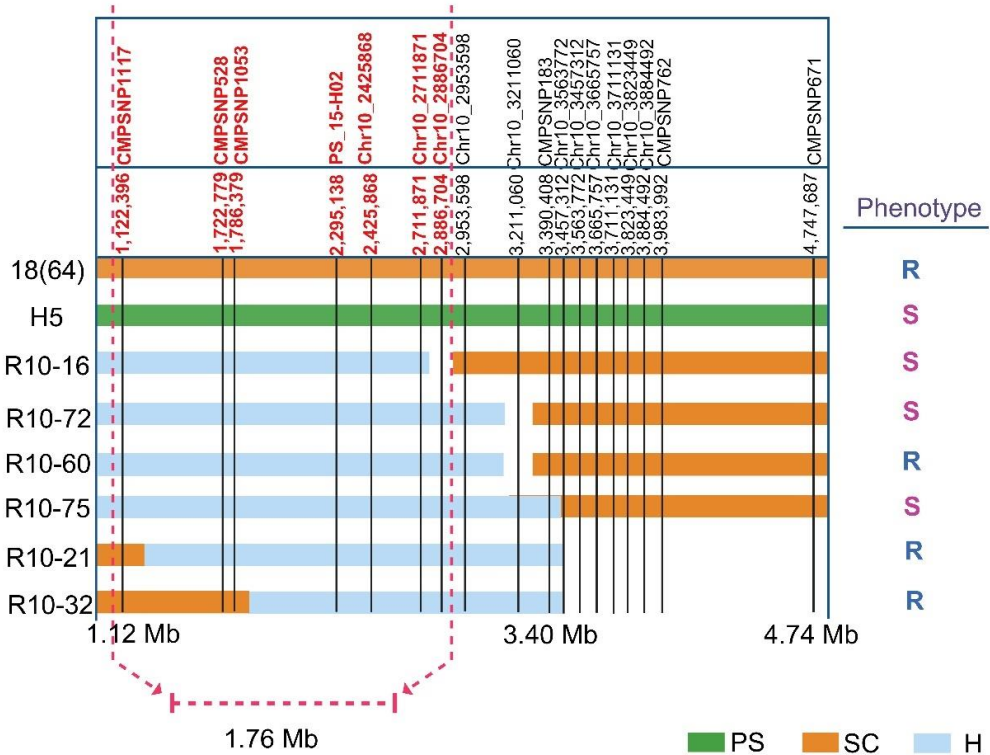
3.6 Genotyping and Phenotyping Association of *cmvqw10.1*

QTL

The interval of the QTL *cmvqw10.1* spanned a physical distance of 3.62 Mb and a genetic distance of 27.2 cM with 569 candidate genes. Despite the small number of phenotyped R10 families, we could perform a fine-mapping association analysis. The fine mapping association using the genotype vs. phenotype results was performed by time points, as we applied in the fine mapping of the QTL *cmvqw3.1*. However, in this case, the selected time points were 13, 16, 20, 24 and 28 dpi. Contingency tables were constructed at each time point, considering the observed infection scores of individual plants. As in the previous section, the individual plants with a score of 0 were considered resistant and those with a score of 1 to 5 were considered susceptible.

Given the late symptoms presented by these R-10 families, for the fine mapping association, we considered the time points 24 and 28 dpi. As shown in Figure 3.14A, we considered six R10 families to perform the association and the data show that there is a putative region of *cmvqw10.1* between 1,122,396 and 2,886,704 bp involved in the resistance to CMV-M6. Therefore, we narrowed it down from 3.62 Mb to 1.76 Mb. However, the fine mapping of the R10 lines was not continued because the phenotyping was difficult, since the minor effect of the QTL *cmvqw10.1* made it challenging to assess the infection phenotypes in most families.

A



B

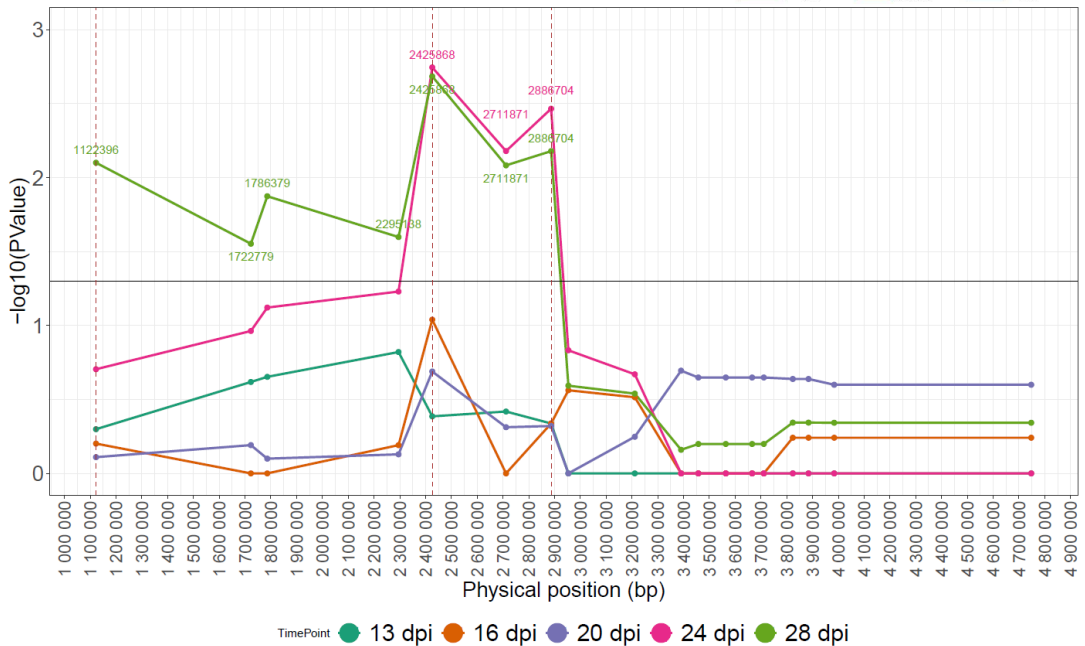


Figure 3. 15 A) Genotypes of six R10 families, the positive (IL Q3-12-H5) and the negative control (IL 3-10-12-18(64)). The molecular markers are distributed along the interval based

Chapter 3-III: Fine mapping of QTL *cmvqw10.1*

on their physical position. The red markers indicate statistically significant SNPs and the black ones mean no association. The red dashed lines mean the fine mapping association. R: Resistant, S: Susceptible, Mb: Megabase. **B)** Fine mapping association of the *cmvqw10.1* in different time points 13, 16, 20, 24 and 28 dpi of infection scores. The physical positions of SNPs within the *cmvqw10.1* interval are distributed along the X-axis, while the Y-axis shows $-\log_{10}(\text{p-value})$. The horizontal line indicates a significance threshold of $\text{p-value}=0.05$.

3.7 Candidate genes of *cmvqw10.1* QTL.

The suggested potential *cmvqw10.1* interval for the gene behind maps between 1,122,396 and 2,886,704 bp, indicating a narrowing down from 3.62 to 1.76 Mb. Thus, from 569 candidate genes, we potentially reduced the number of candidate genes to 294 (For further details check the supplementary Table 1.2 S3 Excel sheet Candidate genes). Among the candidate genes, there are some implicated intracellular trafficking pathways that CMV can exploit, such as a Charged multivesicular body protein 5, a SNAP25 homologous protein SNAP33, an Endosomal targeting BRO1-like domain-containing protein, a Plasmodesmata callose-binding protein 3 and Protein restricted TEV movement 2.

5. General Discussion

5. General Discussion

5.1 Coordination of *cmvqw3.1* and *cmvqw10.1* QTLs with the *cmv1* gene in delaying infection from CMV subgroup I.

The *cmvqw3.1* and *cmvqw10.1* QTLs have a minor effect on resistance and need to cooperate with the major gene *cmv1* in resistance to CMV-M6 and CMV-FNY, strains belonging to SGI (Guiu-Aragonés, et al., 2014; Yan 2018). In contrast, *cmv1* alone can prevent the infection by the SGII strain CMV-LS (Essafi et al., 2009). Yan (2018) observed that the resistance conferred by the two QTL and the *cmv1* gene in melon ILs, under CMV-FNY infection, acts at the phloem entry-level, in the same way as the *cmv1* gene alone does for CMV-LS (Guiu-Aragones et al., 2016). However, CMV-FNY completely overcame the resistance posed by the two QTLs with the *cmv1* gene a few days later, with the plant displaying a full infection with high scores (Yan 2018).

This study aimed to determine a role for the minor QTLs *cmvqw3.1* and *cmvqw10.1*, in resistance to CMV-M6. CMV-M6 infection showed varying mosaic and necrosis symptoms in the melon pyramided lines, with frequent medium to high scores in IL Q10-12-F50 (*cmvqw10.1* QTL and *cmv1* gene), much less in the IL Q3-12-H5 (*cmvqw3.1* QTL and *cmv1* gene) and even less and occasionally in the IL 3-10-12-18(64) (*cmvqw3.1*, *cmvqw10.1* and *cmv1* gene). The same mosaic symptoms were observed when mapping these minor QTLs in melon DHLs, where half of the genome belonged to SC in different introgressions (Guiu-Aragonés et al., 2014). However, their plants did not show necrotic symptoms as we described in our plants. IL 3-10-12-18(64) showed rare mosaic and necrotic symptoms in a few individual plants, but most plants were indistinguishable from the SC lines, which remained symptomless. In contrast, PS showed a gradual mosaic score over time without necrotic tissue. The mosaic symptoms of all melon pyramided lines were statistically different (p-value <0.05) from the PS, whose plants started to show mosaic symptoms around 7 to 10 dpi. Several reports have shown that the mosaic symptoms

5. General Discussion

produced by CMV infections are related to the 2b RNA silencing suppressor, which is involved in viral movement and symptom induction (Lewsey et al., 2009; Hou et al., 2011), but also in the appearance of necrotic symptoms (Inaba et al., 2011; Masuta et al., 2012). Furthermore, satellite RNA may induce necrosis or attenuate symptoms (García-Arenal and Palukaitis 1999; Choi et al., 2001; Palukaitis and García-Arenal 2003, Palukaitis 2016). All melon pyramided lines delayed the appearance of the mosaic symptoms by around 13 dpi (IL Q10-12-F50) and 17 dpi (IL Q3-12-H5) respectively, despite the absence of one of the minor QTL. In the punctate infections of IL 3-10-12-18(64), the infection delay was between 17 and 23 dpi. At a late time post-infection, around 28 dpi, there is a virus burst in the IL Q10-12-F50 and IL Q3-12-H5 lines, and the infected plant reaches high mosaic scores.

Virus presence in the petioles of the inoculated leaves has been studied as a proxy to detect virus entry in the phloem. Melon pyramided lines showed significantly greater resistance to virus phloem entry than PS at all time points. At 7 dpi, PS showed higher virus-relative accumulation in the petiole than in all lines. The low level of virus in PS was sufficient to cause systemic infection, as evidenced by the appearance of mosaic in the youngest leaves at this stage. The amount of virus in the petiole of melon pyramided lines was similar to that of SC. In fact, PS accumulated more virus at 14 dpi but decreased at 21 dpi. In contrast, the virus in the petiole of melon pyramided lines increased, but the levels were always lower than PS. At 21 dpi, it was evident that the production of the virus in the inoculated leaf was ceasing, as we observed a decrease in the amount of virus within the petiole in all lines. Nevertheless, the few viral molecules that had invaded the phloem in some plants of the pyramided lines could have multiplied enough to produce more severe infections with high scores at 28 dpi, as we had already seen in the visual phenotyping. Therefore, the melon gene located in these two minor QTLs could interfere with virus movement towards the phloem, effectively delaying or stopping

systemic infection by CMV-M6. QTL participation in the restriction of virus movement has been observed in other species, such as pepper, where seven major QTLs and several minor QTLs were identified as being involved in the partial restriction of CMV movement (Caranta et al., 2002). In addition, several QTLs have been mapped in pepper that restrict PVY accumulation at the systemic level and become stronger when they are pyramided in a line (Tamisier et al., 2017, Tamisier et al., 2020). In *Solanum tuberosum*, a QTL has been identified on chromosome IX, preventing PVY movement and thus systemic infection (Torrance et al., 2020). In soybean, at least three QTLs are involved in limiting the systemic movement of CMV (Ohnishi et al., 2010).

Since punctate infections were observed in IL3-10-12-18(64), this confirms that additional QTL(s) for resistance to CMV were necessary to stop CMV-M6 and FNY in coordination with *cmvqw3.1*, *cmvqw10.1* and the *cmv1* gene. Our results highlight the valuable role of the minor QTLs *cmvqw3.1* and *cmvqw10.1* in resistance to CMV-SGI strains in melon.

5.2 The *cmvqw3.1* QTL appears to play a more significant role in resistance to CMV-M6 than the *cmvqw10.1* QTL.

Focusing on the resistance carried by the IL Q10-12-F50 and IL Q3-12-H5 lines, we observed a trend towards different levels of resistance. We observed significantly stronger mosaic symptoms, with earlier and faster appearance and, when present, stronger necrosis in IL Q10-12-F50 than in IL Q3-12-H5. The same trend was observed when comparing the IL-Q-10-12-F50 line with the IL-3-10-12-18(64) line. In fact, the IL-Q3-12-H5 and the IL-3-10-12-18(64) lines were not significantly different in terms of mosaic symptoms, with fewer symptoms developing at a much later stage.

5. General Discussion

IL Q10-12-F50 and IL Q3-12-H5 allowed virus entry into the phloem from 14 dpi to 21 dpi. However, although they were not statistically different at any time post-infection, IL Q10-12-F50 appears to be more permissive. Although the amount of virus in IL Q10-12-F50 at 14 dpi was lower than in PS at 7 dpi, some IL Q10-12-F50 plants were infected, as indicated by visual symptoms. Thus, the role of the QTL *cmvqw3.1* seems to be more determinant for restriction to phloem entry and resistance to CMV-M6 than *cmvqw10.1*. The IL-carrying QTL *cmvqw3.1* and *cmv1* gene (IL Q3-12-H5) gets affected at much later times than the IL-carrying the QTL *cmvqw10.1* and *cmv1* gene (IL Q10-12-F50). This finding is different than reported by Yan (2018), who found a greater amount of CMV-FNY in ILs carrying the *cmvqw3.1/cmv1* than in ILs carrying the *cmvqw10.1/cmv1*. However, those ILs still carried additional SC introgressions in other chromosomes outside the QTLs, as seen in Chapter 1, that could affect virus behaviour.

The different roles of the two QTLs *cmvqw3.1* and *cmvqw10.1* have led to several questions. Could the gene(s) located in the *cmvqw3.1* QTL be involved in viral replication, since the virus enters the phloem later? Or perhaps virus inoculation is easier in the IL Q10-12-F50 due to an appropriate host-virus factor interaction? The literature review shows that a recessive gene controls the accumulation of the CMV-CP in *Arabidopsis thaliana*. The *Arabidopsis* mutant RB663 delays the accumulation of CMV-CP in non-inoculated upper leaves, suggesting that virus movement from cell to cell is impaired rather than CMV replication within cells (Yoshii et al., 1998a, 1998b). Additionally, in cucumber, the CMV-CP is involved in long-distance movement (Talianky and Fernando García-Arenal 1995). In contrast, the MP rather than the CP was associated with cell-to-cell movement of CMV-SGII strains in melon plants carrying only the *cmv1* gene (Guiu-Aragonés et al., 2015). Here we have at least three genes (*cmv1* gene, *cmvqw3.1* and *cmvqw10.1* QTL) and the CMV viral factors involved thus, CP could still play a role in the cell-to-cell and systemic

movement of CMV-M6. The C-terminus of MP and CP of cucumoviruses ensures a compatible interaction that establishes viral cell-to-cell movement (Salánki et al., 2004). Perhaps the susceptibility allele(s) located in the minor QTLs in the melon PS plants favour the interaction of CMV MP and CP in the leaves and enhance cell-to-cell movement to establish systemic infection. It is unlikely that the minor QTLs are involved in virus replication since these resistance QTLs collaborate with *cmv1* to generate resistance and *cmv1* is a gatekeeper for movement and phloem invasion (Guiu-Aragonés, 2016). As the understanding of QTLs and their role in CMV resistance advances, it will be beneficial to integrate this knowledge with other approaches. Marker-assisted selection can help accelerate the development of CMV-resistant melon varieties. This could reduce the impact of CMV on melon crops and ensure a sustainable and resilient agricultural industry.

5.3 Laser dissection microscopy is a novel methodology in melon to isolate Bundle Sheath cells.

The resistance conferred by QTL *cmvqw3.1* and *cmvqw10.1*, in coordination with the *cmv1* gene, against CMV-FNY acts at the phloem entry level (Yan, 2018). This mechanism is similar to infection by CMV-LS, from SG II, blocking infection at bundle sheath (BS) cells (Guiu-Aragonés et al., 2016). As we focused on elucidating the role of the *cmvqw3.1* and *cmvqw10.1* QTLs in the resistance mechanism in the BS cell, Laser Dissection Microscopy (LDM) was used to isolate BS cells in the melon pyramided lines however we could not complete the study of the role of the QTLs due to technical challenges.

Despite technical challenges, we proposed a reliable method to isolate specific cell types in melon. As mentioned in the literature review, Gil et al. (2011) developed this method using LDM for CMV-infected melon plants. They studied sucrose accumulation in the phloem of infected melon leaves using PCR quantification.

5. General Discussion

However, they suggested a method that avoids the need for cryogenic samples required for transcriptomic and proteomic analysis. Latrasse et al. (2017) used the LDM protocol to study epigenetic regulation in male and female melon flowers. In this case, they used a cryogenised sample, as we did, but with different reagents, incubation times, microscopes and types of samples.

DNA, RNA and protein can be extracted to analyse large genomics, transcriptomics and proteomics datasets amplified by PCR and qPCR expression profiles associated with infection of plant developmental stages and to study cell relationships in melon. In our case, PCR was used to amplify CMV in the collected BS cells. Nevertheless, we had some cross-contaminated RNA because the procedure is extensive and must be ensured in all steps before cell isolation to avoid contamination. Altogether, we have reported a new method of cell isolation in melon that provides a powerful and advanced approach to studying specific cell types in melon.

5.4 Fine mapping of *cmvqw3.1* revealed two putative intervals

The causal genes in the *cmvqw3.1* and *cmvqw10.1* QTLs are essential for understanding the interaction of CMV with the *cmv1* gene, as well as the viral infection process in melon plants. To map these genes, we genotyped and phenotyped plants recombinant in the QTL *cmvqw3.1* (lines R3) and plants recombinant in the QTL *cmvqw10.1* (lines R10). Phenotyping was complex due to the nature of quantitative resistance. Mosaic symptoms were primarily used as phenotypes, with necrosis also recorded to monitor its evolution in the recombinant families. Infections were recorded every 3-4 days. Multiple fine-mapping association analyses of the QTL *cmvqw3.1* were performed at six different time points (9, 13, 16, 20, 24, 28 dpi) to identify the significant SNPs associated with the resistant phenotype. The QTL *cmvqw3.1* was mapped using these time points excluding the

5. General Discussion

time points 24-28 dpi. Conversely, the time points 13, 16, 20, 24 and 28 dpi were used to map the *cmvqw10.1* QTL, as the R10s infection was not apparent until 11 dpi. Analyses included: 1) Fisher with PS infections, and 2) Fisher without PS infections. For this purpose, contingency tables were constructed to compare individual plant phenotypes between SC (resistant) and PS+H (susceptible) alleles. The phenotype was susceptible (S) when the score was 1-5 and resistant (R) when it was 0. Since the PS infection results skewed the SNP significance in both the *cmvqw3.1* and *cmvqw10.1* QTL intervals, making all markers significant, PS could not filter out any physical region of the QTL, so the infection results of PS were not included in the comparison of R3 and R10 lines. Thus, the melon pyramided lines IL Q3-12-H5 and IL Q10-12-F50 were selected as susceptible controls for the analyses in the two fine mappings.

For each fine-mapping, two different time points post-infection were selected as the critical time to reveal the resistance. For the mapping of *cmvqw10.1*, we chose the times, 24 and 28 dpi (Figure 3.14, Chapter 3-III) and for the fine mapping of *cmvqw3.1*, we chose 16 and 20 dpi (Figure 3.9, Chapter 3-II) The putative final *cmvqw10.1* interval ranges from 1,122,396 to 2,886,704 bp and carries 294 out of the initial 569 genes. Within the QTL *cmvqw3.1* two putative intervals were found, the first interval between positions 5,307,083 and 5,703,825 and the second between positions 8,331,515 and 23,616,908. In the first interval of the *cmvqw3.1* QTL, we managed to narrow down from the initial 1040 candidate genes to 25 candidate genes for the first interval and to 740 genes for the second interval. Further experiments are needed to reveal the candidate genes in the second interval of the *cmvqw3.1* QTL.

Among the candidate genes located in the first interval of the *cmvqw3.1* QTL, two candidates, VPS45 (Gene ID MELO3C008406.2.1) and VPS33 (Gene ID MELO3C029984.2.1), were interesting because of their function in intracellular

5. General Discussion

movement. VPS45 is involved in vesicle trafficking to the vacuole, vacuole biogenesis and vacuole function (Zouhar et al., 2009) and is present in the trans-Golgi network (Bassham et al., 2000). Similarly, VP33 has been implicated in trafficking, organelle morphogenesis and growth (Wang et al., 2011). Both candidate genes could assist CMV trafficking. However, CmVPS45 contains two synonymous variants between SC (genome reference) and PS that do not change the amino acids in the protein and therefore do not alter its biological function. Nevertheless, a putative insertion in the promoter of CmVPS45 could alter gene expression and modify its function. On the other hand, CmVPS33 had an amino acid change Gly (PS) to Glu (SC) at residue 103 (G103E) which could modify its biological function. The same amino acid change “G85E” was identified in CmVPS41 of resistant melon accessions Freeman’s Cucumber, Shirouri Okayama, Pat81, Nanbukin, and Ogon9 (Pascual et al., 2019). Therefore, if we focus on it, CmVPS33 seems to be the best candidate and this single mutation in the coding sequence of CmVPS33 could cause resistance to CMV-M6.

5.5 VPS33 a member of the HOPS and CORVET complex is a candidate gene for the *cmvqw3.1* QTL.

VPS33 is a member of the Homotypic Fusion and Vacuole Protein Sorting (HOPS) and the Class C core Vacuole/Endosome Tethering Factor (CORVET) complexes, which regulate sequential trafficking events during endosomal maturation (Wang et al., 2011; Takemoto et al., 2018). VPS33 is a member of the Vacuolar Protein Sorting (VPS) core (VPS-C), together with VPS11, VPS16, VPS18 and has functions in trafficking, organelle morphogenesis and growth (Wang et al., 2011). In the CORVET complex, VPS-C members interact with additional subunits VPS3 and VPS8 to regulate the transition between early endosome to late endosome. In the HOPS complex, the C core interacts with VPS41 and VPS39 in all vacuole and

5. General Discussion

lysosome fusion events and is also involved in protein sorting in the vacuole (Wang et al., 2011; Balderhaar and Ungermann, 2013).

VPS33 and VPS41 are important in plant vacuole fusion, biogenesis, male fertility and plant development, and in plant vacuole membrane tethering (Lei 2018; Brillada et al., 2018). VPS33 localise to late endosomes, as VPS41 does (Real et al, 2023), consistent with a role in membrane fusion at pre-vacuolar compartments at the vacuole, as part of the HOPS complex (Brillada et al., 2018). Most VPSs have been associated with the vesicle trafficking machinery that viruses use for their intracellular transport during the viral life cycle. In human cells, the Ebola virus, which is internalized into the cells by binding to the cholesterol transporter Niemann-Pick C1, requires also HOPS expression for trafficking and viral entry into the endolysosomal network to reach late endosomal/lysosomal compartments (Bo et al., 2020). In addition, ORF3a of the SARS-CoV-2 virus sequesters HsVPS41, HsVPS39 and HsVPS33 in the late endosome, preventing HOPS complex function in autolysosome formation (Miao et al., 2021). In yeast, a SARS-CoV-2 protein interacts with SC VPS33 and alters membrane trafficking and endocytosis (Klemm et al., 2021).

CmVPS41, encoded by the *cmv1* gene, was the first reported natural plant virus resistance gene implicated in virus movement. It is involved in preventing phloem entry and systemic infection by CMV-SGII strains, like CMV-LS. The PS-susceptible allele (*Cmv1*) of CmVPS41 helps CMV-LS to move through the vacuole and from cell to cell to reach the phloem (Guiu-Aragonés et al., 2016; Real et al, 2023). However, the mutant allele (*cmv1*) restricts viral trafficking by acting as a gatekeeper that stops the virus in the BS cells (Guiu-Aragonés et al., 2016; Giner et al., 2017; Pascual et al., 2019). This means that the mutant CmVPS41 does not require the susceptible alleles of the *cmvqw3.1* and *cmvqw10.1* QTLs to stop CMV-

5. General Discussion

LS infection. Conversely, when infected with CMV-M6, from SGI, the mutant CmVPS41 requires the cooperation of mutant alleles from the *cmvqw3.1* and *cmvqw10.1* QTLs to stop the virus (Guiu-Aragónés et al., 2014). In the cells of PS, CmVPS33 as part of the HOPS complex may interact or communicate with CmVPS41 to promote infection. In the line SC12-1-99, which carries only the *cmv1* gene and the susceptible alleles of the QTLs *cmvqw3.1* and *cmvqw10.1* (Essafi et al., 2009), CmVPS33 and the other gene in QTL *cmvqw3.1* should be able to interact or communicate with the resistant CmVPS41 to promote infection by CMV-M6. Finally, in the resistant accession SC or IL-3-10-12-18(64), the QTL *cmvqw10.1*, the resistant CmVPS33 and resistant alleles of other genes located in the second interval of the QTL *cmvqw3.1* would not be able to cooperate with the resistant CmVPS41 to support CMV-M6infection, thus producing resistance. Figure GD-1 shows a model of resistance given by these genes. Thus, the interaction of all these host factors would regulate the viral movement in the BS cells to allow/prevent phloem entry of CMV-SGI strains and systemic infection

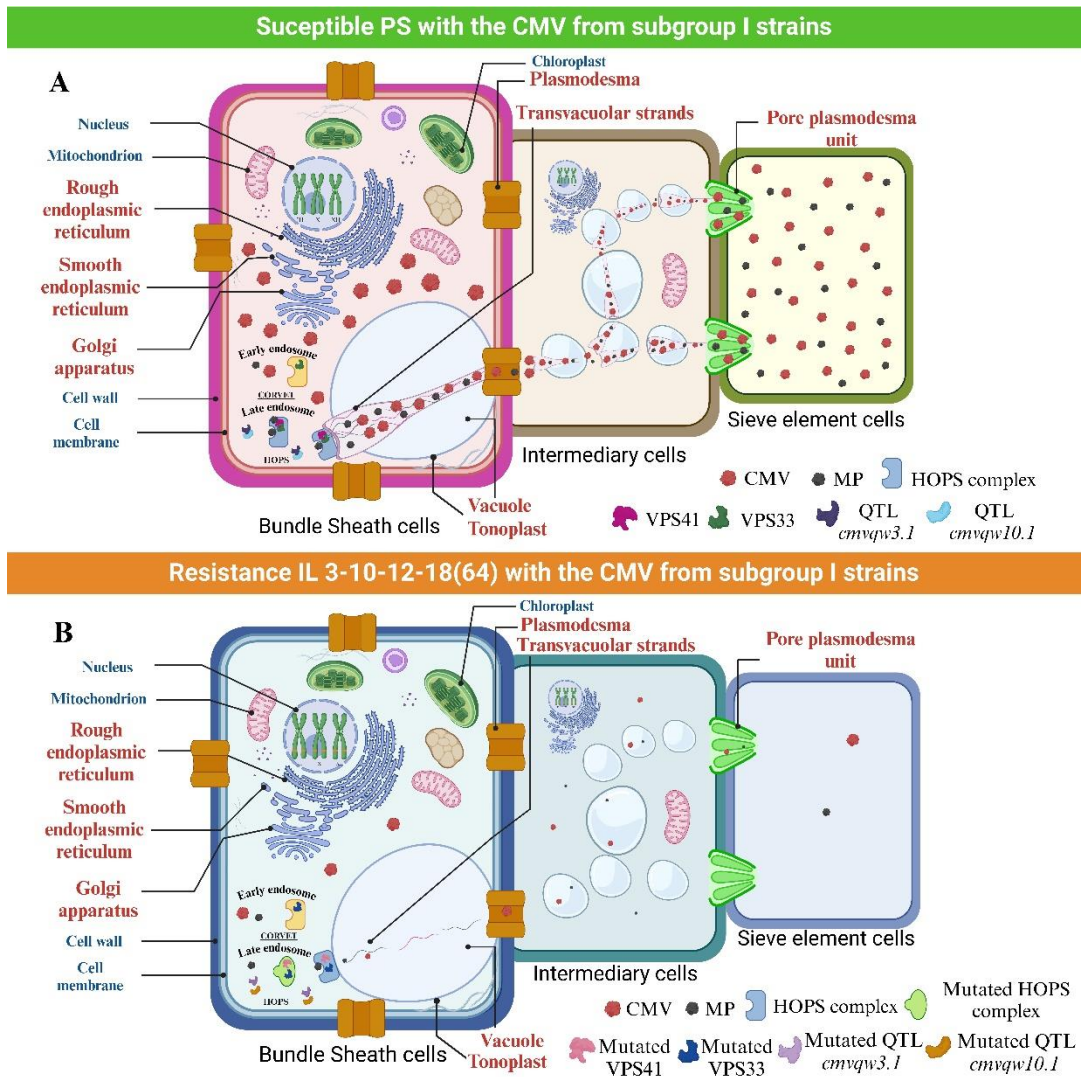


Figure GD-1. Model of resistance conferred by QTL *cmvqw3.1* and *cmvqw10.1* in coordination with the *cmv1* gene. **A)** In susceptible PS plants, CMV SGI particles, once in the cytoplasm, move towards the late endosome, passing through the early endosome where the CORVET complex is located. Once in the late endosome, they interact with VPS41, VPS33 and unknown genes from the *cmvqw3.1* and *cmvqw10.1* QTL within the HOPS complex to hijack the melon cell machinery and move freely within the cell. They then cross the transvacuolar strands in the vacuole and reach the tonoplast to finally enter the plasmodesmata. After that, the virus moves to the intermediate cells to reach the tonoplast of the vacuole and crosses the small transvacuolar strands in the various vacuoles present in ICs until it reaches the pore plasmodesmata unit. Then, the virus crosses the sieve element to establish a systemic infection. **B)** In resistant IL3-10-12-18(64) plants, the CMV SGI strain follows a similar pathway but interacts with mutant versions of VPS33, mutant VPS41 and unknown genes in the QTL *cmvqw3.1* and *cmvqw10.1* within the HOPS complex at the

5. General Discussion

late endosome. The mutant VPS41, in the absence of the susceptible alleles of the other genes, can develop very few TVS and thus, cannot provide the way through the vacuole to the PDs to finally reach the ICs and SE. The very few viruses able to reach the phloem would, at a later time post-infection, have multiplied enough in some plants to produce a systemic infection. VPS41: Vacuolar protein sorting 41, VPS33: Vacuolar protein sorting 33, *cmvqw3.1* QTL: Quantitative trait locus on chromosome III of SC melon, *cmvqw10.1* QTL: Quantitative trait locus on chromosome X of SC melon, CORVET: Class C core vacuole/endosome tethering.

6. Conclusions

6. General Conclusions

6. General Conclusions

1. Two ILs were generated by pyramiding the QTL *cmvqw3.1* and the *cmv1* gene: IL Q3-12-H5 and IL Q3-12-H218, both with minimal genetic contaminations around the *cmv1* locus. IL Q3-12-H5 was used to characterize resistance to CMV-M6, while IL Q3-12-H218 was used to construct mapping populations.
2. Two ILs were generated by pyramiding the QTL *cmvqw10.1* QTL and the *cmv1* gene: IL Q10-12-F50 and IL Q10-12-F193, both with minimal genetic contaminations around the *cmv1* locus. The IL Q10-12-F50 was used to characterise resistance to CMV-M6, while IL Q10-12-F193 was used to construct the fine-mapping populations.
3. The QTLs *cmvqw3.1* and *cmvqw10.1*, in association with the *cmv1* gene, delayed the onset of infection by CMV-M6.
4. The *cmvqw3.1* QTL appears to play a more relevant role than *cmvqw10.1* in resistance to infection by CMV M6.
5. A methodology to isolate specific cell types by Laser dissection microscopy has been developed for melon plants.
6. Two fine-mapping populations for the QTLs *cmvqw3.1* and *cmvqw10.1* were developed by crossing IL Q3-12-H218 and IL Q10-12-F193. This enabled the identification of recombinant plants R3, for the QTL *cmvqw3.1* and R10, for the QTL *cmvqw10.1* for phenotyping assays.
7. For the fine mapping of QTL *cmvqw3.1*, we identified two putative intervals involved in the resistance to CMV-M6, one between positions (v3.6.1 genome

6. General Conclusions

version) 5,307,083 and 5,703,825 bp and the second between positions 8,331,515 and 23,616,908 bp.

8. The first region of QTL *cmvqw3.1* spanned 0.39 Mb, with 25 annotated genes, whereas the second region spanned 15.28 Mb, with 740 genes.

9. CmVPS33 and CmVPS45 mapped to the 0.39 Mb interval and were the best candidates. Both are involved in intracellular movement as mediators of protein trafficking through the endosomal system. However, VPS45 does not have any amino acid changes that could alter the function of the protein in the SC, thus we discard this gene as a candidate.

10. Within the VPS33 coding sequence, there is only one G to A SNP between PS and SC. This results in an amino acid change of Glycine to Glutamic acid at position 103 of the protein (G103E) that could alter the function of the VPS33 protein in SC.

11. VPS33, is a component of the HOPS complex, as VPS41, and is the best candidate in the left region of QTL *cmvqw3.1*.

12. For the fine mapping of QTL *cmvqw10.1*, we proposed a putative interval between 122,396 and 2,886,704 bp involved in resistance to CMV-M6, which narrowed the QTL *cmvqw10.1* down from 3.62 Mb to 1.76 Mb, with 294 genes.

7. Bibliography

7. Bibliography

7. Bibliography

- Abbott, E., Hall, D., Hamberger, B., & Bohlmann, J. (2010). Laser microdissection of conifer stem tissues: isolation and analysis of high quality RNA, terpene synthase enzyme activity and terpenoid metabolites from resin ducts and cambial zone tissue of white spruce (*Picea glauca*). *BMC Plant Biol*, *10*, 106. <https://doi.org/10.1186/1471-2229-10-106>
- Agaoua, A., Bendahmane, A., Moquet, F., & Dogimont, C. (2021). Membrane Trafficking Proteins: A New Target to Identify Resistance to Viruses in Plants. *Plants (Basel)*, *10*(10). <https://doi.org/10.3390/plants10102139>
- Ahmed, M. Z., Saeed, S., Hassan, A., Ghuffar, S., Abdullah, A., Iqbal, R., Shafique, M. S. (2021). *Alternaria alternata* Causing Leaf Spot of Cucumis melo (Muskmelon) in Pakistan. *Plant Disease*, *105*(6), 1853. <https://doi.org/10.1094/pdis-05-20-0973-pdn>
- Alberts, B., Johnson, A., Lewis, J., Raff, M., Roberts, K., & Walter, P. (2002). *Molecular biology of the cell*. New York: Garland Science.
- Alpert, K. B., & Tanksley, S. D. (1996). High-resolution mapping and isolation of a yeast artificial chromosome contig containing *fw2.2*: A major fruit weight quantitative trait locus in tomato. *Proceedings of the National Academy of Sciences*, *93*(26), 15503-15507. <https://doi.org/doi:10.1073/pnas.93.26.15503>
- Amano, M., Mochizuki, A., Kawagoe, Y., Iwahori, K., Niwa, K., Svoboda, J., Imura, Y. (2013). High-resolution mapping of *zym*, a recessive gene for Zucchini yellow mosaic virus resistance in cucumber. *Theor Appl Genet*, *126*(12), 2983-2993. <https://doi.org/10.1007/s00122-013-2187-5>
- Anderson, C. T., & Kieber, J. J. (2020). Dynamic Construction, Perception, and Remodeling of Plant Cell Walls. *Annu Rev Plant Biol*, *71*, 39-69. <https://doi.org/10.1146/annurev-arplant-081519-035846>
- Anwer, M., Akhtar, K. P., Ullah, N., Saleem, M. Y., & Cheema, H. M. N. (2019). First report of cucumber mosaic virus subgroup IB and II isolates infecting tomatoes in Pakistan. *101*(3), 775-775. <https://doi.org/10.1007/s42161-019-00242-5>
- Apalowo, O. A., Adediji, A. O., Balogun, O. S., Fakolujo, T. I., Archibong, J. M., Izuogu, N. B., Atiri, G. I. (2022). Genetic Structure of Cucumber Mosaic Virus From Natural Hosts in Nigeria Reveals High Diversity and Occurrence of Putative Novel Recombinant Strains. *Frontiers in Microbiology*, *13*. <https://doi.org/10.3389/fmicb.2022.753054>
- Argyris, J. M., Ruiz-Herrera, A., Madriz-Masis, P., Sanseverino, W., Morata, J., Pujol, M., Garcia-Mas, J. (2015). Use of targeted SNP selection for an improved anchoring of the melon (*Cucumis melo* L.) scaffold genome assembly. *16*(1), 4. <https://doi.org/10.1186/s12864-014-1196-3>

7. Bibliography

- Argyris, J. M., Díaz, A., Ruggieri, V., Fernández, M., Jahrman, T., Gibon, Y., Garcia-Mas, J. (2017). QTL Analyses in Multiple Populations Employed for the Fine Mapping and Identification of Candidate Genes at a Locus Affecting Sugar Accumulation in Melon (*Cucumis melo* L.). *Frontiers in Plant Science*, 8. <https://doi.org/10.3389/fpls.2017.01679>
- Babu, B., Dankers, H., & Paret, M. L. (2014). First Report of Cucumber mosaic virus Associated with *Capsicum chinense* var. Scotch Bonnet in Florida. *Plant Disease*, 98(7), 1016-1016. <https://doi.org/10.1094/pdis-12-13-1276-pdn>
- Balderhaar, H. J., & Ungermann, C. (2013). CORVET and HOPS tethering complexes - coordinators of endosome and lysosome fusion. In *J Cell Sci* (Vol. 126, pp. 1307-1316). <https://doi.org/10.1242/jcs.107805>
- Barajas, D., Jiang, Y., & Nagy, P. D. (2009). A unique role for the host ESCRT proteins in replication of Tomato bushy stunt virus. *PLoS Pathog*, 5(12), e1000705. <https://doi.org/10.1371/journal.ppat.1000705>
- Barajas, D., Martín, I. F., Pogany, J., Risco, C., & Nagy, P. D. (2014). Noncanonical role for the host Vps4 AAA+ ATPase ESCRT protein in the formation of Tomato bushy stunt virus replicase. *PLoS Pathog*, 10(4), e1004087. <https://doi.org/10.1371/journal.ppat.1004087>
- Bassham, D. C., Sanderfoot, A. A., Kovaleva, V., Zheng, H., & Raikhel, N. V. (2000). AtVPS45 complex formation at the trans-Golgi network. *Mol Biol Cell*, 11(7), 2251-2265. <https://doi.org/10.1091%2Fmbc.11.7.2251>
- Baumgartner, I. O., Patocchi, A., Frey, J. E., Peil, A., & Kellerhals, M. (2015). Breeding Elite Lines of Apple Carrying Pyramided Homozygous Resistance Genes Against Apple Scab and Resistance Against Powdery Mildew and Fire Blight. 33(5), 1573-1583. <https://doi.org/10.1007/s11105-015-0858-x>
- Benitez-Alfonso, Y. (2014). Symplastic intercellular transport from a developmental perspective. *Journal of Experimental Botany*, 65(7), 1857-1863. <https://doi.org/10.1093/jxb/eru067>
- Berkowitz, O., Xu, Y., Liew, L. C., Wang, Y., Zhu, Y., Hurgobin, B., Whelan, J. (2021). RNA-seq analysis of laser microdissected *Arabidopsis thaliana* leaf epidermis, mesophyll and vasculature defines tissue-specific transcriptional responses to multiple stress treatments. *The Plant Journal*, 107(3), 938-955. <https://doi.org/https://doi.org/10.1111/tpj.15314>
- Bezruczyk, M., Zöllner, N. R., Kruse, C. P. S., Hartwig, T., Lautwein, T., Köhrer, K., Kim, J. Y. (2021). Evidence for phloem loading via the abaxial bundle sheath cells in maize leaves. *Plant Cell*, 33(3), 531-547. <https://doi.org/10.1093/plcell/koaa055>

7. Bibliography

- Bhatla, S. C. (2018). Water and Solute Transport. In *Plant Physiology, Development and Metabolism* (pp. 83-115). Singapore: Springer Singapore. https://doi.org/10.1007/978-981-13-2023-1_3
- Bishnoi, R., Kaur, S., Sandhu, J. S., & Singla, D. (2023). Genome engineering of disease susceptibility genes for enhancing resistance in plants. *23*(3), 207. <https://doi.org/10.1007/s10142-023-01133-w>
- Blackman, L. M., Boevink, P., Cruz, S. S., Palukaitis, P., & Oparka, K. J. (1998). The movement protein of cucumber mosaic virus traffics into sieve elements in minor veins of *Nicotiana glauca*. *Plant Cell*, *10*(4), 525-538. <https://doi.org/10.1105/tpc.10.4.525>
- Blokhina, O., Valerio, C., Sokołowska, K., Zhao, L., Kärkönen, A., Niittylä, T., & Fagerstedt, K. (2017). Laser Capture Microdissection Protocol for Xylem Tissues of Woody Plants. *Frontiers in Plant Science*, *7*. <https://doi.org/10.3389/fpls.2016.01965>
- Boevink, P., & Oparka, K. J. (2005). Virus-host interactions during movement processes. *Plant Physiol*, *138*(4), 1815-1821. <https://doi.org/10.1104/pp.105.066761>
- Brillada, C., Zheng, J., Krüger, F., Rovira-Diaz, E., Askani, J. C., Schumacher, K., & Rojas-Pierce, M. (2018). Phosphoinositides control the localization of HOPS subunit VPS41, which together with VPS33 mediates vacuole fusion in plants. *Proc Natl Acad Sci U S A*, *115*(35), E8305-E8314. <https://doi.org/10.1073/pnas.1807763115>
- Bui, H. T., Balkunde, R., & Jackson, D. (2014). Plasmodesmata. In S. Assmann & B. Liu (Eds.), *Cell Biology* (pp. 1-29). New York, NY: Springer New York. https://doi.org/10.1007/978-1-4614-7881-2_7-1
- Bussolati, G. (2022). Fixation in histopathology: the mandate to renew. *Pathologica - Journal of the Italian Society of Anatomic Pathology and Diagnostic Cytopathology*, *114*(4), 275-277. <https://doi.org/10.32074/1591-951X-782>
- Campos, M., Gonzalo, M. J., Díaz, A., Picó, B., Gómez-Guillamón, M. L., Monforte, A. J., & Esteras, C. (2023). A Novel Introgression Line Library Derived from a Wild Melon Gives Insights into the Genetics of Melon Domestication, Uncovering New Genetic Variability Useful for Breeding. *International Journal of Molecular Sciences*, *24*(12), 10099. <https://doi.org/10.3390/ijms241210099>
- Caranta, C., Pflieger, S., Lefebvre, V., Daubèze, A. M., Thabuis, A., & Palloix, A. (2002). QTLs involved in the restriction of cucumber mosaic virus (CMV) long-distance movement in pepper. *Theor Appl Genet*, *104*(4), 586-591. <https://doi.org/10.1007/s001220100753>

7. Bibliography

- Carrington, J. C., Kasschau, K. D., Mahajan, S. K., & Schaad, M. C. (1996). Cell-to-Cell and Long-Distance Transport of Viruses in Plants. *Plant Cell*, 8(10), 1669-1681. <https://doi.org/10.1105/tpc.8.10.1669>
- Castanera, R., Ruggieri, V., Pujol, M., Garcia-Mas, J., & Casacuberta, J. M. (2019). An Improved Melon Reference Genome With Single-Molecule Sequencing Uncovers a Recent Burst of Transposable Elements With Potential Impact on Genes. *Front Plant Sci*, 10, 1815. <https://doi.org/10.3389/fpls.2019.01815>
- Chang, T., & Zhao, G. (2021). Ice Inhibition for Cryopreservation: Materials, Strategies, and Challenges. *Advanced Science*, 8(6), 2002425. <https://doi.org/https://doi.org/10.1002/advs.202002425>
- Chavan, S., Schnabel, E., Saski, C., & Frugoli, J. (2023). Fixation and Laser Capture Microdissection of Plant Tissue for RNA Extraction and RNA-Seq Library Preparation. *Current Protocols*, 3(7), e844. <https://doi.org/10.1002/cpz1.844>
- Chen, J., Liu, X., Hu, Y., Chen, X., & Tan, S. (2023). Cryopreservation of tissues and organs: present, bottlenecks, and future. *Front Vet Sci*, 10, 1201794. <https://doi.org/10.3389/fvets.2023.1201794>
- Choi, H. S., Ryu, J. K., Ahn, K. K., Cho, J. D., & Kim, J. S. (2001). Cucumber Mosaic Cucumovirus-CARNA5 Causing Bud Necrosis on Table Tomato. *17*(3), 169-173.
- Chomicki, G., Schaefer, H., & Renner, S. S. (2020). Origin and domestication of Cucurbitaceae crops: insights from phylogenies, genomics and archaeology. *New Phytologist*, 226(5), 1240-1255. <https://doi.org/https://doi.org/10.1111/nph.16015>
- Cillo, F., Roberts, I. M., & Palukaitis, P. (2002). In situ localization and tissue distribution of the replication-associated proteins of Cucumber mosaic virus in tobacco and cucumber. *J Virol*, 76(21), 10654-10664. <https://doi.org/10.1128/jvi.76.21.10654-10664.2002>
- Clepet, C., Joobeur, T., Zheng, Y., Jublot, D., Huang, M., Truniger, V., Fei, Z. (2011). Analysis of expressed sequence tags generated from full-length enriched cDNA libraries of melon. *12*(1), 252. <http://dx.doi.org/10.1186/1471-2164-12-252>
- Cooper, G. M. (2000). *The Cell: A Molecular Approach. 2nd edition*: Sinauer Associates 2000.
- Corwin, J. A., & Kliebenstein, D. J. (2017). Quantitative Resistance: More Than Just Perception of a Pathogen. *Plant Cell*, 29(4), 655-665. <https://doi.org/10.1105/tpc.16.00915>
- Crang, R., Lyons-Sobaski, S., & Wise, R. (2019). *Plant anatomy: a concept-based approach to the structure of seed plants*. Cham, Switzerland: Springer. <https://doi.org/10.1007/978-3-319-77315-5>

7. Bibliography

- Cui, L., Siskos, L., Wang, C., Schouten, H. J., Visser, R. G. F., & Bai, Y. (2022). Breeding melon (*Cucumis melo*) with resistance to powdery mildew and downy mildew. *Advances of Cucurbitaceae Research*, 8(5), 545-561. <https://doi.org/10.1016/j.hpj.2022.07.006>
- Dahmani-Mardas, F., Troadec, C., Boualem, A., Lévêque, S., Alsadon, A. A., Aldoss, A. A., Bendahmane, A. (2010). Engineering melon plants with improved fruit shelf life using the TILLING approach. *PLoS One*, 5(12), e15776. <https://doi.org/10.1371/journal.pone.0015776>
- Daum, G., Medzihradzky, A., Suzaki, T., & Lohmann, J. U. (2014). A mechanistic framework for noncell autonomous stem cell induction in Arabidopsis. *Proceedings of the National Academy of Sciences*, 111(40), 14619-14624. <https://doi.org/doi:10.1073/pnas.1406446111>
- Dhillon, N. P. S., Ranjana, R., Singh, K., Eduardo, I., Monforte, A. J., Pitrat, M., Singh, P. P. (2007). Diversity among landraces of Indian snapmelon (*Cucumis melo* var. *momordica*). 54(6), 1267-1283. <http://dx.doi.org/10.1007/s10722-006-9108-2>
- Di Donato, M., & Amari, K. (2015). Analysis of the role of myosins in targeting proteins to plasmodesmata. *Methods Mol Biol*, 1217, 283-293. https://doi.org/10.1007/978-1-4939-1523-1_19
- Díaz, J. A., Mallor, C., Soria, C., Camero, R., Garzo, E., Fereres, A., Moriones, E. (2003). Potential Sources of Resistance for Melon to Nonpersistently Aphid-borne Viruses. *Plant Dis*, 87(8), 960-964. <https://doi.org/10.1094/PDIS.2003.87.8.960>
- Diaz, A., Fergany, M., Formisano, G., Ziarsolo, P., Blanca, J., Fei, Z., Monforte, A. J. (2011). A consensus linkage map for molecular markers and Quantitative Trait Loci associated with economically important traits in melon (*Cucumis melo*L.). *II*(1), 111. <https://doi.org/10.1186/1471-2229-11-111>
- Ding, S. W., Shi, B. J., Li, W. X., & Symons, R. H. (1996). An interspecies hybrid RNA virus is significantly more virulent than either parental virus. *Proc Natl Acad Sci U S A*, 93(15), 7470-7474. <https://doi.org/10.1073/pnas.93.15.7470>
- Dogimont, C., Leconte, L., Périn, C., Thabuis, A., Lecoq, H. and Pitrat, M. (2000). Identification of QTLs contributing to resistance to different strains of Cucumber mosaic cucumovirus in melon. *Acta Hort.* 510, 391-398. <https://doi.org/10.17660/ActaHortic.2000.510.62>
- Dos-Santos, N., Bueso, M. C., Díaz, A., Moreno, E., Garcia-Mas, J., Monforte, A. J., & Fernández-Trujillo, J. P. (2023). Thorough Characterization of ETHQB3.5, a QTL Involved in Melon Fruit Climacteric Behavior and Aroma Volatile Composition. *Foods*, 12(2), 376. <https://doi.org/10.3390/foods12020376>

7. Bibliography

- Dou, J., Wang, Y., Yang, H., Niu, H., Liu, D., Yang, S., Yang, L. (2022). Development of branchless watermelon near isogenic lines by marker assisted selection. *Advances of Cucurbitaceae Research*, 8(5), 627-636. <https://doi.org/10.1016/j.hpj.2022.07.003>
- Doyle, J. (1991). DNA Protocols for Plants. In G. M. Hewitt, A. W. B. Johnston, & J. P. W. Young (Eds.), *Molecular Techniques in Taxonomy* (pp. 283-293). Springer Berlin Heidelberg. https://doi.org/10.1007/978-3-642-83962-7_18
- Dwivedi, N., Mishra, M., Sharma, S. S., & Singh, R. K. (2024). Genetic analysis and QTLs identification for resistance to the Begomovirus causing pepper leaf curl virus (PepLCV) disease. 33(1), 34-44. <https://doi.org/10.1007/s13562-023-00855-z>
- Edgley, A. J., Gow, R. M., & Kelly, D. J. (2010). Laser-capture microdissection and pressure catapulting for the analysis of gene expression in the renal glomerulus. *Methods Mol Biol*, 611, 29-40. https://doi.org/10.1007/978-1-60327-345-9_3
- Eduardo, I., Arús, P., & Monforte, A. J. (2005). Development of a genomic library of near isogenic lines (NILs) in melon (*Cucumis melo* L.) from the exotic accession PI161375. *112*(1), 139-148. <https://doi.org/10.1007%2Fs00122-005-0116-y>
- Eduardo, I., Arús, P., Monforte, A. J., Obando, J., Fernández-Trujillo, J. P., Martínez, J. A., van der Knaap, E. (2007). Estimating the Genetic Architecture of Fruit Quality Traits in Melon Using a Genomic Library of Near Isogenic Lines. *Journal of the American Society for Horticultural Science J. Amer. Soc. Hort. Sci.*, 132(1), 80-89. <https://doi.org/10.21273/jashs.132.1.80>
- Eltoum, I., Fredenburgh, J., Myers, R. B., & Grizzle, W. E. (2001). Introduction to the Theory and Practice of Fixation of Tissues. *Journal of Histotechnology*, 24(3), 173-190. <https://doi.org/10.1179/his.2001.24.3.173>
- Endl, J., Achigan-Dako, E. G., Pandey, A. K., Monforte, A. J., Pico, B., & Schaefer, H. (2018). Repeated domestication of melon (*Cucumis melo*) in Africa and Asia and a new close relative from India. *Am J Bot*, 105(10), 1662-1671. <https://doi.org/10.1002/ajb2.1172>
- Eshed, Y., & Zamir, D. (1995). An introgression line population of *Lycopersicon pennellii* in the cultivated tomato enables the identification and fine mapping of yield-associated QTL. *141*(3), 1147-1162. <https://doi.org/10.1093/genetics/141.3.1147>
- Essafi, A., Díaz-Pendón, J. A., Moriones, E., Monforte, A. J., Garcia-Mas, J., & Martín-Hernández, A. M. (2009). Dissection of the oligogenic resistance to Cucumber mosaic virus in the melon accession PI 161375. TAG. *Theoretical*

7. Bibliography

- and applied genetics. *Theoretische und angewandte Genetik*, 118(2), 275–284. <https://doi.org/10.1007/s00122-008-0897-x>
- FAOSTAT, R. (2022). FAOSTAT database. Food Agric. Organ. UN.
- Faulkner, C., & Bayer, E. M. F. (2017). Isolation of Plasmodesmata. In N. L. Taylor & A. H. Millar (Eds.), *Isolation of Plant Organelles and Structures: Methods and Protocols* (pp. 187-198). New York, NY: Springer New York. https://doi.org/10.1007/978-1-4939-6533-5_15
- Fergany, M., Kaur, B., Monforte, A. J., Pitrat, M., Rys, C., Lecoq, H., Dhaliwal, S. S. (2011). Variation in melon (*Cucumis melo*) landraces adapted to the humid tropics of southern India. 58(2), 225-243. <http://dx.doi.org/10.1007/s10722-010-9564-6>
- Gao, X., Wang, C., & Cui, H. (2014). Identification of bundle sheath cell fate factors provides new tools for C3-to-C4 engineering. *Plant Signaling & Behavior*, 9(6), e29162. <https://doi.org/10.4161/psb.29162>
- Gallois, J.-L., Moury, B., & German-Retana, S. (2018). Role of the Genetic Background in Resistance to Plant Viruses. *International Journal of Molecular Sciences*, 19(10), 2856. <https://doi.org/10.3390/ijms19102856>
- García-Arenal, F., & Palukaitis, P. (1999). Structure and functional relationships of satellite RNAs of cucumber mosaic virus. *Curr Top Microbiol Immunol*, 239, 37-63. https://doi.org/10.1007/978-3-662-09796-0_3
- García-Arenal, F., Palukaitis, P., Mahy, B. W. J., & Van Regenmortel, M. H. V. (2008). Cucumber Mosaic Virus. In (pp. 614-619). Oxford: Academic Press. <https://doi.org/10.1016/B978-0-12374410-4.00640-3>
- García-Mas, J., Benjak, A., Sanseverino, W., Bourgeois, M., Mir, G., González, V. M., Puigdomènech, P. (2012). The genome of melon (*Cucumis melo* L.). *Proc Natl Acad Sci U S A*, 109(29), 11872-11877. <https://doi.org/10.1073/pnas.1205415109>
- García-Ruiz, H. (2018). Susceptibility Genes to Plant Viruses. *Viruses*, 10(9), 484. <https://doi.org/10.3390/v10090484>
- Gil, L., Yaron, I., Shalitin, D., Sauer, N., Turgeon, R., & Wolf, S. (2011). Sucrose transporter plays a role in phloem loading in CMV-infected melon plants that are defined as symplastic loaders. *Plant J*, 66(2), 366-374. <https://doi.org/10.1111/j.1365-313X.2011.04498.x>
- Giner, A., Pascual, L., Bourgeois, M., Gyetvai, G., Rios, P., Picó, B., Martín-Hernández, A. M. (2017). A mutation in the melon Vacuolar Protein Sorting 41 prevents systemic infection of Cucumber mosaic virus. 7(1), 10471. <https://doi.org/10.1038/s41598-017-10783-3>

7. Bibliography

- Giordano, A., Santo Domingo, M., Quadrana, L., Pujol, M., Martín-Hernández, A. M., & Garcia-Mas, J. (2022). CRISPR/Cas9 gene editing uncovers the roles of CONSTITUTIVE TRIPLE RESPONSE 1 and REPRESSOR OF SILENCING 1 in melon fruit ripening and epigenetic regulation. *Journal of Experimental Botany*, 73(12), 4022-4033. <https://doi.org/10.1093/jxb/erac148>
- Gomez, S. K., Javot, H., Deewatthanawong, P., Torres-Jerez, I., Tang, Y., Blancaflor, E. B., Harrison, M. J. (2009). Medicago truncatula and Glomus intraradices gene expression in cortical cells harboring arbuscules in the arbuscular mycorrhizal symbiosis. 9(1), 10. <https://doi.org/10.1186/1471-2229-9-10>
- Gonzalo, M. J., Oliver, M., Garcia-Mas, J., Monfort, A., Dolcet-Sanjuan, R., Katzir, N., Monforte, A. J. (2005). Simple-sequence repeat markers used in merging linkage maps of melon (Cucumis melo L.). 110(5), 802-811. <https://doi.org/10.1007/s00122-004-1814-6>
- Gonzalo, M. J., Claveria, E., Monforte, A. J., & Dolcet-Sanjuan, R. (2011). Parthenogenic Haploids in Melon: Generation and Molecular Characterization of a Doubled Haploid Line Population. *Journal of the American Society for Horticultural Science J. Amer. Soc. Hort. Sci.*, 136(2), 145-154. <https://doi.org/10.21273/jashs.136.2.145>
- Gou, M., Balint-Kurti, P., Xu, M., & Yang, Q. (2023). Quantitative disease resistance: Multifaceted players in plant defense. *Journal of Integrative Plant Biology*, 65(2), 594-610. <https://doi.org/https://doi.org/10.1111/jipb.13419>
- Griffiths, H., Weller, G., Toy, L. F., & Dennis, R. J. (2013). You're so vein: bundle sheath physiology, phylogeny and evolution in C3 and C4 plants. *Plant Cell Environ*, 36(2), 249-261. <https://doi.org/10.1111/j.1365-3040.2012.02585.x>
- Gu, F., Crump, C. M., & Thomas, G. (2001). Trans-Golgi network sorting. 58(8), 1067-1084. <https://doi.org/10.1007/PL00000922>
- Guiu-Aragonés, C., Monforte, A. J., Saladié, M., Corrêa, R. X., Garcia-Mas, J., & Martín-Hernández, A. M. (2014). The complex resistance to cucumber mosaic cucumovirus (CMV) in the melon accession PII61375 is governed by one gene and at least two quantitative trait loci. 34(2), 351-362. <https://doi.org/10.1007/s11032-014-0038-y>
- Guiu-Aragonés, C., Díaz-Pendón, J. A., & Martín-Hernández, A. M. (2015). Four sequence positions of the movement protein of Cucumber mosaic virus determine the virulence against cmv1-mediated resistance in melon. *Mol Plant Pathol*, 16(7), 675-684. <https://doi.org/10.1111%2Fmpp.12225>
- Guiu-Aragonés, C., Sánchez-Pina, M. A., Díaz-Pendón, J. A., Peña, E. J., Heinlein, M., & Martín-Hernández, A. M. (2016). cmv1 is a gate for Cucumber mosaic

7. Bibliography

- virus transport from bundle sheath cells to phloem in melon. *Mol Plant Pathol*, 17(6), 973-984. <https://doi.org/10.1111/mpp.12351>
- Gunning, B. E. S., & Steer, M. W. (1996). *Plant cell biology: structure and function*. Boston, Mass.: Jones and Bartlett Publishers.
- Ham, B.-K., Wang, X., Toscano-Morales, R., Lin, J., & Lucas, W. J. (2023). Plasmodesmal endoplasmic reticulum proteins regulate intercellular trafficking of cucumber mosaic virus in Arabidopsis. *Journal of Experimental Botany*, 74(15), 4401-4414. <https://doi.org/10.1093/jxb/erad190>
- Hamann, T. (2012). Plant cell wall integrity maintenance as an essential component of biotic stress response mechanisms. *Frontiers in Plant Science*, 3. <https://doi.org/10.3389/fpls.2012.00077>
- Hashimoto, M., Neriya, Y., Yamaji, Y., & Namba, S. (2016). Recessive Resistance to Plant Viruses: Potential Resistance Genes Beyond Translation Initiation Factors. *Frontiers in Microbiology*, 7. <https://doi.org/10.3389/fmicb.2016.01695>
- Heinlein, M., & Epel, B. L. (2004). Macromolecular Transport and Signaling Through Plasmodesmata. In (Vol. 235, pp. 93-164): Academic Press.
- Hipper, C., Brault, V., Ziegler-Graff, V., & Revers, F. (2013). Viral and Cellular Factors Involved in Phloem Transport of Plant Viruses. *Frontiers in Plant Science*, 4. <https://doi.org/10.3389/fpls.2013.00154>
- Hoffmann, N., King, S., Samuels, A. L., & McFarlane, H. E. (2021). Subcellular coordination of plant cell wall synthesis. *Developmental Cell*, 56(7), 933-948. <https://doi.org/10.1016/j.devcel.2021.03.004>
- Hogekamp, C., Arndt, D., Pereira, P. A., Becker, J. D., Hohnjec, N., & Küster, H. (2011). Laser microdissection unravels cell-type-specific transcription in arbuscular mycorrhizal roots, including CAAT-box transcription factor gene expression correlating with fungal contact and spread. *Plant Physiol*, 157(4), 2023-2043. <https://doi.org/10.1104/pp.111.186635>
- Hou, W. N., Duan, C. G., Fang, R. X., Zhou, X. Y., & Guo, H. S. (2011). Satellite RNA reduces expression of the 2b suppressor protein resulting in the attenuation of symptoms caused by Cucumber mosaic virus infection. *Mol Plant Pathol*, 12(6), 595-605. <https://doi.org/10.1111/j.1364-3703.2010.00696.x>
- Houston, K., Tucker, M. R., Chowdhury, J., Shirley, N., & Little, A. (2016). The Plant Cell Wall: A Complex and Dynamic Structure As Revealed by the Responses of Genes under Stress Conditions. *Frontiers in Plant Science*, 7. <https://doi.org/10.3389/fpls.2016.00984>

7. Bibliography

- Hua, L., Stevenson, S. R., Reyna-Llorens, I., Xiong, H., Kopriva, S., & Hibberd, J. M. (2021). The bundle sheath of rice is conditioned to play an active role in water transport as well as sulfur assimilation and jasmonic acid synthesis. *Plant J*, 107(1), 268-286. <https://doi.org/10.1111/tpj.15292>
- Hull, R. (2009). *Comparative Plant Virology*: Elsevier Science.
- Hull, R. (2014). About the Author. In (pp. xi). Boston: Academic Press.
- Inaba, J., Kim, B. M., Shimura, H., & Masuta, C. (2011). Virus-induced necrosis is a consequence of direct protein-protein interaction between a viral RNA-silencing suppressor and a host catalase. *Plant Physiol*, 156(4), 2026-2036. <https://doi.org/10.1104%2Fpp.111.180042>
- Jacquemond, M., Loebenstein, G., & Lecoq, H. (2012). Chapter 13 - Cucumber Mosaic Virus. In *Viruses and Virus Diseases of Vegetables in the Mediterranean Basin* (Vol. 84, pp. 439-504): Academic Press. <https://doi.org/10.1016/b978-0-12-394314-9.00013-0>
- Joobeur, T., King, J. J., Nolin, S. J., Thomas, C. E., & Dean, R. A. (2004). The Fusarium wilt resistance locus Fom-2 of melon contains a single resistance gene with complex features. In *Plant J* (Vol. 39, pp. 283-297). England. <https://doi.org/10.1111/j.1365-313X.2004.02134.x>
- José, M. A., Iban, E., Silvia, A., & Pere, A. (2005). Inheritance mode of fruit traits in melon: Heterosis for fruit shape and its correlation with genetic distance. *144*(1), 31-38. <https://doi.org/10.1007/s10681-005-0201-y>
- Joshi, M., Narute, T., & Sarnobat, D. (2023). The Cucumber Mosaic Virus: A Review. 35, 253-260. <https://doi.org/10.9734/ijpss/2023/v35i244316>
- Kaeppler, S. M., Phillips, R. L., & Kim, T. S. (1993). Use of near-isogenic lines derived by backcrossing or selfing to map qualitative traits. 87(1), 233-237. <https://doi.org/10.1007/bf00223770>
- Kalluri, N., Serra, O., Donoso, J. M., Picañol, R., Howad, W., Eduardo, I., & Arús, P. (2022). Construction of a collection of introgression lines of “Texas” almond DNA fragments in the “Earlygold” peach genetic background. *Horticulture Research*, 9. <https://doi.org/10.1093/hr/uhac070>
- Kalof, A., Evans, M., Dantey, K., & Cooper, K. (2015). Special Diagnostic Techniques in Surgical Pathology. In (pp. 1-40). <http://dx.doi.org/10.1016/B978-1-4557-7013-7.00001-2>
- Kang, B.-C., Yeam, I., & Jahn, M. M. (2005). Genetics of Plant Virus Resistance. *Annual Review of Phytopathology*, 43(Volume 43, 2005), 581-621. <https://doi.org/10.1146/annurev.phyto.43.011205.141140>
- Kang, B.-H., Anderson, C. T., Arimura, S.-i., Bayer, E., Bezanilla, M., Botella, M. A., Zolman, B. K. (2021). A glossary of plant cell structures: Current insights

7. Bibliography

- and future questions. *The Plant Cell*, 34(1), 10-52. <https://doi.org/10.1093/plcell/koab247>
- Kaplan, I. B., Zhang, L., & Palukaitis, P. (1998). Characterization of cucumber mosaic virus. V. Cell-to-cell movement requires capsid protein but not virions. In *Virology* (Vol. 246, pp. 221-231). United States. <https://doi.org/10.1006/viro.1998.9192>
- Kappagantu, M., Collum, T. D., Dardick, C., & Culver, J. N. (2020). Viral Hacks of the Plant Vasculature: The Role of Phloem Alterations in Systemic Virus Infection. *Annu Rev Virol*, 7(1), 351-370. <https://doi.org/10.1146/annurev-virology-010320-072410>
- Karchi Z., Cohen S., Govers A. (1975). Inheritance of resistance to Cucumber Mosaic virus in melons. *Phytopathology*. 65:479–481. <https://doi.org/10.1094/Phyto-65-479>
- Kerk, N. M., Ceserani, T., Tausta, S. L., Sussex, I. M., & Nelson, T. M. (2003). Laser capture microdissection of cells from plant tissues. *Plant Physiol*, 132(1), 27-35. <https://doi.org/10.1104/pp.102.018127>
- Khaing, Y. Y., Kobayashi, Y., & Takeshita, M. (2020). The 2b protein and C-terminal region of the 2a protein indispensably facilitate systemic movement of cucumber mosaic virus in radish with supplementary function by either the 3a or the coat protein. *Virol J*, 17(1), 49. <https://doi.org/10.1186/s12985-020-01303-3>
- Kiernan, J. A. (2000). Formaldehyde, Formalin, Paraformaldehyde And Glutaraldehyde: What They Are And What They Do. *Microscopy Today*, 8(1), 8-13. <https://doi.org/10.1017/S1551929500057060>
- Kim, M. J., Kim, H. R., & Paek, K. H. (2006). Arabidopsis tonoplast proteins TIP1 and TIP2 interact with the cucumber mosaic virus 1a replication protein. *J Gen Virol*, 87(Pt 11), 3425-3431. <https://doi.org/10.1099/vir.0.82252-0>
- Kim, M. J., Huh, S. U., Ham, B. K., & Paek, K. H. (2008). A novel methyltransferase methylates Cucumber mosaic virus 1a protein and promotes systemic spread. *J Virol*, 82(10), 4823-4833. <https://doi.org/10.1128/jvi.02518-07>
- Kim, S. J., & Brandizzi, F. (2014). The plant secretory pathway: an essential factory for building the plant cell wall. In *Plant Cell Physiol* (Vol. 55, pp. 687-693). Japan. <https://doi.org/10.1093/pcp/pct197>
- Kim, S. J., & Brandizzi, F. (2016). The plant secretory pathway for the trafficking of cell wall polysaccharides and glycoproteins. In *Glycobiology* (Vol. 26, pp. 940-949). <https://doi.org/10.1093/glycob/cww044>
- Kim, K. W. (2020). Methanol fixation for scanning electron microscopy of plants. 50(1), 10. <https://doi.org/10.1186/s42649-020-00028-5>

7. Bibliography

- King, A. M. Q., Adams, M. J., Carstens, E. B., & Lefkowitz, E. J. (2012). Copyright. In (pp. ii). San Diego: Elsevier. <https://doi.org/10.1016/B978-0-12-384684-6.00111-7>
- Kivivirta, K., Herbert, D., Lange, M., Beuerlein, K., Altmüller, J., & Becker, A. (2019). A protocol for laser microdissection (LMD) followed by transcriptome analysis of plant reproductive tissue in phylogenetically distant angiosperms. *15*(1), 151. <https://doi.org/10.1186/s13007-019-0536-3>
- Knapp, E., Flores, R., Scheiblin, D., Modla, S., Czymmek, K., & Yusibov, V. (2012). A cryohistological protocol for preparation of large plant tissue sections for screening intracellular fluorescent protein expression. In *Biotechniques* (Vol. 52, pp. 31-37). England. <https://doi.org/10.2144/000113778>
- Kobayashi, K., Sekine, K.-T., & Nishiguchi, M. (2014). Breakdown of plant virus resistance: can we predict and extend the durability of virus resistance?, *80*(4), 327-336. <https://doi.org/10.1007/s10327-014-0527-1>
- Kobori, T., Ohki, S. T., & Osaki, T. (2000). Movement of Cucumber Mosaic Virus Is Restricted at the Interface between Mesophyll and Phloem Pathway in *Cucumis figarei*. *66*(2), 159-166. <https://doi.org/10.1007/PL00012939>
- Kong, Q., Gao, L., Cao, L., Liu, Y., Saba, H., Huang, Y., & Bie, Z. (2016). Assessment of Suitable Reference Genes for Quantitative Gene Expression Studies in Melon Fruits. *Front Plant Sci*, *7*, 1178. <https://doi.org/10.3389/fpls.2016.01178>
- Kułak, K., Wojciechowska, N., Samelak-Czajka, A., Jackowiak, P., & Bagniewska-Zadworna, A. (2023). How to explore what is hidden? A review of techniques for vascular tissue expression profile analysis. *19*(1), 129. <https://doi.org/10.1186/s13007-023-01109-8>
- Kumar, G., & Dasgupta, I. (2021). Variability, Functions and Interactions of Plant Virus Movement Proteins: What Do We Know So Far? *Microorganisms*, *9*(4), 695. <https://doi.org/10.3390/microorganisms9040695>
- Kumari, R., Kumar, S., Singh, L., & Hallan, V. (2016). Movement Protein of Cucumber Mosaic Virus Associates with Apoplastic Ascorbate Oxidase. *PLoS One*, *11*(9), e0163320. <https://doi.org/10.1371/journal.pone.0163320>
- Lambers, H., Chapin, F. S., & Pons, T. L. (2008). Long-Distance Transport of Assimilates. In *Plant Physiological Ecology* (pp. 151-162). New York, NY: Springer New York. https://doi.org/10.1007/978-0-387-78341-3_4
- Latrasse, D., Rodriguez-Granados, N. Y., Veluchamy, A., Mariappan, K. G., Bevilacqua, C., Crapart, N., Bendahmane, A. (2017). The quest for epigenetic regulation underlying unisexual flower development in *Cucumis melo*. *Epigenetics Chromatin*, *10*, 22. <https://doi.org/10.1186/s13072-017-0132-6>

7. Bibliography

- Lecoq, H., Desbiez, C., & Loebenstein, G. (2012). Chapter 3 - Viruses of Cucurbit Crops in the Mediterranean Region: An Ever-Changing Picture. In *Viruses and Virus Diseases of Vegetables in the Mediterranean Basin* (Vol. 84, pp. 67-126): Academic Press. <https://doi.org/10.1016/b978-0-12-394314-9.00003-8>
- Lee, J.-Y., & Frank, M. (2018). Plasmodesmata in phloem: different gateways for different cargoes. *43 Physiology and metabolism* 2018, 43, 119-124. <https://doi.org/10.1016/j.pbi.2018.04.014>
- Lee, S., Park, G., Choi, Y., Park, S., Kim, H., Lee, O., Park, Y. (2022). Whole-Genome Resequencing of Near-Isogenic Lines Reveals a Genomic Region Associated with High Trans-Lycopene Contents in Watermelon. *Plants*, 11(1), 8. <https://doi.org/10.3390/plants11010008>
- Leegood, R. C. (2008). Roles of the bundle sheath cells in leaves of C3 plants. In *J Exp Bot* (Vol. 59, pp. 1663-1673). England. <https://doi.org/10.1093/jxb/erm335>
- Lefkowitz, E. J., Dempsey, D. M., Hendrickson, R. C., Orton, R. J., Siddell, S. G., & Smith, D. B. (2018). Virus taxonomy: the database of the International Committee on Taxonomy of Viruses (ICTV). *Nucleic Acids Res*, 46(D1), D708-D717. <https://doi.org/10.1093/nar/gkx932>
- Lester, G. E., & Hodges, D. M. (2008). Antioxidants associated with fruit senescence and human health: Novel orange-fleshed non-netted honey dew melon genotype comparisons following different seasonal productions and cold storage durations. 48(3), 347-354. <https://doi.org/10.1016/j.postharvbio.2007.11.008>
- Lewsey, M., Surette, M., Robertson, F. C., Ziebell, H., Choi, S. H., Ryu, K. H., Carr, J. P. (2009). The role of the Cucumber mosaic virus 2b protein in viral movement and symptom induction. *Mol Plant Microbe Interact*, 22(6), 642-654. <https://doi.org/10.1094/mpmi-22-6-0642>
- Li, Q., Ryu, K. H., & Palukaitis, P. (2001). Cucumber mosaic virus-plant interactions: identification of 3a protein sequences affecting infectivity, cell-to-cell movement, and long-distance movement. *Mol Plant Microbe Interact*, 14(3), 378-385. <https://doi.org/10.1094/mpmi.2001.14.3.378>
- Liu, H., McDowell, T. L., Hanson, N. E., Tang, X., Fujimoto, J., & Rodriguez-Canales, J. (2014). Laser capture microdissection for the investigative pathologist. In *Vet Pathol* (Vol. 51, pp. 257-269). <https://doi.org/10.1177/0300985813510533>
- Liu, B., Santo Domingo, M., Mayobre, C., Martín-Hernández, A. M., Pujol, M., & Garcia-Mas, J. (2022). Knock-Out of CmNAC-NOR Affects Melon

7. Bibliography

- Climacteric Fruit Ripening. *Frontiers in Plant Science*, 13. <https://doi.org/10.3389/fpls.2022.878037>
- Liu, Z., & Cheng, J. (2024). C4 rice engineering, beyond installing a C4 cycle. 206, 108256. <https://doi.org/10.1016/j.plaphy.2023.108256>
- López-Martín, M., Sifres, A., Gómez-Guillamón, M. L., Picó, B., & Pérez-de-Castro, A. (2024). Incidence and genetic diversity of cucurbit viruses in the Spanish Mediterranean area. *Plant Pathology*, 73(2), 431-443. <https://doi.org/https://doi.org/10.1111/ppa.13825>
- Lu, J., Hou, J., Ouyang, Y., Luo, H., Zhao, J., Mao, C., Li, X. (2020). A direct PCR-based SNP marker-assisted selection system (D-MAS) for different crops. 40(1), 9. <https://doi.org/10.1007/s11032-019-1091-3>
- Lu, G., Wang, Z., Pan, Y.-B., Wu, Q., Cheng, W., Xu, F., Xu, L. (2023). Identification of QTLs and critical genes related to sugarcane mosaic disease resistance. *Frontiers in Plant Science*, 14. <https://doi.org/10.3389/fpls.2023.1107314>
- Luo, K. R., Huang, N. C., & Yu, T. S. (2018). Selective Targeting of Mobile mRNAs to Plasmodesmata for Cell-to-Cell Movement. *Plant Physiol*, 177(2), 604-614. <https://doi.org/10.1104/pp.18.00107>
- Ma, M., Liu, S., Wang, Z., Shao, R., Ye, J., Yan, W., Che, G. (2022). Genome-Wide Identification of the SUN Gene Family in Melon (*Cucumis melo*) and Functional Characterization of Two CmSUN Genes in Regulating Fruit Shape Variation. *Int J Mol Sci*, 23(24). <https://doi.org/10.3390/ijms232416047>
- Malik, A. A., Vashisht, V. K., Singh, K., Sharma, A., Singh, D. K., Singh, H., Dhillon, N. P. S. (2014). Diversity among melon (*Cucumis melo* L.) landraces from the Indo-Gangetic plains of India and their genetic relationship with USA melon cultivars. 61(6), 1189-1208. <http://dx.doi.org/10.1007/s10722-014-0101-x>
- Malter, D., & Wolf, S. (2011). Melon phloem-sap proteome: developmental control and response to viral infection. *Protoplasma*, 248(1), 217-224. <https://doi.org/10.1007/s00709-010-0215-8>
- Manchali, S., Chidambara Murthy, K. N., Vishnuvardana, & Patil, B. S. (2021). Nutritional Composition and Health Benefits of Various Botanical Types of Melon (*Cucumis melo* L.). *Plants*, 10(9), 1755. <https://doi.org/10.3390/plants10091755>
- Martín-Hernández, A. M., & Picó, B. (2021). Natural Resistances to Viruses in Cucurbits. *Agronomy*, 11(1), 23. <https://dx.doi.org/doi:10.3390/agronomy11010023>

7. Bibliography

- Masuta, C., Inaba, J., & Shimura, H. (2012). The 2b proteins of Cucumber mosaic virus generally have the potential to differentially induce necrosis on Arabidopsis. *Plant Signal Behav*, 7(1), 43-45. <https://doi.org/10.4161%2Fpsb.7.1.18526>
- Matsuno, A., Nagashima, T., Ohsugi, Y., Utsunomiya, H., Takekoshi, S., Munakata, S., Watanabe, K. (2000). Electron microscopic observation of intracellular expression of mRNA and its protein product: technical review on ultrastructural in situ hybridization and its combination with immunohistochemistry. *Histol Histopathol*, 15(1), 261-268. <https://doi.org/10.14670/hh-15.261>
- Maule, A. J., Benitez-Alfonso, Y., & Faulkner, C. (2011). Plasmodesmata – membrane tunnels with attitude. *14/6 Cell biology*, 14(6), 683-690. <https://doi.org/10.1016/j.pbi.2011.07.007>
- Mayobre, C., Santo Domingo, M., Özkan, E. N., Fernández-Borbolla, A., Ruiz-Lasierra, J., Garcia-Mas, J., & Pujol, M. (2024). Genetic regulation of volatile production in two melon introgression line collections with contrasting ripening behavior. *Horticulture Research*, 11(3). <https://doi.org/10.1093/hr/uhae020>
- McDonald, B. A., & Linde, C. (2002). Pathogen population genetics, evolutionary potential, and durable resistance. *Annual Review of Phytopathology*, 40(Volume 40, 2002), 349-379. <https://doi.org/https://doi.org/10.1146/annurev.phyto.40.120501.101443>
- Mellor, N. L., Voß, U., Janes, G., Bennett, M. J., Wells, D. M., & Band, L. R. (2020). Auxin fluxes through plasmodesmata modify root-tip auxin distribution. *Development*, 147(6). <https://doi.org/10.1242/dev.181669>
- Menon, D. S., & Ramana Rao, T. V. (2012). Nutritional quality of muskmelon fruit as revealed by its biochemical properties during different rates of ripening. *19*, 1621-1628. [http://ifrrj.upm.edu.my/19%20\(04\)%202012/45%20IFRJ%2019%20\(04\)%202012%20Rao%20\(337\).pdf](http://ifrrj.upm.edu.my/19%20(04)%202012/45%20IFRJ%2019%20(04)%202012%20Rao%20(337).pdf)
- Miao, G., Zhao, H., Li, Y., Ji, M., Chen, Y., Shi, Y., Zhang, H. (2021). ORF3a of the COVID-19 virus SARS-CoV-2 blocks HOPS complex-mediated assembly of the SNARE complex required for autolysosome formation. *Dev Cell*, 56(4), 427-442 e425. <https://doi.org/10.1016/j.devcel.2020.12.010>
- Mochizuki, T., & Ohki, S. T. (2012). Cucumber mosaic virus: viral genes as virulence determinants. *Mol Plant Pathol*, 13(3), 217-225. <https://doi.org/10.1111/j.1364-3703.2011.00749.x>

7. Bibliography

- Moffett, P. (2009). Mechanisms of recognition in dominant R gene mediated resistance. In *Adv Virus Res* (Vol. 75, pp. 1-33). United States: 2009 Elsevier Inc. [https://doi.org/10.1016/s0065-3527\(09\)07501-0](https://doi.org/10.1016/s0065-3527(09)07501-0)
- Molin, S. O., Nygren, H., & Dolonius, L. (1978). A new method for the study of glutaraldehyde-induced crosslinking properties in proteins with special reference to the reaction with amino groups. *J Histochem Cytochem*, 26(5), 412-414. <https://doi.org/10.1177/26.5.96177>
- Moreno, I. M., Thompson, J. R., & García-Arenal, F. (2004). Analysis of the systemic colonization of cucumber plants by Cucumber green mottle mosaic virus. *J Gen Virol*, 85(Pt 3), 749-759. <https://doi.org/10.1099/vir.0.19540-0>
- Moury, B., & Verdín, E. (2012). Viruses of pepper crops in the Mediterranean basin: a remarkable stasis. In *Adv Virus Res* (Vol. 84, pp. 127-162). United States: © 2012 Elsevier Inc. <https://doi.org/10.1016/b978-0-12-394314-9.00004-x>
- Mrkvová, M., Hančinský, R., Predajňa, L., Alaxin, P., Achs, A., Tomašechová, J., Glasa, M. (2022). High-Throughput Sequencing Discloses the Cucumber Mosaic Virus (CMV) Diversity in Slovakia and Reveals New Hosts of CMV from the Papaveraceae Family. *Plants*, 11(13), 1665. <https://doi.org/10.3390/plants11131665>
- Muñoz-Sanhueza, L. G., Lee, Y., Tillmann, M., Cohen, J. D., & Hvoslef-Eide, A. K. (2018). Auxin analysis using laser microdissected plant tissues sections. *18*(1), 133. <https://doi.org/10.1186/s12870-018-1352-z>
- Murphy, A. M., Jiang, S., Elderfield, J. A. D., Pate, A. E., Halliwell, C., Glover, B. J., Carr, J. P. (2023). Biased pollen transfer by bumblebees favors the paternity of virus-infected plants in cross-pollination. *iScience*, 26(3), 106116. <https://doi.org/10.1016/j.isci.2023.106116>
- Mustafa, A., Cenayko, C., Mitry, R. R., & Quaglia, A. (2012). Laser microdissection microscopy: application to cell culture. *Methods Mol Biol*, 806, 385-392. https://doi.org/10.1007/978-1-61779-367-7_25
- Nagashima, H., Kashiwazaki, N., Ashman, R. J., Grupen, C. G., & Nottle, M. B. (1995). Cryopreservation of porcine embryos. *374*(6521), 416-416. <https://doi.org/10.1038/374416a0>
- Navarro, J. A., Sanchez-Navarro, J. A., Pallas, V., Kielian, M., Mettenleiter, T. C., & Roossinck, M. J. (2019). Chapter One - Key checkpoints in the movement of plant viruses through the host. In *Virus Entry* (Vol. 104, pp. 1-64): Academic Press. <https://doi.org/10.1016/bs.aivir.2019.05.001>
- Navas-Castillo, J., & Fiallo-Olivé, E. (2021). Special Issue "Plant Viruses: From Ecology to Control". *Microorganisms*, 9(6). <https://doi.org/10.3390/microorganisms9061136>

7. Bibliography

- Nicaise, V. (2014). Crop immunity against viruses: outcomes and future challenges. *Frontiers in Plant Science*, 5. <https://doi.org/10.3389/fpls.2014.00660>
- Nishizawa, S., Sakai, A., Amano, Y., & Matsuzawa, T. (1993). Cryopreservation of asparagus (*Asparagus officinalis* L.) embryogenic suspension cells and subsequent plant regeneration by vitrification. *Plant Science*, 91(1), 67-73. [https://doi.org/https://doi.org/10.1016/0168-9452\(93\)90189-7](https://doi.org/https://doi.org/10.1016/0168-9452(93)90189-7)
- Nizan, S., Amitzur, A., Dahan-Meir, T., Benichou, J. I. C., Bar-Ziv, A., & Perl-Treves, R. (2023). Mutagenesis of the melon Prv gene by CRISPR/Cas9 breaks papaya ringspot virus resistance and generates an autoimmune allele with constitutive defense responses. *J Exp Bot*, 74(15), 4579-4596. <https://doi.org/10.1093/jxb/erad156>
- Obando-Ulloa, J. M., Ruiz, J., Monforte, A. J., & Fernández-Trujillo, J. P. (2010). Aroma profile of a collection of near-isogenic lines of melon (*Cucumis melo* L.). <https://doi.org/10.1016/j.foodchem.2009.05.068>
- Oparka, K. J., & Turgeon, R. (1999). Sieve Elements and Companion Cells—Traffic Control Centers of the Phloem. *The Plant Cell*, 11(4), 739-750. <https://doi.org/10.1105/tpc.11.4.739>
- Ohnishi, S., Echizenya, I., Yoshimoto, E., Boumin, K., Inukai, T., & Masuta, C. (2011). Multigenic system controlling viral systemic infection determined by the interactions between Cucumber mosaic virus genes and quantitative trait loci of soybean cultivars. *Phytopathology*, 101(5), 575-582. <https://doi.org/10.1094/phyto-06-10-0154>
- Ouibrahim, L., Mazier, M., Estevan, J., Pagny, G., Decroocq, V., Desbiez, C., Caranta, C. (2014). Cloning of the Arabidopsis *rwml* gene for resistance to Watermelon mosaic virus points to a new function for natural virus resistance genes. *The Plant Journal*, 79(5), 705-716. <https://doi.org/10.1111/tpj.12586>
- Palukaitis, P., Roossinck, M. J., Dietzgen, R. G., Francki, R. I. B., Maramorosch, K., Murphy, F. A., & Shatkin, A. J. (1992). Cucumber MOSAIC Virus. In (Vol. 41, pp. 281-348): Academic Press. [https://doi.org/10.1016/S0065-3527\(08\)60039-1](https://doi.org/10.1016/S0065-3527(08)60039-1)
- Palukaitis, P., & García-Arenal, F. (2003). Cucumoviruses. In (Vol. 62, pp. 241-323): Academic Press. [https://doi.org/10.1016/s0065-3527\(03\)62005-1](https://doi.org/10.1016/s0065-3527(03)62005-1)
- Palukaitis, P. (2016). Satellite RNAs and Satellite Viruses. *Molecular Plant-Microbe Interactions*®, 29(3), 181-186. <https://doi.org/10.1094/MPMI-10-15-0232-FI>
- Park, T. S., Min, D. J., Park, J. S., & Hong, J. S. (2024). The N-Terminal Region of Cucumber Mosaic Virus 2a Protein Is Involved in the Systemic Infection in Brassica juncea. *Plants (Basel)*, 13(7). <https://doi.org/10.3390/plants13071001>

7. Bibliography

- Pascual, L., Yan, J., Pujol, M., Monforte, A. J., Picó, B., & Martín-Hernández, A. M. (2019). CmVPS41 Is a General Gatekeeper for Resistance to Cucumber Mosaic Virus Phloem Entry in Melon. *Front Plant Sci*, *10*, 1219. <https://doi.org/10.3389/fpls.2019.01219>
- Peña, E. J., & Heinlein, M. (2012). RNA transport during TMV cell-to-cell movement. *Front Plant Sci*, *3*, 193. <https://doi.org/10.3389/fpls.2012.00193>
- Peña, E., Niehl, A., & Heinlein, M. (2012). Viral Studies Point the Way: Mechanisms of Intercellular Transport. In F. Kragler & M. Hülskamp (Eds.), *Short and Long Distance Signaling* (pp. 1-43). New York, NY: Springer New York. https://doi.org/10.1007/978-1-4419-1532-0_1
- Pereira, L., Pujol, M., Garcia-Mas, J., & Phillips, M. A. (2017). Non-invasive quantification of ethylene in attached fruit headspace at 1 p.p.b. by gas chromatography-mass spectrometry. *Plant J*, *91*(1), 172-183. <https://doi.org/10.1111/tpj.13545>
- Pereira, L., Santo Domingo, M., Ruggieri, V., Argyris, J., Phillips, M. A., Zhao, G., Garcia-Mas, J. (2020). Genetic dissection of climacteric fruit ripening in a melon population segregating for ripening behavior. *Horticulture Research*, *7*. <https://doi.org/10.1038/s41438-020-00411-z>
- Pereira, L., Santo Domingo, M., Argyris, J., Mayobre, C., Valverde, L., Martín-Hernández, A. M., Garcia-Mas, J. (2021). A novel introgression line collection to unravel the genetics of climacteric ripening and fruit quality in melon. *II*(1), 11364. <https://doi.org/10.1038/s41598-021-90783-6>
- Périn, C., Hagen, S., De Conto, V., Katzir, N., Danin-Poleg, Y., Portnoy, V., Pitrat, M. (2002). A reference map of Cucumis melo based on two recombinant inbred line populations. *Theor Appl Genet*, *104*(6-7), 1017-1034. <https://doi.org/10.1007/s00122-002-0864-x>
- Perpiñá, G., Esteras, C., Gibon, Y., Monforte, A. J., & Picó, B. (2016). A new genomic library of melon introgression lines in a cantaloupe genetic background for dissecting desirable agronomical traits. *16*(1), 154. <https://doi.org/10.1186/s12870-016-0842-0>
- Pestova, T. V., Kolupaeva, V. G., Lomakin, I. B., Pilipenko, E. V., Shatsky, I. N., Agol, V. I., & Hellen, C. U. (2001). Molecular mechanisms of translation initiation in eukaryotes. *Proc Natl Acad Sci U S A*, *98*(13), 7029-7036. <https://doi.org/10.1073/pnas.111145798>
- Pilet-Nayel, M.-L., Moury, B., Caffier, V., Montarry, J., Kerlan, M.-C., Fournet, S., Delourme, R. (2017). Quantitative Resistance to Plant Pathogens in Pyramiding Strategies for Durable Crop Protection. *Frontiers in Plant Science*, *8*. <https://doi.org/10.3389/fpls.2017.01838>

7. Bibliography

- Pitrat, M., & Lecoq, H. (1980). Inheritance of resistance to cucumber mosaic virus transmission by *Aphis gossypii* in *Cucumis melo*. *Phytopathology*, *70*, 958-961.
- Pitrat, M. (2008). Melon. In J. Prohens & F. Nuez (Eds.), *Vegetables I: Asteraceae, Brassicaceae, Chenopodiaceae, and Cucurbitaceae* (pp. 283-315). New York, NY: Springer New York. https://doi.org/10.1007/978-0-387-30443-4_9
- Popovic, R., Beauregard, M., & Leblanc, R. M. (1987). Study of Energy Storage Processes in Bundle Sheath Cells of *Zea mays*. *Plant Physiol*, *84*(4), 1437-1441. <https://doi.org/10.1104/pp.84.4.1437>
- Prabhandakavi, P., Pogiri, R., Kumar, R., Acharya, S., Esakky, R., Chakraborty, M., Palicherla, S. R. (2021). Pyramiding Ty-1/Ty-3, Ty-2, ty-5 and ty-6 genes into tomato hybrid to develop resistance against tomato leaf curl viruses and recurrent parent genome recovery by ddRAD sequencing method. *30*(3), 462-476. <https://doi.org/10.1007/s13562-020-00633-1>
- Prasanth, K. R., Huang, Y. W., Liou, M. R., Wang, R. Y., Hu, C. C., Tsai, C. H., Hsu, Y. H. (2011). Glyceraldehyde 3-phosphate dehydrogenase negatively regulates the replication of Bamboo mosaic virus and its associated satellite RNA. *J Virol*, *85*(17), 8829-8840. <https://doi.org/10.1128/JVI.00556-11>
- R Core Team (2022). R: A language and environment for statistical computing. R Foundation for Statistical Computing, Vienna, Austria. URL <https://www.R-project.org/>.
- Reagan, B. C., & Burch-Smith, T. M. (2020). Viruses Reveal the Secrets of Plasmodesmal Cell Biology. *Molecular Plant-Microbe Interactions*®, *33*(1), 26-39. <https://doi.org/10.1094/mpmi-07-19-0212-fi>
- Real, N. (2022). Study of the resistance to Cucumber mosaic virus controlled by Vacuolar protein sorting 41 in *Cucumis melo*. <http://hdl.handle.net/10803/675240>
- Real, N., Villar, I., Serrano, I., Guiu-Aragonés, C., & Martín-Hernández, A. M. (2023). Mutations in CmVPS41 controlling resistance to cucumber mosaic virus display specific subcellular localization. *Plant Physiology*, *191*(3), 1596-1611. <https://doi.org/10.1093/plphys/kiac583>
- Renner, S. S., Schaefer, H., & Kocyan, A. (2007). Phylogenetics of *Cucumis* (Cucurbitaceae): Cucumber (*C. sativus*) belongs in an Asian/Australian clade far from melon (*C. melo*). *7*(1), 58. <https://doi.org/10.1186%2F1471-2148-7-58>
- Renner, S. S., & Schaefer, H. (2017). Phylogeny and Evolution of the Cucurbitaceae. In R. Grumet, N. Katzir, & J. Garcia-Mas (Eds.), *Genetics and Genomics of*

7. Bibliography

- Cucurbitaceae* (pp. 13-23). Springer International Publishing. https://doi.org/10.1007/7397_2016_14
- Requena, A., Simón-Buela, L., Salcedo, G., & García-Arenal, F. (2006). Potential involvement of a cucumber homolog of phloem protein 1 in the long-distance movement of Cucumber mosaic virus particles. *Mol Plant Microbe Interact*, *19*(7), 734-746. <https://doi.org/10.1094/mpmi-19-0734>
- Riedel, C., Habekuß, A., Schliephake, E., Niks, R., Broer, I., & Ordon, F. (2011). Pyramiding of Ryd2 and Ryd3 conferring tolerance to a German isolate of Barley yellow dwarf virus-PAV (BYDV-PAV-ASL-1) leads to quantitative resistance against this isolate. *123*(1), 69-76. <https://doi.org/10.1007/s00122-011-1567-y>
- Rieu, I., & Powers, S. J. (2009). Real-time quantitative RT-PCR: design, calculations, and statistics. *Plant Cell*, *21*(4), 1031-1033. <https://doi.org/10.1105/tpc.109.066001>
- Risser, G., Pitrat, M., and Rode, J. C. (1977). Etude de la résistance du melon (*Cucumis melo* L.) au virus de la mosaïque du concombre. *Ann Amél Plant* *27*, 509–522
- Rodriguez-Canales, J., Hanson, J. C., Hipp, J. D., Balis, U. J., Tangrea, M. A., Emmert-Buck, M. R., & Bova, G. S. (2013). Optimal molecular profiling of tissue and tissue components: defining the best processing and microdissection methods for biomedical applications. *Methods Mol Biol*, *980*, 61-120. https://doi.org/10.1007/978-1-62703-287-2_5
- Rojas, M. R., Maliano, M. R., de Souza, J. O., Vasquez-Mayorga, M., de Macedo, M. A., Ham, B.-K., & Gilbertson, R. L. (2016). Cell-to-Cell Movement of Plant Viruses: A Diversity of Mechanisms and Strategies. In A. Wang & X. Zhou (Eds.), *Current Research Topics in Plant Virology* (pp. 113-152). Cham: Springer International Publishing. https://doi.org/10.1007/978-3-319-32919-2_5
- Romanov, A., Ly, K., & Kirchoff, B. (2021). Use Of Polyethylene Glycol As An Embedding Medium Produces Results Similar To Those Of Paraffin Wax Embedding. *Edinburgh Journal Of Botany* *78*, Article 382: 1–13
- Roossinck, M. J. (2001). Cucumber mosaic virus, a model for RNA virus evolution. In *Mol Plant Pathol* (Vol. 2, pp. 59-63). England. <https://doi.org/10.1046/j.1364-3703.2001.00058.x>
- Ross-Elliott, T. J., Jensen, K. H., Haaning, K. S., Wager, B. M., Knoblauch, J., Howell, A. H., Mullendore, D. L., Monteith, A. G., Paultre, D., Yan, D., Otero, S., Bourdon, M., Sager, R., Lee, J. Y., Helariutta, Y., Knoblauch, M., & Oparka, K. J. (2017). Phloem unloading in Arabidopsis roots is convective

- and regulated by the phloem-pole pericycle. *eLife*, 6, e24125. <https://doi.org/10.7554/eLife.24125>
- Rossi, M., Pesando, M., Vallino, M., Galetto, L., Marzachì, C., & Balestrini, R. (2018). Application of laser microdissection to study phytoplasma site-specific gene expression in the model plant *Arabidopsis thaliana*. In *Microbiol Res* (Vol. 217, pp. 60-68). © 2018 Elsevier GmbH. <https://doi.org/10.1016/j.micres.2018.09.001>
- Ruggieri, V., Alexiou, K. G., Morata, J., Argyris, J., Pujol, M., Yano, R., Garcia-Mas, J. (2018). An improved assembly and annotation of the melon (*Cucumis melo* L.) reference genome. 8(1), 8088. <https://doi.org/10.1038/s41598-018-26416-2>
- Sakai, A., Kobayashi, S., & Oiyama, I. (1990). Cryopreservation of nucellar cells of navel orange (*Citrus sinensis* Osb. var. *brasiliensis* Tanaka) by vitrification. *Plant Cell Rep*, 9(1), 30-33. <https://doi.org/10.1007/bf00232130>
- Sakai, K., Taconnat, L., Borrega, N., Yansouni, J., Brunaud, V., Paysant-Le Roux, C., Dubreucq, B. (2018). Combining laser-assisted microdissection (LAM) and RNA-seq allows to perform a comprehensive transcriptomic analysis of epidermal cells of *Arabidopsis* embryo. 14(1), 10. <https://doi.org/10.1186/s13007-018-0275-x>
- Salánki, K., Gellért, Á., Huppert, E., Náray-Szabó, G., & Balázs, E. (2004). Compatibility of the movement protein and the coat protein of cucumoviruses is required for cell-to-cell movement. *J Gen Virol*, 85(Pt 4), 1039-1048. <https://doi.org/10.1099/vir.0.19687-0>
- Salánki, K., Kiss, L., Gellért, A., & Balázs, E. (2011). Identification a coat protein region of cucumber mosaic virus (CMV) essential for long-distance movement in cucumber. *Arch Virol*, 156(12), 2279-2283. <https://doi.org/10.1007/s00705-011-1104-y>
- Saltveit, M. E., & Yahia, E. M. (2011). 2 - Melon (*Cucumis melo* L.). In *Woodhead Publishing Series in Food Science, Technology and Nutrition* (pp. 31-45e): Woodhead Publishing. <https://doi.org/10.1533/9780857092618.31>
- Sanfaçon, H. (2015). Plant Translation Factors and Virus Resistance. *Viruses*, 7(7), 3392-3419. <https://doi.org/10.3390/v7072778>
- Sanseverino, W., Hénaff, E., Vives, C., Pinosio, S., Burgos-Paz, W., Morgante, M., Casacuberta, J. M. (2015). Transposon Insertions, Structural Variations, and SNPs Contribute to the Evolution of the Melon Genome. In *Mol Biol Evol* (Vol. 32, pp. 2760-2774). © The Author 2015. Published by Oxford University Press on behalf of the Society for Molecular Biology and Evolution For permissions, please e-mail: journals.permissions@oup.com. <https://doi.org/10.1093/molbev/msv152>

7. Bibliography

- Santo Domingo, M., Areco, L., Mayobre, C., Valverde, L., Martín-Hernández, A. M., Pujol, M., & Garcia-Mas, J. (2022a). Modulating climacteric intensity in melon through QTL stacking. *Horticulture Research*, 9. <https://doi.org/10.1093/hr/uhac131>
- Santo Domingo, Miguel, Carlos Mayobre, Lara Pereira, Jason Argyris, Laura Valverde, Ana Montserrat Martín-Hernández, Jordi Garcia-Mas, and Marta Pujol. (2022b). Fruit Morphology and Ripening-Related QTLs in a Newly Developed Introgression Line Collection of the Elite Varieties ‘Védrantais’ and ‘Piel de Sapo *Plants*, 11(22), 3120. <https://doi.org/10.3390/plants11223120>
- Sáray, R., Fábíán, A., Palkovics, L., & Salánki, K. (2021). The 28 Ser Amino Acid of Cucumber Mosaic Virus Movement Protein Has a Role in Symptom Formation and Plasmodesmata Localization. *Viruses*, 13(2). <https://doi.org/10.3390/v13020222>
- Sasaki, N., Park, J. W., Maule, A. J., & Nelson, R. S. (2006). The cysteine-histidine-rich region of the movement protein of Cucumber mosaic virus contributes to plasmodesmal targeting, zinc binding and pathogenesis. In *Virology* (Vol. 349, pp. 396-408). United States. <https://doi.org/10.1016/j.virol.2006.02.035>
- Sastry, K. S., Mandal, B., Hammond, J., Scott, S. W., & Briddon, R. W. (2019). *Encyclopedia of Plant Viruses and Viroids*. New Delhi: Springer India. <https://doi.org/10.1007/978-81-322-3912-3>
- Schaefer, H., Heibl, C., & Renner, S. S. (2009). Gourds afloat: a dated phylogeny reveals an Asian origin of the gourd family (Cucurbitaceae) and numerous oversea dispersal events. *Proc Biol Sci*, 276(1658), 843-851. <https://doi.org/10.1098/rspb.2008.1447>
- Schaefer, H., & Renner, S. S. (2011). Phylogenetic relationships in the order Cucurbitales and a new classification of the gourd family (Cucurbitaceae). *TAXON*, 60(1), 122-138. <https://doi.org/https://doi.org/10.1002/tax.601011>
- Sebastian, P., Schaefer, H., Telford, I. R. H., & Renner, S. S. (2010). Cucumber (*Cucumis sativus*) and melon (*C. melo*) have numerous wild relatives in Asia and Australia, and the sister species of melon is from Australia. *Proceedings of the National Academy of Sciences*, 107(32), 14269-14273. <https://doi.org/doi:10.1073/pnas.1005338107>
- Seo, J.-K., Kwon, S.-J., Choi, H.-S., & Kim, K.-H. (2009). Evidence for alternate states of Cucumber mosaic virus replicase assembly in positive- and negative-strand RNA synthesis. 383(2), 248-260. <https://doi.org/10.1016/j.virol.2008.10.033>

7. Bibliography

- Sevilem, I., Yadav, S. R., & Helariutta, Y. (2015). Plasmodesmata: channels for intercellular signaling during plant growth and development. *Methods Mol Biol*, 1217, 3-24. <https://doi.org/10.1007/978-1-4939-1523-1>
- Shi, A., Chen, P., Li, D., Zheng, C., Zhang, B., & Hou, A. (2009). Pyramiding multiple genes for resistance to soybean mosaic virus in soybean using molecular markers. 23(1), 113-124. <https://doi.org/10.1007/s11032-008-9219-x>
- Shiono, K., Yamauchi, T., Yamazaki, S., Mohanty, B., Malik, A. I., Nagamura, Y., Nakazono, M. (2014). Microarray analysis of laser-microdissected tissues indicates the biosynthesis of suberin in the outer part of roots during formation of a barrier to radial oxygen loss in rice (*Oryza sativa*). In *J Exp Bot* (Vol. 65, pp. 4795-4806). England: © The Author 2014. Published by Oxford University. <https://doi.org/10.1093/jxb/eru235>
- Shunmugam, A. S. K., Bollina, V., Dukowic-Schulze, S., Bhowmik, P. K., Ambrose, C., Higgins, J. D., Kagale, S. (2018). MeioCapture: an efficient method for staging and isolation of meiocytes in the prophase I sub-stages of meiosis in wheat. 18(1), 293. <https://doi.org/10.1186/s12870-018-1514-z>
- Sicking, C., & Krenz, B. (2022). Rolling circle amplification of begomoviral DNA from a single nucleus isolated by laser dissection microscopy. 308, 114591. <https://doi.org/10.1016/j.jviromet.2022.114591>
- Song, Z., Fang, Q., Gao, S., Zeng, R., Gao, P., Xu, L., & Dai, F. (2024) First Report of Bacterial Leaf Spot on Muskmelon Caused by *Pseudomonas syringae* pv. *syringae* in China. *Plant Disease*, 0(0), PDIS-06-23-1201-PDN. <https://doi.org/10.1094/pdis-06-23-1201-pdn>
- Sopalun, K., Kanchit, K., & Ishikawa, K. (2010). Vitrification-based cryopreservation of *Grammatophyllum spaciosum* protocorm. *Cryo Letters*, 31(4), 347-357.
- Stasolla, C., & Yeung, E. C. (2015). Paraffin and Polyester Waxes. In E. C. T. Yeung, C. Stasolla, M. J. Sumner, & B. Q. Huang (Eds.), *Plant Microtechniques and Protocols* (pp. 45-66). Cham: Springer International Publishing.. <https://doi.org/10.1007/978-3-319-19944-3>
- Su, S., Liu, Z., Chen, C., Zhang, Y., Wang, X., Zhu, L., Yuan, M. (2010). Cucumber Mosaic Virus Movement Protein Severs Actin Filaments to Increase the Plasmodesmal Size Exclusion Limit in Tobacco. *The Plant Cell*, 22(4), 1373-1387. <https://doi.org/10.1105/tpc.108.064212>
- Suzuki, M., Tandon, P., Ishikawa, M., & Toyomasu, T. (2008). Development of a new vitrification solution, VSL, and its application to the cryopreservation of gentian axillary buds. *Plant Biotechnology Reports*, 2(2), 123-131. <https://doi.org/10.1007/s11816-008-0056-5>

7. Bibliography

- Takemoto, K., Ebine, K., Askani, J. C., Krüger, F., Gonzalez, Z. A., Ito, E., Ueda, T. (2018). Distinct sets of tethering complexes, SNARE complexes, and Rab GTPases mediate membrane fusion at the vacuole in Arabidopsis. *Proc Natl Acad Sci U S A*, 115(10), E2457-E2466. <https://doi.org/10.1073/pnas.1717839115>
- Taliansky, M. E., & García-Arenal, F. (1995). Role of cucumovirus capsid protein in long-distance movement within the infected plant. *J Virol*, 69(2), 916-922. <https://doi.org/10.1128/jvi.69.2.916-922.1995>
- Tamisier, L., Rousseau, E., Barraillé, S., Nemouchi, G., Szadkowski, M., Mailleret, L., Palloix, A. (2017). Quantitative trait loci in pepper control the effective population size of two RNA viruses at inoculation. *J Gen Virol*, 98(7), 1923-1931. <https://doi.org/10.1099/jgv.0.000835>
- Tamisier, L., Szadkowski, M., Nemouchi, G., Lefebvre, V., Szadkowski, E., Duboscq, R., Moury, B. (2020). Genome-wide association mapping of QTLs implied in potato virus Y population sizes in pepper: evidence for widespread resistance QTL pyramiding. *Mol Plant Pathol*, 21(1), 3-16. <https://doi.org/10.1111/mpp.12874>
- Tanksley, S. D., & McCouch, S. R. (1997). Seed banks and molecular maps: unlocking genetic potential from the wild. *Science*, 277(5329), 1063-1066. <https://doi.org/10.1126/science.277.5329.1063>
- Tarquini, G., Ermacora, P., Bianchi, G. L., De Amicis, F., Pagliari, L., Martini, M., Musetti, R. (2018). Localization and subcellular association of Grapevine Pinot Gris Virus in grapevine leaf tissues. 255(3), 923-935. <https://doi.org/10.1007/s00709-017-1198-5>
- Teixeira, R., & Pereira, H. (2010). Laser Microdissection applied to plants. In (pp. 986-992)
- Thavarajah, R., Mudimbaimannar, V. K., Elizabeth, J., Rao, U. K., & Ranganathan, K. (2012). Chemical and physical basics of routine formaldehyde fixation. *J Oral Maxillofac Pathol*, 16(3), 400-405. <https://doi.org/10.4103%2F0973-029X.102496>
- Thomas, D. J., Rainbow, J., & Bartley, L. E. (2023). The rapid-tome, a 3D-printed microtome, and an updated hand-sectioning method for high-quality plant sectioning. *I9*(1), 12. <https://doi.org/10.1186/s13007-023-00986-3>
- Thompson, J. R., & García-Arenal, F. (1998). The Bundle Sheath-Phloem Interface of Cucumis sativus Is a Boundary to Systemic Infection by Tomato Aspermy Virus. *Molecular Plant-Microbe Interactions®*, 11(2), 109-114. <https://doi.org/10.1094/mpmi.1998.11.2.109>
- Torrance, L., Cowan, G. H., McLean, K., MacFarlane, S., Al-Abedy, A. N., Armstrong, M., Bryan, G. J. (2020). Natural resistance to Potato virus Y in

7. Bibliography

- Solanum tuberosum* Group Phureja. *133*(3), 967-980. <https://doi.org/10.1007/s00122-019-03521-y>
- Truniger, V., & Aranda, M. A. (2009). Recessive resistance to plant viruses. In *Adv Virus Res* (Vol. 75, pp. 119-159). United States: 2009 Elsevier Inc. [https://doi.org/10.1016/s0065-3527\(09\)07504-6](https://doi.org/10.1016/s0065-3527(09)07504-6)
- Tsutsumi, K., Kawasaki, M., Taniguchi, M., Itani, T., Maekawa, M., & Miyake, H. (2007). Structural and Functional Differentiation of Bundle Sheath and Mesophyll Cells in the Lamina Joint of Rice Compared with that in the Corresponding Region of the Liguleless Genotype. *10*(3), 346-356. <https://doi.org/10.1626/pp.s.10.346>
- Ueki, S., & Citovsky, V. (2007). Spread Throughout the Plant: Systemic Transport of Viruses. In E. Waigmann & M. Heinlein (Eds.), *Viral Transport in Plants* (pp. 85-118). Berlin, Heidelberg: Springer Berlin Heidelberg. https://doi.org/10.1007/7089_2006_101
- Urrutia, M., Bonet, J., Arús, P., & Monfort, A. (2015). A near-isogenic line (NIL) collection in diploid strawberry and its use in the genetic analysis of morphologic, phenotypic and nutritional characters. *Theor Appl Genet*, *128*(7), 1261-1275. <https://doi.org/10.1007/s00122-015-2503-3>
- van de Meene, A. M., Doblin, M. S., & Bacic, A. (2017). The plant secretory pathway seen through the lens of the cell wall. In *Protoplasma* (Vol. 254, pp. 75-94). Austria. <https://doi.org/10.1007/s00709-016-0952-4>
- van Schie, C. C., & Takken, F. L. (2014). Susceptibility genes 101: how to be a good host. *Annu Rev Phytopathol*, *52*, 551-581. <https://doi.org/10.1146/annurev-phyto-102313-045854>
- Vegas, J., Garcia-Mas, J., & Monforte, A. J. (2013). Interaction between QTLs induces an advance in ethylene biosynthesis during melon fruit ripening. *Theor Appl Genet*, *126*(6), 1531-1544. <https://doi.org/10.1007/s00122-013-2071-3>
- Wang, Y. H., Thomas, C. E., & Dean, R. A. (1997). A genetic map of melon (*Cucumis melo* L.) based on amplified fragment length polymorphism (AFLP) markers. *95*(5), 791-798.
- Wang, R. Y., & Nagy, P. D. (2008). Tomato bushy stunt virus co-opts the RNA-binding function of a host metabolic enzyme for viral genomic RNA synthesis. *Cell host & microbe*, *3*(3), 178-187. <https://doi.org/10.1016/j.chom.2008.02.005>
- Wang, T., Ming, Z., Xiaochun, W., & Hong, W. (2011). Rab7: role of its protein interaction cascades in endo-lysosomal traffic. In *Cell Signal* (Vol. 23, pp. 516-521). © 2010 Elsevier Inc. <https://doi.org/10.1016/j.cellsig.2010.09.012>

7. Bibliography

- Wang, A. (2015). Dissecting the Molecular Network of Virus-Plant Interactions: The Complex Roles of Host Factors. *Annual Review of Phytopathology*, 53(Volume 53, 2015), 45-66. <https://doi.org/https://doi.org/10.1146/annurev-phyto-080614-120001>
- Wayne, R. (2010). Chapter 3 - Plasmodesmata. In (pp. 51-60). San Diego: Academic Press.
- Wechter, W. P., Whitehead, M. P., Thomas, C. E., & Dean, R. A. (1995). Identification of a randomly amplified polymorphic DNA marker linked to the Fom 2 Fusarium wilt resistance gene in muskmelon MR-1. *85(10)*, 1245-1249.
- Wildy, P. (1971). *Classification and Nomenclature of Viruses: 1st Report of the International Committee on Nomenclature of Viruses*: S.Karger AG. <https://doi.org/10.1159/isbn.978-3-318-04027-2>
- Wintermantel, W. M., Banerjee, N., Oliver, J. C., Paolillo, D. J., & Zaitlin, M. (1997). Cucumber Mosaic Virus Is Restricted from Entering Minor Veins in Transgenic Tobacco Exhibiting Replicase-Mediated Resistance. *231(2)*, 248-257. <https://doi.org/10.1006/viro.1997.8533>
- Xu, P., Blancaflor, E. B., & Roossinck, M. J. (2003). In spite of induced multiple defense responses, tomato plants infected with Cucumber mosaic virus and D satellite RNA succumb to systemic necrosis. *Mol Plant Microbe Interact*, 16(6), 467-476. <https://doi.org/10.1094/MPMI.2003.16.6.467>
- Xu, M., Cho, E., Burch-Smith, T. M., & Zambryski, P. C. (2012). Plasmodesmata formation and cell-to-cell transport are reduced in decreased size exclusion limit 1 during embryogenesis in Arabidopsis. *Proceedings of the National Academy of Sciences of the United States of America*, 109(13), 5098–5103. <https://doi.org/10.1073/pnas.1202919109>
- Xu, L., He, Y., Tang, L., Xu, Y., & Zhao, G. (2022). Genetics, Genomics, and Breeding in Melon. *Agronomy*, 12(11), 2891. <https://doi.org/10.3390/agronomy12112891>
- Yamaguchi, N., Seshimo, Y., & Masuta, C. (2005). Mapping the sequence domain for systemic infection in edible lily on the viral genome of Cucumber mosaic virus. *71(5)*, 373-376. <https://doi.org/10.1007/s10327-005-0213-4>
- Yan, J. (2018). Study of the resistance to Cucumber mosaic virus aggressive strains in the melon (*Cucumis melon* L.) accession PI 161375. <http://hdl.handle.net/10803/666767>
- Yoshii, M., Yoshioka, N., Ishikawa, M., & Naito, S. (1998a). Isolation of an Arabidopsis thaliana mutant in which accumulation of cucumber mosaic virus coat protein is delayed. *Plant J*, 13(2), 211-219. <https://doi.org/10.1046/j.1365-313x.1998.00024.x>

7. Bibliography

- Yoshii, M., Yoshioka, N., Ishikawa, M., & Naito, S. (1998b). Isolation of an *Arabidopsis thaliana* mutant in which the multiplication of both cucumber mosaic virus and turnip crinkle virus is affected. *J Virol*, 72(11), 8731-8737. <https://doi.org/10.1128%2Fjvi.72.11.8731-8737.1998>
- Yu, X., Zhang, J., Zhang, X., Yang, X., Xu, X., Lin, J., Xiang, W. (2022). Identification and Pathogenicity of Fungi Associated with Leaf Spot of Muskmelon in Eastern Shandong Province, China. *Plant Disease*, 106(3), 872-890. <https://doi.org/10.1094/pdis-06-21-1126-re>
- Zafirov, D., Giovinazzo, N., Bastet, A., & Gallois, J.-L. (2021). When a knockout is an Achilles' heel: Resistance to one potyvirus species triggers hypersusceptibility to another one in *Arabidopsis thaliana*. *Molecular Plant Pathology*, 22(3), 334-347. <https://doi.org/10.1111/mpp.13031>
- Zamecnik, J., Faltus, M., & Bilavcik, A. (2021). Vitrification Solutions for Plant Cryopreservation: Modification and Properties. *Plants*, 10(12), 2623. <https://doi.org/10.3390/plants10122623>
- Zhang, C., & Turgeon, R. (2018). Mechanisms of phloem loading. *43 Physiology and metabolism 2018*, 43, 71-75.
- Zhu, Y., Li, H., Bhatti, S., Zhou, S., Yang, Y., Fish, T., & Thannhauser, T. W. (2016). Development of a laser capture microscope-based single-cell-type proteomics tool for studying proteomes of individual cell layers of plant roots. 3(1), 16026. <https://doi.org/10.1038/hortres.2016.26>
- Zouhar, J., Rojo, E., & Bassham, D. C. (2009). AtVPS45 is a positive regulator of the SYP41/SYP61/VTI12 SNARE complex involved in trafficking of vacuolar cargo. *Plant Physiol*, 149(4), 1668-1678. <https://doi.org/10.1104/pp.108.134361>